IOWA STATE UNIVERSITY
Digital Repository

Retrospective Theses and Dissertations

Iowa State University Capstones, Theses and Dissertations

1974

Particle mixing and circulation in gas fluidized beds of flour and starch

Richard Howard Nielsen
Iowa State University

Follow this and additional works at: https://lib.dr.iastate.edu/rtd

 Part of the Chemical Engineering Commons

Recommended Citation
Nielsen, Richard Howard, "Particle mixing and circulation in gas fluidized beds of flour and starch " (1974). *Retrospective Theses and Dissertations*. 6357.
https://lib.dr.iastate.edu/rtd/6357

This Dissertation is brought to you for free and open access by the Iowa State University Capstones, Theses and Dissertations at Iowa State University Digital Repository. It has been accepted for inclusion in Retrospective Theses and Dissertations by an authorized administrator of Iowa State University Digital Repository. For more information, please contact digirep@iastate.edu.

INFORMATION TO USERS

This material was produced from a microfilm copy of the original document. While the most advanced technological means to photograph and reproduce this document have been used, the quality is heavily dependent upon the quality of the original submitted.

The following explanation of techniques is provided to help you understand markings or patterns which may appear on this reproduction.

1. The sign or "target" for pages apparently lacking from the document photographed is "Missing Page(s)". If it was possible to obtain the missing page(s) or section, they are spliced into the film along with adjacent pages. This may have necessitated cutting thru an image and duplicating adjacent pages to insure you complete continuity.

2. When an image on the film is obliterated with a large round black mark, it is an indication that the photographer suspected that the copy may have moved during exposure and thus cause a blurred image. You will find a good image of the page in the adjacent frame.

3. When a map, drawing or chart, etc., was part of the material being photographed the photographer followed a definite method in "sectioning" the material. It is customary to begin photoing at the upper left hand corner of a large sheet and to continue photoing from left to right in equal sections with a small overlap. If necessary, sectioning is continued again — beginning below the first row and continuing on until complete.

4. The majority of users indicate that the textual content is of greatest value, however, a somewhat higher quality reproduction could be made from "photographs" if essential to the understanding of the dissertation. Silver prints of "photographs" may be ordered at additional charge by writing the Order Department, giving the catalog number, title, author and specific pages you wish reproduced.

5. PLEASE NOTE: Some pages may have indistinct print. Filmed as received.

Xerox University Microfilms
300 North Zeeb Road
Ann Arbor, Michigan 48106

75-3321

NIELSEN, Richard Howard, 1946-
PARTICLE MIXING AND CIRCULATION IN GAS FLUIDIZED BEDS OF FLOUR AND STARCH.

Iowa State University, Ph.D., 1974
Engineering, chemical

Xerox University Microfilms, Ann Arbor, Michigan 48106

THIS DISSERTATION HAS BEEN MICROFILMED EXACTLY AS RECEIVED.

Particle mixing and circulation in gas fluidized beds of flour and starch

by

Richard Howard Nielsen

A Dissertation Submitted to the
Graduate Faculty in Partial Fulfillment of
The Requirements for the Degree of
DOCTOR OF PHILOSOPHY

Department: Chemical Engineering and Nuclear Engineering
Major: Chemical Engineering

Approved:

Signature was redacted for privacy.

In Charge of Major Work

Signature was redacted for privacy.

For the Major Department

Signature was redacted for privacy.

For the Graduate College

Iowa State University
Ames, Iowa

1974

TABLE OF CONTENTS

NOMENCLATURE

a = regression coefficient

A = bed cross sectional area, in^2.

b = regression coefficient

b_o = distance of bubble surface from column wall, cm.

B = general regression coefficient

c = column circumferential coordinate measured from point of observation (shortest normal from wall to bubble), cm.

c = constant

c = regression coefficient

C = conditions effect

C_S = heat capacity of solids, Btu/lb.°F

C.V. = $(S/\bar{X})$ x 100%, coefficient of variation, %

d = particle diameter, microns

d = regression coefficient

d = travel distance of slip surface voids ("cracks"), in.

d_B = diameter of big particles in mixture of two sizes

d_{ls} = length-surface mean diameter, equation 24

d_m = stirrer diameter, cm.

d_{nl} = number-length mean diameter, equation 24

d_{sv} = surface-volume mean diameter, equation 24

d_S = diameter of small particles in mixture of two sizes

d_{wm} = weight-moment mean diameter, equation 24

df = frequency of particles in size range d to d + Δd, %

d.f. = degrees of freedom

D = column diameter, in.

D_b = bubble diameter, cm.

D_c = column diameter, cm.

e = eccentricity (distance of bubble center from column axis, cm.

e = regression coefficient

E = residual error

f = cumulative frequency distribution of particle size, %

f_o = fraction of heat transfer surface covered by gas bubbles, (-)

F = "F" ratio statistic

f = regression coefficient

g = acceleration of gravity, cm./sec^2.

g = regression coefficient

G = superficial mass velocity of fluidizing gas, lb./ft^{2}hr.

G^* = G at minimum fluidization gas flow, lb./ft^{2}hr.

h = mean heat transfer coefficient between bed and heat transfer surface, Btu/ft^{2}hr.$^\circ$F

h_i = instanteous heat transfer coefficient between bed heat transfer surface, Btu/ft^{2}hr.$^\circ$F

H = bed height effect

H = null hypothesis

H = settled bed height, in.

i = index, (-)

j = index, (-)

k = thermal conductivity of a particle, Btu/ft.hr.$^\circ$F

k_e = effective thermal conductivity of the bed, Btu/ft.hr.°F

k_g = value of k in zone adjacent to column wall, Btu/ft.hr.°F

k_{eW} = thermal conductivity of fluidizing gas, Btu/ft.hr.°F

L = length of heater

L = location effect

L = location, height above gas distributor, in.

m = weight of bed, wet basis, lb.

M = mixing index, (-)

$\bar{M}$ = overall mean effect

Ma = material effect

Mo = moisture content effect

M_g = geometric weight mean particle diameter, microns

M_n = geometric number mean particle diameter, microns

M.S. = mean square

n = number of observations, (-)

N = number of particles/g., by microscope count

N = stirrer speed, rpm

N = stirrer speed effect

N_T = total number of particles in a sample, (-)

O = observer effect

p = absolute pressure, psia.

p* = water vapor pressure, psia.

$\bar{p}$ = average proportion of component, equation 7, (-)

p_i = measured proportion of component i, equation 7, (-)

P = power consumption, kilowatts

P = proportion of type A particles in a sample of a mixture of type A and B particles, (-)

P = volumetric fraction of solids

P > F = significance level at which F becomes significant (probability of a larger F value), (-)

P > T = significance level at which T becomes significant (probability of a larger T value), (-)

Q = salt effect

R = gas relative humidity effect

R^2 = coefficient of multiple determination, equation 30

S = set effect

S = $(S^2)^{1/2}$, standard deviation

S^2 = sample variance estimate

S_o = overall vertical displacement of the tracer layer at the point closest to the bubble (c=0), cm.

t = time, min.

$\bar{t}$ = average time, sec.

t' = residence time of packet at heater

t_i = time of ith event, sec.

t_m = mean residence time of packet of solid particles near the heat transfer surface

t_M = minimum mixing time, min.

T = stirrer torque, in-lb.

T = "T" statistic

Tr = tracer effect

u = superficial velocity of fluidizing gas, ft./sec.

u_c = critical fluidization gas velocity, cm./sec.

u_{mf} = minimum fluidization gas velocity, ft./sec.

U = fluidization gas velocity effect

v = velocity

v_i = rate of ith event, in./sec.

$\bar{v}_H$ = harmonic mean rate of downward crack movement, in./sec.

w^2 = population variance due to component under consideration

W = solids superficial mass velocity across a horizontal plane, lb./ft²hr.

X = tracer concentration, mg. metal/g. of dry sample

$\bar{X}$ = steady state tracer concentration, mg. metal/g. of dry sample

X_T = %M/100, total moisture content, lb. of water/lb. of dry stock

$\bar{y}$ = overall mean of y_i

y_i = dependent variable

$\hat{y}_i$ = model estimate of y_i

z = dependent variable

γ = particle specific gravity

γ_g = specific gracity of fluidizing gas

δ_W = thickness of boundary zone adjacent to heater surface

Δd = particle size increment, microns

ΔP_{bed} = bed pressure drop, lb./in².

$\Delta\Pi$ = $(A/m)\,\Delta P_{bed}$, bed pressure drop, (-)

μ_g = gas viscosity, g./cm.sec.

ρ = particle density, g./cm^3.

ρ_B = bulk density of dense phase of fluidized bed

ρ_g = gas density, g./cm^3.

ρ_h = density of heavy particles, g./cm^3.

ρ_l = density of light particles, g./cm^3.

σ = $(\sigma^2)^{1/2}$

σ_g = geometric weight particle diameter deviation, (-)

σ^2 = variance of mixture composition

σ_o^2 = variance of "mixture" composition if components are completely segregated

σ_R^2 = variance of composition of a perfectly random mixture

τ = lag time, min.

X*Y = interaction of X and Y effects

%M = 100X , moisture content, dry basis, %

%RH = relative humidity of fluidizing gas, %

ABSTRACT

The gross rate of downward movement of cohesive solids near the wall of a fluidization column was studied. In addition, the batch mixing of trace amounts (less than 1 wt. %) of powdered, metal salts with wheat flour, flour containing 1.0 wt. % of an antiagglomerate (Cab-O-Sil), and potato starch was investigated.

The statistically designed experiments were conducted in a 6 in. inside diameter by 5 ft. tall, cylindrical column with a porous plate gas distributor. A simple, two-bladed paddle stirrer located just above the distributor promoted fluidization of the cohesive powders by breaking up channels. The rate of solids movement down the wall was measured through the transparent wall at various locations. Mixing was studied by adding an impulse of tracer salt to the top of the fluidized bed and collecting samples from the base of the column as a function of time. The progress of mixing was indicated by plots of tracer concentration versus time. After some experiments, fluidization was abruptly stopped and samples of the settled bed were collected with a sample thief.

The solids were observed to move down the freely bubbling beds in slip-stick flow. At low fluidization velocities, the movement approached plug flow with large segments of the bed moving in unison while at higher gas velocities, the bed had less structure and was broken into smaller seg-

ments which moved more freely.

The rate of solids movement was significantly affected by the fluidization velocity, location above the distributor plate, settled bed height, flour moisture content, and the presence of 0.5% Cab-O-Sil, but was not affected by stirrer speed. The rate of solids movement of pure flour was correlated with the above significant parameters. Wall-to-bed heat transfer coefficients also were correlated with the rate of solids movement.

The rate of mixing was dependent upon the gas velocity, settled bed height, flour moisture content, and material fluidized and independent of stirrer speed. For pure flour the rate of mixing was correlated with the above significant parameters. Fluidization was continued for a long enough time so that the between sample variance of the steady state samples (excluding 5 to 10% of the outlying samples) was independent of all the above factors as well as the amount of tracer added. No segregation of tracer in the bed occurred since the concentration variance of the settled bed samples was independent of elevation or radial location in the bed.

INTRODUCTION

Particulate solids may be classified into two general categories: free flowing and nonfree flowing or cohesive powders. Flour is a familiar example of a cohesive material. It is difficult to pour, having a strong tendency to form aggregates which break away in clumps rather than flow. On a microscopic scale, it is seen that in a free flowing powder the particles can slip over one another when under a stress, while in cohesive powders, there is more frictional resistance, sometimes enough to prevent movement.

Particulate solid heating, cooling, drying, gas adsorption, and gas-solid chemical reactions are several processes where it is desirable to contact particulate solids with a gas. Gas fluidization is the method of contacting a gas with a particulate solid in which fluid properties are imparted to the solids by the passage of a gas stream through the solids.

A gas fluidized bed has important features that are a direct result of particle motion: well mixed solids and high heat transfer rates, both between gas and solid and between the bed and wall. The combined action of these two features results in an isothermal temperature distribution in the bed. This in turn leads to important applications where control of particle temperature is important. The ability to transfer rapidly large amounts of heat enables some very exothermic or endothermic reactions to proceed with little tem-

perature gradient in the bed.

Many of the commerical applications of fluidization as well as almost all the research and theoretical developments have involved free flowing or nearly free flowing solids. Gas fluidization of cohesive powders is of growing interest as new reactions and applications are discovered.

One reaction (29, 60) of interest is the degradation of wheat flour by a reactive gas such as hydrogen chloride followed by neutralization with ammonia. Fluidization of flour was accomplished either by adding a flow conditioner (29) or by slowly revolving a simple stirrer just above the gas distributor plate (9, 10).

The mixing of a small quantity of particulate solid (the trace component) into an order of magnitude larger amount of a second particulate solid (the bulk component) is a process of importance in several industries (3). The solids may be cohesive. In food processing, baking powder and salt are mixed with flour to produce prepared flours. In pharmaceutical production, corn starch is a carrier with which small doses of solid drugs are mixed before being tableted. Gas fluidization would perhaps be a suitable mixing system for trace solids and cohesive powders.

Lloyd and Yeung (71) tabulated about 50 experimental mixing studies according to particle size. They observed that the number of published experiments involving the mixing

of powders of size below 100 microns was few. Powders of size below about 60 microns generally are cohesive (53, 108), whereas those above about 100 microns are generally free flowing (53). So even fewer studies were published on the mixing of cohesive powders.

Because of the above mentioned interest in gas degradation of flour and the general interest in solids mixing, measurement of the fluidization properties of a 6 in. diameter, stirred bed was undertaken (9, 10), including exploratory tests of trace solids mixing (11). Trace amounts of metal salts were placed on the settled bed surface and the gas flow and stirring were quickly started. The steady state metal concentration was achieved within minutes at the operating conditions used. Mixing was very rapid compared to the rate at which samples were then collected and also compared to the time required to achieve steady state fluidization.

In a study (84, 85) of the wall to bed heat transfer of stirred, fluidized flour beds, the need arose for data on the particle residence time on the heat transfer surface. The residence time is a parameter common to several heat transfer models. Moreover, the heat transfer results themselves showed a significant dependence on the elevation of the heat transfer surface above the gas distributor. This suggested that perhaps the residence time was different in the upper and lower areas employed.

Based on these demonstrated needs, an investigation of trace solids mixing and particle residence time on the wall heat transfer areas was planned. Improved mixing study techniques and a method of measuring particle residence time were first developed (87). These techniques were employed in the present study to determine the effect of system variables on the residence time of downward moving solids at wall to bed heat transfer surfaces and to determine the trace solids mixing characteristics of the system.

The statistically designed experiments were performed in a 6 in. inside diameter by 5 ft. overall length, cylindrical column with a porous plate gas distributor. Humidified or dry nitrogen was the fluidizing gas (0.12 to 0.35 ft./sec.). Fluidization was promoted by a simple, two bladed paddle stirrer (19 to 150 rpm) located just above the distributor. (One set of experiments was also performed using flow conditioned flour.) Two columns were used, one a Pyrex glass pipe, the other, a Plexiglas column having 6 pairs of sample ports located at 6 in. elevation intervals. These ports enabled the collection of settled bed core samples. Four moisture content levels (3 to 14%) of flour were used. Bed depths of 12.5, 28, and 32 in. were fluidized. The mixing characteristics of a potato starch bed were also studied.

The residence time of downward moving flour solids was measured at the wall by manually timing particle slip surface

voids (87) moving over grids located at several elevations.

Mixing was studied by adding trace amounts (less than 1 wt. %) of powdered metal salts to the fluid bed. Samples were collected as a function of time by intermittently allowing solids to flow through a small sample tap located just above the gas distributor. After some experiments, fluidization was abruptly stopped and core samples were collected with a sample thief (87) from various locations in the settled bed. Sample metal concentration was determined spectrophotometrically (87).

A gas fluidized bed often is viewed as being composed of two phases: a continuous "dense" phase having a high solid particle concentration, and a discontinuous "bubble" phase which is a gas pocket containing essentially no solids. This picture is the basis of several empirical models of a fluid bed which model the dense phase as a well mixed stirred tank and the bubble phase as a gas bypass stream. Modifications of the basic model include cross flows and dead zones.

Gas fluidization theory and practice have been largely concerned with those free flowing systems which can be readily fluidized and therefore may be called "well-behaved" solids. Successful and promising theoretical developments have been made for those systems which meet the additional requirements or assumptions of the models. These materials may be considered to be "ideal" solids. The "bubble models"

proposed by Davidson and Harrison (22) and by Kunii and Levenspiel (63) are the most widely known. Based upon a set of assumptions, the bubble properties such as size and frequency are related to the fluidization characteristics from which design parameters and operating conditions can be determined. The application to design calculations for most systems, even well-behaved ones, is a future development. At present, once the bubble properties are known or inferred, the theories may be used to fit data and suggest explanations for observed behavior. Since most cohesive powders fail to fluidize unless assistance is provided, for example, by mechanical vibration, stirring, or flow conditioning of the powder, nonfree flowing powders might be expected to behave differently than the well-behaved or ideal solids. The present study may be considered part of a systematic investigation of the fluidization of cohesive solids.

Solids mixing is the process of randomly dispersing two or more particulate solids amongst each other by the random movement of the particles (25). This is an empirical "state of the art" unit operation with several areas of current research activity (26): quantifying the degree of randomness of a mixture, studying the mechanisms and rate of mixing, relating equipment design and selection to the requirements of specific applications, and mathematical modeling or simulation of the mixing process.

The mechanical steps of the mixing process may be described as follows:

1. Trace material must be introduced to the surface of the bulk material.
2. The bulk material must be present in such a state that particle motion exists, at least at the interface, and is of sufficient magnitude for the trace particles to move into the volume vacated by some bulk particles.
3. The process of volume creation or particle displacement must continue.

When examined on a large scale, the resulting powder mixture appears homogeneous in properties such as concentration. The mixture is, however, composed of discrete particles and is ultimately heterogeneous. The smallest sample size which appears to have the required degree of homogeneity is the "minimum scale of scrutiny". A classic illustration of this concept is a cake mix. The package contents are dumped and further mixed as the liquid cake ingredients are added. The minimum scale of scrutiny for the flour cake mixer is the package size (assuming no demixing in packaging). As long as the proper trace component concentration is in the package, the cake will bake well. Now, if only half a recipe is to be made, the minimum scale of scrutiny changes to a smaller value since the half box of cake mix used must

contain the proper concentrations. The required degree of homogeneity will vary with the application.

Solids mixing is utilized in many industries (3) including fertilizer, glass, plastics, and food processing. The system investigated in this study appears to have several possible, direct applications for treating or processing flours and starches, in addition to those mentioned earlier, as well as for other cohesive powders.

The mixing of trace components has several potential applications besides mixing baking powders to produce prepared flours. Benzoyl peroxide has been used as a solid, flour bleaching agent (55). Encapsulated ferrous sulfate may be used to protect flour from rancidity (50). A method (41) for blending agglomerative and nonagglomerative powders used a fluidized bed of nonagglomerative powder into which the agglomerative solids were sifted. This enabled a coating compound to be made without increasing its temperature.

The system investigated here appears to have several possible direct applications for treating or processing flours and starches. The possibility of sugar coating starch in a fluid bed has been demonstrated (32). Granulation of drug powders with 24% potato starch was achieved using a stirred, fluidized bed (90). A method of agglomerating flour using humid air and stirring has been reported (37). The general use of fluidized bed drying in the food industry has

been discussed (27). Fluidization of very cohesive, freeze dried apple juice particles was not achieved by use of a simple mechanical stirrer (73) (nor by any other of the means attempted). Use of the gas solid contacting properties of the system may be advantageous. Flour has been successfully bleached by chlorine gas to produce an improved cake flour (119). Under other conditions, cleavage of flour protein occurred. A steam treatment or heating (46) of flour destroys the gluten forming part of flour protein, a result claimed desirable for several uses. Heating above 120°F in a sealed container pasteurizes flour (31). Heating at 120°C was earlier found to improve cake flour (110). It seems that the good heat transfer properties of a fluid bed might be useful in these heating operations.

PART 1. LITERATURE REVIEW

Several reviewers of the general fluidization literature have discussed the motion of solids in gas fluidized beds (63, 67, 97, 101, 135). A review of the literature published before 1966 pertaining to the gas fluidization of cohesive materials, especially flours and starches, was made by Wheelock (129).

Special techniques were required for achieving successful gas fluidization of cohesive powders. Cohesive powders generally can not be fluidized without assistance due to the formation of channels in the bed through which the gas bypasses the solids. Fluidization has been successfully promoted for many cohesive powders by supplying assistance to particle motion by means of stirring or vibrating the bed, or by the use of a flow conditioner. The promotion of fluidization of flours and starches has been reviewed and studied (9, 29).

A series of studies of flour and starch fluidization characteristics have been conducted at Iowa State University (9, 10, 11, 29, 84, 85, 86, 87, 124). The best column geometry and grid design for these materials was a cylindrical bed with a porous plate gas distributor (29). Fluidization was successfully promoted by either the addition of a fumed silica flow conditioner (29) or by mechanically stirring the bed with a simple, two bladed paddle located just above the

gas distributor (9). The effects of gas velocity, stirrer speed, and bed depth on the fluidization characteristics such as bed pressure drop, expansion, and stirrer torque were measured (9, 10, 29, 84, 85, 87). System properties such as entrainment of solids (9, 29, 124) and the wall to bed heat transfer rate (84, 86, 85) were subjects of further investigations.

The heat transfer coefficients of two heat transfer surfaces, one located in the upper half of the bed, the other in the lower half, were found to be a function of gas velocity, materials fluidized, and location of the surface (84, 85). The lower surface had higher heat transfer coefficients than those of the upper surface.

Some exploratory tests to measure the solids mixing characteristics of these systems were attempted (9, 11). Techniques of studying solids mixing in gas fluidized beds of cohesive materials were further reviewed, developed, and successfully tested (87). Supporting analytical methods required for the description of the powders were also studied (87). Most of the above studies were conducted in batch fluidized beds. A column with continuous solids feed was built (124) and studied (80, 124) also.

In the above studies of the fluidization of flours and starches, the nonideality of fluidization behavior of these cohesive materials compared with that observed for free

flowing powders was noted to be of degree of approach to the values measured for free flowing powders. The general behavior of cohesive powders, once fluidization had been successfully promoted, was found to have much in common with the behavior of freely flowing powders. This also applied to the motion of solids where the basic mechanism of particle movement has been observed to be essentially the same as for free flowing materials but with an additional contribution (108) arising from the cohesive nature of the particles.

SOLIDS CIRCULATION

Early research (67, 92, 135) on gas fluidization was conducted primarily in small diameter (0.5 to 4 in.), cylindrical columns. The solids were generally free flowing materials such as sand, glass beads, or petroleum refinery catalysts, all with a mean size above 100 microns.

The observed solids movement was one where solids moved downward in an outer, annular region and moved upward in the central region. Horizontal movement occurred in two regions, above the gas distributor and near the bed surface. The particles thus circulated in a regular pattern throughout the bed. It was further noted that the bed cross sectional area which contained downward moving particles was considerably larger than the area of upward motion. Hence, the upward traveling particles' linear velocity was greater than that of the downward moving particles.

Some information on particle velocities at the wall of the column was reported (76). Specifically, the vertical motion of 0.028 in. (711 microns) glass beads and 200 mesh (about 74 microns) alumina was very predominant compared to the frequency or extent of horizontal motion. The downward particle velocity at the wall in the 3.75 in. diameter column for the gas velocity range explored was 3 to 5 times larger than the upward velocity at the wall. A main feature of this motion was the alternating fast and slow movement of the par-

ticles. Aggregates of moving particles were commonly observed. Macroscopic solids circulation (117) is the cyclic movement of particles throughout the bed such as from a region in the bed top to a region in the bed bottom and back to the top.

Woollard and Potter (134) showed that Talmor and Benenati's correlation (117) for the macroscopic solids circulation rate in a freely bubbling bed

$$W = 654(G - G^*)\exp(-168.5D_p) \qquad [1]$$

where D_p = particle diameter, in.

adequately correlated the scattered data over the parameter range:

Bed diameter: 1.25 to 4.0 in.

Particle diameter: 67 to 654 microns

$(G - G^*)$: 1 to 250 lb./(sq. ft.)(hr.) (117)

Particle density: 47 to 165 lb./(cu. ft.)

Particle shape: granular to spherical (117)

Size distribution: mixed and uniform

Solids: microspheres, sharp and round sands, silica gel, ion exchange resins, cracking catalyst, and coke.

As the results of more experiments conducted in larger diameter columns were reported, it was apparent that often

the above gross circulation pattern of up in the center, down at the wall was not observed for columns 6 in. in diameter or larger. Instead, particles appeared to be generally moving downward throughout the bed with varying, local regions of upward solids flow.

Woollard and Potter (134) studied the solids movement associated with the passage of single bubbles through an incipiently fluidized bed comprised of a colored bottom layer and a undyed top layer. Glass beads (380 microns average, 95% in the range 300 to 500 microns) were air fluidized in a 4 in. diameter column. Single bubbles of controlled size were injected at the column axis. Displacement profiles of the dyed particles were obtained by bed dissection.

The Talmor and Benenati correlation led to a prediction that the solids transported across the original tracer interface was 40% of the total volume of bubbles passing the original interface for the 380 micron glass spheres. The difference between this value and a value of 30 to 40% for the amount transported by a single bubble required further investigation. As discussed later, recent measurements (112) of the final displacement profiles and wake size compared favorably with those of Woollard and Potter. Woollard and Potter's results showed some, but not complete, agreement with the experiments of Rowe et al. (108) which are also discussed later.

The importance of gas bubbles in promoting solids motion was recognized and investigations were started which have led to general fluidization theories (22, 54, 63) based upon bubble phenomena. These theories have been generally successful in accounting for the gross characteristics of fluidized beds of free flowing solids. The theories are at the stage of development where the bubble properties need to be related to the powder, gas system properties before the more significant, predictive usage of these theories can be made, however.

In discussing the behavior of gas fluidized beds, the column diameter and general design must be considered since different bed geometries such as a tapered or conical bed, can change bubbling behavior and, hence, other characteristics. Also the effect of powder properties, even of free flowing materials, has recently been recognized (34).

EFFECT OF POWDER PROPERTIES

Classification of Systems

Geldart (34) recently suggested criteria based on particle size and density for predicting four categories of gas fluidized bed behavior.

Group A materials have a small size and/or a low particle density (less than about 1.4 g./cm^3). Materials must also be free flowing powders for membership in this group. Beds of these powders expand considerably before bubbling starts as gas velocity is increased. Particle circulation occurs even when only a few bubbles are present. Solids mixing is rapid.

Group B materials generally have a mean size range of 40 to 500 microns, based on the surface volume mean diameter, and a particle density range between 1.4 and 4 g./cm^3. When fluidized, bubbling starts at or just above the minimum fluidization velocity. Bed expansion is small. Little or no particle circulation occurs unless bubbles are present. This is the most frequently studied group. Powders of Groups A and B are rather easy to fluidize and result in a good quality of fluidization and may be thought of as "ideal" materials.

Group C materials are cohesive powders which are identified by being fluidized only with assistance such as

mechanical stirring or vibration to break up channels.

Group D materials are large and/or very dense particles. Not much has been published about the fluidization of these materials. Although dense phase gas velocity is high, solids mixing is relatively poor compared to that of Groups A and B.

Deep beds of dense materials do not fluidize well (70). Tapered or conical beds were often employed in attempts to achieve better quality fluidization of dense particles (70, 81, 109, 113). Relatively sticky particles could be fluidized as there was high particle momentum and fewer particle-particle contacts, This tended to reduce agglomeration.

Particle Size Effects

Geldart (33) investigated the effect of particle size and particle size distribution on the characteristics of gas fluidized beds. He found most of the published work had been concerned with Group B powders. His experiments using a 30.8 cm. diameter column also concentrated on this group.

Analysis of the literature and the results of his experiments showed Geldart that the fluidization characteristics of many powders were independent of both mean particle size and particle size distribution. The effects on bubble size, bed expansion, bed viscosity, and general quality of appearance were discussed.

An expression for mean bubble size as only a function of the gas distributor, observation height above the gas distributor, and the excess gas velocity ($u - u_{mf}$) was derived which gave good agreement with data for Group B powders fluidized in large diameter beds. Some evidence suggested that bubble size in beds of very coarse powders (Group D) may also be predicted by this expression, however. More information was needed for a significant test to be made.

The main effect of increasing the size distribution by adding fines to a material was the accompanying reduction of mean particle size. At equal excess gas velocities, bed expansion increased as also did the solids circulation rate but a decrease in mean bubble size did not result when fines were added.

PARTICLE MOTION

Mechanisms of Particle Motion

Rowe et al. (108) conducted pioneering studies of the mechanisms of solids movement in fluidized beds. Rowe and Partridge (106) and Rowe and Sutherland (109) had previously followed the displacement of layers of colored tracer particles caused by the passage of single gas bubbles through two and three dimensional beds, respectively. These results demonstrated that the solids mixing in gas fluidized beds was not due to the completely random motion of individual particles as assumed by the older diffusion theories of gas fluidized solids mixing. Instead, mixing was the result of a definite, reproducible pattern of particle displacements caused by each bubble passing through a gas fluidized bed.

Bed dissection and X-ray cine photography were the best techniques for studying this particle displacement. (The techniques of studying particle motion and mixing in gas fluidized beds have been recently reviewed (87).) In the studies under discussion, bubble size, location, and frequency were controlled by injecting gas pulses of known volume into a bed fluidized at the incipient fluidization velocity. This type of bubble generation was easier to accomplish when fluidizing a material having a narrow size range.

Generally, fluidized bed bubbles have been observed (101) to have the shape of a partially deflated basketball, Figure 1.

Rowe et al. (108) discovered two distinct solids mixing mechanisms in fluidized beds and a third which combined features of both of the first two mechanisms.

In the first mechanism, solids motion was due exclusively to gas bubble interaction with the particles. Solids motion followed a pattern which was predictable from the known locations of the bubbles. The second mechanism was a purely diffusional mechanism. Since it was found only in liquid fluidized beds, it will not be further discussed. The third mechanism was observed in certain gas fluidized beds to be basically a bubble motion like that of the first mechanism but with bubble induced diffusion contributing to solids motion.

Basic mechanism

Single bubble The bubble action of the first mechanism may be briefly described as follows. According to Rowe et al. (108), as a bubble rose towards an interface between a lower layer of colored particles and an upper layer of colorless particles, the originally horizontal interface was curved upwards. The bubble broke through the interface and was observed to carry colored material up with it, forming a

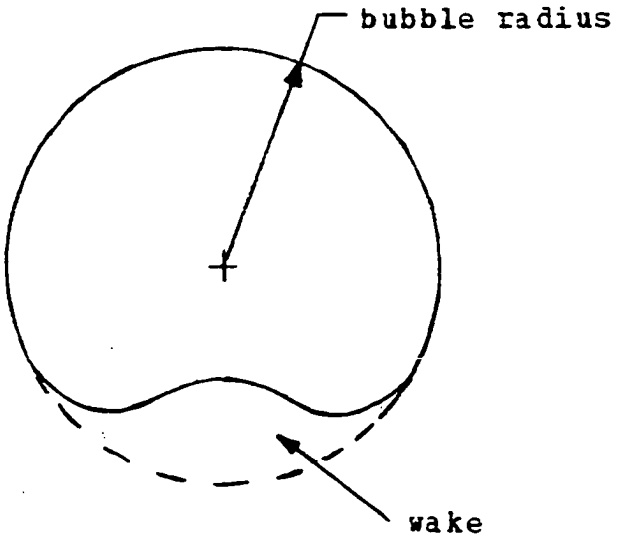

Figure 1. Bubble shape (10 1)

"spout" or "finger" of colored material behind it (Figure 2). The lower one-third of a sphere formed by extrapolating the bubble top's curvature was seen to be occupied by a wake of colored particles. The wake was about one-fourth the volume of the total bubble sphere. Material was shed from the wake as the bubble rose to form the spout and new material was continually added to the wake. When the bubble broke the bed's surface, wake material was dispersed on the surface. The final tracer pattern after the passage of a single bubble, Figure 2, was the main identifying characteristic of this solids motion mechanism.

On closer analysis, the bubble induced mixing was seen to be a result of two processes. In the first process, each bubble gathered underlying particles, some located in the finger following the bubble, and some located in the bubble's wake. The second process followed from continuity. As some material was carried upwards by the bubble, other material was displaced downward to take the place of the material moving upwards. These processes thus generated a convection current with particles moving upward along the path of the bubbles and downward elsewhere.

The size and shape of the spout could be calculated from the bubble size, shape, and path (106). The wake size varied with the size and type of particles (107) and fluctuated in a given bed (108). It did not systematically change with bed

Figure 2. Disturbance of interface caused by a single bubble (from 108)

a. 460 micron diameter ballotini

b. 60 micron diameter Synclyst cracking catalyst

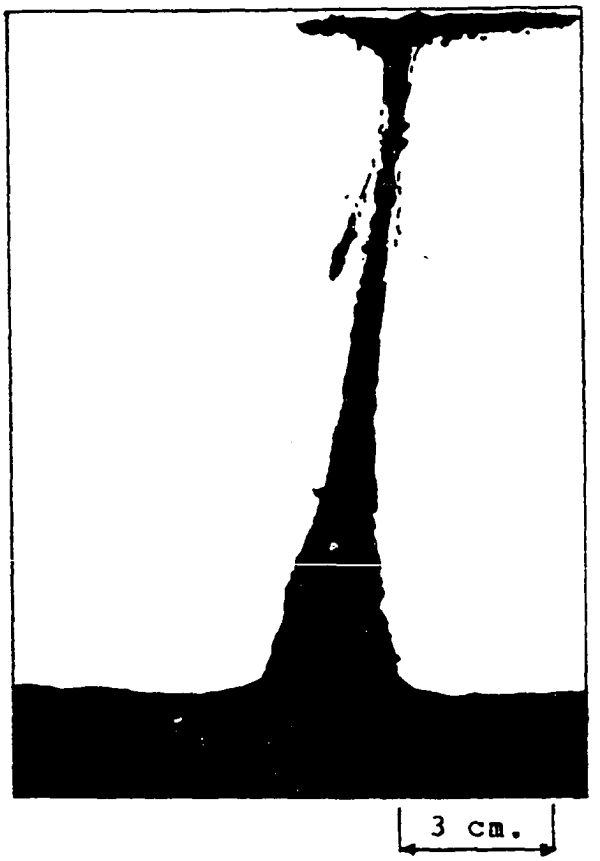

(a)

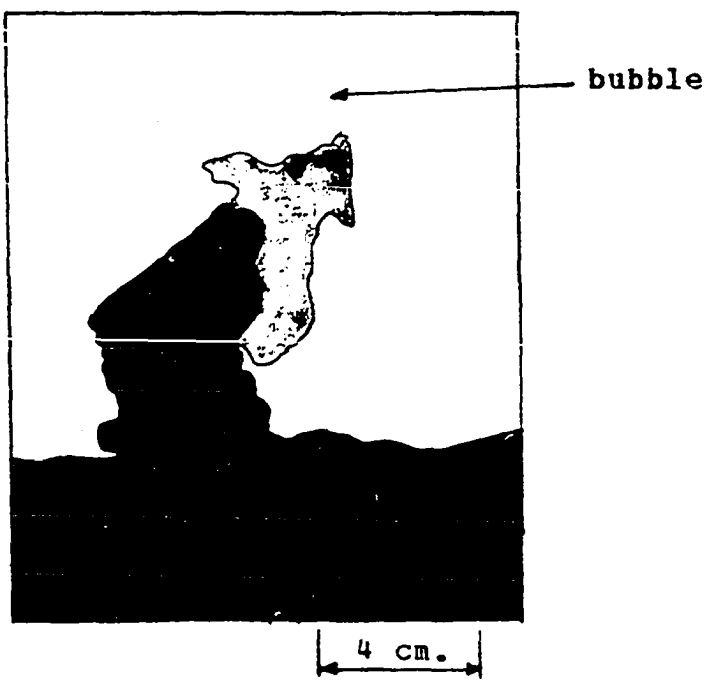

(b)

height. This was demonstrated by a series of experiments using thin tracer layers.

In another experiment, the renewal of wake material was studied. A thin layer of green tracer was laid over a thin layer of red tracer on the column bottom. White particles formed the rest of the bed. A bubble was formed in the red layer and thus initially had a wake comprised of only red particles. As the bubble rose, some of the red wake was shed in the green layer but further shedding in the white section of the bed was a mixture of green particles and red material. An appreciable amount of green, more red, and a small amount of white particles were deposited on the bed surface. It thus appeared that the wake acquired material from a "boundary layer" of particles flowing around the bubble. Furthermore, this boundary layer was thought to be a single particle thick and established by a high shear rate region near the bubble surface which resulted in vigorous particle interference.

Multiple bubbles The action of the passage of the initial, single bubble rising up the bed's axis has been described above. The effects of the passage of another bubble along the same path and of a series of 80 bubbles were also investigated by Rowe et al. (108). In brief, the resulting bed became progressively better mixed, but on a fine scale of scrutiny, the final mixture was not very good. Passage of

more bubbles, would improve results, however. Bubble splitting and the coalescence of bubbles traveling the same path also affect the wake drift particle displacement pattern. Much work has been devoted elsewhere (17, 18, 54, 89) to describing bubble coalescence fluid mechanics.

In a realistic, freely bubbling bed, bubbles would appear frequently and originate at random locations on the gas distributor grid. The resulting particle displacements can be explained by application of the basic bubble mechanism described above. An experimental study of the interaction of bubbles passing, in turn, through the bed at different locations was also performed by Rowe et al. (108). Six bubble generating lines were installed in a circle around a central line and bubbles were generated in random order at the seven locations during a bubbling cycle. The pattern expected from the bubble mechanism resulted, although "spouts" near the sides were not always symmetrical. If the distance between bubble locations was too close, partial cancellation of the particle displacements by each bubble resulted. A less effective degree of solids mixing resulted than would be achieved by an equivalent number of bubbles passing serially up the column axis. For beds having a large diameter compared to the bubble diameter, however, an optimum bubble spacing probably existed which would give more effective solids mixing. A freely bubbling bed was intermediate in

mixing effectiveness between that of a bed passing an equivalent number of bubbles at patterned locations and that of a bed serially passing the same number of bubbles up the column axis.

Rowe et al. (108) concluded that the observed particle displacements were entirely inconsistent with a mechanism of mixing by inter-particle diffusion. Morris et al. (83) had previously found the apparent solids diffusion coefficients to vary considerably from section to section within one gas fluidized bed. These results also contradicted the diffusion mechanism.

Marsheck and Gomezplata (75) showed that in a freely bubbling bed, particles flowed upwards in regions where bubbles rose and downwards elsewhere. They concluded that the bubble flow pattern determines the particle flow pattern. Bed height had little effect on the flow pattern in their 9.5 in. diameter bed of spent silica - alumina catalyst (56 microns), but gas velocity did.

The bubble induced particle displacement mechanism was observed (108) in gas fluidized beds of materials greater than 100 microns in mean diameter. Most of the experiments were performed with narrow size cuts (-30 +36 B.S.S., 460 micron mean diameter) of ballotini fluidized with air for ease of bubble generation. The essential features of this mechanism were also observed with copper, nickel shot and an

irregularly shaped mineral grit. The experiments were harder to perform with wide size distributions, but the same general results were obtained. The mechanism was thus believed to be of general application for materials greater than about 100 microns mean diameter.

Cohesive solids

Mechanism of solids motion For gas fluidized particles less than about 60 microns, the mechanism of solids mixing was intermediate between the mechanism described above and the diffusion mechanism of liquid fluidized beds (108). Beds of these particles exhibited the main features of the bubble mechanism just discussed above but also displayed bubble induced, eddy diffusion as well. For particles in the size range between 60 microns and 100 microns, the mechanism gradually changed from that occurring above 100 microns to that observed below 60 microns.

As single bubbles were passed through beds of particles smaller than 60 microns containing a bottom tracer layer, the approaching bubble disturbed the tracer interface in the same manner as that observed for the coarser materials. Also, a bubble would carry up a "spout" of bottom's material, shedding and replenishing the bubble's wake material. Wake material was finally dispersed at the bed surface. Bubble shape was the same as observed for the coarser materials.

Thus far, the mechansim was identical to the bubble interaction mechanism described for coarse material.

The shape of the spout or finger of underlying material was much distorted. The finger appeared to be broader than that of coarser material, and had points of irregular drift, suggestive of those expected from eddies in a true fluid. This additional turbulent particle motion was not observed unless a bubble passed. A clearer illustration was found in a two dimensional bed of 60 micron particles with a thin tracer layer, Figure 3.

The existence of the eddy diffusion mechanism for particles below about 60 microns and its absence for particles above about 100 microns were related to the particle packing and bed expansion (108). Beds greater than 100 microns were characterized by only slight expansion from the settled bed state at gas velocities near the minimum fluidization velocity. Further expansion of the bed was accounted for by the volume of bubbles within the bed. Beds of fine particles, however, had a larger bed voidage than beds of coarse particles in both the settled state and fluid state. Fine particles expanded further than coarse particles as the gas velocity was increased beyond the minimum fluidization velocity. Bed voidage increased up to 7% before bubbling commenced. Additional bed expansion was then due to bubble volume. Fine particle beds were usually not homogeneously expanded, but

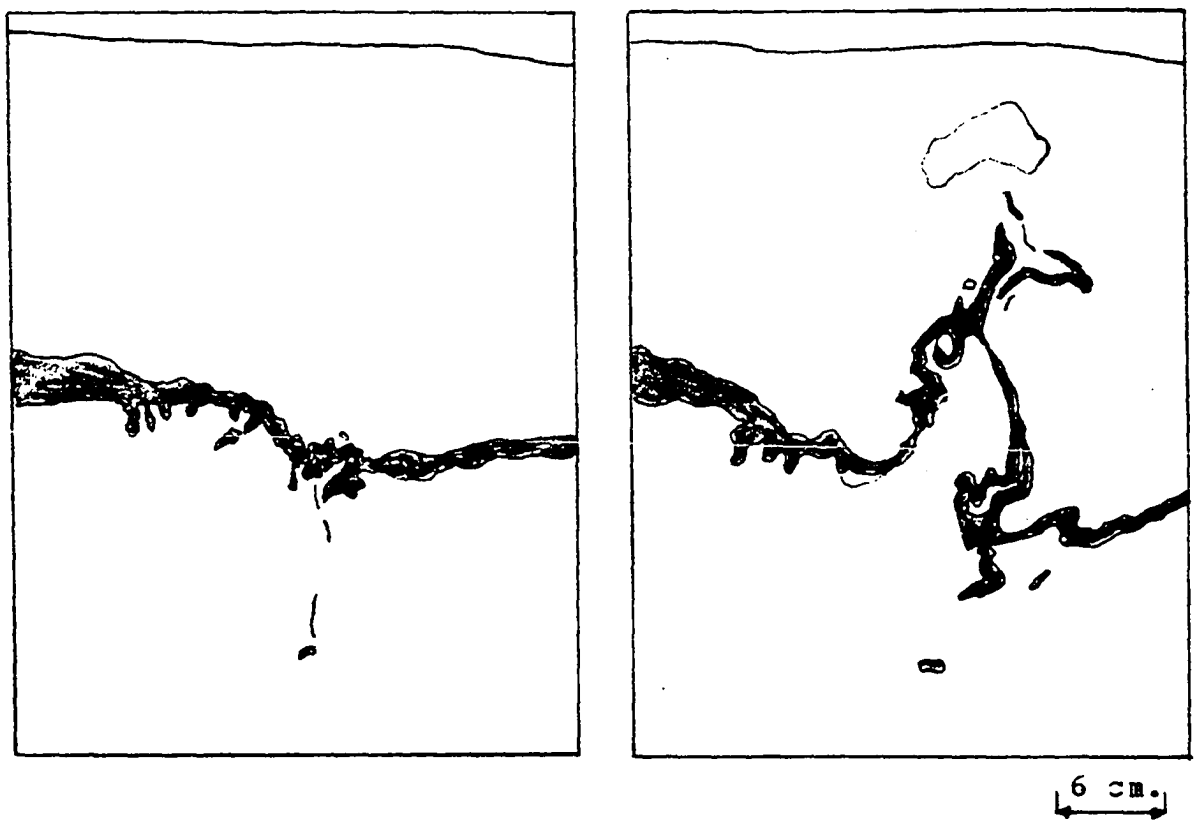

Figure 3. Effect of eddy diffusion (from 108)

a. Undisturbed bed of 60 micron diameter Synclyst cracking catalyst

b. Displacement of colored band after passage of a single bubble

were observed to have groups of particles with the settled bed porosity. This generated space sufficiently large for interparticle movement at the boundaries of these groups. The generation of these relatively dense, local, transient particle groups was a result of bed disturbances such as the passage of a bubble. The particle size for which measurably uniform, dense phase, bed expansion occurred varied with particle shape, density, and size distribution (33, 64).

Rowe et al. (108) have demonstrated the dense phase heterogeneity of fine particle beds by photographing, under conditions of strong back lighting, two dimensional beds of commercial Synclyst catalyst classified into narrow size cuts of 82, 60, and less than 53 micron mean diameters. A freely bubbling bed of the 82 micron fraction clearly had a uniform dense phase. When defluidized, the light transmission was slightly reduced, indicating closer particle packing. The 60 micron bed, also freely bubbling, showed dark and light dense phase regions corresponding to different particle density regions. As the gas was shut off, a dark interface moved up the bed. The smaller than 53 micron fraction showed similar, but more exaggerated, regions of dense packing. Since fluidization was not assisted, a lower, triangular shaped region of unfluidized material developed. In the truly fluidized zone, large numbers of small bubbles were seen within a dense phase of heterogeneous density containing clumps as dense as

the defluidized bed section. These "islands" retained identity for a significant life time and moved about in the dense phase region of lower density.

In summary, the mechanism of solids motion in fluidized beds of fine particles was distinguished by the temporary existence of void regions at the boundaries of moving dense clumps of particles. These void regions allowed interparticle mixing of the less dense phase and also allowed the clumps to move. This occurred in the regions where the shear rate would normally be high if the particles did not separate (108). The very existence of the clumps was probably related to the cohesiveness of the material caused by the surface forses existing between these fine particles. The freedom of movement of the clumps resulted in an eddy diffusion mechanism superimposed on the basic bubble mechanism.

A phenomenon associated with the passage of a bubble through a fluid bed of cohesive powder is the formation of particle slip surfaces.

Slip surfaces It had been noticed previously that fluidized flour beds developed a series of horizontal, plane voids (9, 84) which appeared to move down the bed in regular fashion as the solids moved downward in slip-stick flow. Similar voids had been reported previously for some other cohesive powders.

Rowe and Henwood (103) gave an explanation for the stability of "stationary 'lens shaped' voids". The top particles were described as being stationary while the bottom ones were in agitation.

Partridge et al. (93) showed X-ray photographs of particle slip surfaces found in two dimensional, bubbling fluidized beds. The surfaces appeared as a series of parallel arcs emitting from the bubble. They discussed particle flow around a bubble in free flowing material and related that flow to that of cohesive particles. They stated: "When it is remembered that the streamlines of the particle flow observed, as in the present technique, by a camera at rest would have the appearance of a dipole centered on the bubble center and symmetrical about its vertical axis, the slip surfaces are seen to correspond approximately to the local direction of the solids movement." The surfaces remained after the bubble had passed. The occurrence of slip surfaces was related to the natural angle of repose of the material. Slip surfaces were found for material with an angle of repose greater than about 36°.

Godard and Richardson (38) suggested that a bubble formed a track in its wake with a porosity greater than the bed average, at least for their 126 micron particles. For cohesive materials, instead of a uniform increase in porosity, that slip surfaces form seemed plausible to them.

Nitrogen fluidized flour beds exhibit pronounced particle slip surfaces (87). In a previous study (87), it was concluded that it was possible to manually time the movement of these voids over a distance of up to 3 in. for gas velocities up to about 0.22 ft./sec. (about 2.2 times the minimum fluidization velocity). The mean downward void velocity was reproducible for given operating conditions. The average rate of movement of voids down the column agreed well with the movement of coal char tracer clouds and with the average rate of individual rubber particle tracers. Further evidence also supported the conclusion that the average particle residence time at a wall heat transfer surface corresponds to the mean residence time of the slip surface voids traversing the area.

Observations of Particle Motion

Two dimensional bed

Singh et al. (112) briefly reviewed the displacement of solids caused by the passage of a bubble as modeled by the drift profile resulting from the motion of a sphere moving through an inviscid fluid. From this theoretical development, it was concluded that the net downward displacement of a horizontal line (in a two dimensional bed) of tracer particles after the passage of a single bubble as measured by the area swept out by the line would be equal to the area of the

bubble and its wake. This relationship was experimentally studied using a thin tracer layer of colored particles in a two dimensional bed of 292 micron ballotini fluidized at the minimum fluidization velocity. A single bubble of controlled volume was injected from a tube centrally located in the distributor plate. The tracer movement was filmed.

The sequence (Figure 4) of tracer particle movement during the passage of a typical single bubble through the initially horizontal layer was described (112).

> "As soon as the bubble was injected, there was a motion of particles to accommodate the bubble; at the tracer level this resulted in an upward movement mainly in the center, directly above the bubble (position 2). No further motion was observed until the bubble center was within one bubble diameter of the tracer layer. With subsequent rise of the bubble, the tracer particles near the axial position moved upward while those further away started to descend (position 3). This continued until the leading edge of the bubble reached the tracer layer (position 4); at this stage the center of the bubble was approximately at the initial tracer level, so that this maximum upward displacement was about half the bubble diameter.
>
> "As the bubble passed through the tracer layer, the particles moved rapidly downward, compensating for their rise on bubble injection. This downward motion continued a little further after the bubble had crossed the layer, which reached a lowest position (position 5) at about the time when the trailing edge of the bubble was at the initial level. There had been a net downward movement to replace particles carried across the tracer layer in the bubble wake."

As the bubble rose still further, a peak or finger began to form behind the bubble (position 6). Position 7 shows the final profile.

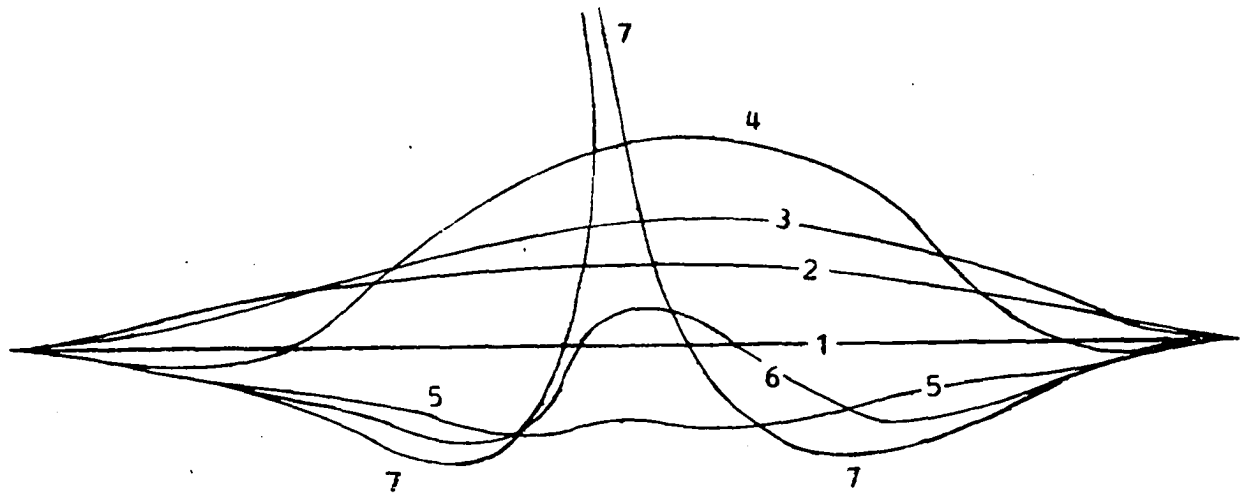

Figure 4. Sequence of tracer layer shape during bubble passage (from 112)

1. Initial tracer level
2. Bubble injected at base
3. Bubble center less than one bubble diameter below tracer
4. Top of bubble touching tracer
5. Bottom of bubble near initial tracer level
6. Bubble passed tracer layer
7. Final tracer profile

Measurements of the final displacement profiles and wake size were made which compared favorably with values obtained by Woollard and Potter (134).

It was observed (112) that particle motion due to the passage of a single bubble existed only in a narrow region extending about one bubble diameter from the bubble axis. An amount of material about equal to 20% of the bubble area was carried up in the bubble wake. A second mechanism, that of a drift in the dense phase, also contributed to the net downward motion. The drift resulted from replacement of material carried up in the wake. A total downward displaced area of about 25% of the bubble area was thus found to be displaced upwards across any horizontal plane in the bed. Singh et al. (112) cited literature that indicated three dimensional beds may behave similarly to two dimensional beds. For either bed geometry, a particle movement dependence on bubble size existed while the effect of particle size was uncertain.

Solids flow pattern at bed wall

Donsi et al. (23) used photography to systematically study the solid flow pattern at the wall of a cylindrical fluidized bed. Single bubbles of controlled size, location, and frequency were injected into beds of 170 to 350 micron alumina catalyst. The effects of two parameters, bubble size and distance of the bubble from the wall, were determined. The ratios of bubble diameter to column diameter, D_b/D_c, and

of bubble diameter to eccentricity of bubble location, $D_b/(D_b + 2b_o)$, were used to measure the relative size and position of bubbles rising along the column axis and of bubbles rising from eccentric locations. (Bubbles intersecting the wall had negative distances from the wall, b_o, estimated by completing the sphere.) Experimental results on particle displacement, particle velocities, and bubble velocities were reported.

The displacement of individual black tracer particles was observed to follow five general motion stages:

a. an initial upward motion as the bubble was injected into the bed,
b. a stationary period as the bubble approached the black particles,
c. further upward motion,
d. a downward movement followed by
e. a smaller upward displacement.

During the last three stages, particles were noticeably circumferentially displaced (moved laterally along the wall). Usually, particles orginally at the wall remained there throughout the cycle even when bubbles passed very close to the wall. Occasionally for relative bubble locations of $D_b/(D_b + 2b_o) < 1$ some particles were lost during filming, indicating some exchange normal to the wall occurred. Thus generally the particle path was an incomplete loop. Depending upon bubble size and the relative position of the bubble in

relation to the particle, one or more of these five stages could be absent.

Four types of particle vertical displacement profiles were observed (Figure 5).

For bubbles rising along the column axis, due to flow symmetry, only vertical motion was found, Figure 5a. The displacement was constant all around the bed circumference and occurred only during stages a and b discussed above. The overall vertical displacement was correlated by

$$S_o/D_b = 0.30(D_b/D_c)^3 \qquad [2]$$

The displacement was essentially zero for $D_b/D_c < 0.20$.

As bubble location approached the wall, the displacement profiles exhibited one (Figure 5b) or two (Figure 5c) minima and even became positive (indicating net upward motion) in the region of wall nearest to the bubble (Figure 5d). For moderate bubble eccentricity [$D_b/(D_b + 2b_o) \leq 0.6$], solids motion was like that of centered bubbles and motion stages a and d only were observed.

For locations closer to the wall, motion stages c and e became progressively more important. The overall displacement was not constant due to the asymmetric flow geometry. Values of the profile's geometric parameters were strongly dependent on bubble location ($D_b/D_b + 2b_o$) but were little

Figure 5. Over-all particle vertical displacements for various bubble locations (from 23)

a. Bubble at column center, $e = 0$

b. Eccentric bubble, $D_b/(D_b + 2b_o) \leq 0.7$

c. Eccentric bubble, $0.7 < D_b/(D_b + 2b_o) \leq 0.9$

d. Eccentric bubble, $D_b/(D_b + 2b_o) \geq 0.9$

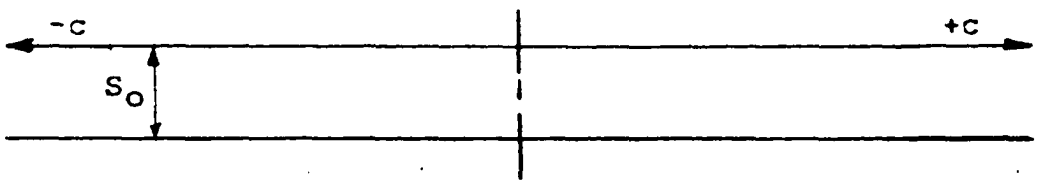

(a)

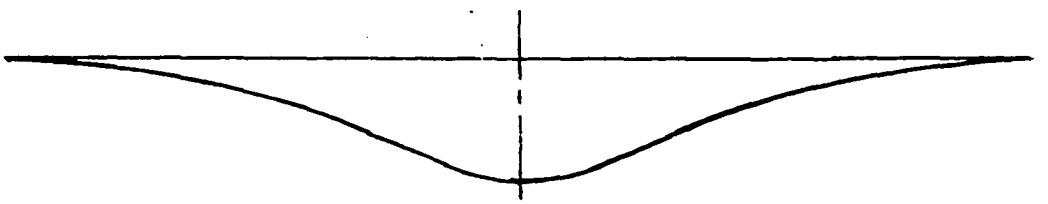

(b)

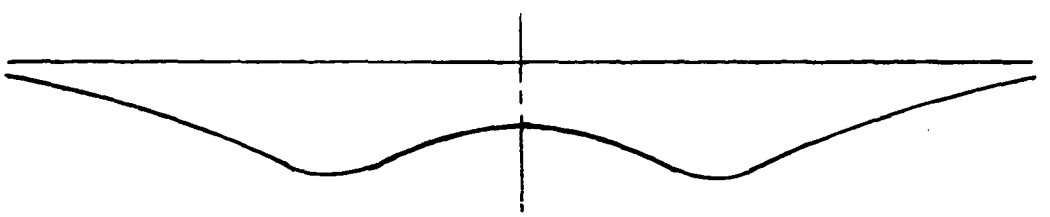

(c)

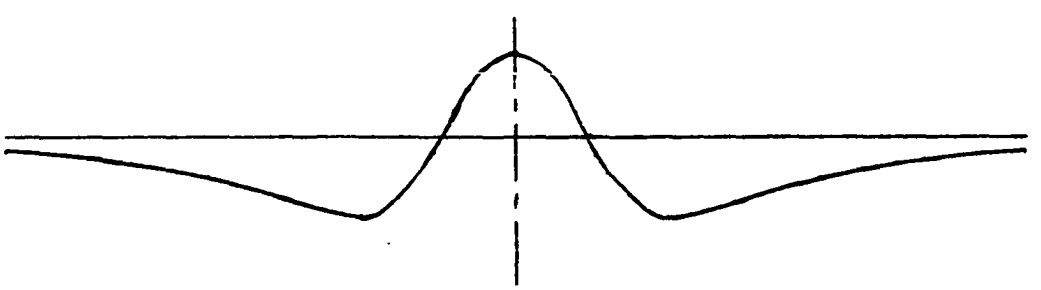

(d)

affected by size (D_b/D_c). Shape correlations were developed.

Circumferential particle displacements became significant only for bubble locations of $D_b/(D_b + 2b_o) > 0.7$, where the vertical profiles exhibited two minima and a maximum. The circumferential displacement was comparable to the largest vertical displacements observed. With a bubble tangent to the wall, $D_b/(D_b + 2b_o) = 1$, a discontinuity occurred such that either large or small circumferential displacements occurred. These large circumferential displacements may depend upon the bubble modifying the solids flow pattern. The large displacements were associated with the occurrence of some tracer particle disappearance or movement normal to the wall. As the bubble "intersected" the wall, $D_b/(D_b + 2b_o) > 1$, circumferential displacement again increased steadily. Occasionally, particle disappearances were encountered here too.

The maximum vertical and circumferential particle velocities were plotted as relative bubble velocities as a function of bubble location. The maximum vertical upward and circumferential velocities were less than one-fifth the bubble velocities. There was much scatter in the data, but the upward velocities appeared to this reader to approximately increase linearly as bubble location approached and intersected the wall over the range of $D_b/(D_b + 2b_o) = 0.4$ up to 1.48, the maximum location. The maximum downward particle

speed reached up to one-half the bubble speed. The increase in speed as the bubble approached the wall was nonlinear. Downward velocities were observed over a wider range of bubble locations, $D_b/(D_b + 2b_o) > 0.2$, than the upward velocities. The bubble size had little apparent effect on either the maximum vertical or circumferential particle velocities. Circumferential velocity was also nonlinear with respect to bubble location.

Comparison of the displacement profiles at the wall with those obtained from cited literature studies of interior bubble locations showed the expected good qualitative agreement. The presence of the wall produced an apparent quantitative distortion in the profiles however. The points of the largest downward displacements and of the points of zero displacement were found at $D_b/(D_b + 2b_o)$ values of 0.70 and 0.90, respectively. This was equivalent to 0.71 D_b and 0.55 D_b from the axis of the bubble. Literature values for these points in undisturbed bubbles were about 0.55 D_b and 0.3 D_b.

The bubble velocity data for axially located bubbles were correlated with the square root of bubble diameter. The correlation for the eccentrically located bubbles was based on a wave theory equation for bubble rise velocity in a fluid and provided a more complex dependence on bubble location.

Donsi et al. (23) concluded from the results of their experiments (discussed above) that solids renewal on a wall

heat transfer surface was sped up by the movement of particles normal to the wall as a bubble "intersected" the wall, causing a local circulation which was superimposed on the gross bed circulation. Thus a substantial increase in solids renewal would be obtained only where the bubble was directly attached to the wall. This condition was frequently observed for free bubbling beds at gas flow rates above twice the minimum fluidization velocity.

Effect of objects in bed

The effect of pairs of vertical rods (1/8 or 1/4 in. diameter) suspended at various spacings in a fluid bed of alumina (Group B) was investigated (102) without finding a condition where the bubbles appeared to be stabilized on the rods. A single bubble could be fairly stably attached to a rod if the bubble symmetrically encased the rod. The rod could be tilted as much as 15° with the bubble still remaining attached. A pair of rods had no measurable effect on the observed bubble pattern, though a high concentration of rods might have.

The bubble pattern was clearly altered by vibrating the vertical rods with a small amplitude transverse oscillation of about 2 Hz. A chain of bubbles formed on the rods and suddenly disappeared when oscillation ceased.

At low gas velocities, horizontal rods and banks of horizontal rods generated bubbles. At higher gas velocities,

the rods were usually completely covered by bubbles, with some being regularly shed. The effect in three dimensional beds was very similar to that previously observed in two dimensional beds.

The effects of a propeller stirrer and a disc turbine were also studied. These were immersed in the middle elevation region of the bed and were not located near the gas distributor. At slow speeds (1 Hz.), the propeller had little success in breaking up bubbles, but did break some up when operated at an intermediate speed (4 Hz). At still higher speeds (6 Hz), more and larger bubbles resulted. (It thus seems that if a cohesive powder tends to act like a Group B material when fluidized, then to minimize large bubble formation, the stirrer speed should not be increased much above that necessary for promoting the best fluidization quality.) The disc turbine behaved similarly to the propeller except at slow speeds where it resembled a flat, horizontal plate.

The movement of solids around a flat plate immersed in a two dimensional fluid bed of FCC catalyst (74 to 149 microns) was complex (72). Some particles were not transported by the gas in the region above the plate and settled on the plate. This dead zone was composed of two regions. Directly above the plate was a parabolically shaped "fixed dead zone" of packed material, the particles of which did not move for long times. The height of this zone was strongly dependent on the

fluidizing gas velocity and moderately dependent on the elevation of the plate in the bed and the type of gas distributor. Height of the fixed dead zone decreased linearly with increasing gas velocity until about 2 to 3 times the minimum fluidization velocity. At this point, the height was essentially constant for up to 5.4 times the minimum velocity, the maximum velocity tested. A "quasi - stable dead zone" existed above the fixed dead zone. Material in this zone was often replenished in intervals of a few seconds or more by surrounding disturbances. The freely fluidized bed material was found only far above the immersed plate.

The effects of baffles and other types of bubble redistributors were briefly reported (102).

It follows that if bubbles were the main mechanism for particle movement that altered bubble patterns caused by objects in the bed should result in altered particle motion patterns. This has been demonstrated also by measurements of local heat transfer coefficients between the bed and objects immersed in it (6, 36, 56, 66, 115).

Small column wall effect

Qualitative evidence for an explanation of the "wall effect" observed in small diameter beds has been recently reported by Rowe and Everett (102). A 30 cm. by 20 cm. by 70 cm. deep rectangular bed of alumina was fluidized at minimum fluidization velocity with a controlled bubble stream. A

flat plate, 12 cm. wide, was vertically inserted into the bed and moved toward the bubble stream. The plate edge and the bubbling bed were viewed by X-ray cine photography. As the plate approached the bubbles, the stream was displaced away from the plate. A distance of approximately one bubble diameter from the bubble axis to the plate surface was constantly maintained by 90% of the bubbles. About 10% of the bubbles attached themselves to the plate and then traveled up the plate as half bubbles.

A similar bubble deflection by the column wall of a small diameter column could concentrate the bubbles in the column center and promote the particle circulation pattern observed in small beds. For large diameter columns, the bubbles would still be deflected, but the concentration would not be greatly changed. The effect on particle motion or circulation would thus be small for a large diameter column.

A solids circulation like that observed in small columns has been induced in large diameter, shallow beds by using a nonuniform distribution of gas flow (77). Solids upflow occurred in the regions of higher gas flow where bubbles tended to be concentrated. Strangely, circulation was strongest when the solids traveled up at the walls and down the bed middle in a rectangular bed having a 0.41 depth to width ratio. Lateral mixing of shallow beds was improved by this gas flow scheme.

Tapered and nontapered columns

Rowe and Sutherland (109) compared trace solids mixing in gas fluidized beds of dense materials (Group D). Cylindrical, annular, and tapered deep beds were compared. Mixing curves showing tracer concentration as a function of bed height and mixing time at several gas velocities from 0.83 to 1.5 times the minimum fluidization velocity were presented for each column. Mixing proceeded from the bed top downward. A distinct tracer "front" was observed to move down the column. The front moved most rapidly down the cylindrical column, and slowest down the tapered column. An earlier study (113) had concluded that the vertical mixing rates of dense materials was reduced by tapering the column for gas flows slower than 1.0 times the minimum fluidization velocity and for beds over 2 ft. in height. A nontapered insert had no effect in that study, however.

The absence of bubbling in the lower bed sections for even the cylindrical beds (109) of these dense materials contributed to the rather slow mixing times compared with other materials. The mixing mechanism definitely had the characteristics described (108) for gas fluidized material greater than 100 microns mean diameter.

Mixing in a continuously fed, tapered column fluidized at the incipient fluidization velocity has also been studied

(81). Radial mixing was observed to be good for small diameter beds, but a sharper radial concentration profile was obtained with larger beds. Concentration profiles of tracer passing through the bed approached plug flow. Also, the larger the particle size and the faster the solids feed rate, the less mixing occurred for the range of conditions studied.

Solids mixing of dense particles (5 g./cm^3.) was also studied (70) in tapered and nontapered rectangular, deep beds (H/D = 8,16). It was concluded that axial mixing was slowed in a tapered bed operating close to minimum fluidization conditions principally by the reduction of mixing occurring in the lower bed section. A slugging, nontapered bed has a reduced rate of uniform particle dispersion. Tapering a formerly slugging bed increased the dispersion rate mainly by increasing the mixing rate at the bed top section.

Models of Particle Motion

A critical survey of the models proposed for the residence time or time of transport of solids through gas fluidized beds has been recently written by Verloop et al. (125). About 17 models were discussed and classified into 5 groups based on their mathematical description. The solids transport was described by

a. combinations of perfect mixing, short - circuiting, piston flow and similar quantities,

b. a number of perfect mixers,

c. diffusivity or a mixing coefficient,

d. circulation patterns, or

e. the existence of different bed layers having different flow characteristics.

Most of the models and data discussed applied to systems with continuously fed solids.

A tracer signal was often used to check these models with the results expressed in terms of an F diagram, C diagram, or I diagram. The F - t curve represents the overall probability, F, for a particle to have a residence time smaller than t. The C - t curve represents the probability, C, for a particle to have a residence time between t and t + dt. The I - t curve represents the probability, I, that a particle having stayed in the system during a period, t, will leave the system in the next period, dt. These functions are not independent, but are related:

$$C = dF/dt \quad \text{and} \quad I = C/(1 - F) \qquad [3]$$

The construction details of making the F diagram from experimental fluidized bed data have been demonstrated (83, 116).

Verloop et al. (125) concluded that each model as initially presented in the literature was only applicable in a limited region of fluidization conditions and that the influ-

ence of the variables on the solids transport process had not yet been adequately described. The major model parameters appeared to be the gas velocity, particle properties, bed geometry, and perhaps the solids feed rate. (As has been reported in other parts of this review, the importance of particle density and size distribution have been recently discussed.)

Verloop et al. (125) offered these concluding opinions on residence time models:

a. Stagnation in solids flow occurred generally in the beds and a model with parallel streams seemed to provide the best description of a fluidized bed.

b. The models often did not include the heterogeneity of the system regarding particle movement. As a result, a single parameter model could only hold if the influence of the bed surface and distributor plate regions could be neglected.

c. The relevance of the parameters, such as the number of mixing stages, circulation rate, or mixing coefficient, of many models was not clear.

d. A model should be evaluated on the basis of the actual system characteristics.

Models for solids mixing have also been reviewed by Gabor (30). He reviewed a random walk model and found that better agreement with experimental data for fluidized beds

containing fixed packings was obtained with this model than with either a diffusion model or a model in which individual particles passed through openings in the particle suspension.

An equation, derived from random walk theory, was presented which related the diffusion coefficient for solids mixing with the average fluidized particle velocity:

$$\bar{v} = D/(0.0558D_p) \qquad [4]$$

where

D_p = fixed packing diameter, ft.

D = diffusion coefficient, sq. ft./sec.

$\bar{v}$ = average particle velocity, ft./sec.

Gabor's motion pictures of large, dense particles fluidized in the voids of large packings showed that the individual particle motions were not random but were in streams of particles traveling vertically due to displacements caused by bubbles. Otherwise, the particles were stagnant. His measurements showed good agreement with the above particle velocity - diffusion coefficient relation.

Verloop et al. (125) discussed the interrelation of some models. A relation between the circulation model and the diffusion model was reported:

$$M/H^2 = (W/\pi^2)(Q_1^{-1} + Q_2^{-1}) \qquad [5]$$

where

Q = weights of layers 1 and 2

W = internal circulation rate

H = bed height

M = mixing coefficient.

SOLIDS MIXING

General Considerations

A general review of the literature pertaining to solids mixing was made by Weidenbaum (127) in 1958. Fan et al. (25) surveyed the literature published from 1958 to 1969. They later reported (26) on the advances published through 1970. Advances, trends, and general problems in solids mixing have been reviewed in several other articles (40, 88, 120, 121). An introductory discussion of solids mixing was written by Clump (19).

Mixer performance depends upon the particle properties of the components, equipment design, and operating conditions. The following are factors which may influence mixing results (19):

Powder characteristics

1. Shape
2. Surface
3. Size distribution
4. Bulk and particle densities
5. Moisture content
6. Friability
7. Flowability
8. Lubricity

Equipment

1. Geometry and size
2. Agitator design
3. Size and location of access openings
4. Materials of construction and surface finishes
5. Design of loading and emptying apparatus

Operating conditions

1. Proportions of components to be mixed
2. Fraction of mixer volume occupied
3. Method, order, and rate of feeding the components
4. Agitation level
5. Time of operation

In evaluating mixer performance, the components to be blended are charged to the apparatus, the mixer is run for a fixed time period, and the resulting mixture is emptied. To follow the course of mixing, representative samples of the mixture are collected as a function of mixing time. The sample size is referred to as the "scale of scrutiny". The sample compositions of the property of interest are determined and an assessment of the final mixture quality is made from samples of the mixture. The effect of different mixing times may be determined by repeating the experiment using different

running times. The occurrence of demixing of a mixture is known as segregation.

The mixing process may be viewed as the result of three basic mechanisms (25, 40, 65, 120, 130): diffusion, convection, and shear. In diffusive mixing, individual particles move short distances relative to one another, generally being scattered by collisions over a freshly formed surface. In convective mixing, clumps of particles are moved from one location in the particle mass to another. Shear mixing involves cutting of clumps by changes in the linear velocity direction due to the establishment of slip planes within the mass. Actual mixers involve more than one major mechanism but usually one or two are dominate. No method for predicting the particle motion is available (19).

Mathematical models only of diffusive mixing have been studied (25) in detail, and then mainly as applied to horizontal, revolving cylinders.

In general, the mixing rate varies approximately exponentially with time until completion is near (122). Eleven rate equations were tabulated by Fan et al. (25, 26). Most assumed mixing was a first or second order process.

$$-dS_g/dt = k(S_g)^r \qquad [6]$$

where

k = rate constant

r = order of process

S_g = degree of segregation

Four applied to diffusive mixing. Mixing characteristics of powders and equipment must be experimentally determined.

The most useful mixers for cohesive powders are those that have predominantly shearing action (71, 122). Purely tumbling or diffusive mixers were deemed the least satisfactory. Williams (130) said diffusive and shear mixing will occur only if the particles have the same properties, especially size, or else these processes lead to segregation. Mechanisms of convection and "percolation" in the mixing of cohesionless powders were discussed (12) and shown to account for a period of well mixed components followed by segregation.

The involvement of the powder properties in the mixing process is more readily indicated by the classifaction of equipment and mixtures as segregating or desegregating (130). Segregating mixtures are generally characterized as composed of free flowing materials having a significant difference in particle size or density. Nonsegregating mixtures, on the other hand, have components which are generally nonfree flowing or which have similar particle properties (120, 130).

A segregating mixture requires a desegregating mixer for attaining good mixing, while any type of mixer may be used for a nonsegregating mixture (130). Of course, other criter-

ia such as tendency to aggregate, friability, or operational ease must be considered in mixer selection (120, 130).

Mixing Indices

Mixing is a statistical process. Statistical concepts are an inherent component of the vocabulary and theory of mixing. The statistics of mixing have been discussed and reviewed frequently (42, 43, 61, 62, 122, 123).

The problem of relating the average composition and standard deviation of the blended product to that of the input batches comprising the blend has been reviewed (8) and extended to include the case of two simultaneous product blend specifications.

Mixing indices are useful for describing the quality or degree of homogeneity of a mixture and as a quantitative measure for comparison of mixer performance.

Over 30 different mixing indices have been summarized (25, 71) and discussed (40, 122). Most apply to binary mixtures; a few are generalized. That numerous indices have been proposed and a large number actually used to report mixing results has negated the mixing indices' comparative function while indicating dissatisfaction with the more common measures.

A simple, frequently used measure of mixture homogeneity is the variance (or its square root, the standard deviation)

about the average of the samples.

$$S^2 = \sum (p_i - \bar{p})^2/(n - 1) \qquad [7]$$

The familiar additive property of the variance enables, for example, the actual mixture variance to be readily calculated from the measured total variance and a known measuring precision (3, 43). The variance measures the industrially significant fluctuation between samples. For this reason and its simplicity, it has been suggested (71) as a universal mixing index for mixer comparison in spite of its considerable disadvantages.

First, the variance depends on sample size (61, 120, 122, 130) and therefore it is said to incorporate uncertainty in comparing mixtures with it since the degree of dependence on sample size may vary between mixtures.

Second, the variance depends on the mean value. Changes in mean value affect the standard deviation (120, 130) and make comparison of mixtures with different mean values difficult to interpret. Williams (130) illustrated this point by comparing two mixtures, one having a mean value of 50% of one component and a standard deviation of 2%, while the other mixture had a mean of 5%, again with a 2% standard deviation. The quality of mixing, however, is not the same. The ratio of standard deviation to mean, known as the coefficient of

variation, is a better index in this regards. Values of the coefficient of variation are 4% and 40% for the respective mixtures, showing the first to be the better mixture.

Third, in general, sample compositions are not normally distributed (3, 130, 131). Nonnormality can affect the prediction of the proportion of samples that will be outside of specified composition limits (130).

The coefficient of variation, the standard deviation divided by the mean value, is commonly used (111) as a mixing index. While having the advantage of allowing comparison of mixture quality of mixtures of differing mean values, the coefficient of variation has been reported as not being precise and to require too many samples (74) as well as having the other disadvantages of the variance (122).

Other frequently used indices relate the mixture condition to that of an ideal mixture or even to the unmixed components. An ideal mixture is a mixture which exists in a maximum state of disorder as indicated by a statistically random variation in composition of representative samples (19, 40).

For a binary mixture of monosized particles of the same density, the ideal variance of composition expressed on a number or volume (130) basis is calculated from the binomial distribution (25).

$$\sigma_R^2 = P(1 - P)/N_T \qquad [8]$$

An expression for the variance of a completely random binary mixture has been derived (61) for the case where each component has a different particle density and size distribution.

$$\sigma_R^2 = \frac{p_A(1 - p_A)}{W}\left[(1 - p_A)\left(\sum f_a w_a\right)_{p_A} + p_A\left(\sum f_a w_a\right)_{p_B}\right]\left(\bar{\rho}^4/\rho_A^2\ \rho_B^2\right) \qquad [9]$$

$$\bar{\rho} = \frac{\rho_A \rho_B}{p_A \rho_B + p_B \rho_A}$$

where

σ_R^2 = variance of random mixture of A and B

ρ_A, ρ_B = particle densities of A, B

f_a = weight fraction of particles in size range "a"

w_a = mean particle weight of size range "a"

p_A = weight proportion of component A in mixture

p_B = weight proportion of component B in mixture

W = mass of sample taken from mixture

The particle density and size distribution by weight are thus

required. Examples of the use of this expression have been published (25, 96). This expression has been generalized for multicomponent mixtures (25, 122).

One mixing index that greatly eliminates the influence of material properties and enables different mixtures to be compared is (122)

$$M = (\sigma_o^2 - S^2)/(\sigma_o^2 - \sigma_R^2) \qquad [10]$$

where σ_o^2 is the variance of the initially completely segregated components (25, 61)

$$\sigma_o^2 = P(1 - P) = P_A P_B \qquad [11]$$

This index is a measure of how far the mixing has proceeded from the original unmixed state (M=0) towards the ideal mixture (M=1) (130). Since σ_R^2 is usually small compared to σ_o^2, this index is essentially independent of sample size (131). The major disadvantage of this index is that it converges too rapidly to 1 to be as useful in practice as desired (120, 122).

A modification (3, 122) of the above index which maintains its advantages and approaches the upper limit more gradually is

$$M = \frac{\log \sigma_o^2 - \log S^2}{\log \sigma_o^2 - \log \sigma_R^2} \qquad [12]$$

This measure was reported (3) to be largely insensitive to mixture composition, but to be more dependent on sample size (131) since $\log \sigma_R^2$ is not insignificant.

It has been suggested (71) that indices using an ideal mixture variance are not necessary since it is very unlikely a random mixture will ever be attained in industrial practice.

An index which avoids the use of the ideal random variance was first proposed (25, 45) and later derived (131) for the variance of samples drawn from a nonrandom mixture.

$$M = 1 - \sigma^2/\sigma_o^2 \qquad [13]$$

This index is independent of sample size if the probability of finding a component is constant for any sample (131). This index unfortunately also approaches 1 rapidly. A similar index was proposed by Michaels and Puzinauskas (78).

$$M = 1 - \sigma = 1 - \sigma_v/\sigma_o \qquad [14]$$

$$\sigma_v = \left[\frac{\sum (C_i - C_o)^2}{nC_o^2}\right]^{1/2}$$

$$\sigma_o = \left[\frac{100 - C_o}{C_o}\right]^{1/2}$$

where

C_i, C_o = fluctuating and required percentage concentrations of component in mixture

n = number of samples

A recent approach to a mixing index has been the application of the coefficient of correlation to mixtures (43, 61, 62). Several common indices were shown to be special cases of this approach. Nonrandom mixtures may be better analyzed as more information is obtained than with simple indices. Specifically, the effect of location of samples in the mixture is incorporated. Also models may be more readily evaluated (43).

Having briefly reviewed the common mixing indices and their advantages and disadvantages, it is apparent that no one index has yet been devised which is satisfactory for completely describing mixture homogeneity. The following has been suggested (130) as one means of describing the mixing state of a component in a mixture:

1. sample size
2. limits of the concentration of component present in samples

3. frequency with which samples must lie within these limits.

Fluidized Bed Solids Mixing

General results

That the gas velocity must be at least 1.2 to 1.3 times the minimum fluidization velocity to obtain any mixing has been reported (83, 109) for beds of particles greater than 100 microns with a density above 1.4 g./cm^3 (Group B). Above 1.5 times the minimum fluidization velocity, mixing was quite fast (83), even in a tapered column (109). The mixing rate increased with increasing gas velocity.

Fomichev and Gvozdev (28) have studied the fluidized bed mixing of mixtures consisting of 90% common salt (2.18 g./cm^3.) and 10% thiodiphenylamine (1.11 g./cm^3.) in columns of aspect ratios (H/D) less than 1. The sieving data reported for these materials indicated mean particle diameters of 680 and 1200 microns respectively with a geometric standard deviation of 3.4 microns for salt. The thiodiphenylamine was a narrow sieve cut, 83% being between 850 and 1600 microns.

For the batch system, the best mixture quality (as measured by the mixing index of Michaels and Puzinauskas (78)) [14] was obtained at a gas velocity 1.5 times the minimum fluidization velocity with the samples being removed midway between the bed top and bottom. Under these conditions, the

best mixture quality was obtained for H/D ratios greater than 0.25. The mixing index was not sensitive enough to indicate any further changes as the bed depth was increased to H/D = 0.85, the highest value reported. Below H/D = 0.25, poor mixing quality was due to the presence of channeling in these thin beds with the gas distributor system used.

A continuously fed solids bed did not function properly with solids removal from the bed middle due to the accumulation of coarse particles at the bed bottom. Removing solids from the bottom corrected that problem.

Leva (68) discussed size segregation in fluidized beds. He concluded that the usual fluidized bed may be unsuitable for solids blending due to economic considerations and also to insufficient product homogeneity.

A stirred, cylindrical fluidized bed was significantly better than a nonstirred bed since a lower gas velocity could be used and a more homogeneous blend was obtained. For the particular stirrer geometry and materials employed in the study, a conical bed minimized dead zones. A curve of mixture homogeneity as a function of time (a mixing curve) for blending 1% salt in sand with a stirred bed showed the approach to steady state composition of samples withdrawn from the bed top and bottom. Operating conditions were not reported, but steady state seemed to be achieved within 2 min. A simple, stirred conical bed was found to be unsatisfactory

for blending cohesive materials such as cements, various fine grained dyes, and soda ash. Nonaerated material was usually found in the area of the air inlet and the slope of the bed wall was not steep enough to prevent material from adhering to the wall.

Kozulin and Kulyamin (59) developed a fluidized bed solids mixing apparatus for mixing cohesive powders. A simple, two bladed stirrer located just above the gas distributor plate in a cylindrical column was successful in promoting fluidization. The stirring prevented the formation of channels which were usually encountered in attempts to fluidize cohesive powders. The fluidization quality was improved by stirring and a stable, evenly fluidized bed resulted for a number of cohesive powders.

Air fluidized columns of 3, 20, and 30 cm. diameter were used. The column had a gas distributor grid covered with "belting" cloth. The stirrer design which was most successful in promoting fluidization utilized a blade diameter equal to 95% of the column diameter. The blade height was equal to 10% of the diameter of the circle described by the rotating blade tips. Stirrer speeds of 20 to 60 rpm were necessary and sufficient to promote fluidization. For speeds greater than 60 rpm, a well-developed vortex was formed in the bed surface.

The materials and their reported properties are listed in Table 1.

Table 1. Materials used by Kozulin and Kulyamin (59)

Powder	Density, g/cm³ bulk	Density, g/cm³ particle	Size, microns range	Size, microns average
Lead oxide	2.32	9.4	0 - 14	12
Barium sulfate	1.84	4.2	0 - 50	20
Coal	0.866	1.72	200 -250	--
Titanium dioxide	0.636	3.84	0 - 30	15
Zinc oxide	0.66	5.6	0 - 20	15
Magnesium oxide	0.26	3.5	0 - 7	5

Two stages of experiments were performed, the first to measure the stirrer power requirements under the full range of operating conditions, and the second to investigate the time required for obtaining the most homogeneous mixture of two materials when operating at a gas velocity three times the minimum fluidization velocity.

The power consumption, or stirrer torque, was observed to decrease linearly as the gas velocity was increased from very small values up to the minimum fluidization velocity. This gas velocity region defines the packed bed state of the system. For higher gas velocities, the bed was fluidized and the power remained at a constant value dependent upon the stirrer speed and diameter.

It was discovered that the intersection of the two linear portions of the power curve was at the point of incipient fluidization.

The power consumption was correlated by

$$K_p = 12.8/Re_u \qquad [15]$$

where

$$K_p = P/(\rho N^3 d_m^5)$$

$$Re_u = (\rho_g N d_m^2)/\mu_g$$

The critical fluidization velocity was found to be a function of stirrer speed and was correlated by

$$u_c = c(N)^{-1/3} \qquad [16]$$

When particle properties were included in the correlation, the data fit the following equation well:

$$Re_{cr}Fr^{1/6} = \frac{Ar}{17.77 + 4.56Ar^{0.5}} \qquad [17]$$

$$Re_{cr} = \frac{u_c d \gamma_g}{\mu_g g}$$

$$Fr = N^2 D_c/g$$

$$Ar = d^3(\gamma - \gamma_g)\gamma_g/\mu_g^2 g$$

where

d = particle diameter

All mixing experiments were performed with H/D = 1.5 and at an optimal gas velocity of three times the critical gas velocity. Materials were blended in weight ratios of 1:1 and 1:2. Samples were withdrawn by flow from the upper and lower bed sections within a time span of 5 sec. of each other.

The best state of homogeneity appeared to be reached in 1 to 5 min. and this state did not deteriorate during a time interval of 1 to 5 min. Segregation as measured by mixture homogeneity occurred for the mixtures reported, starting after 5 to 10 min. Magnesium oxide in titanium oxide was less segregated than a mixture of zinc oxide in titanium oxide. A mixture of lead oxide in barium sulfate was more segregated than the other two mixtures. The best mixture homogeneity for each mixture was reported as "relative percentages" not exceeding ±2% from the expected mixture composition. This was claimed to be a very high degree of homogeneity.

Segregation in fluidized beds

Segregation effects have been observed in fluidized beds of free flowing materials (20, 82, 104, 105). For example, with some iron ores, segregation was prevented by operating the fluid bed near the minimum gas velocity and only fluidizing for a time too short for significant segregation to occur (82). Equal weights of uranium trioxide (6.9 g./cm³.) and alumina (3.5 g./cm³.) having the same size were observed (20) to segregate even at minimum fluidization conditions.

Goossens et al. (39) have proposed a criterion for predicting the occurrence of segregation in fluidized beds of binary mixtures.

$$L = 1 + \frac{(1 - x)R(D - 1)^2}{(x + (1 - x)RD)^2} \qquad [18]$$

where

L = segregation index

x = concentration of heavy component

R = ρ_h/ρ_l, density ratio of heavy to light particles

D = d_h/d_l, diameter ratio of heavy to light particles

For nonsegregating powders, L is equal to 1. As segregation becomes more severe, L increases from 1.

In mixing cohesive powders, the cohesive forces may be strong enough to resist segregation (130). Segregation is also not expected when a very fine powder (less than 10 microns) is mixed with large particles due to coating of the large particles by the small ones.

Rowe et al. (104, 105) made a systematic study of segregation in fluidized beds. Six different combinations of pairs of spherical materials differing in particle size, density, and minimum fluidization velocity were fluidized with air. Narrow sieve cuts, ranging from 82 to 642 microns, of four free flowing materials (steel shot, copper shot, Ballotini, and polystyrene beads) comprising a wide particle density range, 1.05 to 8.86 g./cm^3., were employed. Two materials were placed in the apparatus in a segregated state, fluidized, and the particle behavior observed and photographed.

Segregation was readily achieved when particles of different densities were fluidized. The denser material formed a relatively pure bottom layer, but it was not possible to produce a pure upper layer. Some dense material persisted in staying in the top layer in an approximately uniform distribution. The concentration of dense material in the top layer increased with increasing gas velocity. With large enough gas velocities, it was possible to mix materials of widely differing densities.

Materials of the same density, but of different size ranges were also observed to segregate, but the degree of segregation was small. Particles varying in size by an order of magnitude were mixed fairly uniformly even at moderate velocities. The larger particles tended to concentrate near the bottom.

The relatively greater importance of density as compared to size differences in promoting segregation in gas fluidized beds is contrary to that usually observed in most mechanical mixers.

The steady state bed concentration was measured (105) as a function of height. In all cases, the mid-vertical region of the bed rapidly reached a uniform composition which was a function of gas velocity. Segregation increased with the components density and size ratios as $(\rho_h/\rho_l)^{2.5}$ and as $(d_B/d_S)^{0.2}$ and decreased in a complex manner with increasing gas velocity.

$$y = f(u - u_{cl})(\rho_h/\rho_l)^{-2.5}(d_B/d_S)^{-0.2} \qquad [19]$$

where

y = number fraction of lower particles in upper half of bed

u_{cl} = minimum fluidization velocity of light material

At low gas velocities, $f(u - u_{cl})$ was an approximately linear term. Two practical, real materials were fluidized to verify these results.

Segregation was observed to involve four distinct particle motion mechanisms (104). The most important mechanism was the action of rising bubbles lifting particles in their wakes. This mechanism, under certain circumstances may promote segregation, but was more often observed to cause mixing which counteracted segregation. This was the only mechanism by which particles that were both less dense and smaller than the other material could get to the bed top.

A second mechanism involved particles which were both of large density and large diameter. These particles were observed to descend through the bed by falling through bubbles. For particles which were only a little more massive than the rest, the upward gas velocity would not be sufficient to support them. This was almost the only method observed for large particles to descend.

Smaller yet denser particles moved by a third mechanism. They may descend by inter-particle percolation but only under the special conditions occurring in the track of recent bubbles. Inter-particle percolation was never observed to occur throughout the bulk of the bed. These particles have a lower minimum fluidization velocity than the rest. In the

bulk of the bed, they would be descending against an upward gas stream of greater velocity and lifting force and, hence, could not descend.

The fourth mechanism was observed to preserve but never to cause segregation. A quasi hydrostatic effect resulted in particles appearing to "float" on a fluid bed of denser particles. Less dense particles were never seen sinking, but also never were seen to rise through the dense phase like a submerged tennis ball rising through water.

PART 2. MATERIALS AND APPARATUS

MATERIALS

Fluidization Materials

Gas

The fluidizing gas was regular grade compressed nitrogen (Chemistry Stores, Iowa State University, Ames, Iowa). The nitrogen was used as received (dry) or the humidity was adjusted to 17% or 28% relative humidity by bubbling the gas through water.

Powders

Powders for the fluidization experiments were sifted through a 1000 micron screen to remove large lumps and pieces of paper packaging material. The storage of the materials has been previously discussed (87).

Flour The flour was a straight grade, Michigan soft white winter wheat flour (King Milling Company, Lowell, Michigan). This flour was unenriched and unbleached and labeled "King Kookie Flour". The following three batches were obtained:

a. Flour I was the batch used previously by Brekken (9), Nazemi (84), and Nielsen (87).
b. Flour II was received in September, 1970, and used for one mixing run, Set 14.
c. Flour III was received in June, 1971 (lot: May

241971) and used in the other flour mixing and residence time experiments. The as received moisture level was about 16%.

Potato starch One set of mixing experiments was performed using Crown Potato Starch (Penick and Ford Limited, Cedar Rapids, Iowa). It was the same batch as used in a starch slurry study (15). This was a different batch than that used by Nazemi in his heat transfer study (85), however.

Flow conditioner The flow conditioner used was Cab-O-Sil (Cabot Corporation, Boston, Massachusetts). This was a fumed silica material having an ultimate particle size of 0.015 microns (29) and a very low bulk density, 0.037 g./ml. The material itself was a white powder which formed large flocs.

Microthene Microthene MN 710 (U.S. Industrial Chemical Corporation, Tuscola, Illinois) is a low density polyethylene powder. Although it felt "sticky" to one's touch, this powder was fairly free flowing and was easily fluidized without mechanical assistance such as stirring. In the present work, Microthene was used for comparison of its fluidization characteristics with those of flour and potato starch, two cohesive powders that fluidized only when assisted by stirring or flow conditioning.

Tracer salts The salts selected for use as tracer materials to mix with flour were copper II sulfate pentahydrate, zinc acetate dihydrate, and nickel acetate tetrahydrate ("Baker Analyzed" reagents, G. T. Baker Chemical Company, Phillipsburg, New Jersey). These salts were primarily selected for their low density, moisture stability, and acceptibility for the two analytical processes employed (87) to measure sample tracer concentration. The copper sulfate was also used in some previous, exploratory experiments (9, 11) and was chosen for use in the present study to afford a direct comparison with those experiments.

The crystals were ground with 1% by weight Cab-O-Sil in a 4 in. diameter jar mill to pass a 74 micron screen. These flow conditioned, ground salts were designated as copper tracer, zinc tracer, and nickel tracer, respectively.

Reagents

All reagents were "Baker Analyzed" reagents (J. T. Baker Chemical Company, Phillipsburg, New Jersey).

The distilled water was condensed boiler steam which was redistilled with a Barnsted Water Still (Barnsted Still and Sterilizer Company, Boston, Massachusetts) with a glass receiving vessel. This water was used directly through most of the work, but when the addition of ammines in the boiler

water treatment was started, it was necessary to deionize the water with a Standard Barnsted hose type cartridge D8901 (Barnsted Division, Sybron Corporation, Boston, Massachusetts).

Powder Properties

The powder properties are summarized in Tables 2 and 3.

General properties

The particle densities (Table 2) of the flours and potato starch were not significantly different. The bulk densities of the flours in settled beds which had been fluidized briefly were very close. That of potato starch, however, was significantly more dense. Adding a flow conditioner reduced the flour bed bulk density.

The static angle of repose is the angle between the side and base of the cone formed by lifting a cylindrical mold, containing the loosely poured powder, from a circular pedestal. The static angle of repose data have been previously discussed (87). Briefly, the flour did not flow to form a cone as required by the method, but instead, chunks of flour broke off the cylinder. This resulted in irregular, haystack shaped piles of flour remaining on the pedestal from which the listed values were calculated. For at least Flours II and III, 90° may be a better estimate than the values determined from the very irregular cones. The potato starch

Table 2. Powder density and angle of repose

Material	Particle density g./cm³	Bulk density[1] g./cm³	Angle of repose[2] degree	%M at angle of repose measurement
Flour I	1.46[3]	0.55	63	8.8
		0.52[4]	66	11.9
Flour II	1.48	0.50	67	9.4
			90	10.5
Flour III	1.46	0.50	69	15.
			(90)	15.
Potato starch	1.47[3]	0.72	90[3]	16.
Cab-O-Sil treated flours:				
Flour III, 0.5%	1.46[5]	0.47	--	---
Flour I, 1%	1.46[5]	0.53[4]	58[3]	12.
Flour III, 1%	1.46[5]	0.43	--	---
Copper tracer	2.28[6]	0.87	--	---
Nickel tracer	1.74[6]	0.53	--	---
Zinc tracer	1.74[6]	0.56	--	---
Microthenes:				
MN 701	0.91	0.28	49	0.03
MN 710	0.91	0.41	44	0.03

[1]Wet basis.

[2]From Nielsen (87).

[3]From Nazemi (84).

[4]From data of Brekken (9).

[5]Pure flour.

[6]From (126).

Table 3. Particle size and shape

Material	Shape	Particle Size[1] M_g microns	σ_g	M_n microns	Sizing method
Flour I	irregular	18 100		14.5	Coulter Counter
Flour II	irregular	18 75		15.5	
Flour III	irregular	18 75		15.5	
Potato starch	spherical, ellipsoidal	32	1.39	23	
Copper tracer	angular[2]	35	1.89	10.4[3]	Electro-
Nickel tracer	angular[2]	36.5	1.92	10.2[3]	mesh
Zinc tracer	angular[2]	37	1.93	10.1[3]	sieving
Microthenes:					
MN 701	mixed[4]	280	1.49	173[3]	Regular
MN 710	irregular	180	1.45	119[3]	seiving

[1] All had simple log-normal distributions except flour, which was bimodal.

[2] Assumed.

[3] Calculated from weight distribution.

[4] Mostly round, but had flakes, ribbons, and beads with tails.

actually remained in the form of the cylindrical mold. The flow conditioner did significantly reduce the angle of repose of the flour. The angle of repose ranks the apparent flowability of the flours and starch in correct order.

Particle shape (Table 3) (as determined from scanning electron microscope photomicrographs) of all flours was irregular. The smaller particles appeared to be more rounded, but the larger (greater than 70 micron) particles appeared more angular. Nazemi (84) presented photomicrographs of the smaller particles. The potato starch was composed of essentially spherical particles for the small ones, while some of the larger particles were ellipsoidal. From the crystalline nature of the salt tracer, one would expect the salt tracer to be angular in shape.

Size distributions

Results The measured particle size distributions of the simple powders such as potato starch were log normal or appeared approximately so. The flours did not have simple distributions, but were bimodal. The geometric mean averages and the geometric standard deviation are summarized in Table 3. The geometric mean volumetric average, the geometric mean weight average, and the weight average are equivalent (1, 48).

The measured distributions of the flours and potato starch are plotted in Figures 6 and 7. (The measured weight distributions of the remaining materials have been included in Appendix A, Figures 50 and 51.) The number distributions were recalculated (see Procedures) from the volumetric distribution and the total number of particles counted. (Total counts were 55,203; 50,812 and 56,052 for Flours I, II, and III respectively; and 34,507 for potato starch.)

The straight line fit (Figures 6 and 7) of the potato starch cumulative distributions indicates a log normal distribution. The fact that the measured deviation of the volumetric and number distributions were equal indicated that the data fit the log normal distribution well. Various statistical averages can then be calculated for this distribution (1, 48). The log normal distribution has been assumed for the sieved materials of Table 3 and the geometric number mean average calculated from the weight mean and deviation.

The bimodality of the flour distributions is clearly indicated in the relative volumetric percentage frequency distribution, Figure 8. The geometric weight means of the two apparent component distributions occur at the peaks in this plot. The values reported in Table 3 for the larger diameter peak were best estimates based upon the series of determinations of each flour. More scatter in the data for this peak was expected since fewer particles comprise the upper peak

Figure 6. Volumetric cumulative size distribution of flour and potato starch

X Flour I

o Flour II

● Flour III (showing range of samples)

+ Potato starch

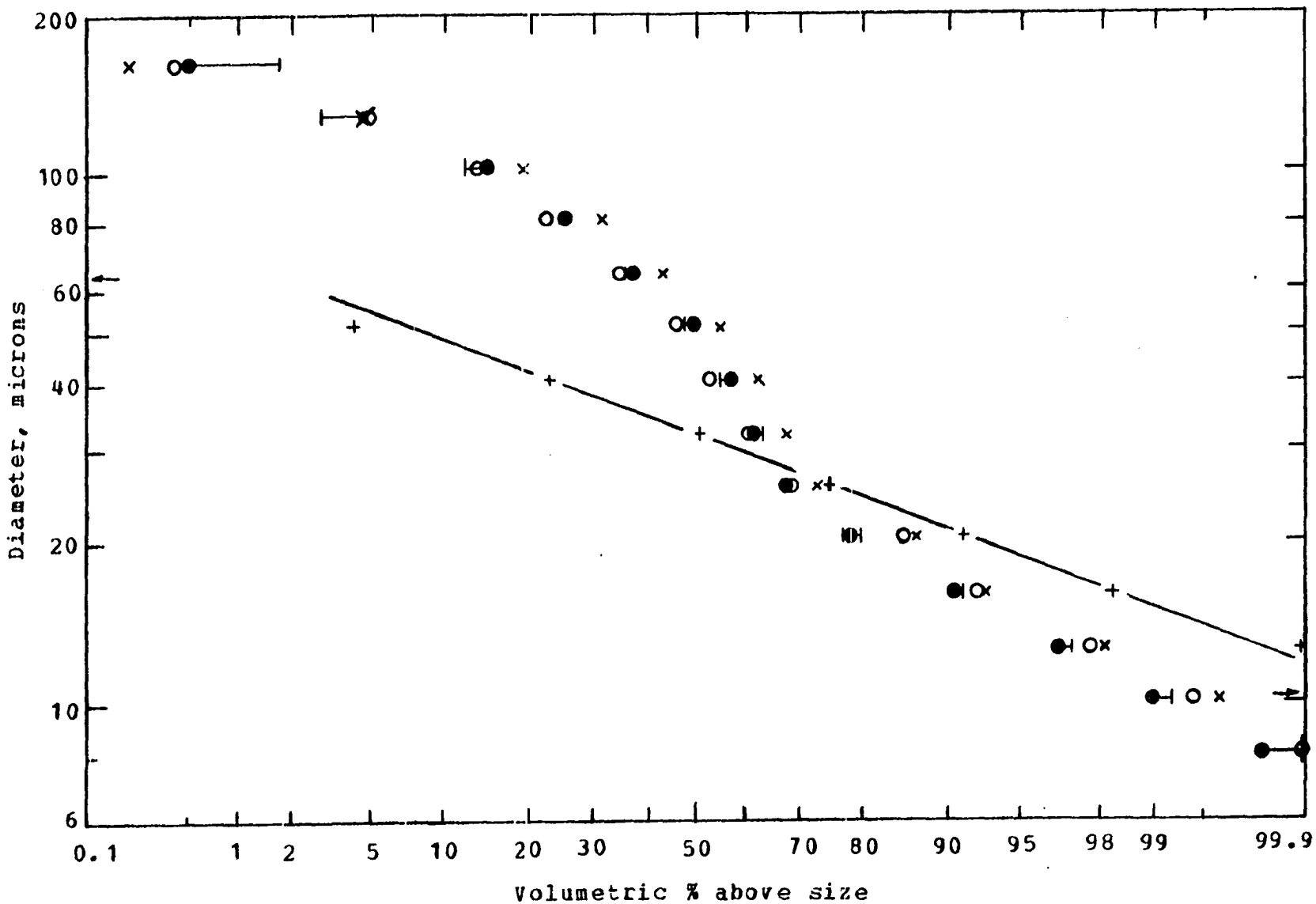
200
100
80
60
40
20
10
6
Diameter, microns
0.1
1
2
5
10
20
30
50
70
80
90
95
98
99
99.9
Volumetric % above size

Figure 7. Numerical cumulative size distribution of flour and potato starch

x Flour I

O Flour II

● Flour III (showing range of samples)

+ Potato starch

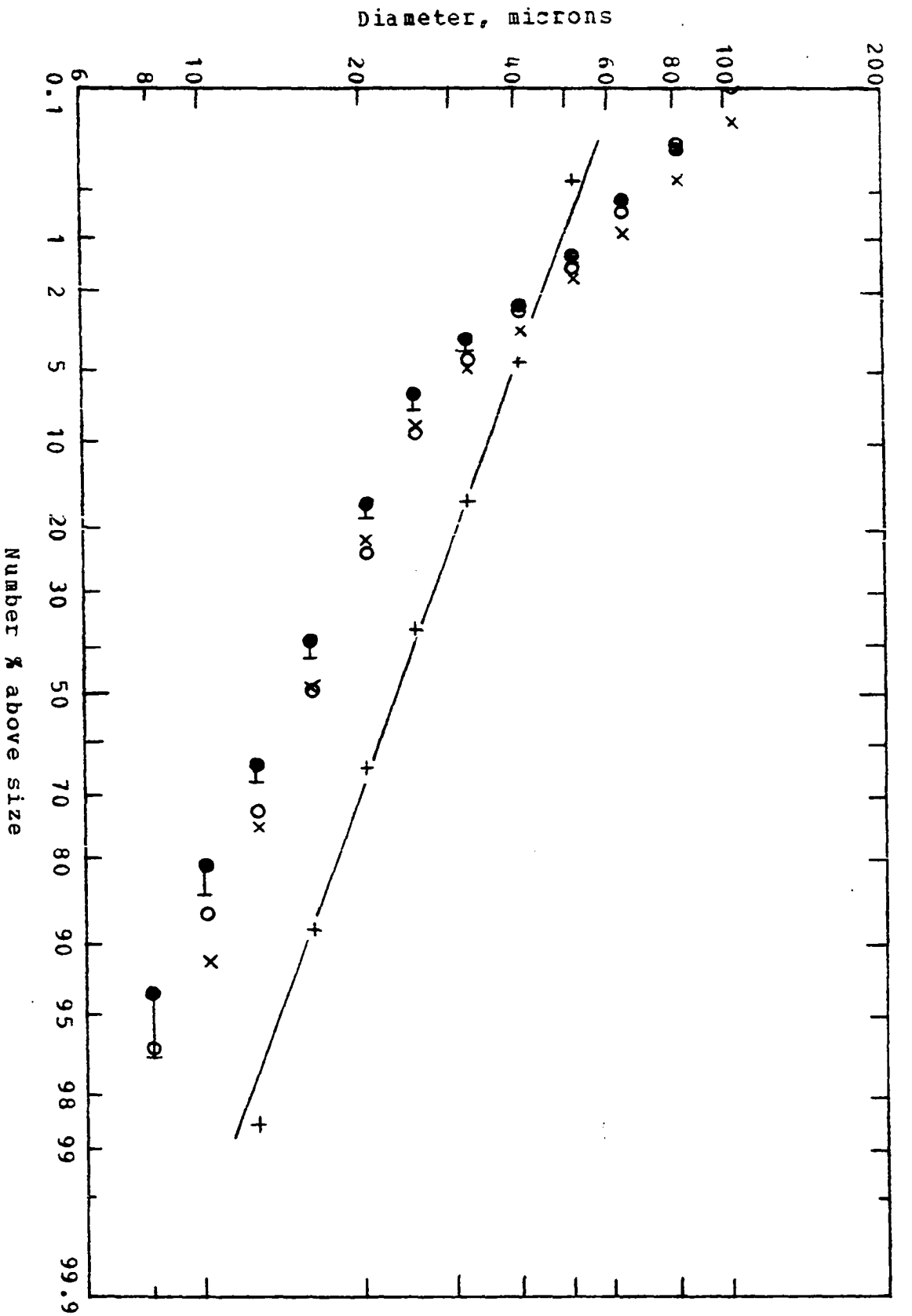
Diameter, microns
6
8
10
20
40
60
80
100
200
0.1
1
2
5
10
20
30
50
70
80
90
95
98
99
99.9
Number % above size

Figure 8. Relative volumetric percentage frequency distribution of flour size

--- Flour I

—— Flour III

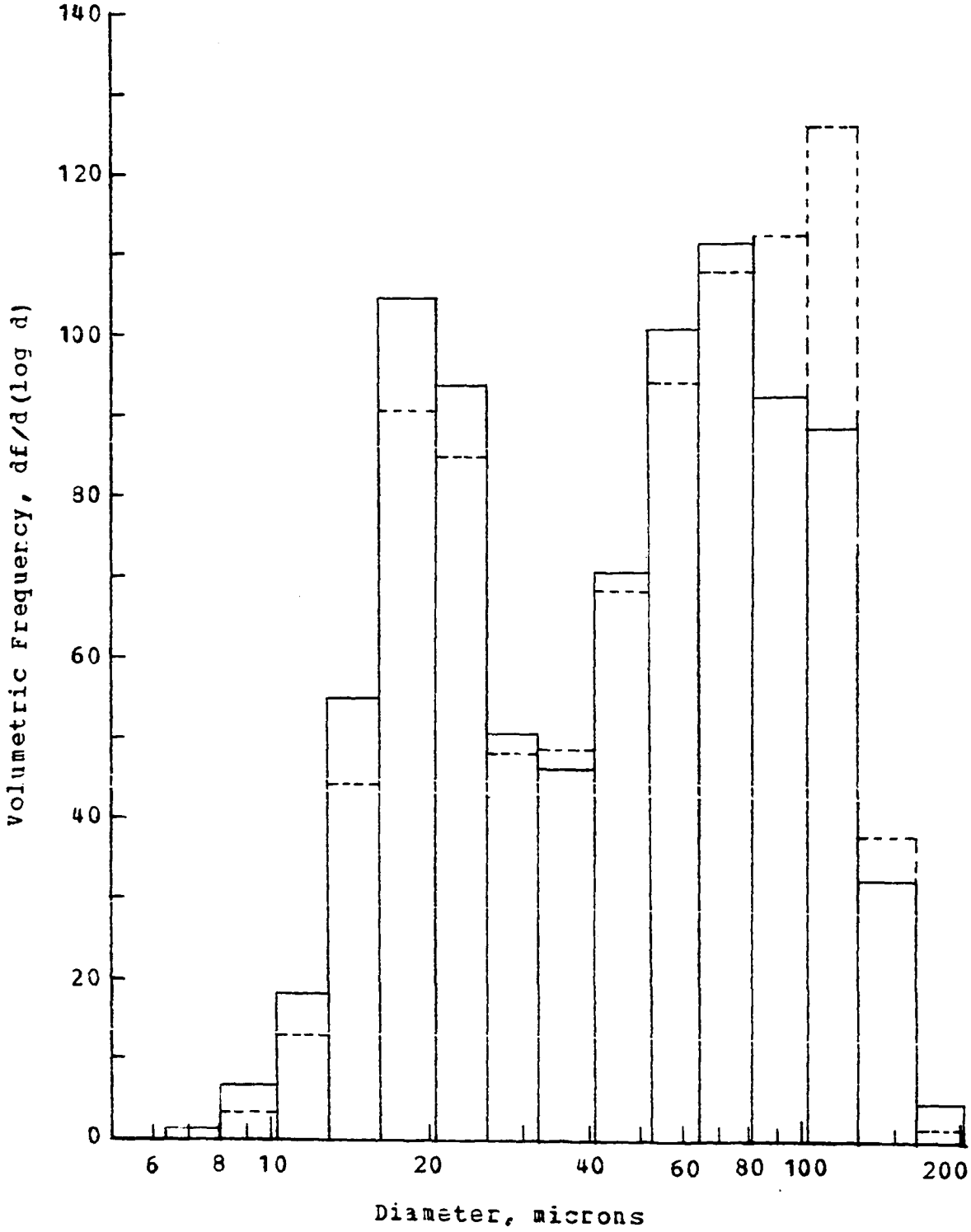
140
120
100
80
60
40
20
0
Volumetric Frequency, df/d(log d)
6
8
10
20
40
60
80
100
200
Diameter, microns

than comprise the lower peak. Instrument accuracy was perhaps a little less in this region also. From the nature of the cumulative distribution, it appears that the deviations and fraction of each component may be determined by fitting an empirical formula discussed by Irani and Callis (48).

The cumulative number distribution appeared to be best fitted by two intersecting, straight lines. The interpretation of this plot appeared to be complicated by the presence of a lower size detection limit of the instrument which introduced an asymptotic curve to the data (48). When the data was replotted with the lower limit diameter subtracted from the size, the resulting curve was asymptotic to two almost parallel straight lines.

Discussion The record of attempts made to determine the size of Flour I is interesting. The earliest attempt was a Coulter Counter number distribution obtained by others only after liquid classifying the sample. Details of the technique used were not reported. The reported result was just a number frequency plot showing a definite peak at about 17 microns with an upper shoulder at 3 microns which may have been background counts. The size range covered was 2.4 to 39 microns.

Nazemi (84) had some electron microscope photomicrographs made. From a total sample of about 300 particles, he found a single number peak at about 3 microns (geometric num-

ber mean of 3.9 microns) and no particles smaller than 1 micron, nor larger than 27 microns. Most of the particles, 89%, were less than 10.5 microns. The calculated weight geometric mean value was 16 microns. This was in good agreement with the smaller diameter component mean of about 18 microns found by the current analysis. (Apparently the larger particles were either lost in sample preparation or were not present in large enough numbers to be evident in a 300 particle sample.)

An attempted Coulter Counter analysis[1] using an unclassified sample resulted in quick plugging of a 100 micron orifice. Both scanning electron microscope photomicrographs made showed particles present which were on the order of 400 microns with many in the 20 to 50 micron size range. It was concluded[1] that "It would be difficult to determine a size distribution by any technique." In the current analysis, it was possible that the extremely large particles were not counted because of segregation during sampling or because they were not suspended at the elevation of the orifice.

---

[1]Princen, L. H., U. S. Dept. of Agriculture, Agricultural Research Service, Peoria, Illinois. Electron micrographs of flour and glass beads. Private communication. 1970.

Conclusion The present analysis was successful in better defining the range and nature of the flour size distribution of these particular flours. It has been possible to explain the apparent differences in the previous analyses. It was demonstrated that there were no significant differences in particle size distribution or density between the three flours. One then would expect the same degree of cohesiveness or flowability of the flours. With these basic powder properties essentially identical, comparison of the fluidization process can be made without regard to the flour batch.

APPARATUS

The fluidization apparatus consisted of a gas supply and treatment system, column wind box and gas distributor plate, either one of two 6 in. inside diameter by 5 ft. high cylindrical fluidization columns, stirrer and top plate assembly, and an entrainment filter. The basic apparatus was that used by Brekken (9) but with modifications and improvements (87). A major change was the addition of a gas humidifier previously used by Nazemi (85) and the use, in at least half of the experiments, of a new, plastic column. The column was supported at the top flange by 3 leveling bolts mounted on a new supporting structure. The gas distributor plate was 23 in. above the floor and the column was located for easy access to all sides.

Gas Supply and Treatment

Commercial compressed gas was supplied from either of two shipping cylinders, through pressure regulators (Airco Oxygen Regulator No. 456, with a nitrogen adaptor, Air Reduction Company, Inc. and a nitrogen regulator, Model 8, Matheson Gas Products, Division, Will Ross Incorporated, Joliet, Illinois) attached to a manifold (Figure 9). Cylinders could thus be changed without interrupting gas flow.

Figure 9. Gas supply system flowsheet

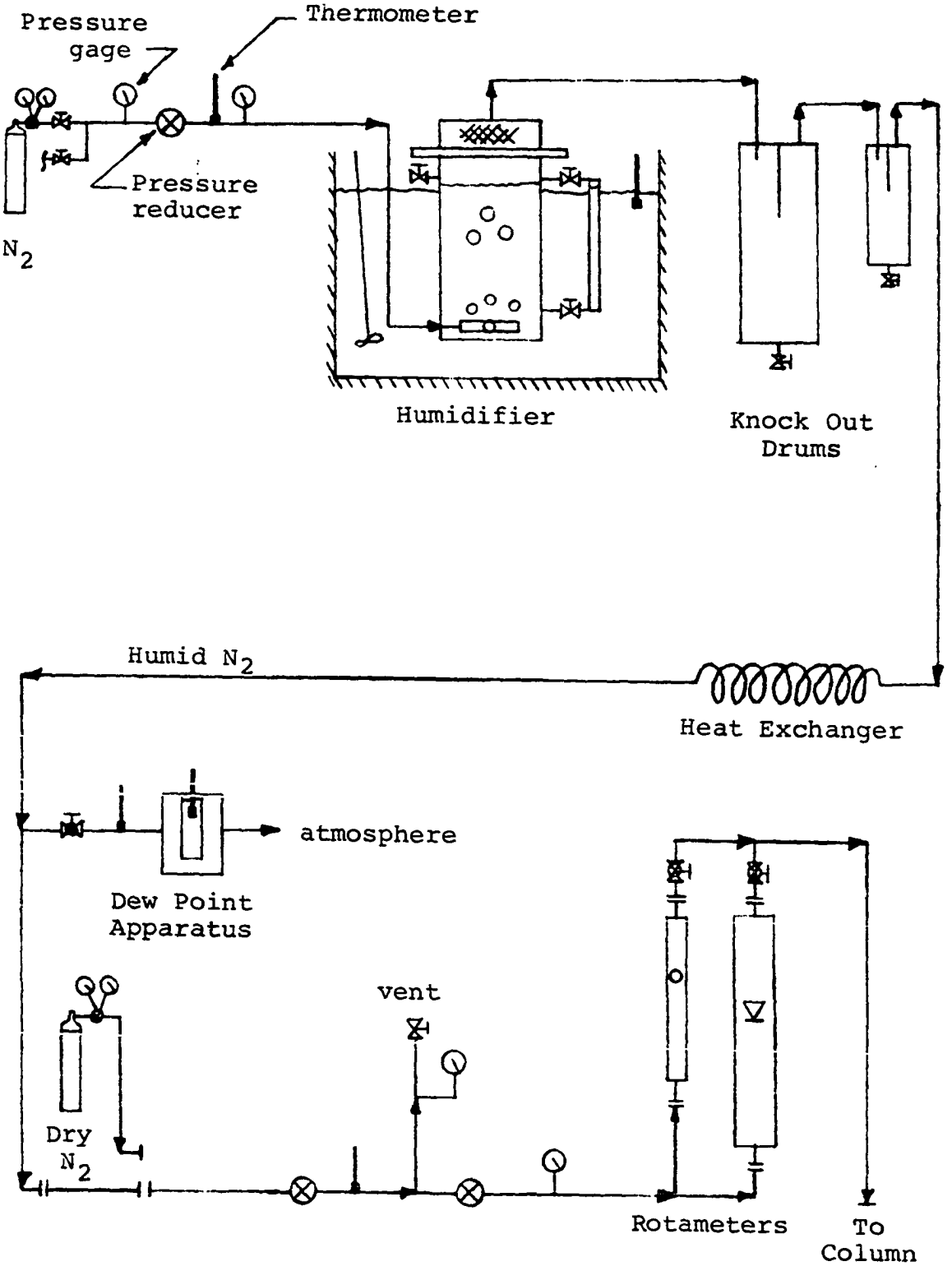
Pressure gage
Thermometer
Pressure reducer
N_2
Humidifier
Knock Out Drums
Humid N_2
Heat Exchanger
atmosphere
Dew Point Apparatus
vent
Dry N_2
Rotameters
To Column

The humidifier (86) was a constant pressure (34 psig), water bubbler. The vessel was a 4.75 in. inside diameter by 13.75 in. tall, brass cylinder of 1/8 in. wall thickness. The gas distributor was made of 1/4 in. copper tubing having 44 small holes (about 1/16 in. diameter) on the top and sides. The vessel was immersed up to the water inlet valve in a constant temperature bath (55°F for 17%RH gas, 72°F for 28%RH) (Lo - temp Bath, Wilkens - Anderson Company, Chicago, Illinois). Distilled water was added batchwise. A glass gage with isolation valves indicated the water level (8 in.) in the depressurized vessel. A 5 in. (at no gas flow) water disengaging space was sufficient to prevent most droplet entrainment. A demister containing stainless steel turnings was located at the vessel top. A 10.5 in. long, 1/4 in. copper pipe led to the first knockout drum (4 in. diameter, 14 1/4 in. tall, brass cylinder) and a small commercial steam trap. A 40 ft. coiled length of 1/4 in. copper tubing (84) provided time for the gas to reach room temperature, 72°F. A small sample stream could be bled to the dew point indicator.

For operation with dry gas, the humidifier could be bypassed by removing a spool and attaching the cylinder regulator line.

The main gas line pressure was reduced by a variable setting pressure reducing valve. A thermometer (1°F least scale division) inside the line indicated gas temperature. A

fixed pressure reducer lowered pressure further. By adjusting the upstream variable pressure reducer, the desired rotameter inlet pressure (indicated by a 1/16 psig least scale division gage) was set.

The gas flow rate was measured with either of two calibrated rotameters. The rotameters were calibrated (7) with a dry gas displacement meter (Model A1 - 175, American Meter Company, Nebraska City, Nebraska). Very small gas flows were calibrated by water displacement.

A 1/4 in. tapered rotameter tube (Precision Bore Flowrator Tube No. 2-F 1/4-20-5, Fischer and Porter Company, Warminster, Pennsylvania), using the same spherical float Brekken (9) used, measured flow rates up to 0.067 ft./sec. (based on the 6 in. diameter column) at 7 psig. Flow rates from 0.066 to 0.31 ft./sec. (at 9 psig) were measured with a 1/2 in., tapered rotameter (Precision Bore Tube No. 48-25 E3-1147, Dwg. G-15154, Fischer and Porter Company, Warminster, Pennsylvania) equipped with a stainless steel, 8.5 g. float (87). (A heavier float gave a slightly higher flow range (87).) Gas flow was controlled by globe valves (1/4 or 1/2 in.) immediately after the rotameters. Gas then flowed about 12 ft. in a 3/4 in. copper pipe to the column wind box.

Wind Box and Gas Distributor

A wind box (Figures 10 and 11) is a gas chamber provided for maintaining uniform gas flow through the porous distributor plate. The 3 in. deep wind box and the distributor plate mounting were made of Plexiglas. The whole assembly bolted to the bottom of either column. A 11/16 in. thick, Plexiglas ring (9) interfaced with the glass column.

The distributor plate was an 8 in. diameter, 1 in. thick, porous Alundum disc (Mixture P2120, Norton Company, Worcester, Massachusetts). Fried (29) had concluded that a porous plate was the best type of several gas distributors and that this plate had a good permeability.

At the start of this project, it was noticed that the central area of the disc had a uniform, white coloration compared to the gasket covered periphery. Measurement of the pressure drop across the plate (Figure 12) showed a change in plate permeability. Since little change had occurred during Brekken's mixing experiments, it appeared that a steady state condition had been reached. During the preliminary experiments, it became evident that the permeability was still changing and had significantly deviated from Brekken's conditions.

Reversing the gas flow or fluidizing a sand bed did not reduce the plate pressure drop.

Figure 10. Fluidization column schematic

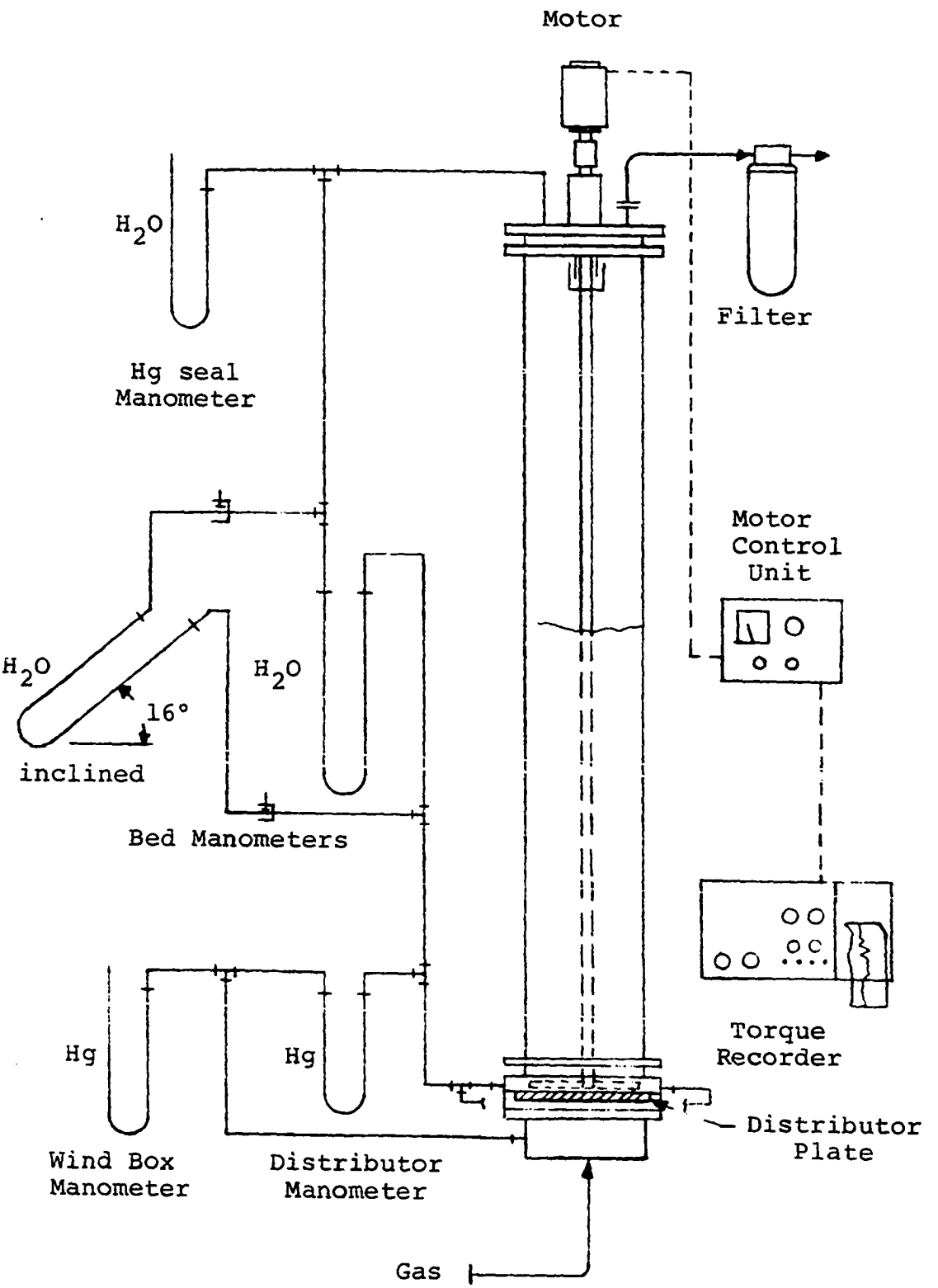
Motor
H_2O
Hg seal
Manometer
Filter
Motor
Control
Unit
H_2O
16°
inclined
H_2O
Bed Manometers
Torque
Recorder
Hg
Hg
Wind Box
Manometer
Distributor
Manometer
Distributor
Plate
Gas

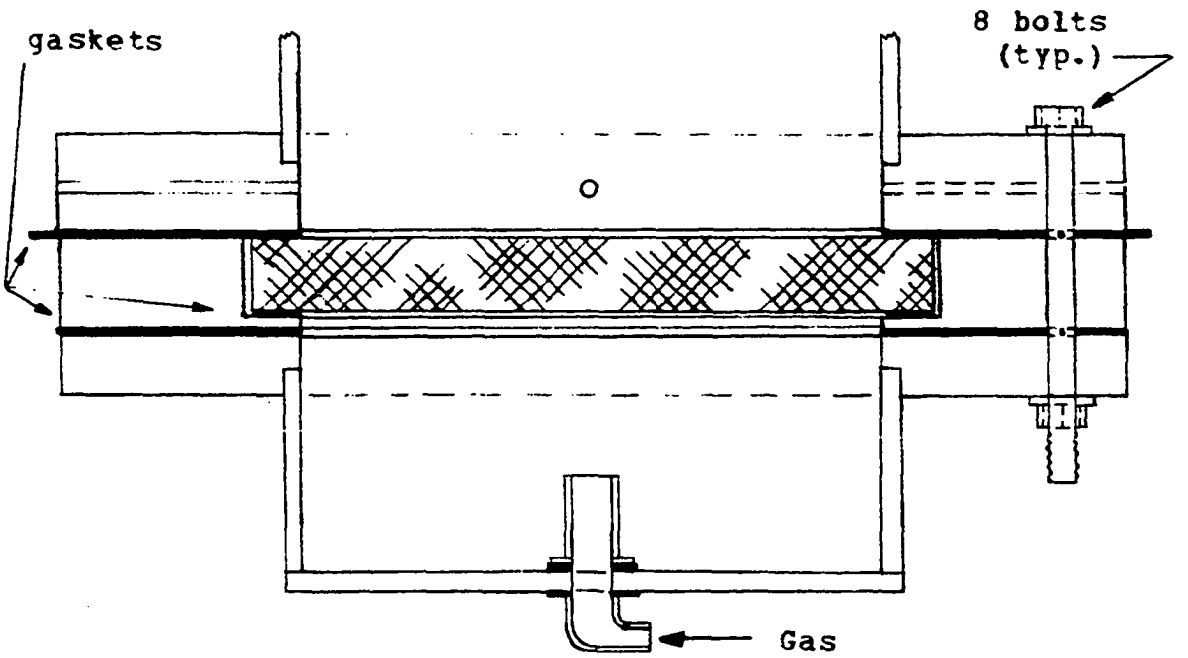

Figure 11. Wind box and gas distributor

Figure 12. Distributor plate pressure drop

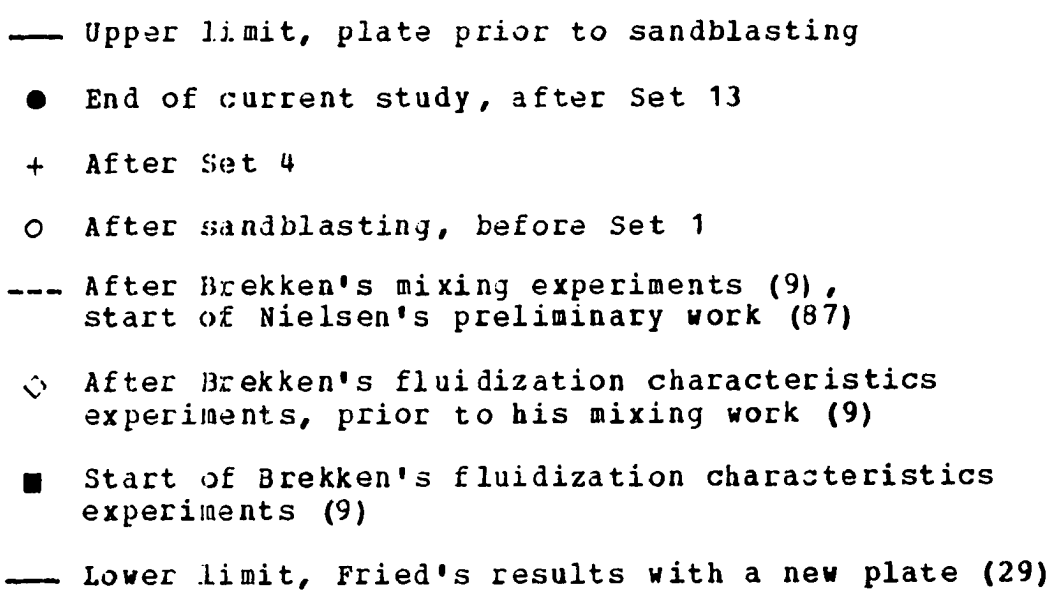

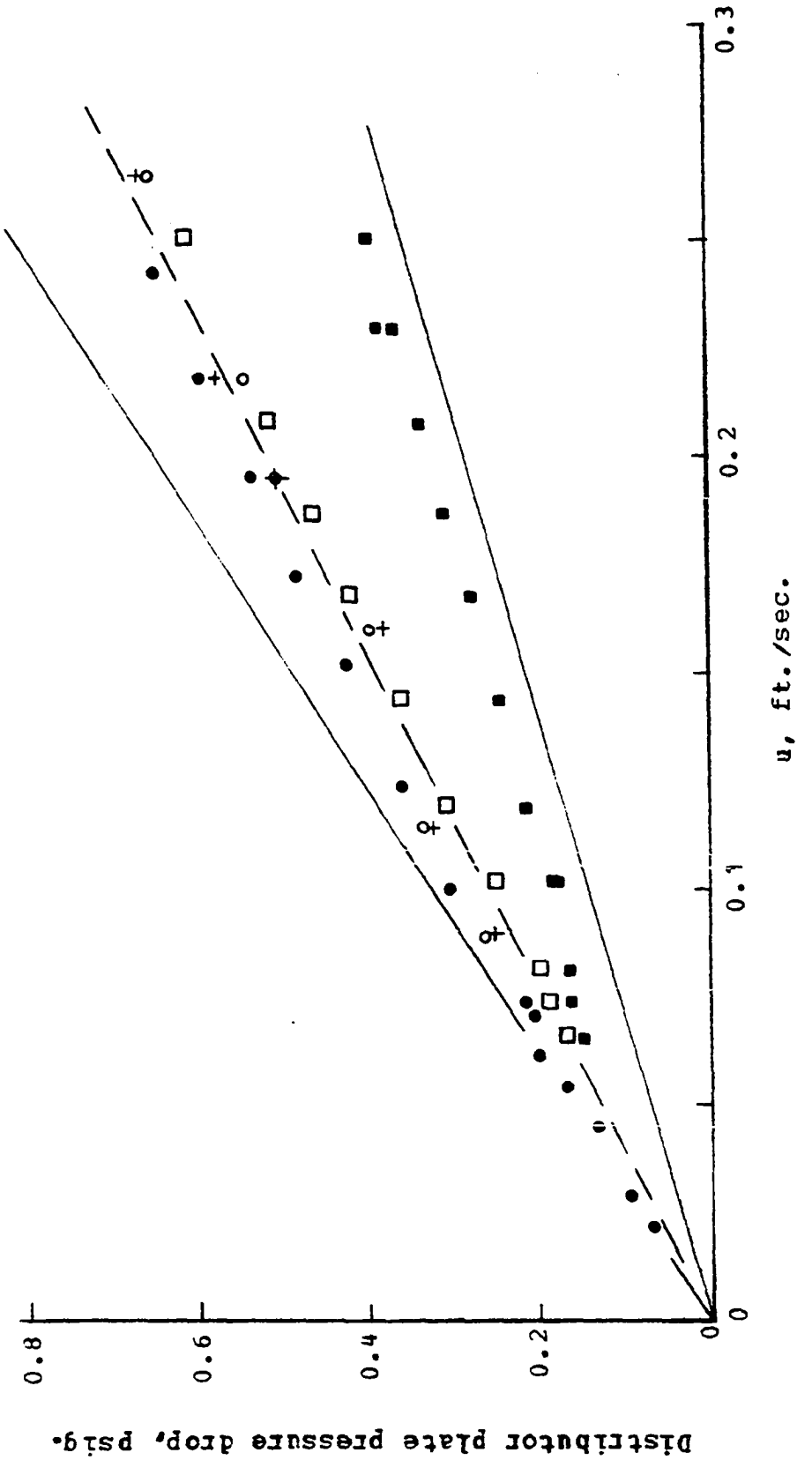
0.8
0.6
0.4
0.2
0
0
0.1
0.2
0.3
u, ft./sec.
Distributor plate pressure drop, psig.

The plate was sandblasted with very light, short strokes over the top surface using regular sand. Two applications were required to remove the coloration and restore the pressure drop to a level of Brekken's mixing experiments. A total of 0.003 to 0.0045 in. was removed, leaving the surface considerably rougher and slightly nonuniform in thickness. The surface, however, was still considerably smoother than some newer plates which had not been as finely manufactured. The plate was flipped over and used with the smooth side on top.

During the current experiments, the permeability decreased slightly (Figure 12). The pressure drop across Nazemi's plate (84) was measured after the conclusion of his experiments and found to be close to the range of the current experiments.

It is evident that distributor plate plugging, presumably with fine flour particles, must be accounted for in future fluidized bed designs.

Columns

The first column was a 6 in. inside diameter by 5 ft. tall Pyrex glass pipe that Brekken (9) had used. A metal tape measure (1/16 in. least scale division) was taped to the column for measuring bed height. The residence time grids were also taped on the wall. A 11/16 in. thick Plexiglas

ring between the distributor plate and glass column contained three 3/8 in. outside diameter copper pipe taps, 90° apart; two were pressure taps and one was used for sampling the fluid bed.

The pressure taps were 1/4 in. diameter brass tubes machined to fit inside the 3/8 in. copper pipe. Pieces of 270 mesh screening soldered across the fluid bed end prevented (84) particles from entering the 1/4 in. Tygon tubing manometer lines. The taps were periodically cleaned with a brush.

The manometer system is diagramed in Figure 10. All manometers were made of 8 mm. glass tubing with Tygon tubing "U" sections and had 0.1 cm. least scale division scales. The wind box pressure (generally a 29 in. Hg manometer) and the pressure drops across the bed (33 in., water with side filling tap) and mercury seal (filter) (16 in., water) were measured during each experiment. The distributor plate pressure drop was frequently determined by the pressure balance.

Samples of the fluid bed were collected through a previously described (87) 8.75 in. long, curved piece of 1/8 in. diameter "Polypenco Nylaflow" pressure tubing. The tube was inserted through a cork and aligned in the Plexiglas ring's sampling tap so that the withdrawal point was flush with the column wall and at the stirrer bottom.

The second column (Figures 13 and 14) used the same sampling tube and manometer system as the first column (without the ring). The second column was also 6 in. inside diameter by 5 ft. tall, but was constructed of Plexiglas. The plastic column was designed for collecting core samples of the settled bed (87). This was accomplished through a series of 6 sets of holes in the lower part of the column at 6 in. elevation intervals. Two additional holes in the upper part of the column were used in filling the column and could be used for inserting a horizontal tracer feeding mechanism. One wall sector contained the grids for the residence time measurements. Again the metal tape measure indicated bed height.

During fluidization, the sample ports in the bottom flange (Figure 13) were closed by the insertion of two pressure taps with cork bushings, the 1/8 in. sampling tube, and a 1/4 in. pipe and bushing through which the column was emptied.

The five pairs of sample holes in the column wall were closed (Figure 15) with polyethylene film (obtained from "Alligator" Baggies, Colgate-Palmolive Company, New York, N. Y.). A 2 in. square of film was first taped (cellophane tape) to the wall above the port. Then a cardboard retaining ring (1/16 in. thick by 1/4 in. deep), cut to fit the hole snugly, was inserted until the film was flush with the inside

Figure 13. Plastic column

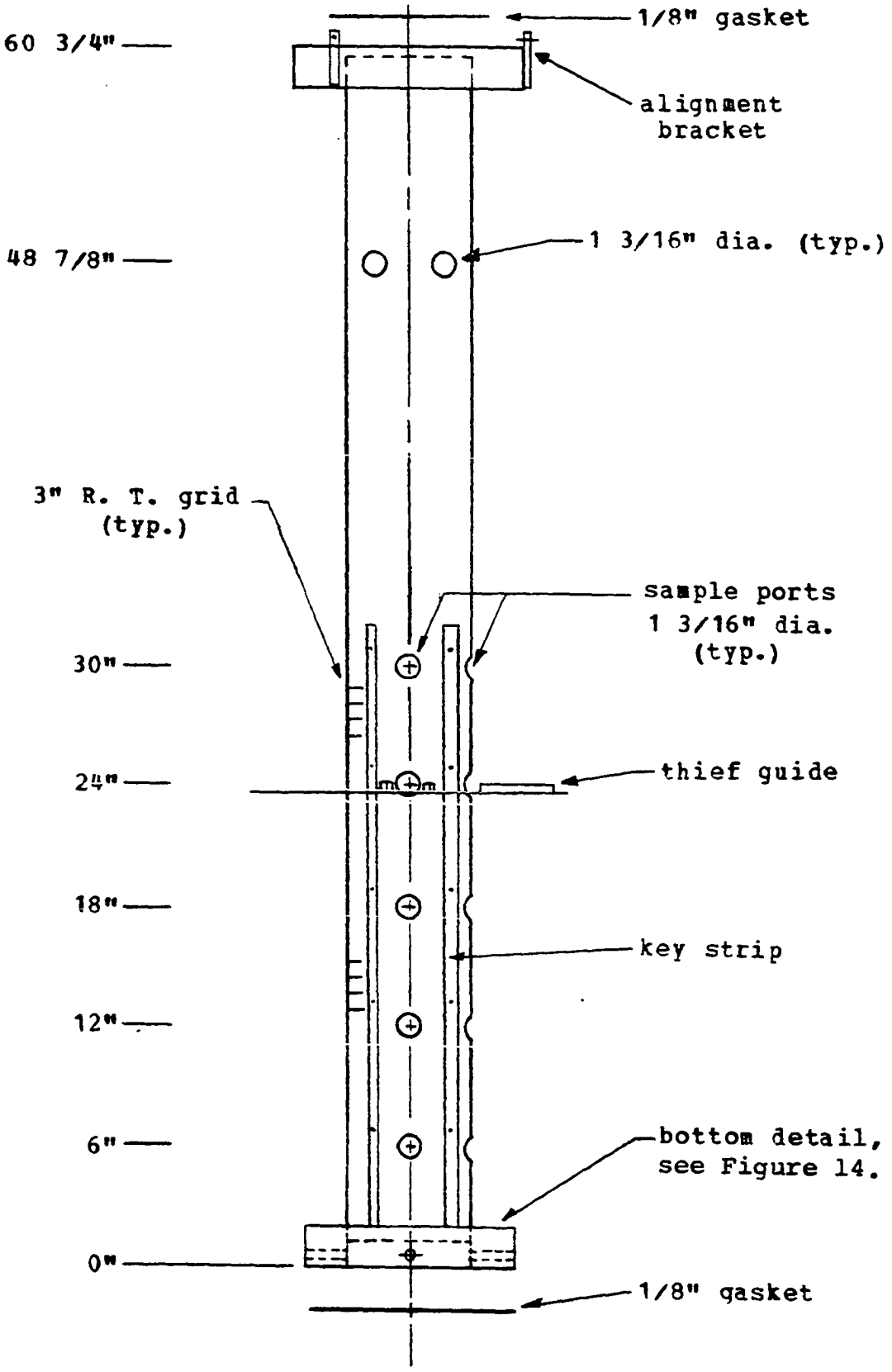
1/8" gasket
60 3/4"
alignment bracket
48 7/8"
1 3/16" dia. (typ.)
3" R. T. grid (typ.)
sample ports 1 3/16" dia. (typ.)
30"
24"
thief guide
18"
key strip
12"
6"
bottom detail, see Figure 14.
0"
1/8" gasket

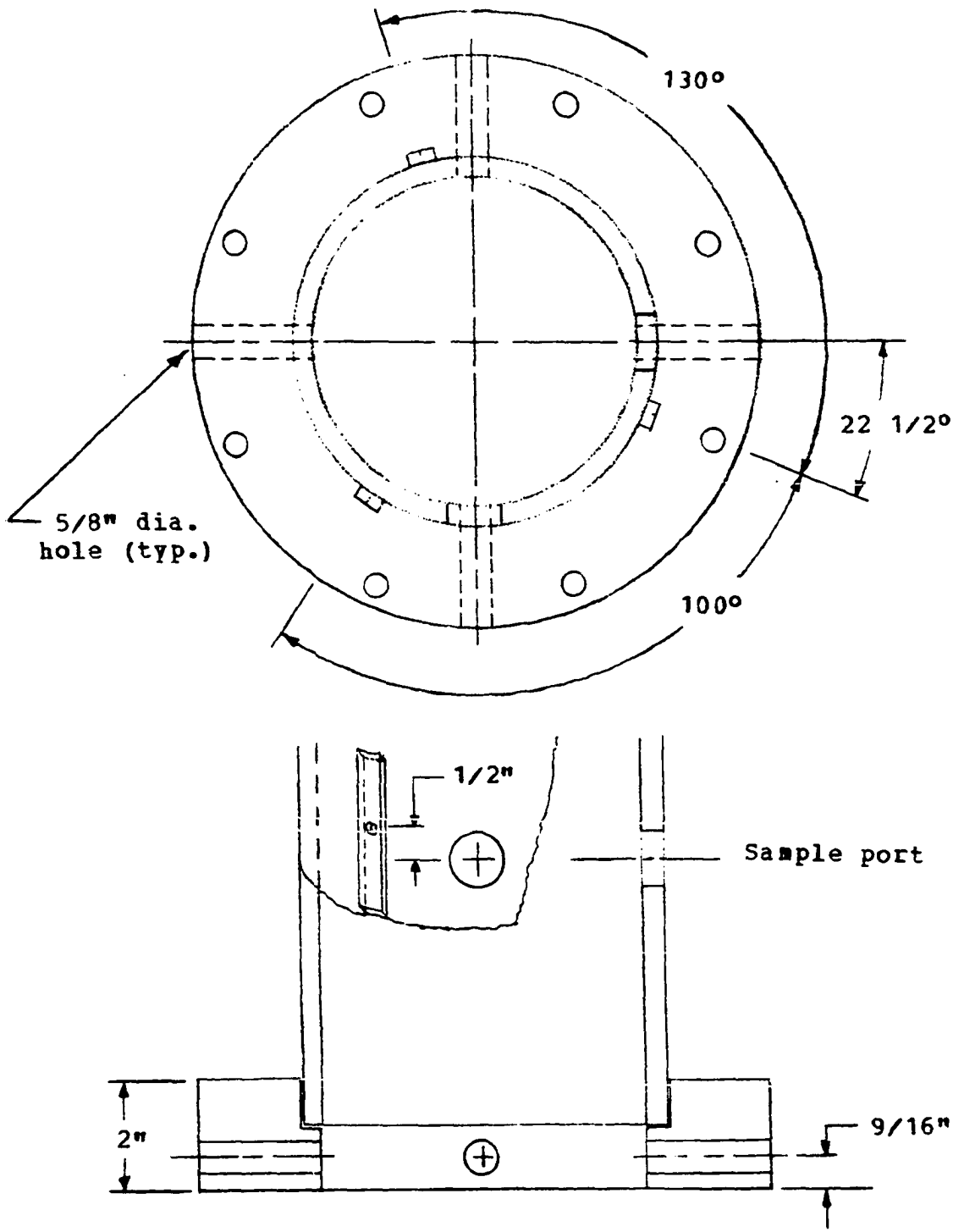

Figure 14. Bottom detail of plastic column

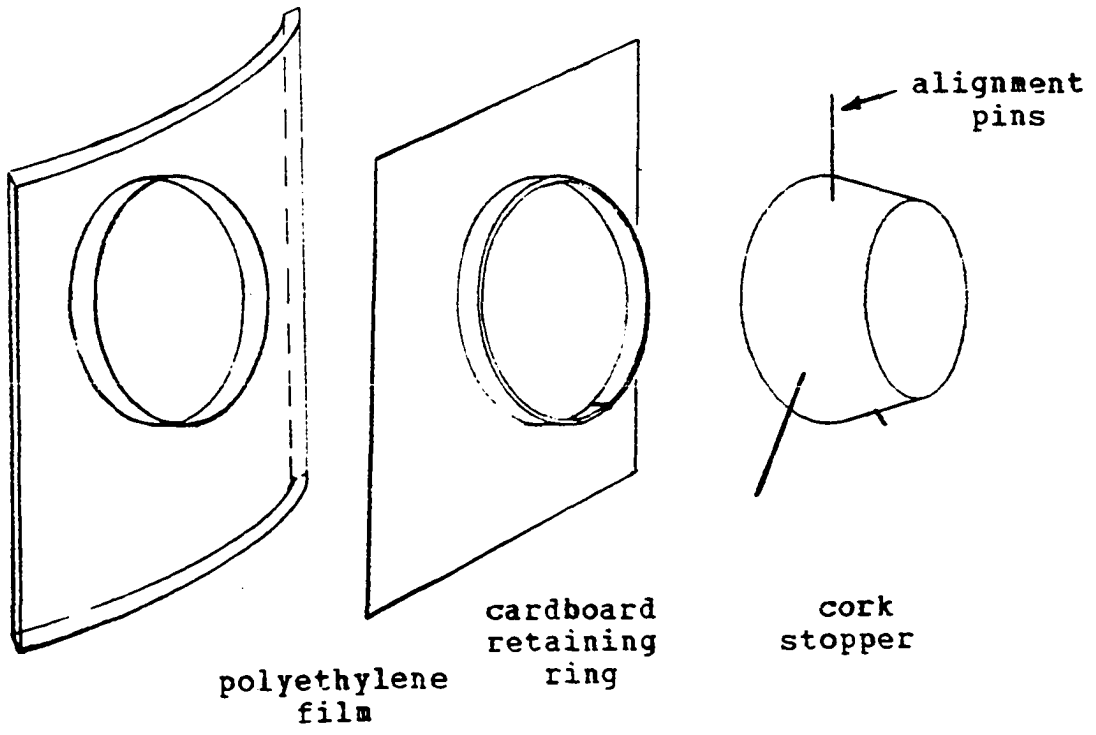

Figure 15. Sample port detail

wall. The film was pulled taut while the ring was inserted. The extending edges of the film were now trimmed and taped, leaving no gas leaks. To prevent the film from stretching or blowing out under pressure, a cork stopper whose diameter was almost equal to the diameter of the inside retaining ring, was inserted. Three alignment pins maintained the film flush with the wall. The stopper was now firmly taped (using an "X" pattern) to the wall. For additional strength at high gas velocities (0.35 ft./sec.) the retaining ring was also taped.

Settled bed samples were collected using a sample thief (87). This required a thief guide (Figure 13 and 16) for the accurate determination of sample location. The guide was an aluminum plate with Plexiglas mounting brackets and guide blocks. The mounting brackets aligned the guide's location with the key strip's pin holes (Figure 13) on the column at each sample port (Figure 14) elevation except at the flange. Three pins firmly locked the guide's position. Guide blocks directed the thief into the column along the desired path. Thiefs of different diameters required different sized blocks and Plexiglas risers (not illustrated) upon which the thief sat. The guide was constructed so that at each sample hole, the thief could be inserted in two possible directions.

The plastic column also was equipped with alignment brackets (Figures 13 and 17) for aligning the top plate and

Figure 16. Thief guide detail

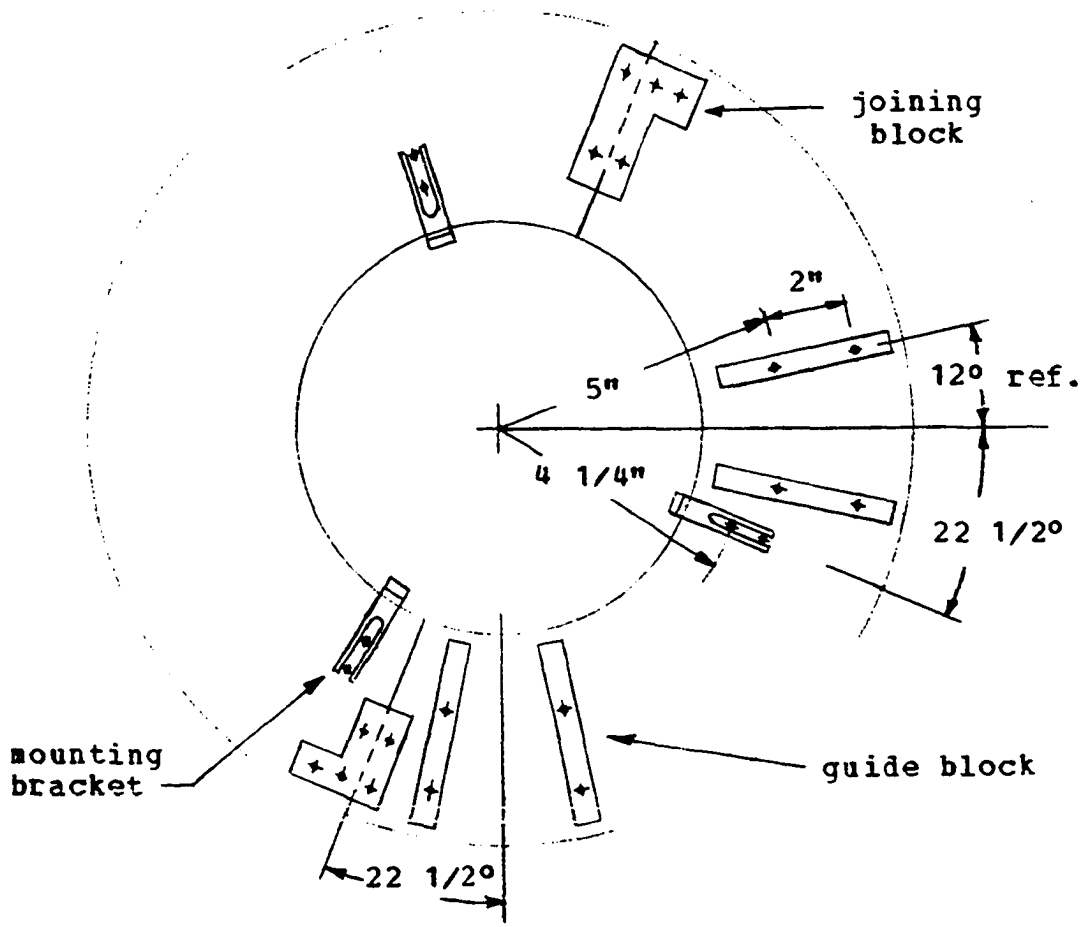
joining block
2"
5"
12° ref.
4 1/4"
22 1/2°
mounting bracket
guide block
22 1/2°

(a)

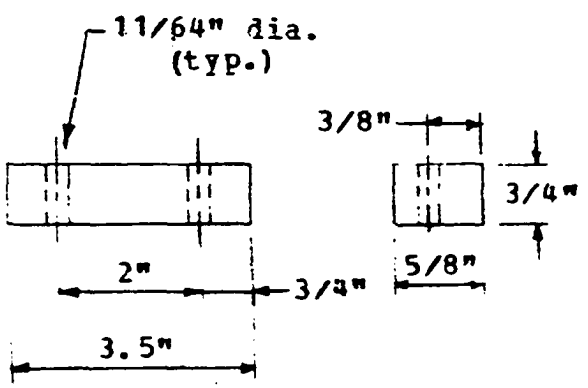
11/64" dia. (typ.)
3/8"
3/4"
5/8"
2"
3/4"
3.5"

(b)

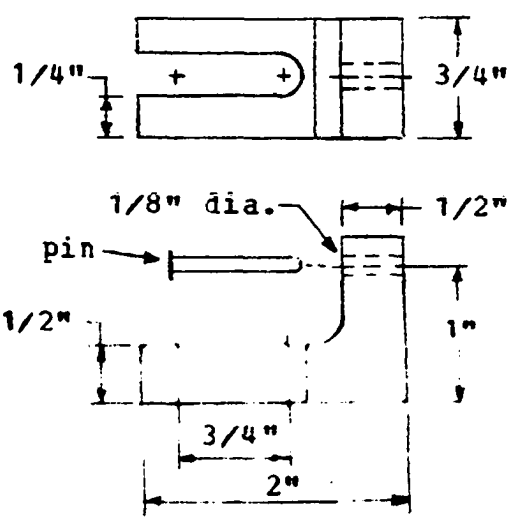
1/4"
3/4"
1/8" dia.
1/2"
pin
1/2"
1"
3/4"
2"

(c)

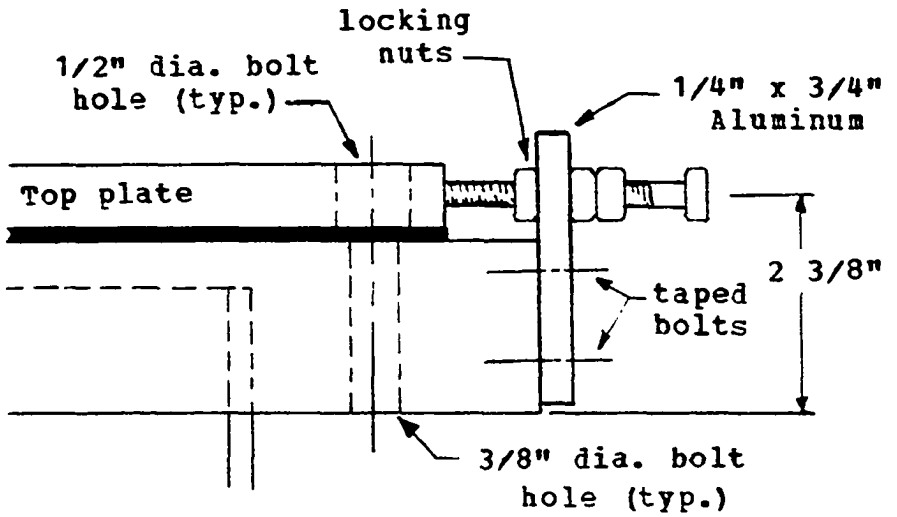

Figure 17. Alignment bracket detail

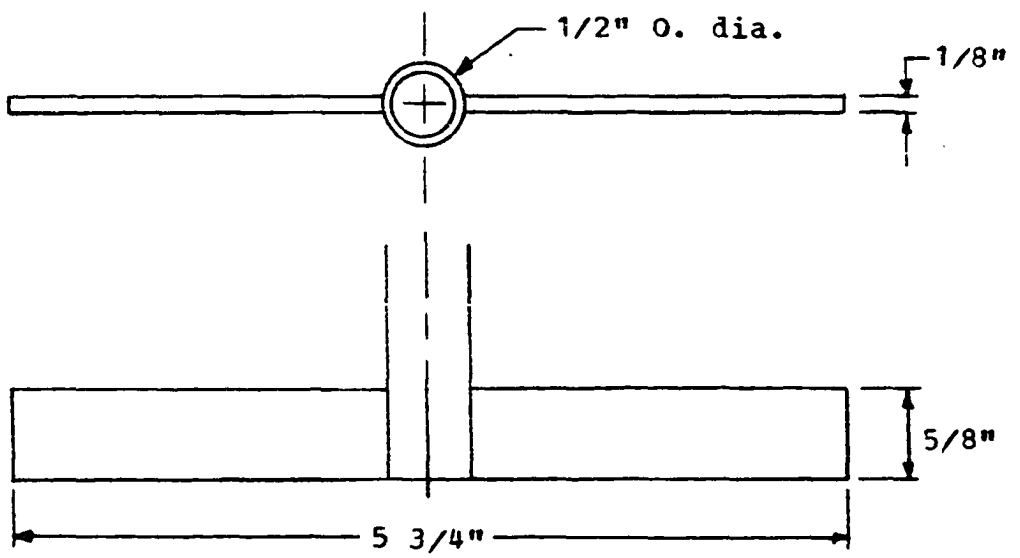

Figure 18. Stirrer detail

stirrer. This device also enabled the top plate and stirrer to be removed from the empty column and then returned with the same alignment.

Stirrer and Top Plate

A simple, two bladed paddle stirrer (Figure 18) was used to promote fluidization. This stirrer was similar to that used by Kozulin and Kulyamin (59) and Nazemi (84, 85). The stirrer was supported by a new pair of sealed, single row radial bearings (Nice, no. 1616 -DC) mounted on the top plate (Figure 19). The clearance between the gas distributor and paddle was maintained at just under 3/16 in. by a collar riding on the upper bearing. The shaft was free to move up, since it was only restrained by the 3 in. long, vacuum hose shaft coupling, but usually did not.

The mercury barometric seal located just under the top plate also protected the bearings from dust.

The stirrer was driven at a constant speed by a Servodyne Lab Drive System (Model 4420, Cole - Parmer Instrument and Equipment Company, Chicago, Illinois). The stirrer speed indicator was calibrated with an electric timer or a stroboscope. The drive unit generated a current proportional to the motor torque. This signal was recorded on a direct current modified Beckman Offner Recorder (Type RS Dynograph, Model 462) with heat sensitive chart paper.

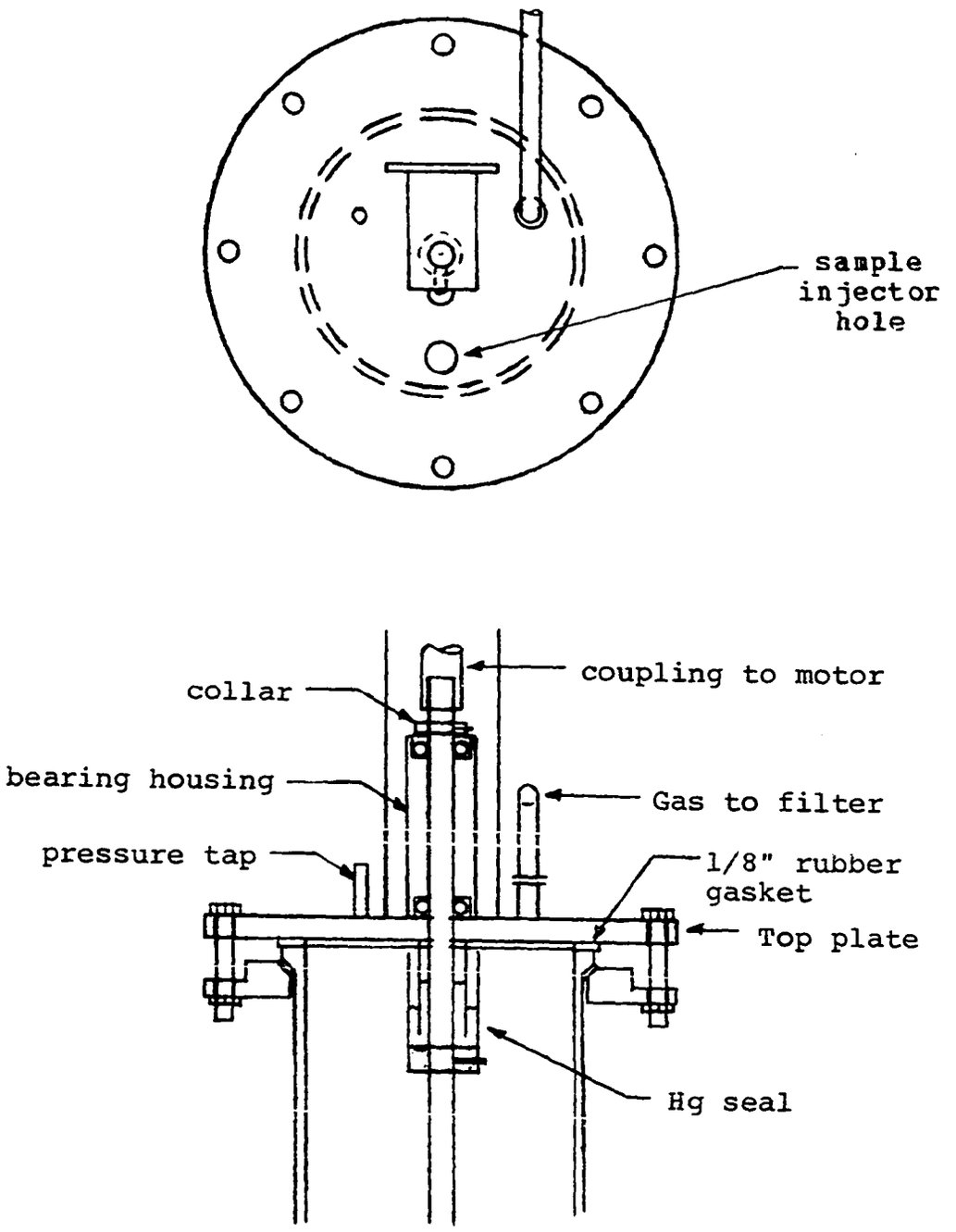

Figure 19. Top plate detail

The torque signal indicator was calibrated as a function of stirrer speed by applying a known torque provided by lifting weights. A monofilament nylon fishline was attached to the mercury seal cup. The line was then passed over a 2 in. diameter pulley. Weights were raised about 6 ft. with the line being wound in a single layer on the cup. From the known moment arm and weight, the torque was calculated. With this calibration method, the effect of stirrer bearings was included in the calibration.

The top plate was made of 1/2 in. thick aluminum. In addition to the bearing housing and motor, it had several 5/8 in. diameter access holes, a 1/4 in. diameter pressure tap, and the gas outlet line fitting.

Alignment of the top plate was critical for stirrer performance. Alignment was easier with the column on a floor stand since one could sight down the access hole. The plastic column was easier to align since the alignment brackets could be used to maintain a location or could be used to move the plate slightly in a controlled direction. The glass column had no restraint on the plate and alignment was mostly trial and error. After final alignment, the column was lifted onto the supporting structure.

Filter

The gas left either column through a 3/4 in. diameter pipe rising vertically 7 in. and then traveling 9 in. horizontally into the filter. A Pall cartridge filter (Model MCC1001EC16, T. M. Pall Corporation, Cortland, New York) with a 3 micron, 4.5 sq. ft. paper cartridge (Pall, type MCS1001EC) removed entrained solids. Each cartridge was used for only one material. The filtered gas was discharged to the atmosphere.

Residence Time Apparatus

The residence time experiment involved measuring particle slip surfaces over measured distances. For this purpose, two grids of four parallel lines 1 in. apart were ruled on a thin plastic sheet and then inked (87). The grid lines were about 6 in. long. These grids were then taped at the desired elevations (see Table 4) on the outside column wall. Similarly, two grids with 1 in. travel distance were made.

The particle slip surfaces were timed with a 0.1 sec. least scale division electric timers hooked to a manually operated switching circuit (87).

Mixing Apparatus

Figure 20 shows the general arrangement of equipment for a mixing curve experiment where samples were collected as a function of time. Tracer salts were added to the top of the fluidized bed with a tracer injector tube (87) having a conical plugged bottom. On releasing the plug, the weighed salt flowed down, over the plug and was distributed on the bed surface.

Flow samples from the fluid bed bottom were collected in 13 by 100 mm. lipless test tubes (87). Time of sampling was determined by test tube location on a constant speed, rotary disc sample table (87).

Settled bed samples were collected using a thin, well polished, 1/2 in. diameter sample thief (87).

The tracer concentration of each sample was determined by dissolving the salt tracer and measuring the solution concentration with either a Model 290 or a Model 305 Atomic Absorption Spectrophotometer (Perkin - Elmer Corporation, Norwalk, Connecticut).

Figure 20. Apparatus arrangement for mixing curve experiment

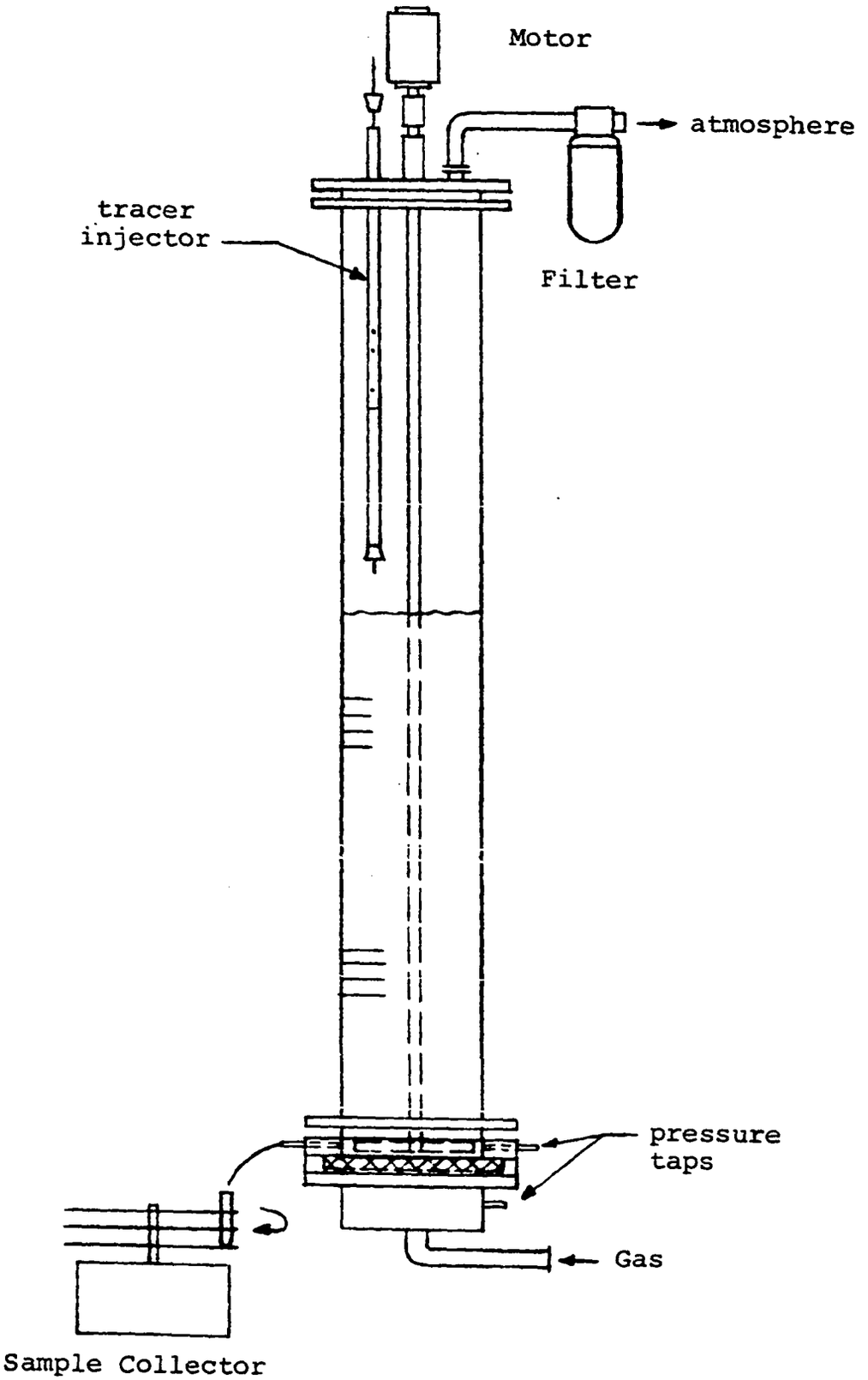
Motor
atmosphere
tracer
injector
Filter
pressure
taps
Gas
Sample Collector

PART 3. EXPERIMENTAL METHODS

PROCEDURES OF FLUIDIZATION EXPERIMENTS

Drying of Flour

The stored Flour III moisture content was about 13.6 to 14.6% on a dry basis. To produce the moisture levels desired for investigating the effect of moisture on the fluidized bed behavior, the flour had to be dried. Flour was slowly dried by exposing it to the atmosphere for a few weeks followed by fluidizing it with dry gas. A low moisture content flour was obtained by drying flour in a vacuum oven. Flour III of 11.6% moisture (Set 8) was made by exposing a open paper shipping bag of flour to the atmosphere. After several weeks, the moisture content was about 12.3%. The flour was further dried by fluidizing with dry nitrogen at 0.15 ft./sec. for 1 hr. (12.0% moisture was obtained). Drying occurring during the characteristic run resulted in the desired 11.6% moisture level.

Flour with 7.9% moisture (Set 9) was prepared by air drying the higher moisture content flour to 11.4% moisture and then drying this material by fluidization at 0.15 ft./sec. for 26 hr. in order to reach the 7.9% moisture level.

The 2.8% moisture flour was obtained by vacuum drying (28 in. Hg vacuum) flour spread in sheets about 1/2 in. thick for 2 hr. in the Unit Operations Laboratory oven. The steam

jacket pressure was very low, 4 to 5 psig. The oven was preheated for 22 hr. The batches were mixed together by rolling them in a "jerri can" container before charging the flour to the column.

Bed Installation

A weighed amount of flour or potato starch was charged to the column via nitrogen gas transport from a plastic "jerri can". The material was fluidized for 1 min. to level the top of the bed and then was settled. The settled bed depth was then recorded.

One bed of flour (Set 11, runs 5 to 11, see General Plan) was made less cohesive by flow conditioning it with Cab-O-Sil. The Cab-O-Sil was mixed with flour by an improved technique compared to using a cement mixer (9) or mixing it by hand (84). In the current work, enough Cab-O-Sil was to be added to the flour to produce a concentration of 0.5% wt. Later more Cab-O-Sil was added to this bed to raise the Cab-O-Sil concentration to 1.0% wt., the minimum concentration needed to provide a free-flowing flour (29).

The desired weight of Cab-O-Sil (32.5 g.) was pneumatically conveyed from a 1 l. vacuum flask to the bottom of the fluidized bed. A 2 ft. long piece of 1/4 in. diameter Tygon tubing connected the flask with the 1/4 in. diameter pipe which was also used in emptying the column. This pipe entered the column wall at the level of the stirrer blade

(see Columns section). Nitrogen gas was supplied to the vacuum flask from a cylinder with a pressure regulator having a valve for controlling small rates of gas flow. Gas flow was stopped with a pinch clamp placed on the rubber tubing used to connect the regulator to the flask.

To minimize Cab-O-Sil loss from the system, the entrainment filter was prepared by allowing the cake of flour built up during the two previous experiments (runs 3 and 4 of set 11) to remain on the filter. Without the flour cake, the pores of the filter would be large enough to pass Cab-O-Sil particles.

The bed was fluidized at a gas velocity high enough to provide complete fluidization without excessive bubbling. A stirring speed of 50 rpm was used. A gas velocity of 0.15 ft./sec. was used for the pure flour bed and a velocity of 0.007 ft./sec. was used for the flour bed already having 0.5% wt. of Cab-O-Sil. As Cab-O-Sil was added and mixed with the flour, the fluidizing gas velocity was reduced since the minimum fluidization velocity decreased as the flour became more free flowing.

To add the Cab-O-Sil to the bed, a "C" clamp on the Tygon tubing was opened fully and the pinch clamp was removed. Gas flow from the cylinder was started and increased until Cab-O-Sil was being conveyed into the bed when the flask was inverted so as to feed solids into the Tygon

tubing. A slow Cab-O-Sil feed rate was used to provide time for the Cab-O-Sil to be dispersed without having a locally large Cab-O-Sil concentration in the bed near the entry point. Also, with a slow feed rate, bubble generation due to the transport gas stream was reduced too since the transport gas flow rate was was less.

After the Cab-O-Sil was added (about 15 min. was required for the addition), the bed was fluidized at the initial gas velocity specified above for 10 min. to mix the Cab-O-Sil with the flour. A few flocs of Cab-O-Sil were seen circulating in the bed, but became fewer and smaller with further fluidization.

Fluidization Characteristics

The fluidization characteristics of the bed were measured in the following manner: The bed was prepared by fluidizing for about 3 min. with a gas velocity of 0.26 ft./sec. with 50 rpm stirring speed. A pair of samples for moisture analysis were collected. The stirrer and gas were quickly shut off and the bed was allowed to settle. The initial bed depth was then recorded. The bed was next fluidized at the highest gas velocity and the desired stirring speed, 50 rpm. Steady state appeared to have been reached within minutes at the high gas velocities. The following steady state parameter values were recorded: column inlet

pressure, pressure drop across the seal or filter, bed pressure drop, fluid height (maximum and average) and stirrer torque. The gas velocity was decreased incrementally and the steady state parameters were again measured. In this manner, the gas velocity was decreased incrementally until severe channeling occurred or the apparatus torque limit was reached. From a dimensionless plot of bed pressure drop as a function of gas velocity, the minimum fluidization velocity can normally be determined for free flowing powders. Bed expansion and stirrer torque were also plotted. The column was sealed air tight at the completion of the characteristics experiments to await the next experiment.

Residence Time Experiment

The bed was installed and a fluidization characteristic run was made according to the procedures given above.

Before each crack movement measuring experiment, the bed was conditioned by fluidizing at 0.265 ft./sec. gas velocity and 50 rpm stirring speed for 3 min., then without shutting down, the operating conditions were set. After steady state was established, the following fluidization characteristics were recorded.

Static bed depth (noted before conditioning)

Fluid bed height

Column inlet pressure

Bed pressure drop

Mercury seal pressure drop

Stirrer torque.

A sample of flour for moisture analysis was taken at this time.

Particle slip surface voids descending into the grid area were timed for travel over 1, 2, and 3 in. according to the following rules:

1. The void must have been in downward motion above the highest or "zero inch line" of the grid. The void must not have been at rest on the zero line.
2. As the void crossed the zero line, the three timers were simultaneously started.
3. Void identity must have been constantly maintained. A particular identifying feature such as a point on the edge was timed. The rest of the void might have changed shape. When identity of the specific point was lost, all timers were stopped and the event was recorded as not having gone the required distance.
4. As the void passed the "one inch line", the first timer was stopped; as the "two inch line" was passed, the second clock was stopped; and as the "three inch line" was reached, the third timer was stopped.
5. Times were then recorded; the timers were not reset

to zero, but left as is. Cumulative times were recorded so that the individual times could be found by subtraction of the before and after clock readings.

6. The net travel time was measured. A void might have crossed either the one or two inch line, but later be slowed or driven upward before reaching the next line. If void identity was maintained, even though the void was driven up past the last line, when it finally did reach the lower line, then the timer was stopped.
7. Either about 70 voids were measured or the run was terminated after 1 hr.

The fluidization characteristics were again determined after the voids were measured.

Final samples of flour for moisture analysis were taken just before the bed was shut down. The entrainment during the residence time or mixing experiments was determined by measuring the gain in filter weight during the timed period of fluidization.

It should be noted that the same void was measured over the 1, 2, and 3 in. of travel. The times for the 2 and 3 in. of travel were cumulative times since they included the time for travel over the previous intervals. Thus the three times were not completely independent.

The average travel time for a given fixed distance was computed along with the standard deviation about that average by employing the following relations.

$$\bar{t} = (\sum t_i)/n \qquad [20]$$

$$S = \left([\sum (t_i - \bar{t})^2]/(n - 1)\right)^{1/2}$$

(Voids requiring longer than the semi-arbitrary limits of 25, 50 and 75 sec. for 1, 2, and 3 in. of travel were excluded from the calculations since most of the values were below these limits and the ones above these limits would have undue influence on the statistics. Few points were outside these limits and these points were the result of voids which were pushed up by bubbles.) From the average time and the fixed travel distance, the harmonic mean void rate was calculated.

$$1/\bar{v}_H = \sum v_i^{-1} \quad \text{or} \quad \bar{v}_H = d/\bar{t} \qquad [21]$$

Mixing Experiments

The process of mixing a trace amount of salt added to the surface of a fluidized bed was studied using two types of sampling methods (87). Samples were collected as a function of time while the bed was fluidized and, after fluidization, as a function of location in the settled bed. In addition,

the scale of scrutiny was briefly studied.

All mixing runs performed in this investigation involved measuring the "mixing curve", that is, the course of mixing a tracer with the flour or starch as a function of time. In these experiments, the course of mixing was followed by intermittently collecting samples of solids from a tap located just above the gas distributor. The tracer concentration of each sample was later measured and the concentration plotted as a function of time. These plots were then used to determine values of the mixing performance characteristics.

Settled bed sampling involved collecting samples from known locations in the settled bed after fluidization. In the present study, samples of the settled bed were collected after certain mixing curve experiments during which steady state mixing should have been obtained. In this case, time was not a variable and the sample variation with location could have indicated the existence of segregation in the bed. Comparison of the bed samples with those obtained during the mixing curve experiment were expected to indicate any segregation due to withdrawal of material from the bottom of the fluidized bed.

In the scale of scrutiny experiment, the effect of sample size on the apparent mixture homogeneity was determined. Smaller sizes of steady state mixture samples were taken from flow samples collected just after each of 30 regular samples

and from settled bed locations adjacent to each of 36 regular sample sites. The tracer concentration variances of the smaller samples were compared with the regular sized samples.

Fluid bed sampling

The mixing curve experiments were executed according to the previously discussed and tested procedure (87) described below. A modification of this procedure required for sampling the settled bed is also discussed. The basic procedure was performed as follows:

1. If needed, make-up solids were added. The bed was conditioned by fluidization for 20 min. at a gas velocity of 0.24 ft./sec. with a 50 rpm stirring speed, then fluidization was stopped. The filter was weighed, emptied, and reweighed.
2. The tracer injector, filled during the conditioning period with weighed tracer salt, was fitted into the column.
3. The bed was fluidized at the experimental operating conditions.
4. Two moisture samples were taken.
5. The bed characteristics were measured at the run conditions.
6. Simultaneously, tracer was added to the bed, sampler rotation was started, and the sample flow was started for the first sample.

7. Filled test tubes were removed manually from the disc and empty ones added at the proper locations on the disc.
8. When the time interval was long enough, the solids flow was stopped between samples and restarted just before the sample was collected to purge the line.
9. After the last mixing sample was collected, the bed characteristics were recorded and two moisture samples were collected.
10. The solids flow rate was measured by weighing the flour collected in a tared vacuum flask during a period of about 20 sec.
11. Fluidization was stopped and the settled bed depth recorded.
12. The purged flour was swept up and weighed.
13. Grab samples were taken of the weighed and mixed filter material collected by the entrainment filter during the run.
14. Tracer salt adhering to the injector was recovered by washing with water.
15. Later, the samples were analyzed by methods described below.
16. The tracer metal concentration was plotted as a function of time. After the material balance was completed, the metal concentration was made dimen-

sionless by dividing by the steady state concentration and plotted as a function of time.

When sampling of the settled bed was to be performed, the fluid bed sampling procedure had to be modified. The mixing curve experiment was performed by the same procedure (steps 1 to 8 above) except that the bed was shut down abruptly at the instant the last sample was collected. This was achieved in the following manner:

Two moisture samples were collected at intervals between collection of the last five mixing samples. An attempt to measure the solids flow rate was also made. The fluidization characteristics were not measured at the end of the experiment. As the last mixing curve sample was collected, the stirrer and gas flow valve were turned off simultaneously. The bed was allowed to settle and the settled bed depth was recorded. Steps 12 to 16 were performed as with the other mixing curve experiments.

Settled bed sampling

Settled bed samples were collected as a function of bed location after a mixing curve experiment was performed by the modified procedure described above in which fluidization was abruptly stopped at a known time.

The development of this sampling procedure and the sample thief employed have been discussed elsewhere (87).

This procedure could be performed only in the plastic column which was equipped with a series of sample ports (see Apparatus). Samples were collected at the locations indicated in Figure 21 and Table 4.

Table 4. Location of settled bed samples

Sample letter	Elevation in.	Sample number[2]	Location[1] in core, in.
A	30	1 or 7	0.25
B	24	2 or 8	0.88
C	18	3 or 9	1.75
D	12	4	3.5
E	6	5 or 10	4.88
F	0.8	6 or 11	5.5
		12	2.88

[1]Distance along core from the thief blade to center of sample, except at elevation F where samples 1, 4, 7 and 10 were 0.25 in. from the wall; samples 2, 5, 8 and 11, 0.88 in.; samples 3, 6, 9 and 12, 2.25 in.

[2]See Figure 21.

The procedure is described for a bed of cohesive solids such as flour. It was difficult to extract a full 5.75 in. flour core sample, uncompacted, from the thief. Smaller samples, up to about 3 in. long or so, could be recovered uncompacted by the described technique. A modified technique

Figure 21. Cross sections of column showing radial location of settled bed samples and annuli of equal areas (for key, see Table 4)

a. Elevations A through E

b. Elevation F

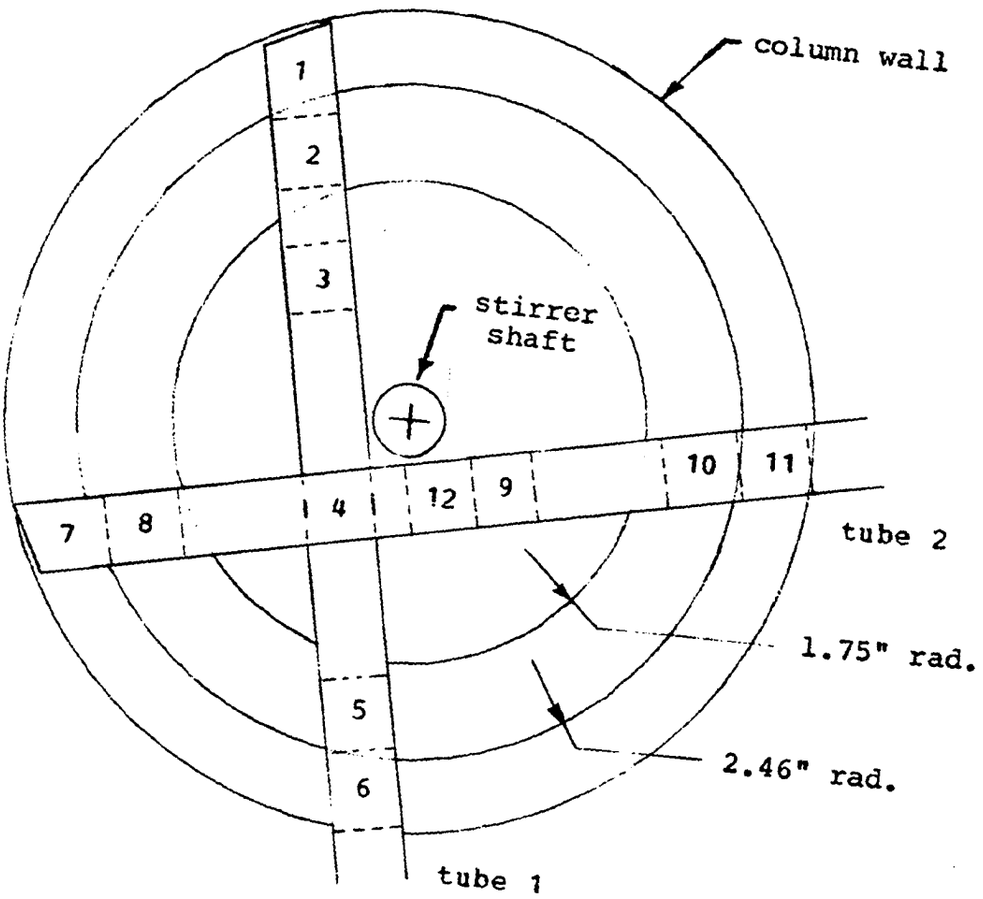
column wall
1
2
3
stirrer
shaft
10
11
7
8
4
12
9
tube 2
1.75" rad.
5
2.46" rad.
6
tube 1

(a)

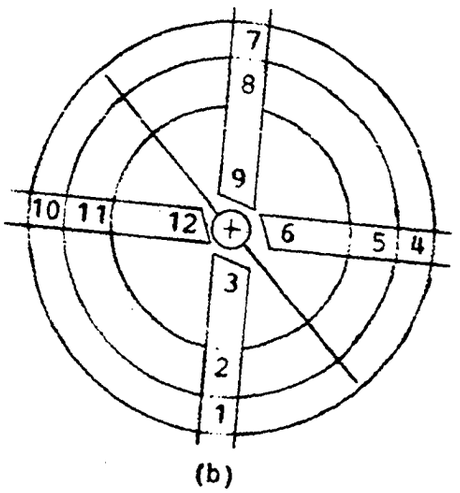
7
8
9
10
11
12
6
5
4
3
2
1

(b)

was used for sampling beds of free flowing solids.

The sample intervals of the core to be collected were marked with pencil in reverse order on the thief tube with an allowance for the column wall thickness. The samples were collected in the following manner:

1. The thief guide was positioned at the highest elevation level and the mounting block pins inserted into the guide strip holes.
2. With a razor blade, an "X" of size just smaller than the tube diameter was cut in the polyethylene film of the front port for insertion of the sample thief.
3. The sample thief (with the rod drawn back as needed) was placed against the guide block with the beveled end parallel to the far wall section.
4. The sample thief was slid slowly along the guide block and was inserted into the cut film, which stretched to accommodate the thief.
5. Samples 1 and 2 were usually removed at the same time. The tube was inserted until the end mark or location 2 was adjacent to the outer column wall. The rod was maintained near the powder bed.
6. The tube was given about a quarter twist to shear the sample from the flour bed. Occasionally, a slight lateral movement was required.

7. The thief assembly was carefully slid back along the guide block, removed from the port, and horizontally carried, holding the tube and rod, to a convenient table top.
8. The thief's sample end was placed on glassine paper and the thief assembly held at a slight angle with horizontal. The rod was held fixed, and the tube was slid back, up the rod. The sample was left on the paper. A razor was used to cleanly cut the two samples which were then transferred to tared papers.

   Alternately, tared glassine paper was used initially and the first sample only was similarly removed from the thief, the sample being cut from that remaining in the tube. The second sample was similarly placed on its tared paper.
9. The condition of the bed sample "tunnel" was checked to see that all the sample had been extracted with the thief. Any remaining pieces were recovered with the thief or a thin spatula.
10. The samples were weighed. If a sample required more material, it was collected from the corresponding location in the tunnel floor or ceiling. The samples were transferred to 125 ml. Erlenmeyer flasks for tracer concentration measurement.
11. The tube was cleaned with an air hose and the rod

was wiped clean.

12. The next bed core section was removed by the technique indicated in Steps 3 to 11. Material between samples was collected and used for an average moisture measurement of that elevation's samples. Excess material was discarded.

13. After samples 1 to 6 had been removed from the bed, another tube (the retaining tube) was inserted to prevent the tunnel from caving in while a second series of samples were collected normal to the first series.

14. The second series (7 to 12) of samples, up to the retaining tube, were collected as described in steps 3 to 12. Note that the locations of the second series of samples along the core corresponded with those of the first series, except for number 12. The retaining tube was removed and the remaining samples were similarly collected.

15. After all samples at an elevation had been collected, the thief guide was lowered to the nest elevation as in step 1. The finished sample ports were closed with cut off rubber stoppers.

16. The bottom samples were collected in a slightly different manner. The pressure taps and sample taps were removed. The 5/8 in. diameter holes in the

bottom flange served as the thief guide with the thief resting on the bottom of the hole. The innermost samples were collected as close to the stirrer as possible.

In sampling free flowing solids, the complete core sample was removed from the bed. On inserting the tube, the rod was held against the sample during the whole process. The angle of repose of the material would limit the length of core which could be obtained (87) and also caused the end sample to be smaller. For very free flowing materials, the traditional thief designs (87) are more suitable than the cohesive powder thief.

Scale of scrutiny

The effect of sample size on the apparent mixture homogeneity was investigated using mixing curve and location samples.

1. An additional 30 smaller samples of the steady state mixture were collected in some mixing curve experiments by placing a second test tube just after the regular test tube.
2. The material in the test tube was mixed with a spatula.
3. Various small sample sizes were weighed out and the tracer concentration was determined.
4. The mixture homogeneity indicated by the small sam-

ples was compared with that determined from the regular sized samples and with each other.

5. Samples were also collected from the settled bed at locations adjacent to the regular sized samples and steps similar to steps 2 to 4 above were performed.

ANALYTICAL TECHNIQUES

Powder Properties

Angle of repose

The static angle of repose was determined by pouring a cylindrical mold full of powder, leveling the top, and raising the mold from its pedestal. As the mold was raised, powder flowed out, leaving a cone of material. From the known pedestal radius and the measured cone height, the angle of the surface of the cone with the base could be calculated. This is the static angle of repose. The detailed procedure and its application were discussed in a previous study (87).

Bulk density

Bulk density of the fluidized materials was determined from the bed mass charged to the column and the settled height of the briefly fluidized bed. The density of Cab-O-Sil was determined by the weight contained in a 1.00 l. graduated Erlenmeyer flask filled to the 900 ml. mark. The material was packed as loosely as possible. The bulk density of the salt tracer was estimated from the weight of material poured loosely into a graduated cylinder.

Moisture content

The moisture content of a powder was determined by weight loss during 24 hr. of drying in a vacuum oven at

105°C. Samples were usually about 2 g. Details of this procedure were discussed in a previous study (87).

Particle Density

The procedure used to determine the particle density was essentially that used by Nazemi (84). A liquid of known density was sought which wetted, but did not dissolve the particle and was not absorbed by the particle. By adjusting the solution density with another suitable, completely misicible liquid until the particles remained in suspension, the particle density was found.

The liquid system used for flour and starches was carbon tetrachloride and ethyl benzene. For Microthene and other less dense materials, methanol and water were used.

The particle density was determined as follows:

1. A small amount of particles was placed in a 10 ml. beaker containing the pure dense liquid. The contents were stirred and the particles allowed to settle or rise.
2. Similarly, a small amount of particles were placed in the pure light liquid.
3. When the density of the particles was bracketed by the pure liquids, solutions of intermediate density were made by mixing various amounts of the pure liquids. Particles were added to a series of inter-

mediate solutions and settling or rising was noted.

4. About 250 ml. of the solution having a density close to the particle density was made up. The density of this solution was adjusted until the solution density was such that the particles remained suspended for at least 2 hr.
5. If the particles settled in this solution, more of the dense liquid was added; if they rose, more of the light liquid was added. Tests were now made in graduated cylinders. To account for evaporation, the tests were performed with about an inch of liquid in the cylinder with the particles. At least 70 ml. of the solution was stored in a similar cylinder. Both were covered with watch glasses.
6. After the suspension remained for at least 2 hr., 50 ml. of the solution was pipetted into a tared volumetric flask. From the weight of the 50.00 ml. of solution, the density of the solution was calculated.
7. The particle density was taken as being equal to the solution density which maintained the suspension for at least 2 hr.

Particle Shape and Size

Literature review

Flour shape A particle shape factor relates particle size based on the definition of one type of particle diameter to that based on another type. The general topic of particle shape is discussed in several publications (1, 44, 98).

Wilson and Donelson (133) reported that flour particles have a thickness to length ratio of about 0.5. It was their experience that flour particles appeared to be irregularly shaped since the particles usually became oriented on a microscope slide with the largest diameter normal to the optical axis. Examples of calculating the linear and volumetric shape factors were given (133).

From microscope data, the linear shape factor, a_l, is determined:

$$a_l = (6x10^{-12}/\pi\rho N(d')^3)^{1/3} \qquad [22]$$

where

N = Number of particles/g. from microscope count

$(d')^3 = \sum nd^3/\sum n$

The linear shape factor is related to the volumetric shape factor a_v

$$a_l = (a_v)^{1/3} \qquad [23]$$

since

$$a_v = 6a_v'/\pi$$

where

$$a_v' = 1/\rho\ N\ (d')^3$$

The linear shape factor as a function of flour size fraction was determined (133) for a given flour. The linear shape factor ranged from 0.641 to 0.877 as particle size increased. Most values were around 0.76.

Another method of calculating shape factors is based on the fact that different measuring techniques measure different particle diameters. For example, the statistical average diameters are calculated from uncorrected Coulter Counter data and microscope data (133).

$$d_{nl} = \sum nd/N \qquad d_{ls} = \sum nd^2/\sum nd$$

$$d_{sv} = \sum nd^3/\sum nd^2 \qquad d_{vm} = \sum nd^4/\sum nd^3 \qquad [24]$$

The ratio for each average diameter (i) is then calculated:

$$a_l = d_i \text{ Coulter Counter}/d_i \text{ microscope} \qquad [25]$$

This value should be equal to the linear shape factor comput-

ed above. The moments used to calculate d_{nl} and d_{ls} are more sensitive to sampling variation and counting error than those of d_{vs} and d_{wm}.

Sizing considerations Size is the fundamental property of a particle which best describes its state of subdivision (1). Likewise, the particle size distribution is a fundamental characteristic of a powder. A powder's flowability, solubility, gas adsorptivity, chemical reactivity, and its interaction with fluids are several phenomena influenced by particle size and its distribution. Because of its extensive effect on powder behavior, the particle size distribution is generally the most informative powder parameter.

Allen (1) summarized eight definitions of particle size based upon different particle properties, as well as various statistical diameters.

The first step in particle size analysis involves measuring the size distribution. The general features of the commonly used particle size measurement techniques have been adequately discussed (1, 14, 44, 48, 91).

The second step in particle size analysis involves summarizing and then interpretating the data. Generally for purposes of comparison of powders and for economy in publishing particle size data, the experimental size distribution is fitted by one of several frequency distributions (98).

Frequently, the fitted distribution may be expressed by two parameters, an average size and a deviation measure. Many powders are fitted at least approximately by the log-normal distribution. The details of fitting this distribution and the subsequent calculation of the common statistical averages have been described by Irani and Callis (48). The use of graph paper with special coordinates provides a short cut (114). Randolph and Larson (98) discussed the gamma distribution, a distribution which results naturally in crystallization processes. They extensively tabulated and discussed the total, average, and cumulative parameters for the normal, log-normal, and gamma distribution functions. The reader is referred to the works of Allen (1), Irani and Callis (48) and Randolph and Larson (98) for a full discussion of statistical average sizes, size distribution fitting, and utilization.

Even though particle size measurement has been studied thoroughly and well-known techniques are available, a brief discussion of the methods used in the current work is warranted because of the difficulty encountered in determining the flour particle size distribution. Differences in size were reported previously (10, 84) for samples from the same flour shipment.

Two particle size measurement techniques were employed for determining the size distribution of the powders used in the current study. The size distributions of flour and

potato starch were determined using a Coulter Counter. The size distributions of the tracer salts used in the mixing study were measured by dry, electro-mesh sonic sifting. The Microthenes were measured by ordinary dry sieving.

Coulter Counter A Coulter Counter measures the volume of a particle suspended in an electrolytic solution and counts the number of particles in a size interval (1, 21). A small, controlled amount of suspension is caused to flow through a sapphire orifice in the side of a glass tube. Electrodes immersed on each side of the tube measure the electrical resistance across the orifice. As a particle passes through the orifice, the electrical resistance changes. A voltage pulse proportional to the volume of the particle is generated and counted. The response is independent, in practice, of the electrical resistivity of the particle. This enables the instrument to be calibrated by use of standard, monosized powders of known diameters for each electrolyte and orifice diameter.

Lines (69) discussed sampling procedures for the Coulter Counter and compared instrument models for reproducibility. Instrument reproducibility of the multichannel Model T, measuring polypropylene beads as a function of total number of particles counted, was reported as an average 2 standard deviations at each size level of ±0.70 wt. % for 100,000 particles, ±1.5 % for 10,000 particles, and ±4.2 % for 2700 parti-

cles. The use of electronic conversion of the raw number data to volume data feature of the Model T gave results within 0.3% of manual calculation.

One coning and quartering operation on a 0.5 kg. cement sample resulted in a spread of up to 6 % at any size level in the cumulative distribution. A random grab sample lead to an error up to ±6.5 % (2 standard deviations) on the same cement sample. The apparent reproducibility value of single channel instruments normally includes sampling, dispersion, and statistical deviations.

The theoretical errors induced in the transformation of particle size distributions determined on a number basis to a mass basis have been calculated and discussed (51) for log-normal distributions differing in size range and sample size. It was found that order of magnitude errors could occur, especially for small populations. The confidence level of the number distribution was shown and data relating the magnitude and probability of occurrence of error in the mass distribution to the absolute number of particles counted and the type of parent size distribution were presented. The greater the number distribution confidence, the smaller the transformation error was. At a constant confidence level, the greater the size range was, the larger the error became. It was concluded that if the errors were to be small, that the number distribution data could be transformed to mass distribution

data only when a large sample of narrow size range was considered.

Application of the Coulter Counter to flour particle sizing has been discussed (47, 49, 132, 133) and the results compared with those obtained by other techniques (47, 49, 133). The electrolytic solution used was 4 or 5 wt. % ammonium thiocynate in anhydrous isopropanol (47, 132, 133). The alcohol freely dispersed the particles. The particles did not swell or contract even after 6 hr. of immersion (132). Standard procedures were followed.

Irani (47) compared the results of analyzing flour with a Coulter Counter with those obtained by sedimentation and microscopic electronic sizing and counting. Different operators and two Coulter Counters were used. All the samples tested followed the log-normal distribution. The geometric mean diameter and the geometric standard deviation on a weight basis were evaluated in the size range of 10 to 100 microns with a precision of ±2 microns and ±0.08, respectively, at the 95% confidence level. It is claimed (47) that if the ratio of the largest to smallest diameter drawn through a particle's center of mass does not exceed four, the size (as defined as the average of all diameters through the center of mass) should be independent of measurement technique within an experimental error of ±5%. Sedimentation and microscope techniques agreed well. However, Irani used a novel calibra-

tion procedure to correct the Coulter Counter results in order to obtain agreement with the other methods. Since good agreement was obtained between methods used to determine the size of irregular glass particles without a shape factor correction, Irani believed the correction for flour and some other materials to be more complex than that due to just shape. The Coulter Counter results for a flour of large average size (geometric mean of 45 microns) did not require correction (49) but those for a flour of small average size (8 micron) did.

In a later study, Wilson and Donelson (133) compared Coulter Counter and microscopic analyses. Two independent comparisons were used. First linear shape correction factors for the microscopic measurements were calculated and applied. Good agreement resulted. Secondly, linear shape correction factors calculated from the ratios of the moments of the uncorrected microscopic and Coulter Counter distributions were calculated and compared. Agreement within experimental error was obtained. It was concluded that the microscopic method was oversizing and that the shape correction factors should be applied to the microscope data to obtain good agreement between the two methods.

Sizing procedures

Coulter Counter The particle volumetric size distributions of the flours and potato starch were determined using a Model TA Coulter Counter (Coulter Electronics, Incorporated, Hialeah, Florida). The general instrument operating procedure and settings were those recommended by the manufacturer (21).

A 4% by weight solution of ammonium thiocynate in anhydrous isopropanol was the electrolytic solution (47, 133). The solution was filtered through a 4 to 5.5 micron, fritted glass filter. Since the background count was negligible, no background correction was required.

Grab samples of previously coned and quartered flour samples were used. Potato starch samples were grab samples of a larger grab sample. Two or three determinations on each slurry sample were made. For each material, two or three slurries were made from each of the original samples of flour.

A slurry density of about 0.15 g. of flour/liter was used. Unfortunately, more dilute slurries were not used, and thus the coincidence of two particles passing through the orifice simultaneously was not shown to be insignificant. Coincidence at this slurry level was not expected to be significant, however. No statistical corrections for coin-

cidence were applied.

The particles dispersed freely. A round bottom, well stirred, 250 ml. glass beaker was used.

A 280 micron orifice was selected since it adequately covered a size range from 6 to 120 microns. A wide size range for flour was expected. No blockage was encountered. Calibration of the orifice was performed with standard, monosized (19 to 20 micron) ragweed pollen. The instrument was equipped with an "external Size Calibrator". The main ragweed peak was placed in channel 7 with the half as large peak occurring in channel 6.

The Model TA Coulter Counter determines the size distribution from a single sample of slurry flowing through the orifice. The distribution is divided into size intervals and recorded in up to 16 channels. Usually 15 channels were active for flour and 13 for potato starch. This model counter electronically converts the measured number distribution into the volumetric distribution. This distribution and the total number of particles counted (in the sample and within the size range) are the instrument's output. These were read from the digital display.

In the reported results, about 50,000 flour particles and 30,000 potato starch particles were counted per sample using the instrument's time mode of operation. Sampling time was set at 15 sec. During that time, about 4.9 ml. of slurry

was drawn through the orifice.

From the total particle count (N_T) and the volumetric frequencies (V_i, i = 1 to 16 channels), normalized to total 100%, the number distribution was calculated[1]. Each volume percent in a given channel represents a relative number of particle pulses (P_i) where

$$P_i = 2^{(16 - i)}, \quad i = 1 \text{ to } 16 \text{ channels} \qquad [26]$$

The relative number of pulses in each channel, VP, are reduced to actual numbers by setting the sum of all relative numbers proportional to the total number count

$$(\sum V_i P_i)K = N_T \qquad [27]$$

The number of particle pulses in channel i is thus $V_i P_i K$.

The cumulative percent above the given size distributions were calculated and plotted in the usual manner in log, probability graphs from which the geometric means and the geometric standard deviation were determined, assuming log-normality.

---

[1] Kinsman, Shepard. Coulter Electronics, Incorported, Hialeah, Florida. Conversion of volumetric frequencies to number frequencies. Private communication to Dr. M. A. Larson, Ames, Iowa. 1972.

Electro-mesh sieving The size distributions of the salt tracers were determined using electro-mesh screens in a Sonic Sifter, Model L3P (Allen-Bradley Company, Milwaukee, Wisconsin). In this sieving technique, sonic vibration is used to promote powder fluidity and break up agglomerates. By using carefully manufactured fine sieves, smaller sizes can be separated than with regular sieving apparatus. Weighings were made on a 0.01 mg. least scale division balance. Experimental procedures were carried out in a constant temperature and controlled humidity room.

The analysis was performed according to the following procedure:

1. Carefully handling the sieves without gloves or tongs, accurately weigh and assemble the first screen stack of electro-mesh sieves: fines collector, a deep 45 micron sieve, shallow 53 micron sieve, deep 60 micron sieve, shallow 74 micron sieve, and top cone and diaphragm. (Be sure "top" side of the latex diaphragm is up.)
2. Weigh accurately about 2.00 g. of tracer material on a folded, tared glassine paper. Then transfer the sample to the top screen. Reweigh the glassine paper.
3. Replace the cone and diaphragm on the stack and

lock the assembly.

4. Place the stack in the sifter, unlock, and check stack alignment. Sift 6 min. at a sift setting just large enough to cause the largest particles to move about on the top screen (sift = 3 used) and adjust pulse setting to a value high enough to break up agglomerates (pulse = 5 for copper and nickel tracers, 8 for zinc tracer).
5. After 6 min., lock the stack and remove it from the sifter.
6. Accurately weigh the cone and diaphragm, each sieve, and the fines collector, saving all material.
7. Weigh accurately and assemble the second sieve stack: fines collector no. 2; deep 10, 20, 30 micron sieves; and the cone and diaphragm.
8. Reweigh the fines collected in stack 1. By gently pouring, analytically transfer these fines to the top screen of stack 2. Replace the cone and diaphragm and lock the stack. Reweigh the "empty" fines collector of stack 1.
9. Place stack 2 in the sifter. Sift 6 min., adjusting the sift and pulse settings as in Step 4 (sift = about 2 and pulse = 10 were needed for these smaller particles).
10. Repeat Steps 5 and 6.

11. Observe the particles on the screens under a binocular microscope for shape, and agglomeration state.

12. Empty and clean the sieves, fines collectors, and cone and diaphragm according to special handling techniques. The cleaning procedure consists of first holding the sieve so that the screening is in a vertical plane. Then rinse the sieve with distilled water running at a slow rate from a rubber hose in such a manner that the stream is never directed on to the screens (or latex of the fines collector or diaphragm). Instead, the flow is impacted on the upper, plastic rim such that a film of water flows down the screen. The stream is moved gently aroung the rim on both sides of the screen. Be sure to always keep the screen vertical. The weight of the water film or the stream impact on the fine screens may cause tears. Next, the sieves are individually, vertically immersed in soapy, distilled water and put into a sonic cleaner for 5 min. After that time, the sieve, still vertical, is removed and rinsed. The sieves are placed, still vertical, on a paper towel in a hood for air drying. The latex fines collector is turned inside out for cleaning by holding the metal ring and

simultaneously rising and twisting the metal base plate. The collector is wetted by directing a slow distilled water stream on to the base plate, allowing water to flow down the latex sides. A soap film is formed by rubbing soap particles between one's thumb and first finger until no particles can be felt. The soap film is then gently spread over the latex. The collector is rinsed in the same manner by which it was first wetted. The collector, still inside out, is supported on a pedestal by the metal base plate and allowed to air dry. Maintaining the diaphragm in a vertical position, it is similarly washed, rinsed, and dried.

13. The weight distribution is calculated from the weight of sample on each screen with allowance for incomplete recovery of the stack 1 fines.

Regular sieving A sieve analysis of the Microthenes was made using standard 8 in. diameter sieves and a Ro - Tap shaker. Sieves of 707, 595, 500, 420, 354, 250, 210, 177, 149, 125, 105, and 88 microns and a pan were run in two stacks. Loading guidelines suggested in ASTM Methods (2) were followed. Three 50g. samples were run. A shaking time of 15 min. was used as no significant changes occurred on shaking an additional 10 min. The difference between the sum of weights on each screen and the initial test sample weights

were within the allowed closure limits (about 0.9 g.). Some electrostatic charging occurred as some particles repelled one another when poured into a graduated cylinder. Some material adhered to the screen walls and glassware, but no material was on the screen wall immediately after shaking.

Gas Humidity

The general procedure and apparatus for measuring gas humidity used in the present work was used by Nazemi (84). The dew point of a gas stream bled from the main line (see apparatus) was determined. Also knowing the dry bulb temperature allowed the relative humidity to be calculated from tabulated (94) vapor pressure data. From the measured relative humidity, the humidifier efficiency could be calculated from the pressures at the instrument and humidifier.

The dew point indicator was of the silvered mirror cup type (Model DP1 - 86A, Weighing and Control Components, Incorporated, Hatboro, Pennsylvania). The mercury thermometers used to measure the temperature of the gas in the line and of the brine in the cup had 1°F least scale divisions. An insulated beaker was used to store crushed ice. A dropper was used to remove and add water to the silvered cup.

Distilled water and reagent grade sodium chloride were used to form a brine solution cooled with crushed ice made from distilled water.

The procedure was performed as follows:

1. Carefully clean, so as not to scratch or abrade, the mirrored cylindrical surface. Clean the viewing window also. Dry the apparatus by passing air through it.
2. Attach the dew point apparatus to the humidifier bleed line connection with dry Tygon tubing. Check the dry bulb thermometer alignment.
3. Put large chunks of ice in the storage beaker along with a little water. The ice will keep for a couple hours this way.
4. Since the dew point may vary from about 24 to 40°F depending on the humidifier pressure, estimate the expected dew point from the expected relative humidity and dry bulb temperature:

$$\%RH = \frac{p^*_{\text{dew point}}}{p^*_{\text{dry bulb}}} \times 100\% \qquad [28]$$

5. Add ice, salt, and water to cup. Stir with the thermometer until the expected dew point temperature is nearly reached. Allow about 15 min. for the surface of the cup to reach temperature equilibrium.
6. Now slowly pass gas through the apparatus and look for fogging of the mirror. If necessary, cool the mirror further by adding small amounts of ice,

trying to keep the outer and inner cup surface temperatures near equilibrium. At the instant fogging starts, record the brine temperature, dry bulb temperature, and the humidifier temperature and pressure. (The flow rate of gas through the indicator did not seem to affect the reading, but using a slow flow rate helped prevent rapid accumulation of moisture drops on the mirror.)

7. Remove ice or add slightly warmer water while stirring continuously and noting the temperature at which fog disappears. Keep the light furnished by a small wattage bulb off except for brief times near the fogging point and then use it only momentarily.
8. Again cool the mirror slightly and note the appearance of fog. Then repeat Steps 7 and 8 so as to narrow the temperature range between appearance and disappearance of fog.
9. Take the average of the last three dew point temperatures found on the first appearance of fog after the temperature range has been sufficiently narrowed.
10. The percent relative humidity of the gas at atmospheric pressure and dry bulb temperature is calculated from equation 28.
11. The percent relative humidity in the humidifier is

calculated from the gas humidity at the measuring conditions:

$$\frac{\%RH_{humidifier}}{\%RH_{measured}} = \frac{P_{humidifier}}{P_{atmosophere}} \times \frac{P^*_{dry\ bulb}}{P^*_{humidifier}} \qquad [29]$$

The time required for one determination is about 30 to 45 min.

Tracer Metal Concentration

The tracer metal concentration in the mixing experiments was determined by either of two procedures, both of which were studied and discussed in detail (87).

The samples from a few early runs (Runs 10 and 11 of Sets 1,2,3; Set 2, Run 12; and half of Set 4, Run 10) were analyzed with the Dilute Sulfuric Acid Procedure (87). With this procedure, the sample was transferred to a 100 ml. volumetric flask; 20 to 30 ml. of distilled water were added followed by 4.0 ml. of 50% by volume sulfuric acid. The flask was heated to 85 to 92°C for 2 hr., cooled, and 7.0 ml. of concentrated ammonium hydroxide was added. The solution was brought to the mark with distilled water, centrifuged, and the solution metal concentration measured by flame atomic absorption spectrophotometry.

The samples which were not analyzed by the above procedure were analyzed by a much easier procedure, that of Metal

Extraction by EDTA. In this procedure, the sample was Transferred to a 125 ml. Erlenmeyer flask, 5 ml. of methanol was added, and allowed to stand 10 min. Then 10.0 ml. of an aqueous EDTA solution containing 16.0 micromole/ml. was added and the solution was allowed to stand 20 min. The solution was then filtered into 100 ml. volumetric flasks, brought to the mark with distilled water, and the metal concentration was measured by flame atomic absorption spectrophotometry. For procedural details and tests, see Nielsen (87).

PART 4. RESULTS AND DISCUSSION

One kind of macroscopic solids circulation and two kinds of microscopic circulation have been defined (117). Macroscopic circulation is the cyclic movement of particles throughout the bed such as from a region near the bed top to a region near the bed bottom and return. Microscopic solids circulation is a similar, cyclic movement of particles located either near the bed wall or in the bed interior. Three different solids circulation rates are then possible.

Timing the movement of particles observed through the transparent wall of the fluidization column provides a measure of the mean particle velocity along the bed wall, one microscopic circulation rate. Timing the movement of tracer particles within the bed by means of X-ray cine photography yields a mean velocity of the interior particles, another microscopic circulation rate. Finally, timing the movement of tracer particles from the bed top to bottom gives a measure of the macroscopic circulation rate (117), a mean rate of movement down the whole bed. These three circulation rates are not generally expected to be equal (117). However, they might be equal in special cases as for example where very cohesive solids appear to move down the column in slip-stick flow.

In the present investigation, two kinds of experiments were performed. The first measured the rate of downward par-

ticle movement at the column wall. This was accomplished by a previously developed technique (87) of timing the movement of particle slip surface voids. The results of this kind of experiment are discussed below. In the second kind of experiment, a small amount of a salt tracer was quickly distributed over the fluid bed surface and samples of the bed were collected as a function of time from the bed bottom. The results of these experiments are discussed further on.

GENERAL PLAN

The effects of operational parameters on the downward rate of solids movement at the column wall and on the mixing of trace amounts of metal salts were investigated.

Manual timing of the downward movement of particle slip surfaces (cracks) across a grid was carried out until about 70 cracks had been timed or a 1 hr. observation period had expired. Travel distances of 1, 2, and 3 in. were used. The average residence time (and the variation about that average) for each distance was computed and used as the individual element in a statistical analysis.

Mixing was studied by adding a known amount of tracer to a fluid bed's surface and collecting samples at the bed bottom as a function of time. This kind of experiment was sometimes extended to include collecting samples from various locations in a settled bed following fluidization for a long enough period of time so that the degree of homogeneity should have reached steady state. In another experimental variation, the size of the samples was reduced to see how small a scale of scrutiny the mixture could be subjected to and still have essentially the same mixture homogeneity.

The residence time and mixing studies were conducted with thirteen different beds of flour (referred to as Sets) following the statistical design of Figure 22. Set 14 reproduced the operating conditions used by Brekken (9, 11) with

Figure 22. General statistical design

Set No.	1	2	3	4	5	6	7	8	9	10	11	12	13	14
Experiments	Residence time and mixing											Mixing only		
Column	Glass				Plexiglas									Glass
%RH[1]	28							Dry						17
Material	Flour III										III[2]	[3]	III[4]	II[5]
Bed Depth	27"				31"		12.5"	31"						12.5"
% Moisture	13.9							11	7.8	2.9	14	18	13.5	7.7
Speed, rpm	25, 50, 100, 150[6]				50									19
u, ft./sec.	0.12, 0.15, 0.175[6], 0.20										[7]	[8]	0.35	0.33
Set No.	1	2	3	4	5	6	7	8	9	10	11	12	13	14

[1]Relative humidity of fluidizing gas (nitrogen).

[2]Half of runs used flow conditioned Flour III.

[3]Potato Starch.

[4]Flour III.

[5]Flour II.

[6]Condition run once.

[7]Flow conditioned flour runs: 0.07, 0.08, 0.11 ft./sec. and 0.06 and 0.08 ft./sec.

[8]0.15 and 0.20 ft./sec.

Flour I and was run to test the apparatus and procedures (87) of the mixing experiments. Sets 1 to 13 were performed (See Procedures of Fluidization Experiments.) in the listed set order.

The basic statistical "Star" design (Figure 22) of these sets was chosen for its ability to handle the rather large number of parameters involved in the study with a minimum of experimental determinations. Sufficient levels of the parameters were available for correlating the data. In this design, some combinations of parameters were repeated more than others. Furthermore, not all combinations of the parameters were run, which meant many of the factors of the statistical tests to be performed on the data were nonorthogonal. As discussed in Appendix D, the usual analysis of variance procedure was not applicable since orthogonality of factors is assumed in that method. The multiple regression model is not as restrictive, however. Briefly, the procedure followed in determining significance of the factors was to carry out analysis of variance calculations in a regression format.

The following parameters were varied between sets: column wall material (two levels), gas humidity (two levels), material fluidized (three levels), bed depth (two levels), and flour moisture content (four levels). Three levels each of gas velocity and stirrer speed were used within each set. An additional level of gas velocity and stirrer speed were

each run once during the residence time experiments. The set was also a parameter of the experimental design (a "blocking factor"). The "set effect" represents the possible differences between the beds which is not accounted for by other factors.

As mentioned above, three distances were used for the measurement of the rate of bed crack movement. Four different observers and four locations of the crack measurement grid relative to the gas distributor were employed in measuring crack movement. Two levels of tracer were used in the mixing experiments. The copper and nickel tracers were added in amounts ranging from 3.5 to 4 times that of the zinc tracer.

Each set was composed of a number of runs of the residence time experiment and the mixing experiment. The gas velocity and stirrer speed of each run are shown in Figures 23 and 24. The range of fluidization conditions for each type of experiment is summarized in Tables 5 and 6. The specific operating conditions for each run are listed in Table 16 of Appendix B for the residence time experiments and Table 21 of Appendix C for the mixing experiments. The gas velocity and stirrer speed level were randomly selected for each run in Sets 1 to 4 as a group. These runs were performed first to determine if stirrer speed had a significant effect on the residence time. An analysis of the residence time data of

Figure 23. Statistical design of residence time experiments for gas velocity, stirrer speed, and observers

The numbers are identified as follows:

1.5 = fluidization gas velocity x10, ft./sec.

50 = stirrer speed, rpm

Set Number

Run Number	1	2	3	4	5	6	7	8	9	10	11
1	1.5 50	1.2* 50	1.5 50	1.5 150	1.5 50	1.5 50	1.2 50	2.0 50	1.5 50	1.5 50	1.5 50
2	1.5* 25	1.2 50	1.7 50	1.5 100	2.0 50	1.2 50	2.0 50	1.5 50	1.2 50	1.2 50	1.2 50
3	2.0 50	1.2 50	1.5 100	2.0 50	1.2 50	2.0 50	1.5 50	1.2 50	1.5* 50	2.0 50	2.0 50
4	1.2 50	1.5 25	2.0 100	1.2 100	1.5 50	1.5 50	1.5 50	1.5* 50	2.0 50	1.5 50	1.5 50
5	1.5 100	2.0 50	1.5 25	1.5 25	---	---	---	---	---	---	1.1 50
6	1.5* 25	1.5 100	1.2 50	1.2 50	---	---	---	---	---	---	0.8 50
7	1.5 25	1.5 50	2.0 25	1.2 25	---	---	---	---	---	---	0.7 50
8	2.0 50	2.0 50	1.5 50	1.5 50	---	---	---	---	---	---	0.8 50
9	---	---	1.5 50	1.5 50	---	---	---	---	---	---	---
	1	2	3	4	5	6	7	8	9	10	11

Set Number

*Observers switched locations they timed.

Run Number	Set Number 1	2	3	4	5	6	7	8	9	10	11	12	13	14
10	1.5 25	1.2 50	2.0 100	1.2 50	2.0 50	2.0 50	1.5 50	2.0 50	2.0 50	2.0 50	1.5 50	1.5 50	3.5 50	3.3 19
11	1.2 50	1.5 25	1.2 25	1.2 100	1.5 50	2.0 50	2.0 50	1.5 50	2.0 50	1.5 50	2.0 50	2.0 50	3.5 50	
12	1.5 100	2.0 50	1.5 25	2.0 25										
	1	2	3	4	5	6	7	8	9	10	11	12	13	14

Set Number

Figure 24. Statistical design of mixing experiments for gas velocity and stirrer speed

The numbers are identified as follows:

1.5 = fluidization gas velocity x 10, ft./sec.

50 = stirrer speed, rpm

Table 5. Range of residence time fluidization conditions

Material	Moisture content %	Settled bed depth in.	Gas humidity %RH	u ft./sec.	u/u_{mf}	N rpm
Flour III	3 - 15	12.5, 28, 32	0,28	0.12 - 0.20	1.2 - 2.0	25 - 150
Flour III with 0.5% Cab-O-Sil	13.2	31	0	0.07 - 0.11	1.0 - 1.5	50

Table 6. Range of solids mixing fluidization conditions

Material	Moisture content %	Settled bed depth in.	Gas humidity %RH	u ft./sec.	u/u_{mf}	N rpm
Fluid sampling (mixing curves):						
Flour III	3 - 14	12.5, 28, 32	0, 28	0.12 - 0.35	1.2 - 3.5	25 - 100
Flour III with 1.0% Cab-O-Sil	12.5	31	0	0.06, 0.08	1.5, 2.0	50
Potato Starch	18.	32	0	0.15, 0.20	---, 4	50
Settled bed sampling:						
Flour III	3 - 14	12.5, 32	0, 28	0.15 - 0.35	1.5 - 3.5	50
Flour III with 1.0% Cab-O-Sil	12.6	31	0	0.08	2.0	50
Potato Starch	18.	32	0	0.20	4	50

Sets 1 through 4 was performed and stirrer speed was found to be an insignificant factor. The remaining sets were performed using a convenient stirrer speed, 50 rpm.

In Sets 5 to 10, the gas velocity for each residence time run was randomly selected with the constraint that each set must include all three levels and the middle level twice. A similar constraint held for each material in Set 11.

The residence time experiment involved additional parameters. Two observers were generally used to time the movement of cracks across two or four grid locations (Table 7). Each observer was assigned to one or two grids for each run. One observer generally timed the upper-grid and mid-grid locations while the other timed the lower two locations. Occasionally the assigned areas were switched (Figure 23), enabling a test for observer bias to be made. The same slip surface was timed as it traveled three distances in Sets 1 to 4; two in Sets 5 and 6; and only one distance in Sets 7 to 11.

Since the addition of tracer might of had a flow conditioning effect (29) on the bed, the residence time experiments were generally performed on a bed before the mixing experiments. The exception was run 9 which was performed after the mixing experiments as a test for the possible presence of a flow conditioning effect caused by the tracer salts.

Table 7. Additional residence time parameters

Set no.	1-4	5-6	7	8	9-11
Location, inches from gas distributor to top line of grid:					
Upper	29 1/4	29 1/4	10 7/8	29 1/8	29 1/8
Mid	---	---	8 1/2	22 7/8	22 7/8
Lower	13 3/4	13 3/4	5 1/4	13 3/4	13 3/4
Lowest	---	---	3 1/4	8 3/4	8 3/4
Travel distances, in.	1,2,3	1,3	1	1	1,2[1]
Operators, code no.	1,2	1,3,4	1,3	1,4	1,4

[1]Flow conditioned flour only.

In conducting the mixing experiments, for reason of analytical convenience, copper tracer was always added in run 10; zinc, in run 11; and nickel, in run 12 of each set. The tracer concentration level was constant for each metal in all sets. The amounts of each salt, however, were different. For example, usually 27.9 g. of copper tracer was added in run 10 of each set, 8.0 g. of zinc tracer in run 11, and 32.2 g. of nickel tracer in run 12.

FLUIDIZATION CHARACTERISTICS

Three kinds of bed behavior were observed in aerated, stirred beds of flour. Between the familiar freely bubbling bed observed at high gas velocities (0.15 ft./sec. or greater for flour) and the clearly channeled, packed bed occurring at low gas velocities (less than about 0.074 ft./sec. for flour) was a transition region of "zone fluidization". In this kind of bed behavior, some large sections of the bed are fluidized while other parts are in a dense state of solids compaction. This is an enlarged version of the "clumps" seen by Rowe et al. (108) discussed in the Literature Review. Large agglomerates or "chunks" of the denser material were seen moving down the column and also were observed to cause an increase in stirrer torque as they were chopped up on encountering the stirrer. As gas velocity was decreased to 0.1 ft./sec., the frequency and length of the periods of higher torque increased. The chunks became larger in height and cross sectional area. The bed surface was level. At still lower gas velocities, half or even two-thirds of the bed cross section appeared to be in a slowly downward moving, compacted mass which extended to the bed surface. Meanwhile, the remainder of the bed was in a bubbling fluidization state. The height of the fluid region oscillated but was frequently observed to be higher than the compacted region. The compacted region itself was higher than the settled bed.

For fluidization to have occurred at the low end of the gas velocity range for zone fluidization, the local gas flow in the fluid zone must have been greater than that in the compacted sector since the total gas velocity was less than the minimum fluidization velocity. At the interface of the fluidized and compacted sectors, shearing of the compacted region occurred. At low gas velocities, the fluidized zone rotated slowly around the column axis in the direction of the stirrer.

Various degrees of zone fluidization were observed over a wide range (0.24 to 0.10 ft./sec.) in the potato starch bed; that is, agglomerates were observed at 0.24 ft./sec. and a substantial packed region existed at 0.10 ft./sec. Zone fluidization was not observed in the flour beds containing Cab-O-Sil nor after the potato starch bed was flow conditioned by the addition of tracer salts during the mixing experiments.

For both flour and potato starch, at gas velocities below those resulting in zone fluidization, the beds exhibited channeling of the completely packed bed. Spouting occurred over a very narrow range of gas velocity, but usually at very low velocities (less than 0.074 ft./sec.), the gas carried few solids.

One bed of flour (Set 11, runs 5 to 11) was made less cohesive by flow conditioning it with Cab-O-Sil added to a

concentration of 0.5% wt. for the residence time experiments (runs 5 to 8) and to 1.0% wt. for the mixing experiments (runs 10 and 11). The Cab-O-Sil was mixed with the flour in the fluid bed itself (see Bed Installation) which was a better method compared to using a cement mixer (9) or mixing by hand (84). The very low bulk density, very small particle size, and a strong tendency to agglomerate make Cab-O-Sil a difficult material to mix with flour by the latter two methods. The flocs readily segregate from flour. Cab-O-Sil is easily suspended in air. Just pouring flour into a vessel containing Cab-O-Sil resulted in sufficient air currents to suspend some of the Cab-O-Sil. When stirred by hand or tumbled, Cab-O-Sil flocs tended to rise to the top and were not readily mixed with the flour. A lot of time and effort were thus required in the hand mixing procedure, but the resulting mixture composition was more accurately known than when mixed for 1.5 hr. in the cement mixer.

Shear mixing is required to break up agglomerates of Cab-O-Sil. In a tumbling type of mixer, shearing occurs at the interface of the downward flowing layer and the lower, static layer. The very light bulk density of the Cab-O-Sil flocs resulted in a tendency for flocs to move to the top of the flowing layer, away from the shearing zone. Shearing in a stirred, fluidized bed of flour occurs as gas bubbles pass through the bed and also as the stirrer blade sweeps material

laterally.

Adding the Cab-O-Sil to the bottom of the stirred, fluidized bed was an easy and successful method. Very little Cab-O-Sil was entrained in the gas stream above the bed. The flour in the entrainment fliter was found to not contain any flocs of Cab-O-Sil and appeared to not have been flow conditioned. A few flocs of Cab-O-Sil were seen circulating in the bed, moving straight down the bed wall at a rapid rate. Further fluidization after the 10 min. mixing period resulted in smaller and still fewer flocs. (After run 5, only a very few flocs could be found at all.)

Bed Properties

The bed pressure drop, bed expansion, and stirrer torque were routinely measured as a function of gas velocity while using a stirring speed of 50 rpm as described in the Procedures of Fluidization Experiments. These characteristics of fluidized beds have been widely discussed in the literature (4, 5, 9, 10, 29, 63, 67, 84, 87, 124, 135) and are shown in Figure 25 for a typical, freshly installed 28 in. deep flour bed. The results are similar to those previously reported (9, 10, 84).

On decrementally reducing the gas velocity from 0.31 to 0.10 ft./sec., the bed pressure drop and bed expansion decreased while stirrer torque remained constant at a small

Figure 25. Fluidization characteristics of Flour III, before Set 3

Small symbols denote maximum value; large symbols, average value

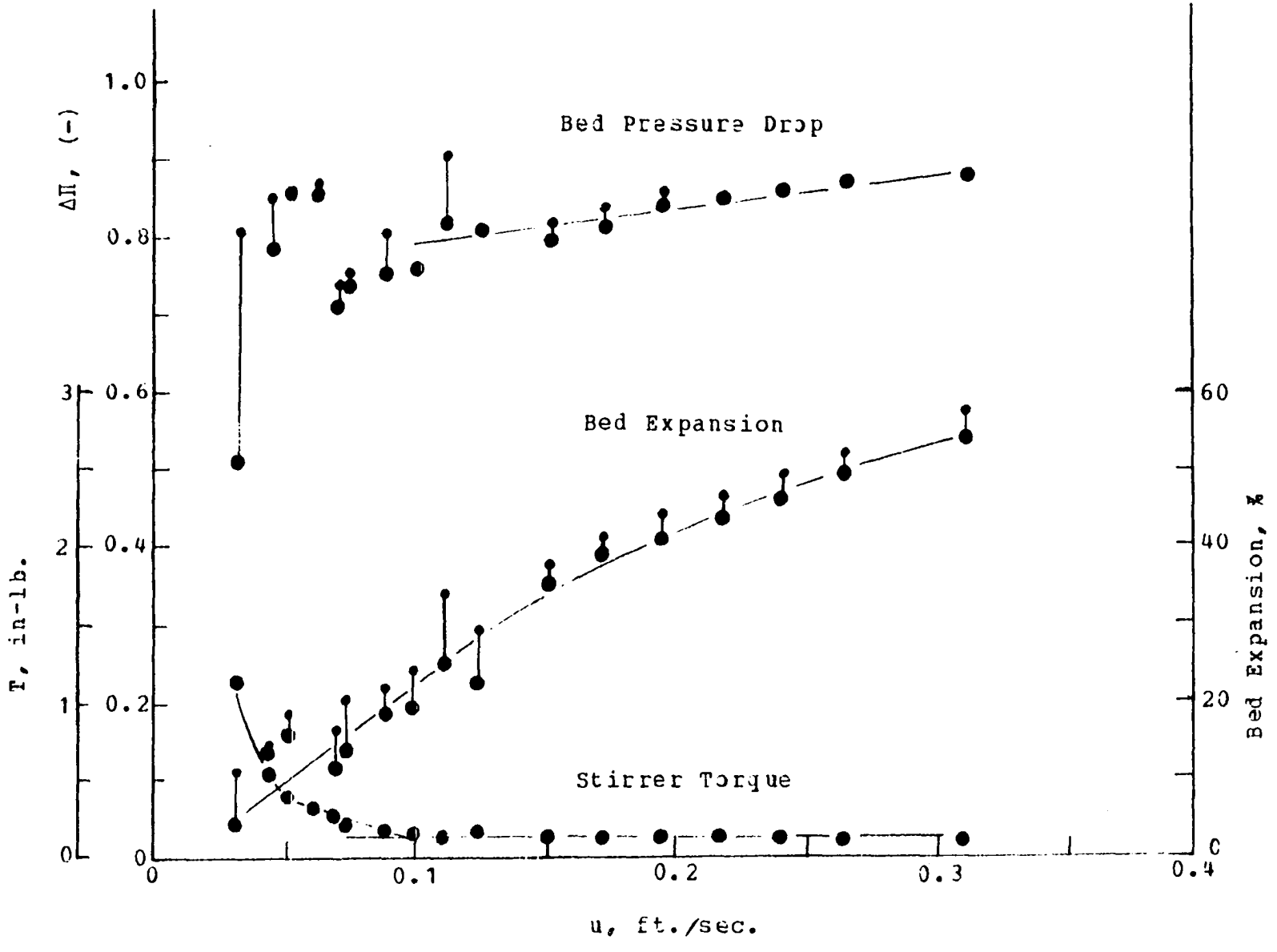
Bed Pressure Drop
Bed Expansion
Stirrer Torque
ΔΠ, (-)
T, in-lb.
Bed Expansion, %
u, ft./sec.
1.0
0.8
0.6
0.4
0.2
0
3
2
1
0
60
40
20
0
0.1
0.2
0.3
0.4

value, 0.15 in-lb. The bed bubbled vigorously for gas velocities down to at least 0.15 ft./sec. The dimensionless bed pressure drop was always significantly less than unity which indicated some structure remained in the bed (5) even under vigorously bubbling conditions. The decreased pressure drop with decreased gas velocity indicated that the percentage of the bed weight supported by the bed structure increased at the lower gas velocities. The bed pressure drop manometer exhibited small amplitude, high frequency oscillations. These oscillations were due to the passage of bubbles through the bed and the resulting changes in bed height at a given gas velocity.

The bed height was cyclic. Figure 25 shows the average and maximum bed expansion. The period of oscillation increased as gas velocity decreased. The amplitude of oscillation changed little until the gas velocity was reduced to lower than 0.15 ft./sec. Lower than that, the magnitude of oscillation increased with decreasing gas velocity. The period also increased.

As gas velocity was reduced from 0.1 ft./sec., the bed pressure drop oscillated at a larger amplitude and period, which is indicative of channeling (63). The stirrer torque increased linearly with decreasing gas velocity until a relatively low gas flow rate was reached.

The fluidization characteristics of the bed which provided the data of Figure 25 were also determined after the mixing experiments were performed with the bed, Figure 26. In this example, the bed expansion in the freely bubbling region was slightly larger than before, but generally no significant differences were observed in characteristics of flour beds before and after the mixing and residence time experiments.

The fluidization characteristics of potato starch, Figure 27, were similar to those of flour. The fluidization quality was less, however. As mentioned above, pronounced zone fluidization occurred over a larger gas velocity range than with flour. The dimensionless pressure drop across the freely bubbling potato starch bed was the same as observed for flour, about 0.82. Bed expansion was considerably less for potato starch than for flour (16% versus 53% at u = 0.31 ft./sec.). Having less expansion and a greater bed mass, it was not surprising that the stirrer torque of the potato starch bed was greater than that of the flour bed.

Figure 28 shows the fluidization characteristics of a free-flowing polyethylene powder, Microthene MN 710. On comparing the flour characteristics (Figure 26) with those of Microthene, several differences are apparent. The maximum bed pressure drop of the Microthene was close to unity (0.98) and constant over much of the bubbling bed region. A com-

Figure 26. Fluidization characteristics of Flour III, after Set 3

+ after Set 3

o before Set 3 (same as Figure 25, for comparison)

Small symbols denote maximum value; large symbols, average value

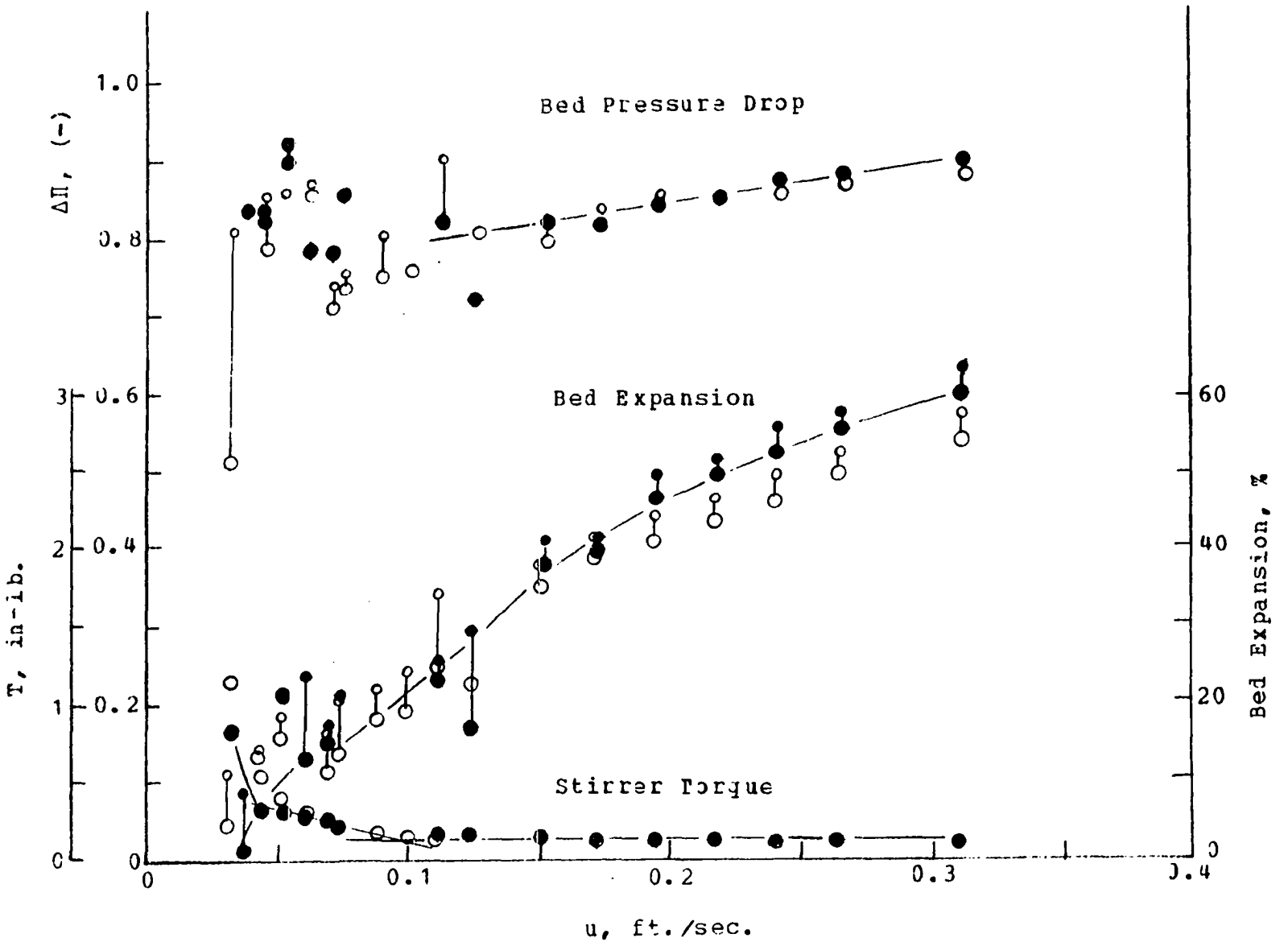
Bed Pressure Drop
Bed Expansion
Stirrer Torque
ΔΠ, (-)
T, in-lb.
Bed Expansion, %
u, ft./sec.
1.0
0.8
0.6
0.4
0.2
0
3
2
1
0
0.1
0.2
0.3
0.4
60
40
20
0

Figure 27. Fluidization characteristics of potato starch

Small symbols denote maximum value; large symbols, average value

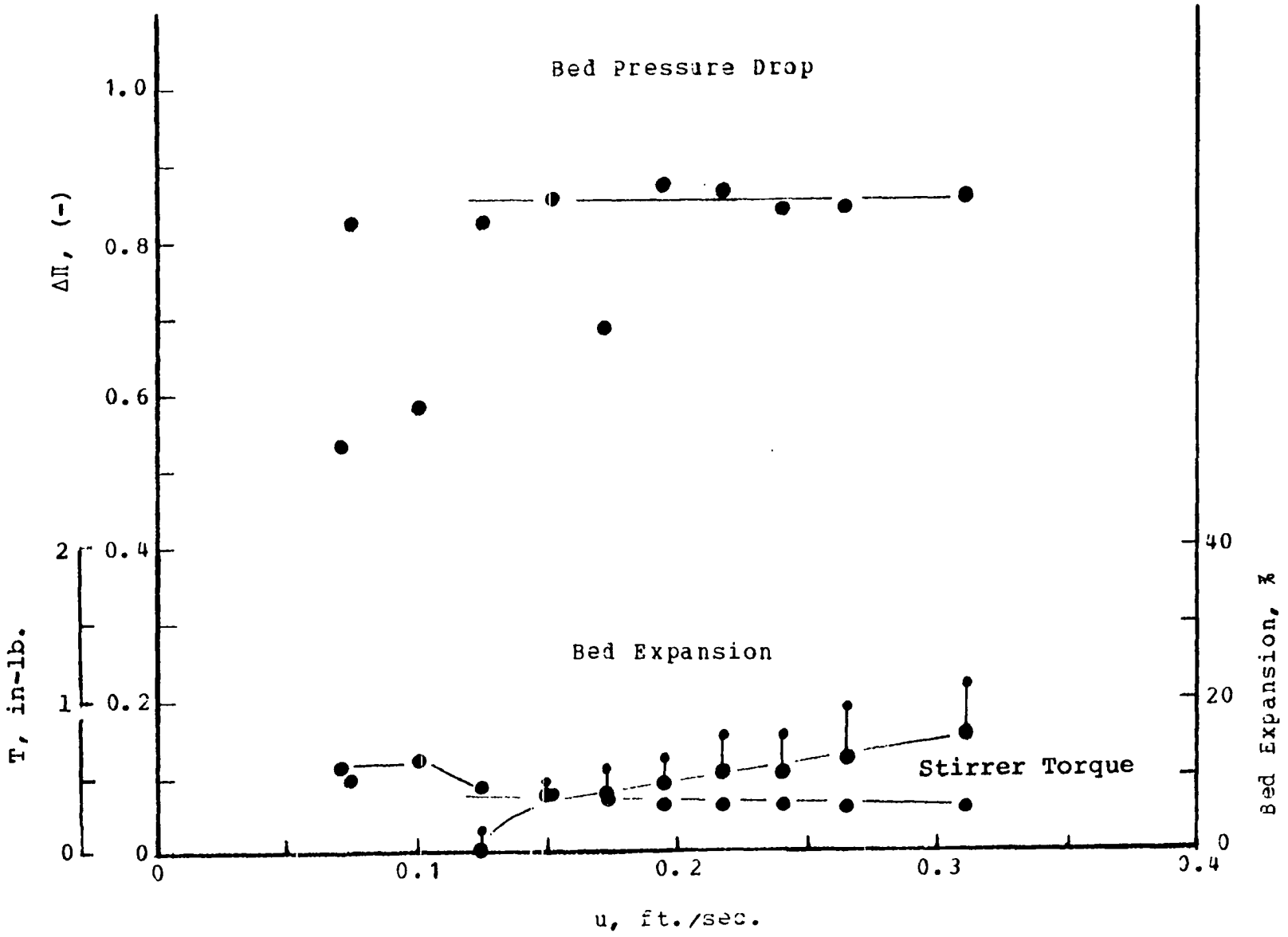
Bed Pressure Drop
Bed Expansion
Stirrer Torque
ΔΠ, (-)
T, in-lb.
Bed Expansion, %
u, ft./sec.
1.0
0.8
0.6
0.4
0.2
0
2
1
0
40
20
0
0.1
0.2
0.3
0.4

Figure 28. Fluidization characteristics of Microthene MN 710

Parameters: 30 in. deep bed, 25 rpm stirring, 0 %RH nitrogen gas

o trial 1

□ trial 2

▽ trial 3

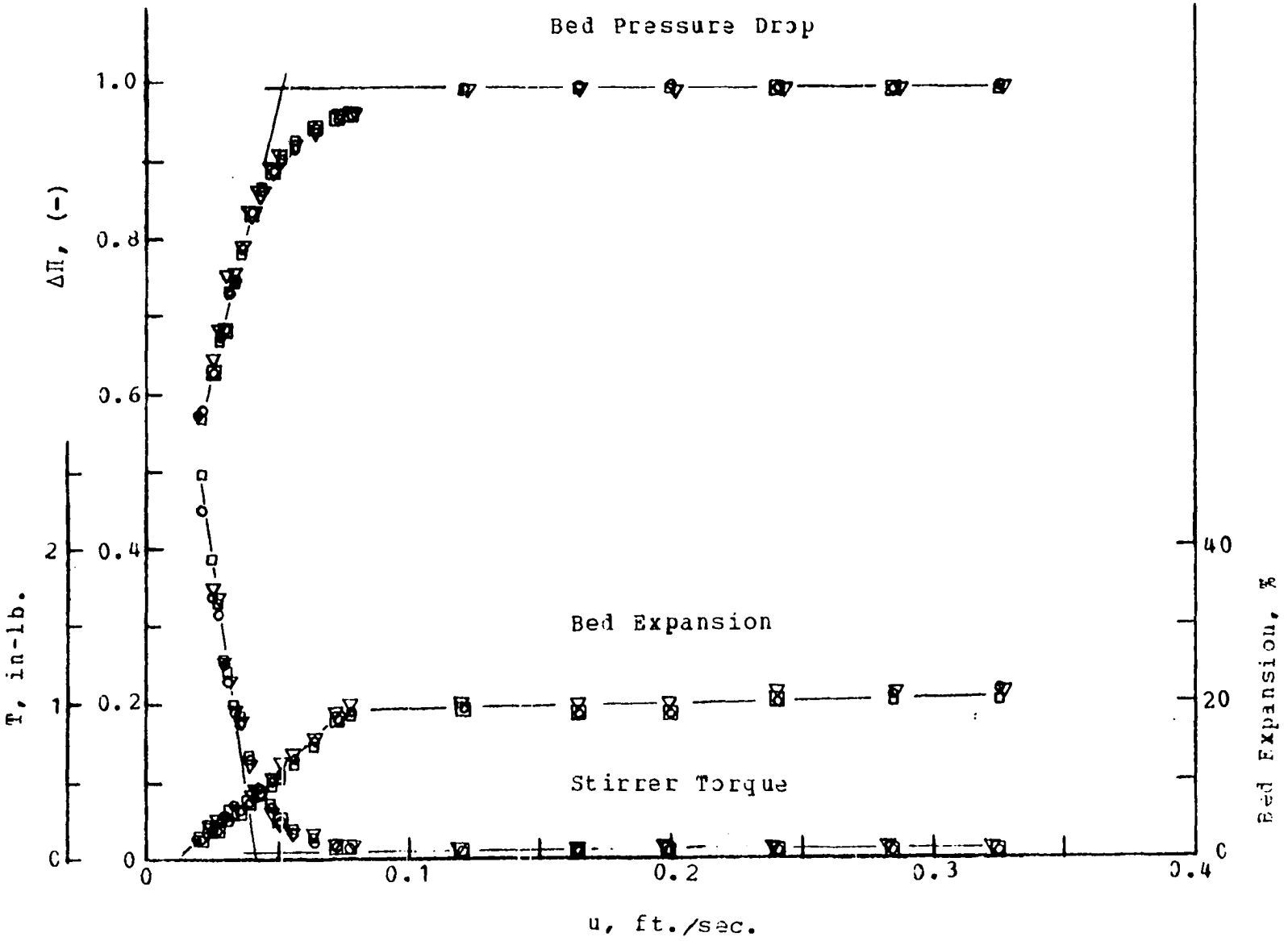
Bed Pressure Drop
Bed Expansion
Stirrer Torque
ΔΠ, (-)
T, in-lb.
Bed Expansion, %
u, ft./sec.
1.0
0.8
0.6
0.4
0.2
0
2
1
0
40
20
0
0.1
0.2
0.3
0.4

pletely structureless bed would have a pressure drop of unity(5). The pressure drop decreased linearly with decreasing gas velocity at low flow rates corresponding to the fixed bed state. The bed pressure drop oscillated some in the freely bubbling bed, but diminished as gas velocity was decreased in the fixed bed region.

The bed expansion of the fluidized Microthene bed was essentially constant and was smaller than that observed for flour. At low gas velocities (below 0.08 ft./sec.), bed height decreased linearly with decreasing gas velocity. The Microthene bed did not exhibit oscillations in bed height. If any bed height cycling existed, the period of oscillation would have to be very long compared to that of flour.

Like the flour bed, the stirrer torque of the fluidized Microthene bed was constant but slightly smaller in value.

As Cab-O-Sil was added to the fluid bed of flour, bed expansion increased from the 34% expansion of the pure flour bed to 53% when the Cab-O-Sil concentration was 0.5% wt. At another gas velocity, the bed expansion increased from 48% to 57% as Cab-O-Sil concentration was raised from 0.5% to 1.0%. The settled bed height increased 10.5% (from 30.8 in. for pure flour to 34.0 in. for 0.5% Cab-O-Sil flour) but only increased another 4.2% when the Cab-O-Sil concnetration was raised to 1.0%.

The other fluidization characteristics of the flour bed were also modified by flow conditioning with Cab-O-Sil (Figures 29 and 30). The dimensionless fluidized bed pressure drop became constant and increased (from 0.86 for pure flour to 0.94 for 0.5% Cab-O-Sil flour and to 0.96 for 1.0% Cab-O-Sil flour) as the bed was made free-flowing. Channeling was reduced and a linear fixed bed pressure drop curve resulted. Maximum bed expansion remained about the same, but was reached at lower gas velocities. (The decrease in the expansion curve for the flour bed containing 1.0% Cab-O-Sil was unexpected from previous results (9, 84).) The fluidized bed stirrer torque was essentially unchanged but the torque of the fixed bed was reduced.

The potato starch bed was unintentionally flow conditioned by the tracer salts added in the mixing experiments. The characteristics of this bed (Figure 31) reflect changes similar to those discussed above for the flow conditioned flour beds. When flow conditioned, the dimensionless pressure drop across the bed of potato starch was comparable to that of the flour conditioned with 1.0% Cab-O-Sil but instead of being constant over the fluidized region, bed pressure drop in the potato starch bed increased slightly with increasing gas velocity. This indicated that better quality fluidization was occurring at the higher fluidization velocities. The bed expansion increased when the bed was flow con-

Figure 29. Fluidization characteristics of 0.5% Cab-O-Sil Flour

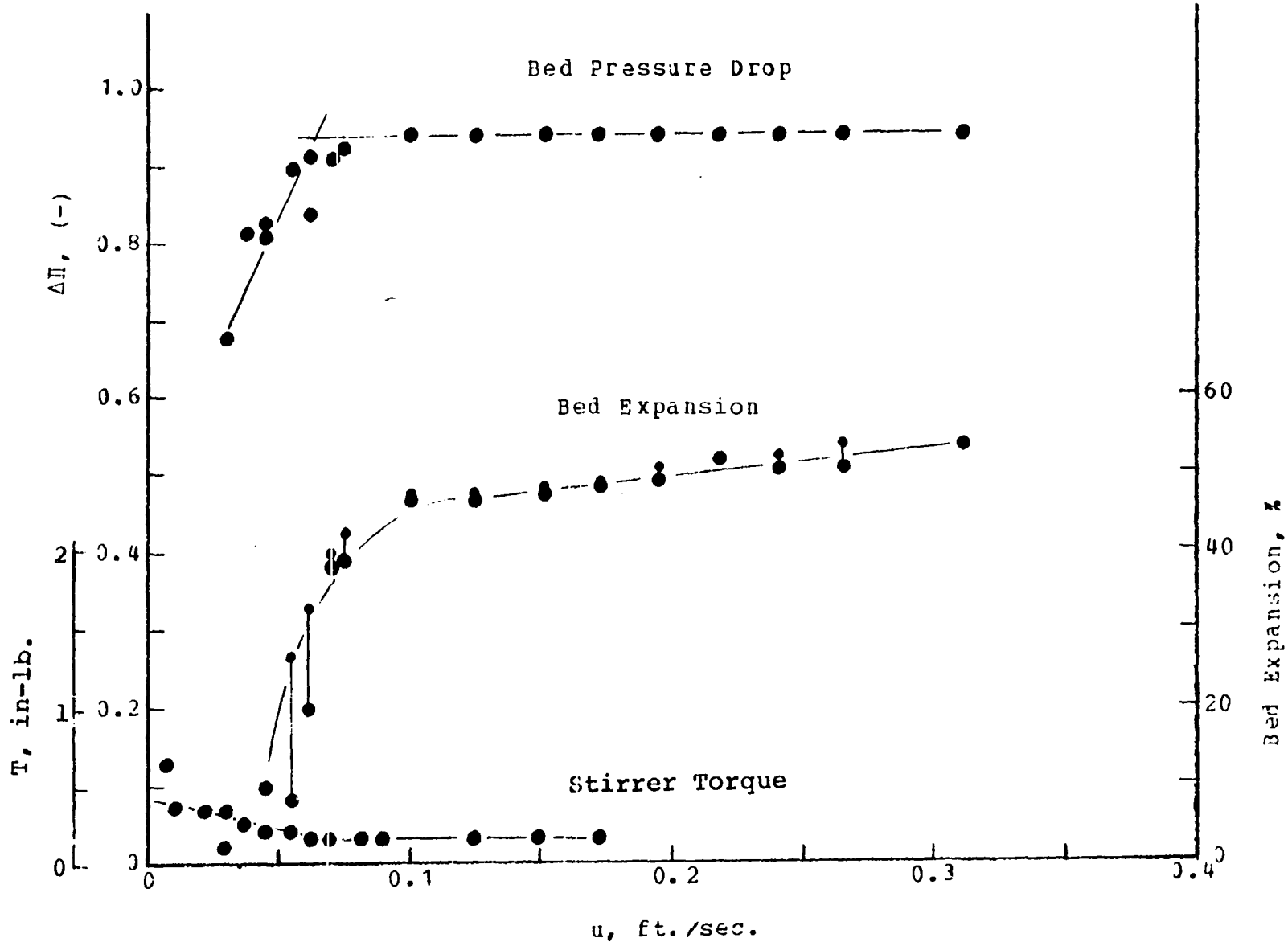
Bed Pressure Drop
Bed Expansion
Stirrer Torque
ΔΠ, (-)
T, in-lb.
Bed Expansion, %
u, ft./sec.
1.0
0.8
0.6
0.4
0.2
0
2
1
0
0.1
0.2
0.3
0.4
60
40
20
0

Figure 30. Fluidization characteristics of 1.0% Cab-O-Sil Flour

Small symbols denote maximum value; large symbols, average value

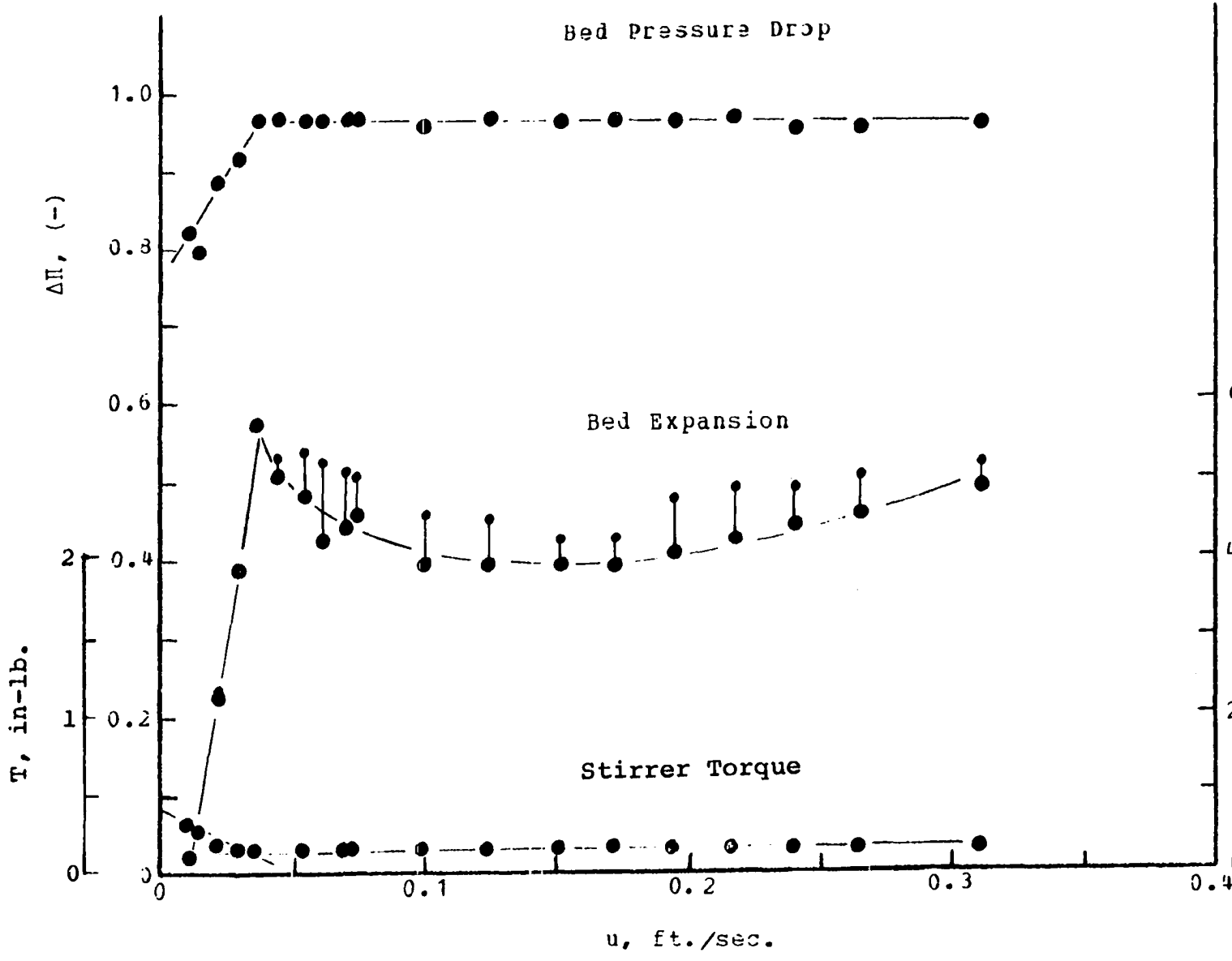
Bed Pressure Drop
Bed Expansion
Stirrer Torque
ΔΠ, (-)
T, in-lb.
Bed Expansion, %
u, ft./sec.
1.0
0.8
0.6
0.4
0.2
0
2
1
0
60
40
20
0
0.1
0.2
0.3
0.4

Figure 31. Fluidization characteristics of potato starch, after run 11

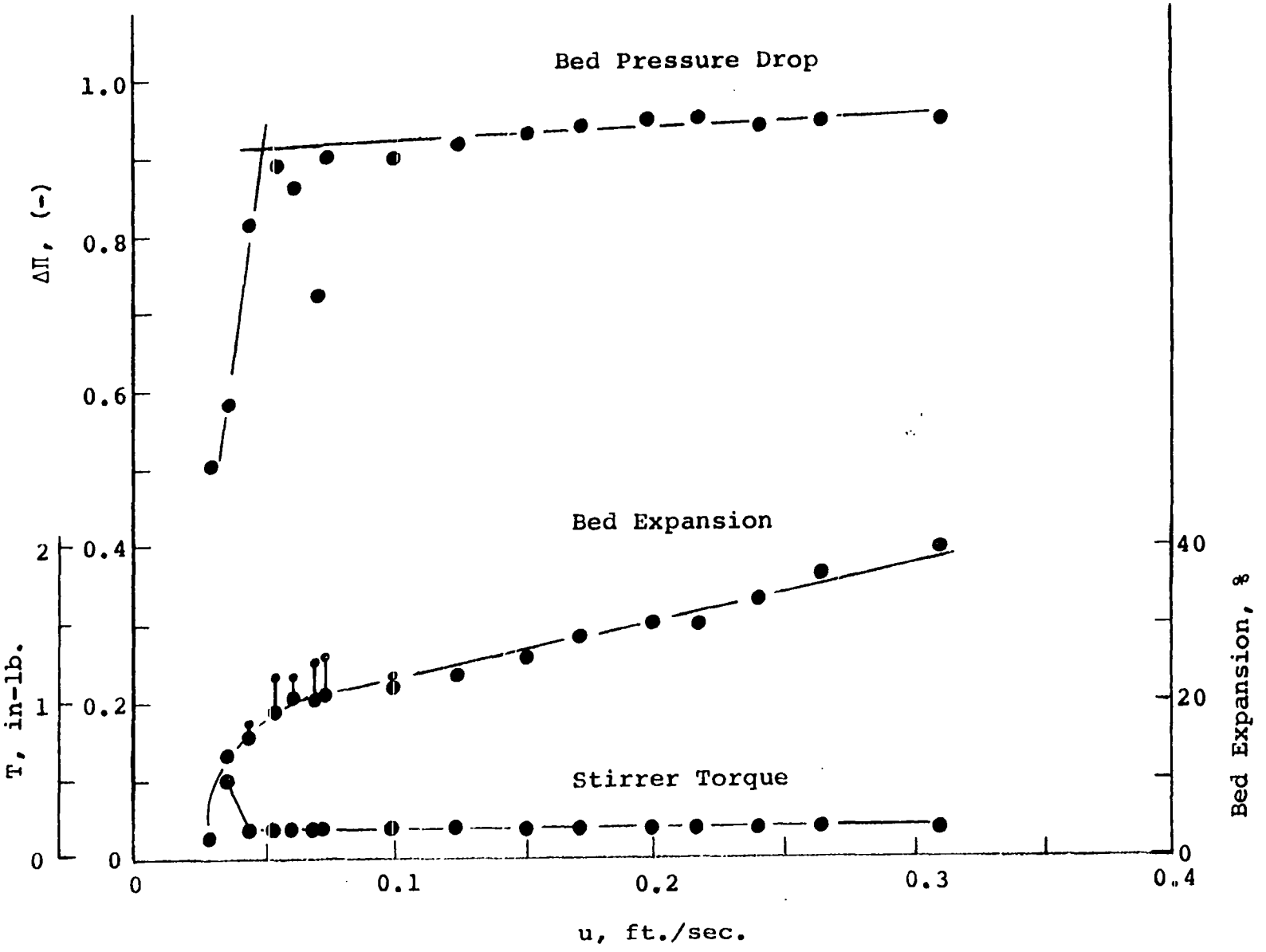
Bed Pressure Drop
Bed Expansion
Stirrer Torque
ΔΠ, (-)
T, in-lb.
Bed Expansion, %
u, ft./sec.
1.0
0.8
0.6
0.4
0.2
0
2
1
0
40
20
0
0
0.1
0.2
0.3
0.4

ditioned. As one might expect from the larger bulk density and smaller bed expansion of potato starch, the stirrer torque was still slightly larger than that of flour.

An important characteristic of the fluidized solids is the minimum gas velocity required for achieving a state of fluidization. The minimum fluidization velocity of more free-flowing powders used in the present study was determined in the usual manner from the bed pressure drop curve (63). The intersection of the linear portion of the curve representing the fixed bed region and the extrapolated line drawn from the portion of the curve representing the bubbling bed region was taken to be the minimum fluidization velocity.

The determination of the minimum fluidization velocity of the cohesive flour and potato starch beds was difficult. The pressure drop indicated approximately the start of fluidization by the diminishing of the large, slow oscillations of the channeled, fixed bed and the start of a small rate of pressure increase with increasing gas velocity (Figure 26). Bed expansion gave no indication. The oscillatory nature of the bed pressure drop and bed height reduced the accuracy of these measurements.

The stirrer torque may be used to indicate the minimum fluidization gas velocity (9, 10). When the bed is fluidized, the stirrer torque is small in value and essentially independent of gas velocity. When stirring a packed bed, the

stirrer torque increases linearly as the gas velocity is decreased. The intersection of the straight lines drawn through the fixed bed region and the fluidized region corresponds to the minimum fluidization velocity. This was generally a good indicator of the minimum fluidization velocity, but some difficulties were encountered.

In the present work, two kinds of deviation from linearity were observed for the packed bed torque curve.

The first deviation occurred after a small linear region. When gas flow was reduced to lower values, a region of sharply increased torque was encountered as illustrated in Figure 26. The stirrer drive system was not powerful enough to stir a nonaerated or slightly aerated bed. At some point, the stirrer failed to turn on further reduction of gas flow. Near this point, torque sharply increased.

The second deviation occurred when a region of low solids compaction was created near the stirrer. The cohesiveness of the packed solids in the bed above the stirrer resulted in the formation of arches reaching across the column. Most of the bed weight was then supported by the column wall. The stirrer rotated in a cavity filled with loosely packed solids. The result was a higher torque value than in the fluid state, but a further increase did not occur as the gas velocity was reduced (Figure 27).

The minimum fluidization velocities of flour and potato starch were determined by a consideration of stirrer torque, bed pressure drop behavior, and visual observation of the bed.

Table 8. Summary of minimum fluidization velocity

Material	u_{mf}, ft./sec.
Flour III	0.10
Flour III with 0.5% Cab-O-Sil	0.07
Flour III with 1.0% Cab-O-Sil	0.04
Microthene MN 710	0.047
Potato Starch	0.12
Potato Starch with tracer salts	0.05

The minimum fluidization velocity of the materials studied are summarized in Table 8. The minimum fluidization velocities of the cohesive materials, pure flour and potato starch, were significantly greater than that of the free flowing Microthene MN 710. Reduction of powder cohesiveness by adding a flow conditioner such as 1% by weight Cab-O-Sil resulted in a free flowing powder having a significantly lower minimum fluidization velocity (29). A partial reduction of cohesion, such as was achieved by adding only 0.5%

Cab-O-Sil, resulted in an intermediate value of the minimum fluidization velocity roughly proportional to the amount of flow conditioner added. A reduction in minimum fluidization velocity was obtained for potato starch when the tracer salts were added during the mixing experiments.

Entrainment

Entrainment is the removal of solids from a fluidization column by suspension of the solids in the exit gas stream. As discussed in the Literature Review of solids motion, some of the solids of the bubble wake are thrown into a "cloud" above the bed when the bubble bursts. Most of the particles rain down on the bed. The superficial gas velocity of the exit gas stream is very frequently (in cylindrical columns) larger than the free fall terminal velocity of the smaller diameter particles. Once suspended in the exit stream, these particles are swept from the column (unless, due to their cohesive nature, they impinge upon another particle and the agglomerate falls to the surface.) Some of the larger particles may also be entrained because they do not have time to settle before being swept from the column. The above simple description is complicated by the existence of local areas of temporarily high gas velocity caused by bursting bubbles and by the effects associated with changes in the gas velocity profile from the turbulence of the bed surface to laminar

flow further up the column.

Some of the solids dispersed by bursting bubbles hit and adhered to the wall. In both the glass and Plexiglas columns, the wall above the bed became speckled with a thin, splotchy layer of solids. The accumulation was heaviest just above the bed and hindered observation of the bed surface. The amount of solids would build up enough locally to overcome adhesion to the wall and periodically, some patches of solids would fall back to the bed. A discontinuous monolayer extended for several inches above the multiparticle layer. Population density of the specks decreased with elevation above the bed. At most, a couple of grams of solids were stuck to the wall at any one time.

The height of the column from the fluidized bed surface to the gas outlet is called the freeboard. Given sufficient time, particles having a free fall terminal velocity greater than the exit gas stream settle out of the stream. The freeboard at which particles of terminal velocity greater than the exit gas velocity would just have sufficient settling time is the transport disengaging height.

The rate of entrainment from the fluidized beds used in the current study was determined by measuring the gain in weight of the filter provided to collect entrained particles during timed periods (30 to 60 min.) of fluidization under the constant operating conditions occurring during either the

residence time or mixing experiments. No attempt was made to maintain a constant freeboard since the column length was fixed and constant settled bed depths were required in the residence time and mixing experiments. The freeboard was dependent upon the bed expansion characteristics of the materials. For the rather small gas velocity range employed, the change in bed expansion for a given material was usually insignificant so that an approximately constant freeboard resulted. The freeboard was assumed to be smaller than the unknown transport disengaging height.

The terminal velocity of 10 micron flour or potato starch particles was calculated (63), assuming the particles were spherical, to be 0.015 ft./sec., a 32 micron particle to be 0.15 ft./sec., and a 100 micron particle to be 1.87 ft./sec.

The average entrainment rates as a function of gas velocity for 27 to 32 in. deep settled beds are summarized in Figure 32. Three points based on measurements made by Brekken (9) with 29 and 30 in. deep beds of flour of unknown moisture content were included. The flour moisture content was otherwise 14%. The entrainment data for potato starch is not representative of the pure starch. The salt tracer added in the mixing experiments flow conditioned the bed, increasing bed expansion and reducing the minimum fluidization velocity. The 0.15 ft./sec. data point was obtained during the

Figure 32. Entrainment rate versus fluidization velocity

● Flour III

o Flour I, Brekken (9)

✗ 0.5% Cab-O-Sil Flour

■ 1.0% Cab-O-Sil Flour

□ 1.0% Cab-O-Sil Flour, Brekken (9)

▲ potato starch, (Set 12, run 10)

△ potato starch, (Set 12, run 11)

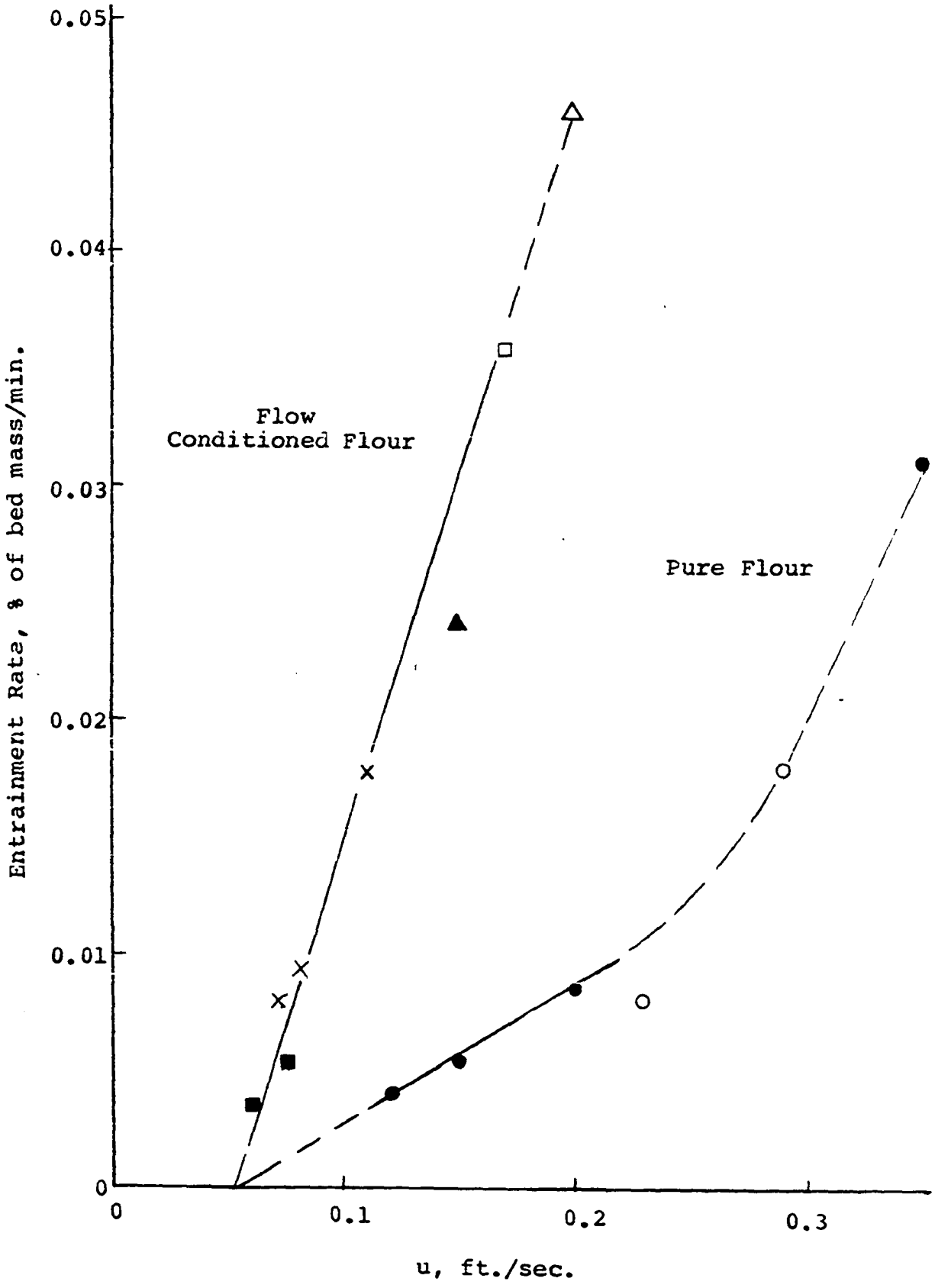
0.05
0.04
0.03
0.02
0.01
0
0
0.1
0.2
0.3
Entrainment Rate, % of bed mass/min.
u, ft./sec.
Flow
Conditioned Flour
Pure Flour

mixing of the first tracer into the pure bed while the 0.20 ft./sec. point was obtained when a second tracer salt was added later.

The entrainment curve for pure flour was linear for the lower gas velocities (less than 0.25 ft./sec.) but the rate of entrainment increased faster at the higher gas velocities. The increased bed expansion at the higher velocities over that at lower velocities resulted in a significant reduction of freeboard (from 15 to 19 in. of freeboard at the lower velocities compared to 10 to 12 in. at the higher velocities) which might account for the increased entrainment rate. Brekken (9) pooled his entrainment results for 18 to 30 in. deep beds and found a linear increase in entrainment rate over the gas velocity range of his data, 0.23 to 0.37 ft./sec. His data indicated that freeboard, over the 12.5 to 31 in. range, was rather insignificant. In the present work, the entrainment rate obtained at 0.35 ft./sec. agreed with Brekken's curve. These results are explained if the transport disengaging height were about 12 in. One would expect the size distribution of material collected in the filter to shift towards larger sizes than expected from terminal velocity considerations at the higher gas velocities.

One straight line could be drawn through the entrainment data of both levels of flow conditioned flour and the data point of the flow conditioned potato starch bed containing

both the copper and zinc tracer salts. This line and the one for pure flour had a common interceptat 0.05 ft./sec. The rate of entrainment from the flow conditioned flour beds was larger than from pure flour beds operated at the same gas velocity.

The rate of entrainment from the pure flour bed was less because the flour probably existed as larger agglomerates in the pure flour bed than it did in the flow conditioned flour beds. Agglomerates of the pure bed frequently were not broken up when bubbles burst. The particles dispersed above the bed had a large effective particle diameter and thus a large terminal velocity. The entrainment rates from the bed of 0.5% Cab-O-Sil flour and from the bed of 1.0% Cab-O-Sil flour were equal. Apparently both flow conditioned flour beds contained a large percentage of individual particles and agglomerates of just a few particles. The rate at which material was tossed above the bed apparently was not the rate controlling factor (or else was equal for both flow conditioned flour beds). Since the bubble rise velocity depends upon the excess gas velocity $(u - u_{mf})$ while particle properties usually have a fairly small effect (101), it seems plausible that the rate at which material was ejected from the bed was not the factor controlling the entrainment rate.

The bed expansion of both flow conditioned flours was about the same, 40 to 45%.

The entrainment rate was influenced more by the superficial gas velocity than the relative gas velocity. The same excess gas velocity ($u - u_{mf}$), 0.04 ft./sec., resulted for the flour with 0.5% Cab-O-Sil at 0.11 ft./sec. (a relative gas velocity of 1.5) as did for the flour with 1.0% Cab-O-Sil at 0.08 ft./sec. (relative gas velocity of 2.0). Approximately equal volumetric rates of gas passed through each of these two beds as bubbles. The entrainment rate from the bed of flour with 1.0% Cab-O-Sil was larger than that from the bed of flour with 1.0% Cab-O-Sil. Since the excess gas velocity was the same in these two cases, bubble rise velocity, and hence the approximate momentum of the particles in the bubble wake, was also the same. The rate at which particles were tossed above the bed is thus expected to be about the same too. Once a particle is dispersed into the gas, however, the particle will settle quicker from the slower gas stream and the terminal velocity of more particles are likely to be larger than the exit gas velocity. Particles are thus less likely to be entrained from the bed operated at the lower gas velocity even though the relative and excess gas velocities might be the same or larger. One would expect that flour treated with Cab-O-Sil at some level below 0.5% would have an intermediate entrainment rate.

The flow conditioned potato starch entrainment rate was that expected for flour flow conditioned with 0.5%, or more,

Cab-O-Sil.

The bed expansion of the potato starch (30%) was less than that of the flow conditioned flour (40 to 45%). Two parameters which largely determine the free fall terminal velocity, particle density and size, were similar for the two materials. The minimum fluidization velocity of the potato starch bed which contained both copper and zinc tracer salts was between that of the flow conditioned flours (Table 8). With particle terminal velocity and fluidization characteristics similar to flow conditioned flour, the entrainment rate of flow conditioned potato starch would be expected to be similar to that of the flow conditioned flour.

The common intercept, 0.05 ft./sec., of both the pure and flow conditioned flour entrainment curves indicated that no particles could be entrained at this gas velocity or lower. Only the finest particles (about 10 microns or less) had a terminal velocity which was lower than this gas velocity. Even these particles could not be readily entrained since they could not be dislodged from the bed. Even though the 1% Cab-O-Sil flour bed was still fluid at this gas velocity, it was not freely bubbling. The other beds were definitely in the fixed bed state.

RESIDENCE TIME EXPERIMENTS

Observations

The general appearance of the fluidized beds of flour was essentially the same as described in a discussion of preliminary experiments (87). The dominant visual features of these beds were the rippling of the downward moving solids by the faster, upward moving gas bubbles and the existence (9, 84, 87) of quasi-stable discontinuities (particle slip surface voids) in the solid phase. These discontinuities, in contrast to the rounded bubbles, were irregularly shaped, horizontal, plane voids which looked like cracks in the bed. Their length (up to 3 in.) was long compared to their height (about 1/32 to 1/8 in.). The voids extended into the bed to various, undetermined depths. The voids observed during the current work appeared to be more crooked than those photographed in the preliminary experiments (87). The flour beds were strikingly different in appearance from the uniformly expanded beds of freely flowing solids such as 107 micron diameter glass beads or of Microthene MN 710.

The particle slip surface voids were also observed in the beds of flour which had been flow conditioned with 0.5 or 1.0% Cab-O-Sil, as well as in the potato starch bed. The voids in the bed of flour with 0.5% Cab-O-Sil were manually timed as they moved past a grid on the column wall. The

voids in the bed of flour with 1.0% Cab-O-Sil and in the potato starch bed were too small or short lived to be timed. It was observed that as the flour was made more free flowing by adding Cab-O-Sil, the size and "life expectancy" of the voids decreased.

Photographic (87) and direct observation of the flour beds showed the voids to be formed by the passage of bubbles through the bed. It was previously demonstrated (87) that the slip surface voids move down the bed with the solids in the vicinity of the void. The height and shape of the voids were observed to change with time but the voids remained long and narrow.

The passage of a bubble near a void had a direct effect on the void's motion qualitatively like that measured for solids motion by Donsi et al. (23), see Figure 5. Donsi et al. followed the path of individual black tracer particles as bubbles passed at known distances from the wall. Details of their results were discussed in the "Solids flow pattern at bed wall" section of the Literature Review. In pure flour and flour treated with 0.5% Cab-O-Sil, a bubble approaching a void was observed to stop the downward motion of the void and either to promote rapid descent of the void or to cause the void to rise. After the gas bubble had completely passed, the void continued its descent. Frequently, a closely passing bubble resulted in a rapid change in the void's shape

or in closing of the void. The outcome of whether a void immediately descended, rose, or lost its identity to the observer depended upon the lateral distance of closest approach between the bubble and void. The closer the bubble was to the void, the more likely the void was to be lost. Separations just large enough for identity to be maintained resulted in upward motion of the void. As separation increased still further, the magnitude of upward displacement decreased and with further separation of the bubble and void, downward displacement resulted. Beyond some additional distance, the bubble had no effect on the void.

The effects of two or more bubbles on a void were additive. Thus one half of a void was observed to move down while the other half of the void was stationary or even moved up. This shearing usually resulted quickly in closure of the void. Movement of voids distributed across a horizontal section of the bed wall was not constant. The voids of one section could be moving down while those of another section were stopped or moving up. This behavior was more noticeable at the lowest gas velocity (0.12 ft./sec.) where solids motion was slower and stagnant periods were longer than at higher gas velocities.

Bubbles passing serially near a void, but not close enough to annihilate it, were observed to have sequential effects on the void. For instance, the downward motion

promoted by the passage of the first bubble was nullified by the approach of a second bubble. The void did not move before it received a downward thrust by the passage of the second bubble. Thus the serial passage and interaction of gas bubbles appeared to result in the observed slip-stick solids flow. In such solids flow, material moves down the column, stops for a short time interval, and then continues downward for an irregular period. The cycle is repeated over and over.

As mentioned in the discussion of "Fluidization Characteristics", the bed height was oscillatory. The amplitude and period of fluctuation increased as gas velocity was decreased. This phenomenon was accompanied by changes in solids motion, especially when bed height was increasing. During this phase, many voids were observed to slow down, stop, and then rise until the maximum bed expansion was achieved. Then the net motion again was downward. These changes in particle motion were more pronounced at the lower gas velocities. The presence of larger or more frequent bubbles during the bed expansion phase could not be determined by direct observation.

The existence of particle slip surface voids in fluidized beds of flour was utilized in the procedure described above for measuring solids residence time at a wall-to-bed heat transfer surface. The technique was employed to deter-

mine the influence of fluidization conditions such as gas velocity, stirrer speed, and type of material on the residence time of the voids, and hence solids, on heat transfer surfaces. The heat transfer coefficients determined by Nazemi (84) for heat transfer surfaces in contact with beds of flour fluidized with nitrogen were correlated with this residence time data.

Results

The arithmetic average and variance of the times required for individual particle slip surfaces voids ("cracks") to travel 1, 2, and 3 in. were calculated from the record of cumulative times for each run and location (as described in Procedures of Fluidization Experiments). In Sets 1 to 6, the cracks were measured over a distance of 3 in. In Sets 7 to 11, cracks in the pure flour beds were only timed over 1 in. of travel. The increased speed of the cracks in the bed of flour flow conditioned with 0.5% Cab-O-Sil (Set 11, runs 5 to 8) necessitated measurement over a travel distance of 2 in.

In all sets, cracks traveling slower than 0.04 in./sec. were excluded from the averages. These few cracks were largely cracks which traveled upward a considerable distance during measurement. Including cracks traveling slower than the 0.04 in./sec. limit would have greatly distorted the averages and variances as well as clouded interpretation of the

results as downward travel times.

Table 9. Summary of cracks meeting criteria of traveling the full grid distance at a rate of 0.04 in./sec. or faster

u, ft./sec.	Location	Ave. % passed	No. failed/no. passed d = 1 in.	d = 3 in.
0.12	upper	75	0.06	0.19
	lower	89	0.012	0.05
0.15	upper	82	0.07	0.21
	lower	95	0.013	0.05
0.20	upper	55	0.032	0.90
	lower	93	0.03	0.08

For each gas velocity, Table 9 summarizes the percentage of all cracks (for which an attempt was made to measure thier downward movement) which passed the criteria of (1) traveling the full grid length (as discussed above) and (2) at a rate greater than 0.04 in./sec. In addition, the average ratio of the number of cracks failing to travel 1 or 3 in. to the total number of cracks which traveled the full grid length at a rate greater than 0.04 in./sec. is presented. For each run, the percentage of all cracks meeting both criteria and the ratios of those cracks failing to travel 1 or 3 in. to those that passed both criteria are listed in Tables 17 and

18 of Appendix B.

To compare times measured over different travel distances, a velocity is usually calculated. The harmonic average velocity was convenient for eliminating travel distance since it could be directly calculated from the average time, equation 21. Expressing average residence time as the harmonic average is preferable for correlation since the residence time for other travel distances may be more readily calculated.

The residence time data, summarized as the arithmetic average and its variance for each run, location, and travel distance is listed in Tables 19 and 20 of Appendix B. The levels of the operating conditions of each set and run are summarized in Figures 22 and 23 and Table 7. The actual values of the operating conditions are listed in Table 16 of Appendix B. The residence times (Tables 19 and 20 of Appendix B) increased proportionately with the travel distance. The variances showed that the spread of the distribution of individual crack times was wide. Variance increased with increasing travel distance. Both the residence time average and variance were greater for the upper measurement location than for the lower. Further qualitative information was obtained by plotting the data as functions of the operating parameters.

The mean average residence time for each gas velocity of Sets 1 to 4 is plotted in Figure 33 for the two locations and three travel distances. The residence time decreased nonlinearly with increasing gas velocity. The variance of the cracks also decreased (Figure 34), indicating that the crack velocities were closer to the average. This decrease was linear for the 1 and 2 in. travel distances. The downward crack velocity increased linearly with gas velocity at both the upper and lower areas (Figure 35). The slopes of the curves for the upper and lower areas were slightly different.

For a given run and travel distance the cracks timed at the upper area were slower than those timed at the lower area (Table 19, Appendix B). The relationship of these times with those of the mid- and lowest-locations (Table 20, Appendix B) was not apparent from the tables of data. The harmonic velocity of the cracks timed in Sets 8 and 9 are plotted in Figure 36. This plot shows that there was an interacting relation of the harmonic velocity of the downward moving cracks and the gas velocity and height above the gas distributor. At the 0.15 ft./sec. gas velocity, both the sets showed a linear increase of crack velocity as the cracks traveled down the column. For higher and lower gas velocities, the crack velocity passed through a maximum, linearly increasing until between 8.8 and 13.8 in. above the distributor, crack veloci-

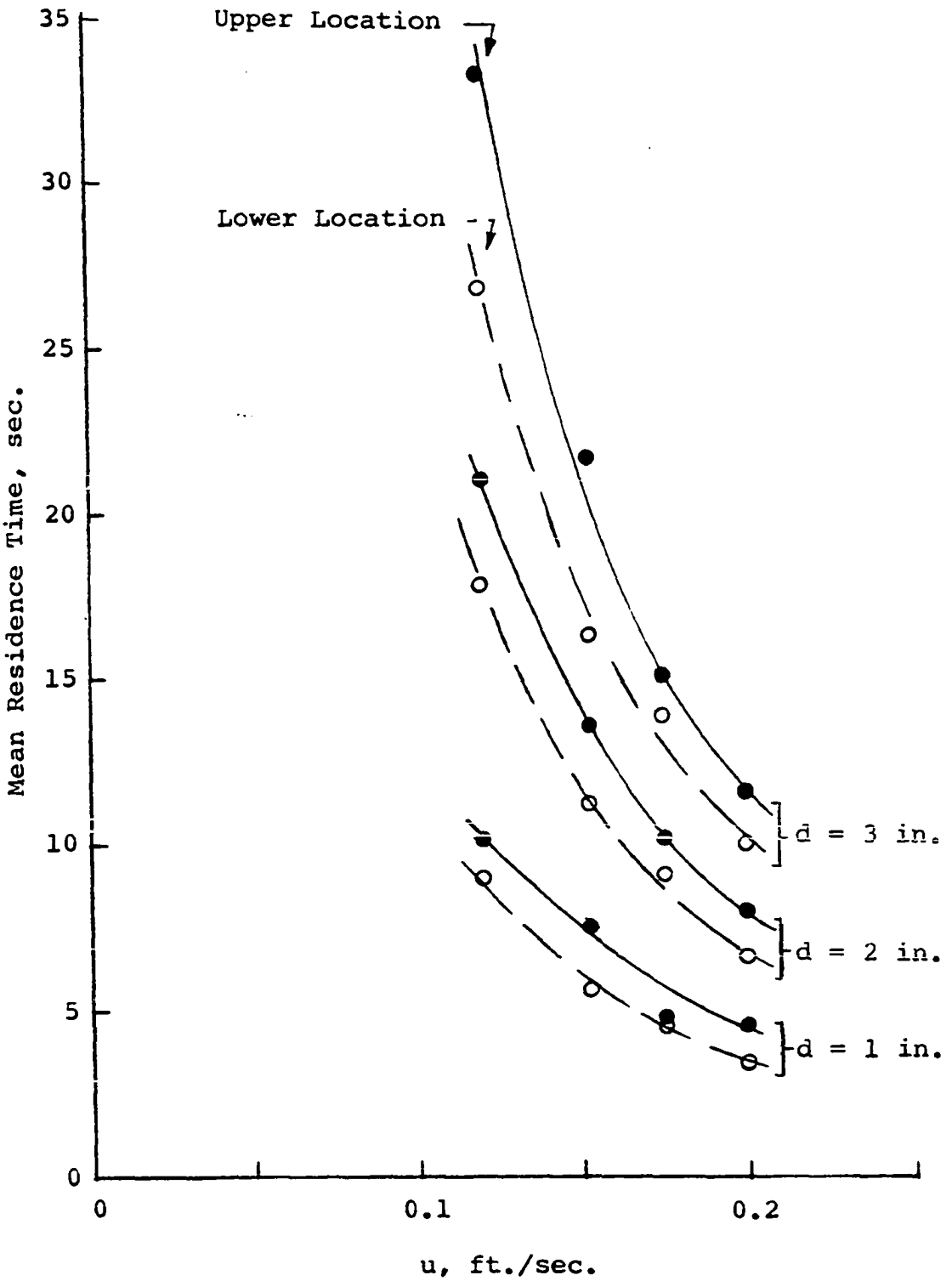

Figure 33. Mean residence time versus gas velocity for cracks measured over three distances of travel, Sets 1 through 4

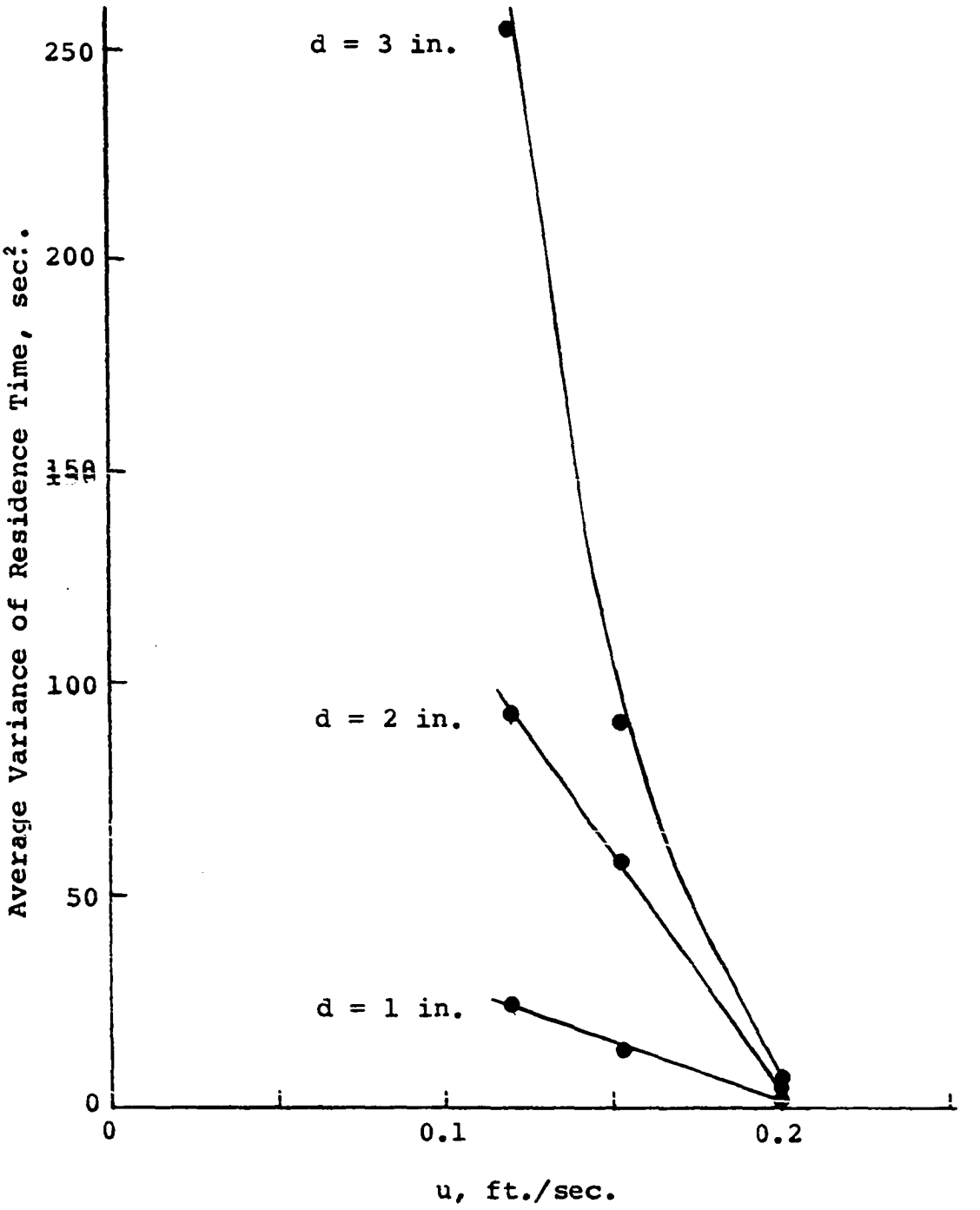

Figure 34. Average variance of crack residence time for upper grid location, Sets 1 through 4

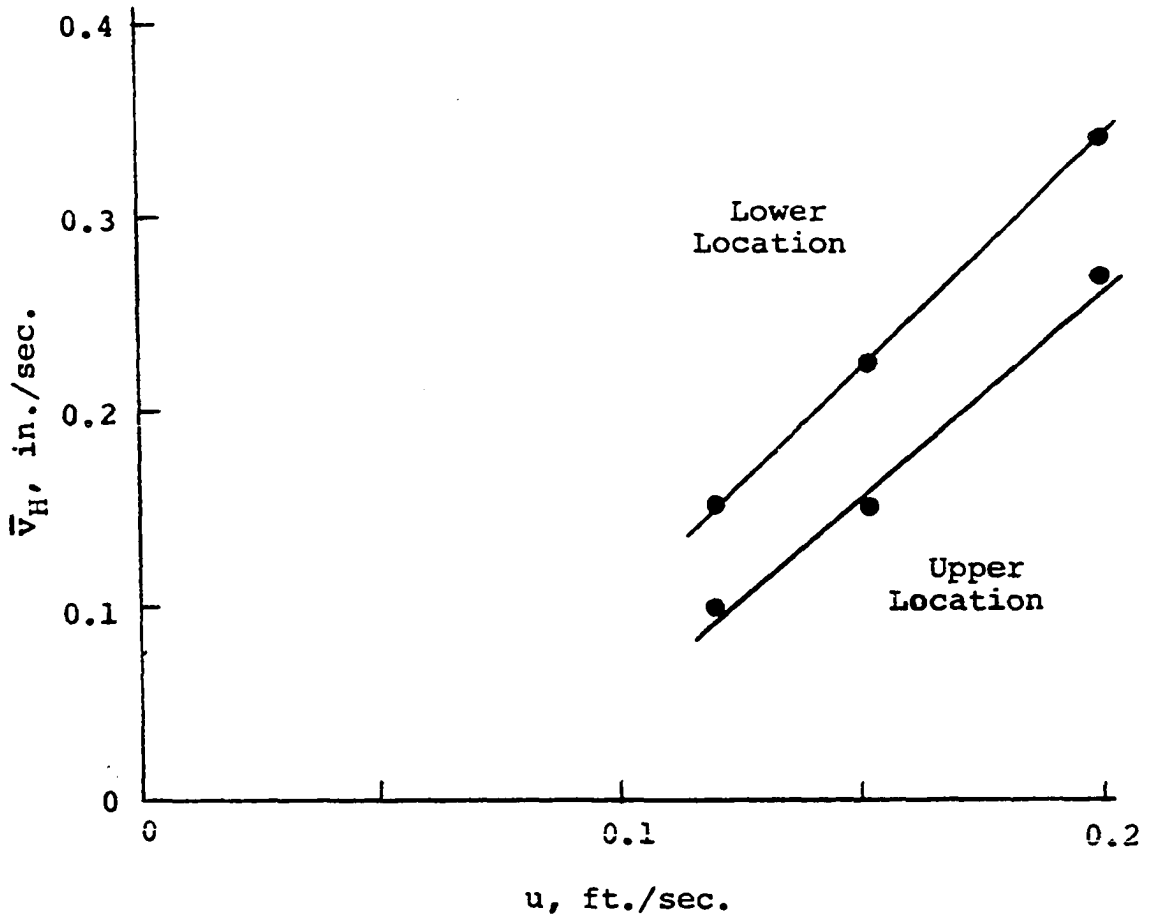

Figure 35. Downward mean harmonic average velocity of cracks versus gas velocity, Sets 5 and 6

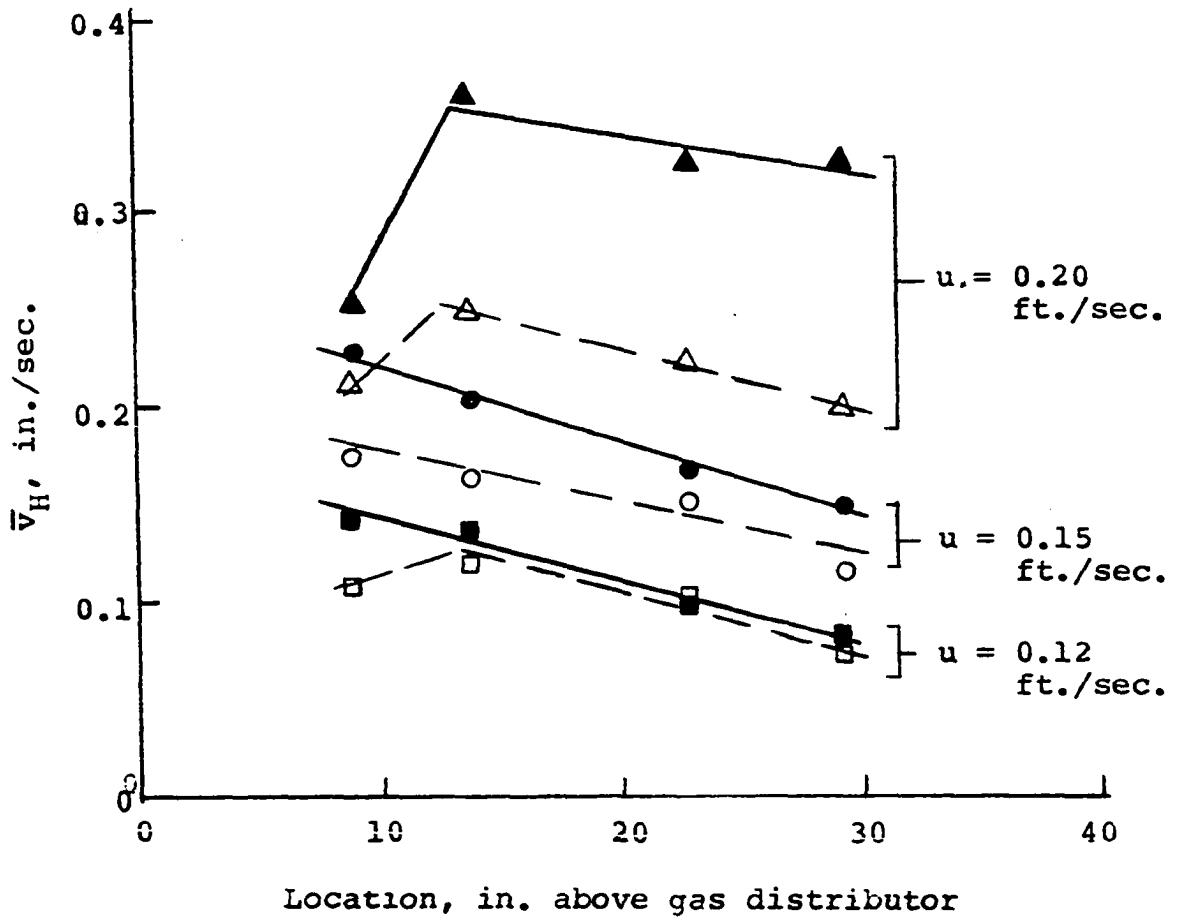

Figure 36. Downward mean harmonic average velocity of cracks versus location above the distributor plate

▲, ●, ■ = Set 8

△, ○, □ = Set 9

ty was reduced. The slopes of the linear regions above 13.8 in. varied little.

Information about the effect of some properties of the fluidized solids on the residence time was also obtained. The flour moisture content, as suggested by the data plotted in Figure 36, had a higher order effect on the residence time as illustrated by Figure 37. Figure 37 shows graphs of the harmonic velocity at the upper and lower areas as a function of flour moisture content for Sets 5 to 11. Some data collected while drying the flour bed preparatory to conducting the experiments of Set 9 are included. These additional measurements were made during an observation period of about 12 min. at each location during which about 50 cracks were timed. The flour moisture content had a quadratic effect on the harmonic average velocity although the data were scattered. A moisture content of about 8% generally resulted in the slowest crack movement. A moisture content of 11 to 13% resulted in the fastest motion at a gas velocity of 0.20 ft./sec. while at 0.12 or 0.15 ft./sec., a moisture content higher than 12% gave slightly faster motion. The 0.20 ft./sec. gas velocity curve showed a cubic effect of moisture content.

Flow conditioning the flour with 0.5% Cab-O-Sil increased the crack rate and also the rate of increase of crack velocity as gas velocity increased, Figure 38. The harmonic

Figure 37. Downward harmonic average velocity of cracks versus moisture content of pure flour, Sets 5 to 11

a. Upper location

b. Lower location

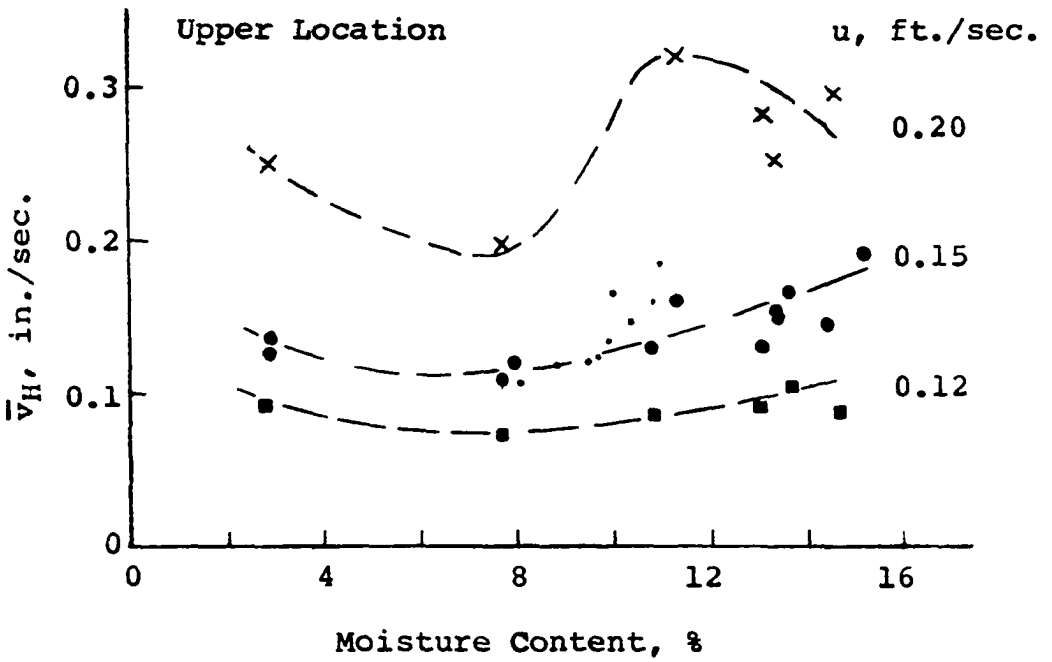
Upper Location
u, ft./sec.
0.20
0.15
0.12
$\bar{v}_H$, in./sec.
0.3
0.2
0.1
0
0
4
8
12
16
Moisture Content, %

(a)

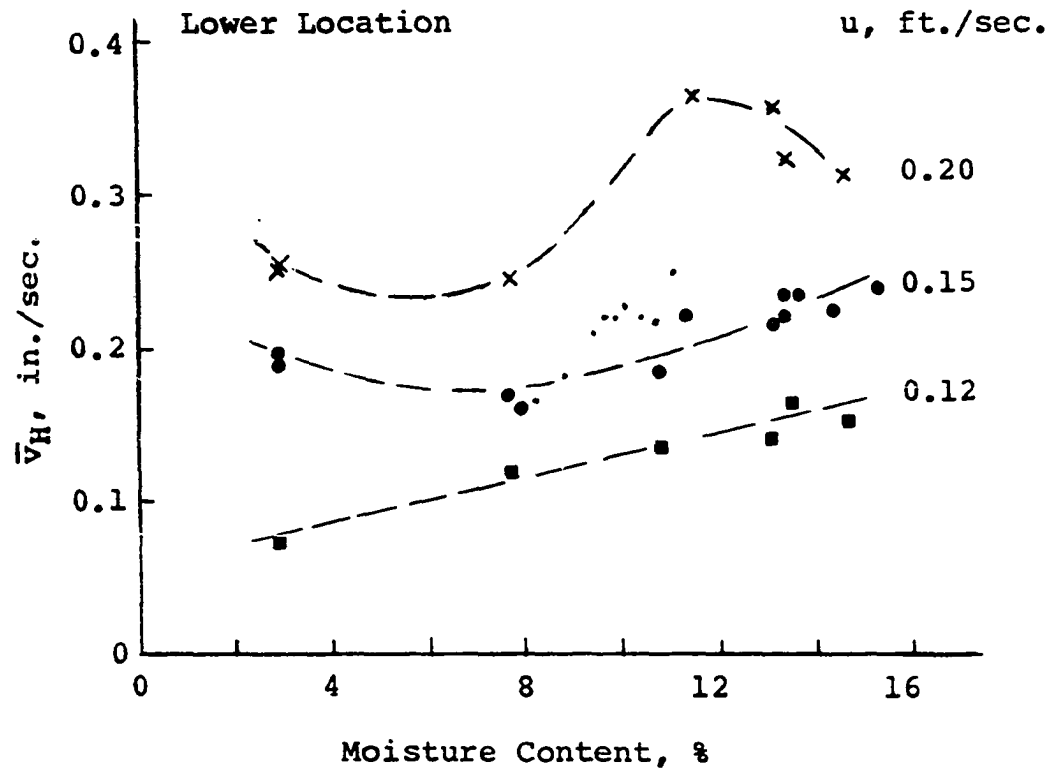
Lower Location
u, ft./sec.
0.20
0.15
0.12
$\bar{v}_H$, in./sec.
0.4
0.3
0.2
0.1
0
0
4
8
12
16
Moisture Content, %

(b)

Figure 38. Harmonic average velocity of cracks versus gas velocity for a 0.5% Cab-O-Sil Flour bed and for the pure flour bed, Set 11

a. Upper location

b. Lower location

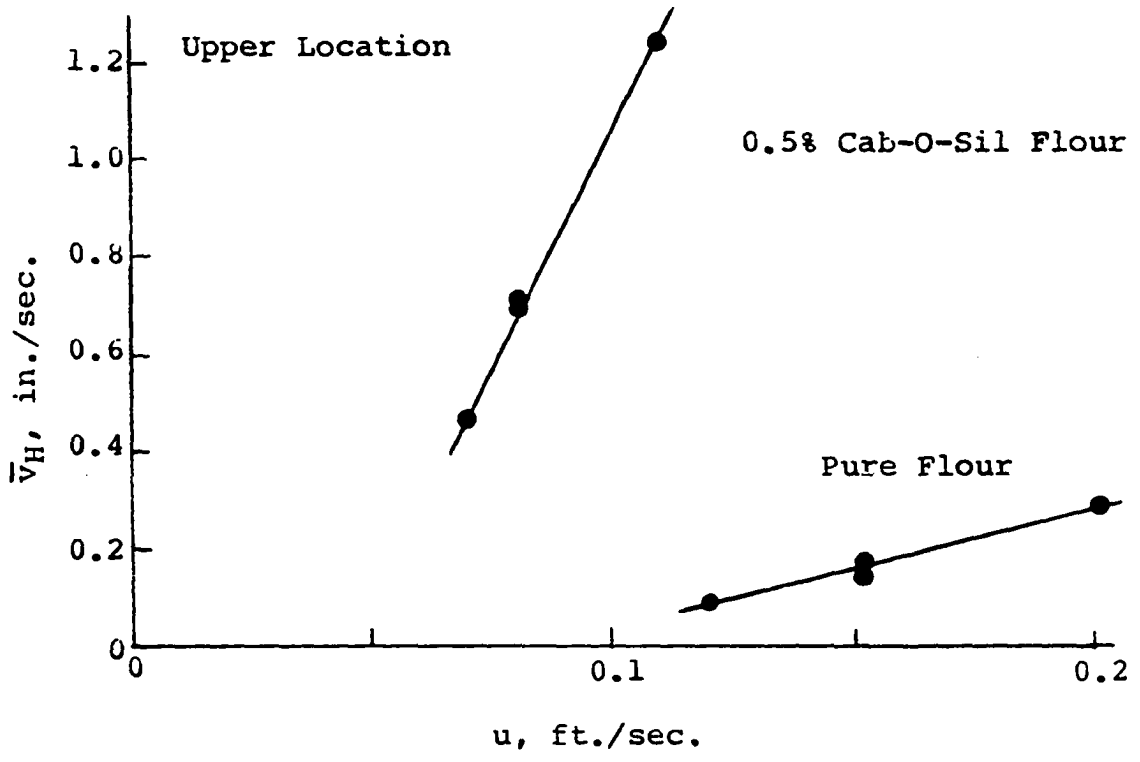
Upper Location
0.5% Cab-O-Sil Flour
Pure Flour
1.2
1.0
0.8
0.6
0.4
0.2
0
0
0.1
0.2
$\bar{v}_H$, in./sec.
u, ft./sec.

(a)

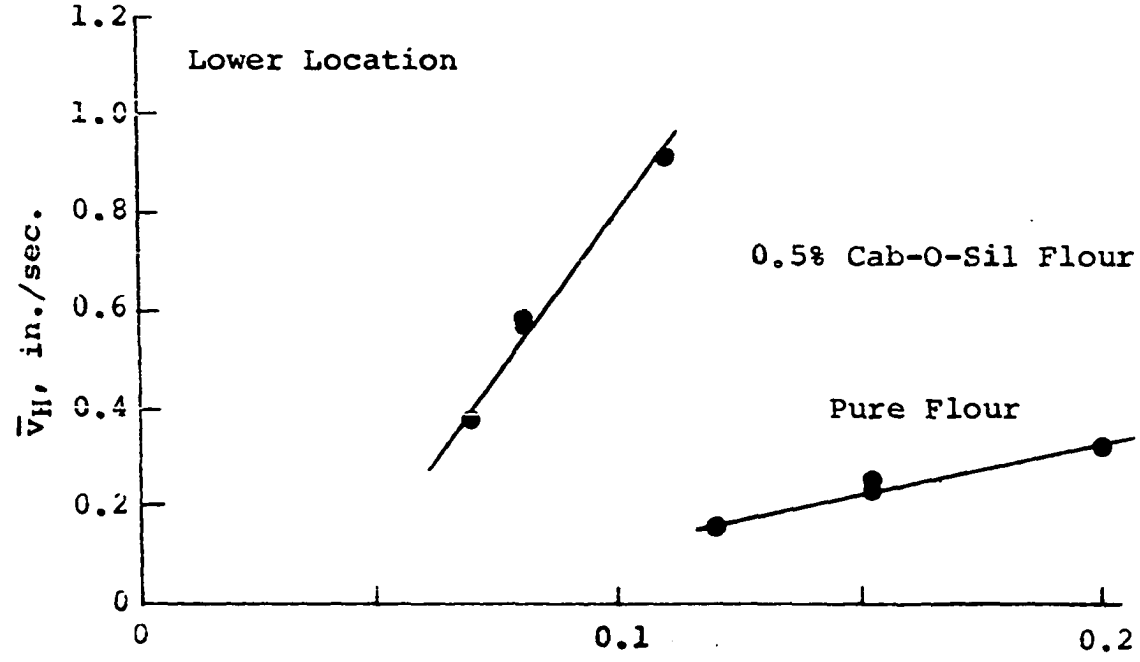
Lower Location
0.5% Cab-O-Sil Flour
Pure Flour
1.2
1.0
0.8
0.6
0.4
0.2
0
0
0.1
0.2
$\bar{v}_H$, in./sec.
u, ft./sec.

(b)

crack velocity was still a linear function of gas velocity. Cracks moved faster in the upper area than the lower area of the flow conditioned flour bed, opposite the results found for pure flour beds.

Statistical Analysis

In the statistical analysis, the run average residence time (or the harmonic velocity) for each travel distance and measurement location was treated as the individual element of the analysis. This was necessitated by the impossibility of computing the analysis using the 19,165 individual crack residence times from which the 324 averages were calculated. The run average residence time will continue to be referred to simply as the residence time.

A plot of the average of the within run variance about the average residence time of each run for Sets 1 to 4, Figure 34, showed the variance to decrease as gas velocity increased. Since it is assumed in analysis of variance and in regression analysis that this variance is constant, a transformation of the residence times (and also of the harmonic average velocity) was necessary. For this type of variance dependency, taking the natural logarithm of the residence time (and of the harmonic velocity) was the proper transformation (13) since a constant variance then resulted. (An alternate possible transformation, taking the square

root, did not yield a constant variance.) The usual statistical tests could then be performed on the transformed time (or harmonic velocity).

In some tests for determining the significance of certain parameters (such as observer bias), the runs between which the parameter of interest was varied also included several levels of other possibly significant parameters. In this case, lumping or combining the effects of the other parameters into one term, the "conditions" parameter, was perferable to the alternative of individually including these parameters in the analysis. Lumping parameters made economical use of the limited data by enabling one degree of freedom to account for several peripheral parameters. For example, by lumping gas velocity, stirrer speed, and set effects as conditions in an analysis for observer differences, Table 38, Appendix D, only one degree of freedom was used whereas including these effects separately would require three degrees of freedom. By using the conditions parameter, two degrees of freedom were made available for determining the residual error. This resulted in a better error estimate and consequently an improved analysis compared to the alternative procedure. The meaning of the conditions parameter varied from analysis to analysis depending upon which parameters required lumping in each test.

In the experimental design of the residence time experiments (Figures 22 and 23), more replications of some combinations of parameters were made than for others; some were not run. In other words, many factors were nonorthogonal, a condition which violated an assumption of the usual analysis of variance tests. As discussed in Appendix D, in cases of nonorthogonality, a less restrictive regression technique was employed in the analysis of variance testing.

The residence times (or the harmonic average velocities computed from the residence time with equation 21) were statistically tested for effects of the following factors

observer
travel distance
set effect
gas velocity
stirrer speed
location
bed depth
gas humidity
flour moisture content
trace levels of salt from the mixing experiments
material

Two approaches to the testing of a group of parameters for the significance of each member exist, the "backwards elimination" and the "all possibilities" procedures.

In the backwards elimination procedure, a general model that incorporates all of the parameters and their interactions is proposed and then tested with the full data set. The results of this test usually indicate that some terms are insignificant. These terms are eliminated from the model which is then retested. By repeating this process, a model composed of only the significant factors is developed. The number of possible terms of the initial model increases very rapidly with the number of parameters and their levels.

In practice, a limit to the number of terms that may be accurately tested for significance exists. Some variance is attributed to the terms later judged to be insignificant at the conclusion of the test as well as to the significant terms of the model. Several insignificant terms appearing "early" in a model may remove enough error so that later terms have little of the total sum of squares left to account for, even if they are truly significant. Thus accumulation of error in the insignificant terms of a many termed model reduces the accuracy of the test, even if enough degrees of freedom are available to accommodate the number of terms. With a limited amount of data, the residual error of a many termed model is likely to have only a small number of degrees of freedom and be a less accurate of an estimate of the true error than one having more error degrees of freedom. The backwards elimination procedure is most helpful when only a

small group of parameters is being considered and when enough data are available for orthogonality of the factors.

The alternative approach, the all possibilities method, is generally more capable of handling a large number of parameters than the backwards elimination method. The factors need not be orthogonal. In this approach, the final model containing only significant parameters and which fits the data satisfactorily is built up from smaller models describing the effects of only a few of the significant factors. A subset of the data points is selected over which the levels of a few parameters are varied while the other parameters are present at only one level. A model of the desired parameters and their likely interactions is proposed which has few enough terms so the residual error has sufficient degrees of freedom for accuracy. The model is tested with the selected data subset. The results of this test indicate the significance of each model term. The model is revised by elimination of insignificant terms and possibly by including new terms such as the square of a parameter, in an attempt to account for more of the subset data variance. The revised model is tested and similarly improved until a model which satisfactorily fits the subset data is found. Next, another subset of all the data is selected over which another parameter or two are varied while the others are either constant or of known insignificance. The new parameters and those of

known significance are included in another small model which is tested with the second subset data. This procedure is continued until all parameters have been examined and a model containing all the significant parameters is developed that satisfactorily accounts for the complete data set.

In the statistical analysis of the residence time data, the all possibilities method described above was used since the significance of a rather large number of parameters was to be tested with a minimal amount of data. Guided by the significance of individual model terms and the amount of variance of the subsets accounted for by the models as indicated by the coefficient of multiple determination, R^2, satisfactory models were developed.

$$R^2 = \frac{\sum (\hat{y}_i - \bar{y})^2}{\sum (y_i - \bar{y})^2} \qquad [30]$$

The data of the first four sets were analyzed before conducting the experiments of Sets 5 to 13 (Figures 22 and 23). The following factors were tested for significance in this preliminary analysis:

observer

travel distance

stirrer speed

gas velocity

location

presence of the mixed salt tracer

As discussed shortly, the first three factors were insignificant, the next two were significant, and the last was of borderline significance, all at the 5% significance level. This feedback of results enabled the more efficient design of Sets 5 to 13 since the insignificant parameters were not further varied (except as expedient) and two additional levels of location were added.

The results discussed in the following section are based on an analysis program considering all the data of Sets 1 to 13. A significance level of at least 5% was used for deciding whether a particular factor had a significant effect on the residence time.

The statistical design allowed testing for parameter significance to progress through a series of parameters with increasing complexity of the tests. Since the possible influence of the measurement technique parameters would extend through all the data, the effects of observer bias, travel distance of the voids, and the set effect were investigated first. The possible significance of various operating parameters and materials fluidized were then determined. Finally, regression models incorporating the significant parameters were fit to the data.

Technique factors

Observer In the eleven sets of residence time experiments, three pairs of observers (identified as observers 1 and 2, 1 and 3, and 1 and 4) were employed. During a given run, one pair of observers was used to time the movement of the voids. One person normally measured voids at the upper two grid locations (See Apparatus), while the other person normally timed voids at the lower locations. For predetermined runs (shown in Figure 23) the assigned observation areas were switched so that the usual "upper grid observer" (number 1) worked at the lower grids for these runs while the usual "lower grid observer" (number 2, 3, or 4) worked at the upper grid. This reassignment minimized over-specialization of labor and also allowed for testing of observer bias by comparing these results with those obtained with the same bed and the usual grid assignments.

Two analysis of variance tests for observer effect were performed. The first test (Table 38, Appendix D) showed that observers 1 and 2 had no effect on the residence time results of Sets 1 through 4. A second test (Table 39, Appendix D), using the data of Sets 8 and 9, similarly showed no significant effect between observers 1 and 3 or between observers 1 and 4. Furthermore, no interaction between location and observers 1 and 2 was found (Table 38, Appendix D).

It was concluded that any observer bias that did exist was uniform among all four observers, none of whose measured times were significantly different from those determined by the others. Thus individual response time and selection of voids to time appeared similar. Observers were not considered in the statistical tests later performed to determine the effects of various operating parameters.

Travel distance An analysis of variance test (Table 40, Appendix D) of the residence times of Sets 8 through 10, expressed as the harmonic average velocities, showed there was no significant difference in the harmonic average velocities determined by timing the same void over distances of 1 or 3 in. at either the upper or lower grid locations. This result agrees with an earlier experiment (87). The insignificance of travel distance supports the idea that the cracks, and hence the solids, moved down the column at constant rate until they encountered upward moving gas bubbles which interacted with the solids movement either by reducing solids velocity, pushing the solids up, or laterally transferring particles into the bed as described in the above "Observations" section.

For long travel distances, the location above the gas distributor became significant, as discussed below.

"Set effect" The "Set effect" is a measure of the differences observed between different flour beds prepared

and operated under supposedly identical conditions. This effect may be interpreted as a "between bed error" or as an indicator of the reproducibility of the operating conditions. Hysteresis effects, such as differences in settled bed bulk density caused by minor differences in installing the bed, contribute to this effect. The distribution of operating conditions among the runs in any given set could also contribute to this effect. A set containing more runs at high gas velocities, for instance, may yield different residence time values for the set as a whole than a set containing more runs at low gas velocities, other parameters being the same.

Set effect was insignificant (Table 41, Appendix D) for the two sets (5 and 6) having otherwise identical preparation and operating conditions (Figures 22 and 23). Set effect was also insignificant in Sets 1 through 4 (Table 42, Appendix D) if the effects of the operating parameters were previously accounted for in the analysis of variance model. The set effect was thus insignificant in both the Plexiglas and glass columns.

The insignificance of the set effect meant that under identical operating conditions, the average movement of the cracks was the same for identical beds if observed for a significantly long period. This suggested that the major significant parameters of particle motion had been included in the experimental design or had been held at a constant level

by the methods employed in preparing the column and in conducting the residence time experiments.

Operating factors

Column It was not possible to test reliably for the effect of the different column materials of construction with the experimental design used for these experiments. The Plexiglas column required a slightly deeper bed for the mixing experiments. Bed depth and column used were changed at the same time. The column effect was believed to be insignificant, however, as indicated by the good regression fit, discussed later, of the data obtained with both columns.

Gas velocity The fluidization gas velocity was consistently significant (Tables 40, 42, and 43 of Appendix D), both by itself and in interaction with grid location. The gas velocity had a linear effect on the harmonic average crack velocity (Figure 35) at all locations of the residence time grid. A test for a quadratic gas velocity effect (Table 44, Appendix D) in addition to the linear effect, showed the higher effect to be insignificant.

The results agreed with those found in a preliminary study (87). In those experiments, the arithmetic average crack velocity was found to have a linear effect with gas velocity.

These results were in harmony with the bubble induced particle motion mechanism discussed in the Literature Review. Quantitative relations were not available, but the mechanism accounted for gas velocity effects as follows. As gas velocity was increased, proportionately more gas passed through the bed as bubbles. More or larger bubbles resulted in a larger solids circulation rate. Downward particle velocity was increased with the increased gas velocity. Interaction effects with bubbles slowed the net increase in downward crack velocity at the upper location more than at the lower measuring location. The more frequent passage of bubbles at the highest gas velocity resulted in a larger percentage of cracks that failed to travel 1 or 3 in. at this velocity compared to the middle velocity (Table 9). At the slowest gas velocity, the downward crack velocity was slow enough so that the less frequent bubbles resulted in more cracks failing to travel the measurement distance than at the middle velocity. The middle gas velocity appeared optimum in terms of cracks traveling the grid distance between bubbles.

Nazemi's empirical model (84) for the wall-to-bed heat transfer coefficient of the lower heating surface (7.9 to 13.8 in. above the gas distributor) was essentially linear while that of the upper surface (23.8 to 29.8 in.) was dependent on gas velocity to the 1.2 power.

Stirrer speed Sets 1 through 4 contained runs between which the stirrer speed was varied from 25 to 150 rpm while the levels of the other parameters were unchanged. Analysis of variance tests of this data (Table 42, Appendix D) showed stirrer speed to be insignificant over the above range. In addition, there were no two way interactions of stirrer speed with gas velocity or location nor was the three way interaction of these parameters significant over the tested range of 25 to 100 rpm (Table 42, Appendix D).

These results support the mechanism that the stirrer breaks up channels in the vicinity of the gas distributor plate and does not otherwise affect solids motion in the upper bed regions.

The finding of insignificant stirrer speed effect agreed with the results of a heat transfer study done with a similar nitrogen fluidized bed of flour (84), where stirring speed in the range of 25 to 100 rpm had an insignificant effect on the wall-to-bed heat transfer coefficient.

Location The elevation of the voids above the gas distributor had a very significant influence on their residence times (Tables 42, 44, and 45 of Appendix D) for both the shallow (12.5 in.) and deep (28 and 32 in.) beds. The residence times at the upper grid location were 10 to 40% longer than those observed at the lower location (Figure 33) while the harmonic velocity was 12 to 37% slower than at the

lower locations (Figure 36). Location had a consistently significant interaction with gas velocity.

The measured wall-to-bed heat transfer coefficients in a similar fluidized flour system (84, 85) were very significantly lower (14 to 27%) at the upper heat transfer surface over a similar range of operating conditions.

Gas humidity There was no significant effect due to using nitrogen either dry (as received) or with a relative humidity of 28% as the fluidization gas (Table 46, Appendix D). This was expected (79) since the gas density and viscosity were only slightly different (less than 1% and 0.7%, respectively) (94) between the dry and 28% relative humidity nitrogen. No electrostatic effects were observed at the rather low fluidization velocities employed.

Bed depth At the same relative distance (elevation/settled bed depth) above the gas distributor, the 12.5 in. settled bed (Set 7) had significantly different harmonic average crack velocities than the 28 or 31 in. beds (Tables 46 and 47, Appendix D). At the upper location, the shallow bed had the same solids velocity as the deeper beds (Sets 5 and 6) except at 0.12 ft./sec. where velocity was larger in the shallow bed. At the lower location, the shallow bed's crack velocity was consistently less than in the deep beds. The cracks of the shallow bed varied less with location than those of the deep bed (Sets 8 to 10, having different mois-

ture content levels). Two levels of bed depth were not sufficient to test for the interaction of of bed height and gas velocity or location. The solids circulation in shallow beds is likely to have significant radial character compared to the dominant axial displacements of solids in deep beds due to the larger percentage of the shallow bed which is occupied by the turbulent regions near the gas distributor plate and bed surface.

Material factors

Moisture content The moisture content of the flour was found to be very significant (Tables 43, 46, and 47 of Appendix D) as illustrated in Figure 37. Higher order dependence on moisture was indicated since the square and even the cubic terms of the models tested (Table 47, Appendix D) were significant. However, the overall fit was only slightly improved by inclusion of the higher order terms. Since the cubic term was the last factor added to the regression model, and it had a small sum of squares compared to the error, the cubic term could be ignored without significantly affecting the values of the other coefficients. The data (Figure 37) indicated that near 0.20 ft./sec., the cubic term should be included. The finding of a significant moisture effect, and even a square or cubic dependency agreed with some preliminary residence time experiments (87). In a discussion of

powder flowability (87), measurements of the cohesion of wheat starch as a function of moisture content were cited. Moisture had a quadratic effect on cohesiveness with maximum cohesion occurring at 15 to 17% moisture. Above that value, flow of the powder occurred with slippage between agglomerates and not individual particles. The residence time results indicated that the effective maximum flour cohesiveness was obtained with an 8% moisture content (Figure 37). The more cohesive the flour became, the larger the force required to shear two particles apart. A fluidized bed has conditions favorable to agglomerate formation compared to the fixed bed used in cohesiveness testing. Easier formation of agglomerates might account for the shift in the moisture level of apparent maximum cohesion. At moisture levels higher than those used in this study, water condenses on the particles. The surface tension of this water film increases cohesion between particles and reduces powder flowability.

Salt tracer It was concluded that the addition of 28 g. copper tracer, 8 g. zinc tracer, and 32 g. nickel tracer to a 28 in. deep flour bed had an effect of borderline significance on the residence times (Table 48, Appendix D). No "salt effect" was indicated when analysis of variance tests were performed with pooled data from upper and lower locations nor was there a significant interaction between the presence of salt and location. The degrees of freedom of the

tests were small and the estimate was considered rather poor.

Flow conditioning Regression analysis to determine the effect of adding 0.5% Cab-O-Sil to flour was carried out. The material effect under discussion is thus one of powder cohesiveness rather than mean powder size or particle density.

Using the data of Set 11 (Figure 38), the harmonic average crack velocity was related to relative gas velocity by three different models (Table 49, Appendix D). In model 1, both the treated and untreated flour harmonic average velocities were represented as linear functions of gas velocity with the corresponding straight lines having a common slope but different intercepts for the two materials. Model 2 also allowed the slopes of each material's line to be different. The possible influence of location was incorporated into model 3. In this model, each combination of material and location was represented by individual straight lines which could each have a unique slope and intercept. "Partial F" tests were performed to indicate which model fit best (Table 49, Appendix D). It was concluded that model 2, with a different slope and intercept for each material, was adequate. Model 1 did not account for as much variance of the data as model 2 did. Furthermore, since model 3 did not result in an improved fit compared to model 2, location was not an important factor influencing the slopes of the lines. Thus flow

conditioning the flour (reducing powder cohesiveness) resulted in a significantly increased velocity of the downward moving cracks. Comparison of Figures 37 and 38 indicates that flow conditioning had a much larger effect on residence time than moisture content changes.

Cohesiveness of the fluidized solids also had a significant effect on the measured heat transfer coefficients (84, 85). The reduction of cohesiveness resulted in increased heat transfer when the flour was flow conditioned with 1% Cab-O-Sil.

Correlations

Having determined the significant parameters for the residence time of cracks along the wall grid areas, the data were then correlated. It was convenient to express the residence times as the harmonic average velocity (equation 21) since a linear relationship with gas velocity resulted (Figure 35) and the effect of travel distance was removed. To remove the dependence of residence time variance on gas velocity (Figure 34), the dependent term of the regression models was the natural logarithm of the harmonic average velocity (see Analysis of Data section above).

The range of the data over which the models were tested is summarized in Table 10. Since the flow conditioned flour was observed only over a small range of conditions compared to pure flour, separate models were developed for each

Table 10. Range of applicability of residence time correlations

Item	Flour	Flour with 0.5% Cab-O-Sil
Column diameter, in.	6	6
Column material[1]	glass, Plexiglas	Plexiglas
Settled bed depth, H, in.	12.5 - 32	31
Moisture content, % dry basis	2.9 - 15.4	12.9 - 13.6
Fluidizing gas	nitrogen	nitrogen
Gas humidity[2], %RH	0 - 28	0
Gas velocity, ft./sec.	0.12 - 0.20	0.07 - 0.11
Stirrer speed[2], rpm	25 - 150	50
Relative location[2], elevation/H	0.27 - 1.04	0.28 - 0.95

[1] Believed insignificant.

[2] Tested as insignificant for flour.

material.

Two models fit the pure flour data almost equally well. The first model was composed of only linear terms

$$\ln \bar{v}_H = -3.446 + 7.313u - 0.0467L + 0.0207H + 0.200uL + 2.02X_T \quad [31]$$

Multiple linear regression was used to evaluate the coefficients of this model and to test them for significance (Table 46, Appendix D). All terms were highly significant at the the 0.01% level of significance. The coefficient of multiple determination (R^2=0.88) was good. Although this model was fit with all the data, it was shown previously that the moisture content had a third-order effect (Figure 37).

The second model included the higher order crack velocity dependency on the flour moisture content.

$$\ln \bar{v}_H = -2.605 + 7.315u - 0.0469L + 0.0212H + 0.200uL - 0.386X_T + 0.504x10^4 X_T^2 - 0.184x10^4 X_T^3 \quad [32]$$

Multiple regression was used to evaluate the coefficients and to test them for significance (Table 47, Appendix D). As was the case with the first model, all terms were again highly significant, the least significant being significant at the 0.02% level. The second model's coefficient of multiple determination ($\bar{R}^2$=0.89) was also good, but not much improvement

in total fit resulted over that of the linear model. In consideration of the results shown in Figure 37, it is recommended that equation 32 be used when gas velocity is near 0.20 ft./sec.

The data for flour conditioned with 0.5% Cab-O-Sil were fit very well (R^2=0.95) by the following correlation (Table 50, Appendix D)

$$\bar{v}_H = -1.031 + 17.34u + 0.0108L \qquad [33]$$

The harmonic velocity was not transformed since the range of the residuals was small. The gas velocity and location were the only parameters which were varied for 0.5% Cab-O-Sil flour. The range of the operating conditions over which the correlation applies are summarized in Table 10.

WALL-TO-BED HEAT TRANSFER

The combination of particle motion and a high rate of heat transfer between particles results in the establishment and maintenance of an isothermal temperature distribution in a fluidized bed. Particle motion in a fluidized bed promotes a high rate of heat transfer from the column wall to the bed compared to a fixed bed or an empty tube. The rate of heat flow, q, across a wall heating surface of area A exposed to a fluidized bed is proportional to the temperature difference between the heater surface and the fluid bed, $(T_W - T_B)$. The proportionality factor, h, is known as the wall-to-bed heat transfer coefficient

$$h = q/A(T_W - T_B) \qquad [34]$$

The general literature pertaining to heat transfer in fluidized beds has been reviewed and discussed many times (16, 35, 58, 63, 67, 135). Heat transfer in fluidized beds of cohesive material such as flour and starches has also been discussed (5, 84, 85).

The wall-to-bed heat transfer coefficient increases linearly at a slow rate as gas velocity is increased over the fixed bed velocity range. For gas velocities just above the minimum fluidization velocity, the heat transfer coefficient increases rapidly with increasing gas velocity but at a declining rate of increase. A maximum heat transfer coeffi-

cient value is reached at an optimum gas velocity. The heat transfer coefficient is observed to decrease only slightly over a range of higher gas velocities. Then further increases in gas velocity result in a continued lowering of the coefficient. This decline is not as fast as the rate of increase occurring before the optimum gas velocity.

The wall-to-bed heat transfer coefficient has been previously observed to vary with elevation above the gas distributor plate. The vertical profile of the heat transfer coefficient has been observed to have a flat maximum located about midway up the bed (52) or to be higher near the distributor but to decrease rather steadily as elevation increases (118).

Mechanisms

Four mechanisms have been identified through which heat may be transferred from a wall heating surface to a gas fluidized bed (63) at low to moderate temperatures where radiative heat transfer may be neglected. The mechanisms are as follows:

1. The rate is controlled by heat transfer through a thin gas film on the heater surface. This gas layer is believed to be on the order of a particle diameter or less in thickness. The particle radius has often been used to estimate this thickness (35).

This mechanism is controlling for residence times of solids on the heating surface of less than 0.030 sec.

2. The rate is controlled by heat transfer occurring in the vicinity of particle-surface points of contact accompanied by frequent replacement of particles at the surface. Mechanism 1 often occurs in conjunction with this mechanism.
3. The rate is controlled by unsteady state heat absorption by fresh emulsion which is swept up to and away from the surface. This mechanism is the basis of surface renewal models for the emulsion phase. For short contact times, this mechanism leads to the prediction that the wall-to-bed heat transfer coefficient is inversely proportional to the square root of the residence time.
4. The rate is controlled by steady state heat conduction through an emulsion layer which is seldom swept away. This mechanism represents a film model for heating the emulsion phase. For long contact times, the heat transfer coefficient is predicted to be independent of the residence time.

Mechanisms 1 and 2 often are found to operate in parallel with mechanism 3 or 4 or a combination of these mechanisms (63).

Surface Renewal Model

Various models for predicting the heat transfer coefficient in a fluidized bed have been proposed. Those based on heat conduction through a boundary layer have not been generally successful since they do not account for the effects of the thermal properties of the particles on heat transfer (35). A more successful approach has been to consider the heat transfer to occur mainly by mechanism 3. The several "surface renewal and penetration theory" models (16, 35, 79, 58, 63) are illustrative of this approach.

The surface renewal model proposed by Mickley and Fairbanks (79) has been often discussed (35, 63) and seems especially applicable to the physical conditions existing in heat transfer to fluidized beds of cohesive solids. In this model, the fluidized bed is visualized as containing small groups or agglomerates of particles called "packets" which freely move as individual units throughout the fluid bed. The packets are assumed homogeneous and to have a void fraction, density, and thermal properties similar to those of the quiescent bed at the minimum fluidization state. Transient heat transfer occurs to packets at the heater surface. Packets are periodically displaced from portions of the surface by gas bubbles to which relatively little heat is transferred.

The rate of heating depends on the rate of heating the packets and the fraction of heat transfer surface covered by bubbles. The rate of heating the packets depends upon the packet thermal properties and the packet residence time. The heating rate of the packets decreases as residence time increases, eventually declining to the steady state heat transfer rate. The maximum in the heat transfer coefficient- gas velocity curve is attributed to the competing effects of decreased residence time and increased number of gas bubbles at the heater as gas velocity is increased from the minimum fluidization velocity.

The particle motion in the radial direction is usually negligible. For free flowing glass beads, copper, alumina and aluminum particles, Koppel et al. (58) stated that

"During the present work it was observed that particles tended to move in groups downward along the wall, with only a few particles (less than 5%) moving away from or towards the wall in a radial direction. Such downward motion is typical of particles at fluidized bed walls. This would imply that the particles are representative of the packets and that particle residence times are virtually the same as packet residence times. Since some particles do move away from and towards the surface radially, one should expect that particle residence times are in general slightly shorter than packet residence times."

The mean residence time is said to be approximately the time between two successive gas bubbles (35).

Mathematical analysis of the packet model (35, 63, 79) results in the following expression for the instantaneous heat transfer coefficient:

$$h_i = \left[\frac{k_e C_S \rho_B}{\pi\, t'}\right]^{1/2} \qquad [35]$$

where t' is the time the packet is in contact with the heater.

The model may be modified (35, 79) to account for the possible difference of particle packing arrangement in a packet located at the heater surface compared to the interior. An additional resistance in series with the thermal resistance of the packet itself ($1/h_i$) is added to the model. This "contact" resistance is approximately independent of time and depends on the thickness of this zone adjacent to the wall and an effective thermal conductivity (35)

$$R_W = \delta_W / k_{eW} \qquad [36]$$

The instantaneous heat transfer coefficient applies only to the local transfer of heat at one point of the heater to a packet of age t at that location. The mean heat transfer co-

efficient is obtained by averaging the instantaneous heat transfer coefficient over the range of particle residence times and then averaging over all points of the heater. The results of this integration for several boundary conditions have been summarized and discussed for the whole range of contact resistance (35). For zero contact resistance and a constant wall temperature (35), the mean heat transfer coefficient is given by

$$h = 2(1 - f_o)\left[\frac{k_e C_S \rho_B}{\pi t_m}\right]^{1/2} \qquad [37]$$

where t_m is the mean contact time of the packet and f_o is the fraction of heater surface covered by bubbles at the given fluidization conditions.

For the case of plug flow of solids with no radial motion, the mean heat transfer coefficient for constant wall temperature and negligible bubble coverage is (79)

$$h = 2\left[\frac{k_e C_S \rho_B}{\pi L}\right]^{1/2} v^{1/2} \qquad [38]$$

where v is the constant downward velocity of particles moving past a heater of length L.

Expressing the mean contact time of equation 37 in terms of the length of the heater results in the harmonic average velocity, equation 21, which is not equivalent to the arithmetic velocity of equation 38 unless the residence time distribution is uniform. These two solutions (equations 37 and 38) are thus equivalent for pure plug flow, but not for other distributions such as the one measured in the current work. For a known (or measured) residence time distribution, the mean residence time may be obtained by integrating the distribution using a weighting factor (63).

Criticisms of the packet model are the square root dependence on heat capacity, and possibly the dependence on thermal conductivity (16, 63) of the packet. The heat transfer coefficient has been found to be dependent on the heat capacity of the particles (63), but it was found to be essentially independent of the thermal conductivity of metallic particles even though conductivity was varied over a wide range (16).

Correlation With Residence Time Data

The heat transfer coefficients measured by Nazemi (84) were correlated with the crack velocity.

The heat transfer coefficients corresponding to the measured gas velocities in the present work were obtained by interpolation of Nazemi's data with a linear correlation of

the heat transfer coefficients and gas velocity (Table 51, Appendix D). The heat transfer coefficients were then correlated with the residence times expressed as harmonic average velocities. Two models were fitted. The first was a linear model (Table 52, Appendix D) (R^2 = 1.0)

Upper location

$$h = 7.073 + 83.42\bar{v}_H \qquad [39]$$

Lower Location

$$h = 2.342 + 63.54\bar{v}_H$$

which fit the data well, as expected from the fact that the heat transfer coefficients had been calculated from linear models themselves. In the second model (Table 53, Appendix D), the heat transfer coefficients were a function of the square root of the harmonic average velocities (R^2 = 0.99)

Upper location

$$h = 53.63\bar{v}_H^{-1/2} \qquad [40]$$

Lower Location

$$h = 35.02\bar{v}_H^{-1/2}$$

This model was of the form of the theoretical relation derived from the packet surface renewal model, equation 37. The good fit of the square root regression model agrees well with that theory.

The coefficient of the square root regression model was estimated from the packet model, equation 37, as described below.

For the particles used in the present investigation, the contact resistance, as estimated using the average particle radius for the contact layer thickness, was negligible compared to the packet resistance.

The assumption was made that bubble frequency at the wall was small enough so particles traveled the full length of the heater, 6 in., between bubbles. This also implied that the fraction of heater surface covered with bubbles was small, an implication supported by observation. It was also assumed that the 6 in. heater length was small enough so that the downward particle velocity was constant over this distance. With the above assumptions, the equation for the packet model for the mean heat transfer coefficient in terms of the harmonic velocity became

$$h = \left(\frac{k_e C_S \rho_B}{\pi d}\right)^{1/2} (\bar{v}_H)^{1/2} \qquad [41]$$

The parameters of this equation were either measured or were estimated from published correlations. The fluidization conditions used in the calculations were as follows

Cross sectional bed area = 0.1963 ft^2.

Temperature = 72 °F

Flour moisture content = 13.6%, dry basis

Flour particle density = 91.4 $lb./ft^3$.

Bed mass = 15.97 lb.

Settled bed depth = 27 in.

Minimum fluidization velocity = 0.10 ft./sec.

Bed expansion at minimum fluidization = 20%, (Figure 26)

Nitrogen thermal conductivity = 0.014 Btu/ft.hr.°F

The average bulk density of the fluidized bed at minimum fluidization, 30.2 lb./ft^3., was used as the packet density. The porosity of the bed was calculated (63) from the bed height to be 0.67.

The flour particle heat capacity was calculated from a published correlation (128), based on temperature and moisture content, to be 0.389 Btu/lb.°F. The effective thermal conductivity was estimated to be that of a packed bed of porosity equal to that of the bed at minimum fluidization. The flour particle thermal conductivity was approximated by that of corn starch (99, 100) as 0.125 Btu/hr.ft.°F. This value was for the particle in a vacuum. Several correlations for determining the thermal conductivity of gas-solid packed beds exist (99, 100). It was not known which of these correlations most closely applied to a flour or starch bed. The effective thermal conductivity was calculated from four correlations. The values calculated from the "Lord Rayleigh" and the "Maximum Limit" equations bounded the estimated conductivity at 0.027 to 0.051 Btu/hr.ft.°F, respectively.

Maximum Limit equation:

$$k_e/k_g = (1 - P) + PK \qquad [42]$$

Lord Rayleigh equation:

$$\frac{k_e}{k_g} = \frac{KP^{2/3} + (1 - P^{2/3})}{K(P^{2/3} - P) + (1 - P^{2/3} + P)} \qquad [43]$$

where $K = k_e/k$

The other values were 0.029 and 0.033 Btu/hr.ft.°F.

The travel distance was the length of the heat transfer surface, 6 in.

Substituting the above values into equation 41, the coefficient of the packet model was calculated to be 0.904 to 1.236 Btu/(ft.)$^{3/2}$ (hr.)$^{1/2}$ (°F), for the predicted range of thermal conductivity values. When the units were converted to those of the experimentally determined coefficients for each location, it was seen that the coefficient had been underestimated at best by a factor of 2.2 for the lower surface location and 1.9 for the upper surface location (15.7 to 21.3 calculated, 39.8 and 46.6 Btu sec$^{1/2}$/ft^2 hr.°F in$^{1/2}$., measured, at the upper and lower locations respectively).

Since it was not possible to time most of the cracks for further than 3 in. under the range of gas velocities used, it seemed reasonable to suppose that the average crack did not

travel much more than 3 in. before being swept from the heater surface by a bubble. Under this condition, the heat transfer coefficient for a 3 in. long heater is not likely to be much greater than for a 6 in. heater (79). The packet theory with the higher estimate of effective thermal conductivity predicted a coefficient value of 30.1 for these conditions. This value was reasonably close to that measured for the upper heater, since radial mixing was not completely absent from the flour bed.

The differences in the coefficients of the upper and lower locations could not be accounted for by the packet model. It is unlikely that the packet heat capacity or effective thermal conductivity would vary much between the two locations. The bed density difference was calculated from the bed pressure drop across each heater (84) and was found to be only slightly different at each location.

It was noted in the residence time "Results" section that the identity of cracks in the upper section was much more frequently lost to the observer than for those in the lower section. This agreed with the general behavior of gas bubbles in fluidized beds. Bubbles increase in size as they rise through the column due to the decreasing pressure and also due to coalescence. At the upper location, the bubbles, being larger than at the lower location, influence the motion of particles at a greater distance between particle and

bubble. Some bubbles, which passed the lower heat transfer surface without disrupting downwards solids movement, have grown enough by the time they are at the upper location to exert a disruptive influence on the solids downward motion. Packets are swept into and away from the interior more frequently at the upper location as well as moving downward slower due to larger upward forces exerted by larger bubbles at greater separations.

The measured heat transfer coefficients and the correlation are shown for both heater locations as a function of gas velocity in Figure 39.

Figure 39. Fit of heat transfer coefficients with harmonic average velocity

a. Average heat transfer coefficient (84) versus square root of harmonic average velocity

b. Predicted (equations 31 and 40) values of heat transfer coefficient versus observed values (84)

c. Observed (84) and calculated (equations 31 and 40) heat transfer coefficients versus gas velocity

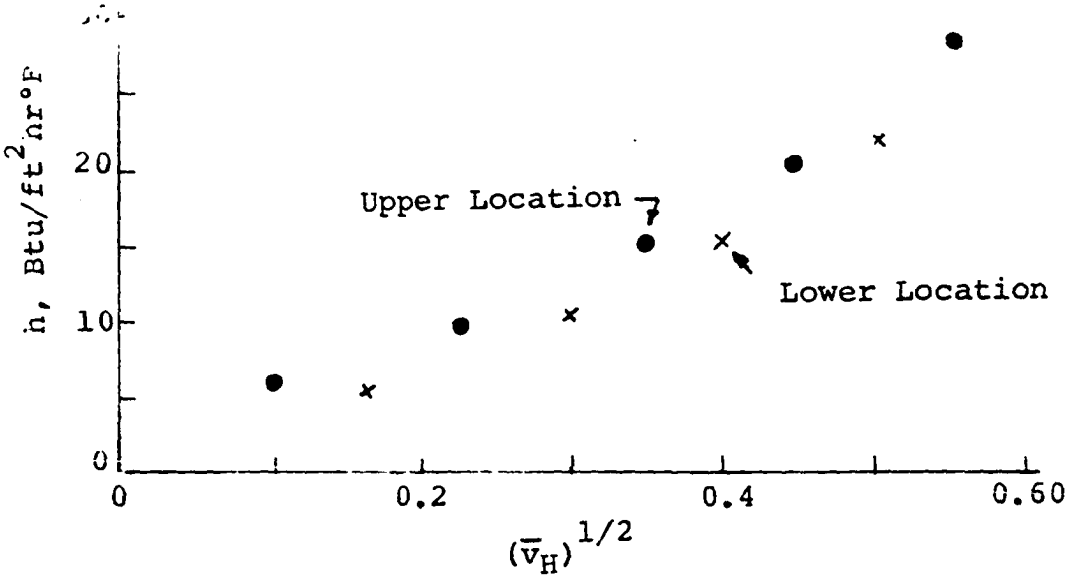
h, Btu/ft^{2}hr°F
20
10
0
Upper Location
Lower Location
0
0.2
0.4
0.60
$(\bar{v}_H)^{1/2}$

(a)

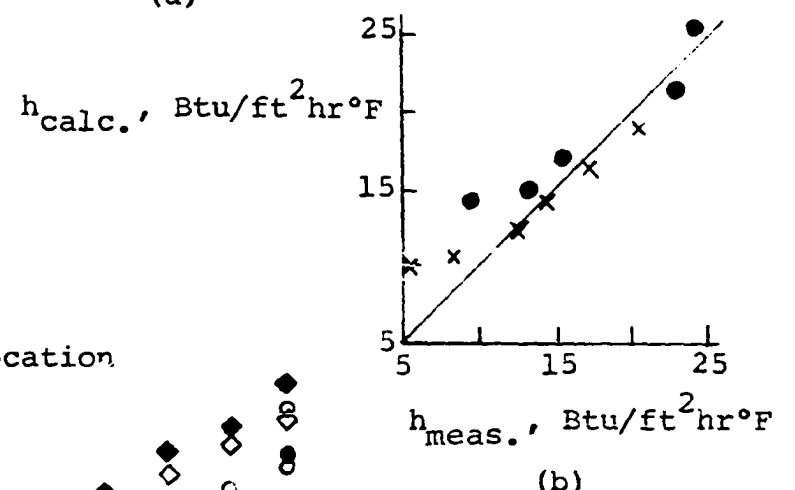
$h_{calc.}$, Btu/ft^{2}hr°F
25
15
5
5
15
25
$h_{meas.}$, Btu/ft^{2}hr°F

(b)

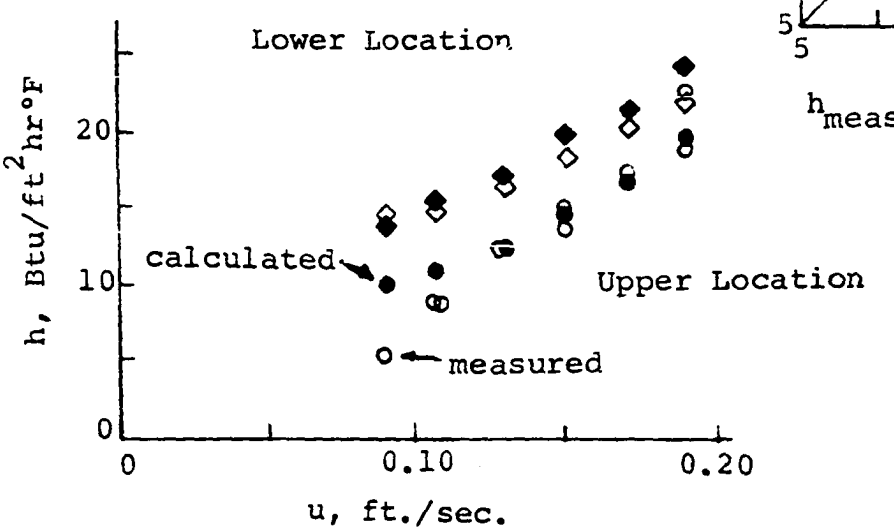
Lower Location
h, Btu/ft^{2}hr°F
20
10
0
calculated
Upper Location
measured
0
0.10
0.20
u, ft./sec.

(c)

MIXING EXPERIMENTS

The process of mixing a trace component (less than 1%) of metal salt in fluidized beds of flour or potato starch was investigated. The salt was distributed over the top of the fluidized bed. Samples were collected as a function of time, metal concentration was measured, and the mixing curve was constructed from this information. In this manner, the mixing curve for every experimental mixing run (numbers 10, 11, and 12) in each Set of the experimental design shown in Figures 22 and 24 was constructed. The mixing curve contains information on both transient and steady state mixing.

After fluidization, the settled beds of run 11, Sets 5 to 13, were sampled at known locations. This was done to show whether or not segregation occurred or whether the steady state mixture was homogeneous.

The tracer concentration variance as a function of sample size of samples collected from steady state mixtures was compared for each material. This indicated the scale of scrutiny the mixture could be subjected to and still appear homogeneous.

Mixing Curve

A mixing curve (97) shows the progress of mixing. In the current work, the progress of mixing a small amount of tracer salt distributed over the surface of a fluidized bed

was followed. Samples of 0.5 to 1.2 g. were withdrawn at known times from an intermittent effluent stream flowing from a sampling tap located just above the gas distributor plate. A time of 1.3 sec. or less (87) was required for the actual collection of each sample. Mixing was continued for 20 to 35 min., long enough to achieve a steady state distribution of tracer. The tracer concentration of each sample was determined by dissolving the salt and spectrophotometrically measuring the concentration of metal tracer (as described in Analytical Procedures).

The mixing curves for the mixing runs (numbers 10, 11, and 12) of each set in the experimental design (see Figures 22 and 24) were constructed. The weight of tracer metal in the sample per gram of sample was calculated and plotted as a function of time. These values were normalized (9, 11, 97) by dividing each sample concentration by the average concentration of the steady state mixture. The mixing curves were these normalized values plotted as a function of time. Normalization made visual comparison between curves easier and provided a common steady state value, 1.0, about which sample variance could be calculated.

In these mixing experiments, the fluidization conditions were varied over the range indicated in Table 6. The detailed conditions for each run are listed in Table 21, Appendix C. Batch operation of each bed was approximated to a

high degree. The sample tube was purged just prior to collecting a sample. About equal amounts of material was purged as was collected. The total average change in bed mass due to sampling was 4.4% for collecting about 90 samples (Table 22, Appendix C lists the data). The total change in settled bed depth during an average run was 4.9% (Table 22, Appendix C), including that lost by entrainment.

Results

Five representative mixing curves (runs 10, 11, and 12 of Set 2 and run 10 of Sets 3 and 13) are shown in Figures 40 to 44 while the mixing curves for the remaining runs are in Appendix C, Figures 52 to 77.

The major features of the mixing curves are described by four characteristics discussed below: the lag time, the minimum mixing time, the percentage of steady state samples having concentrations outside the range of most steady state samples, and a steady state mixing index.

Before examining the mixing curves further, it is convenient to summarize the qualities which an ideal or perfect mixer of solids would exhibit in terms of the above characteristics. First, the lag time would be zero. On adding the tracer to the mixer top, some would immediately be transported to the bottom. Second, and more importantly, the minimum mixing time would also be zero. Solids would be

Figure 40. Mixing curve of Set 2, run 10

Parameters: u = 0.12 ft./sec.

N = 50 rpm

%M = 13.0%

H = 26.8 in.

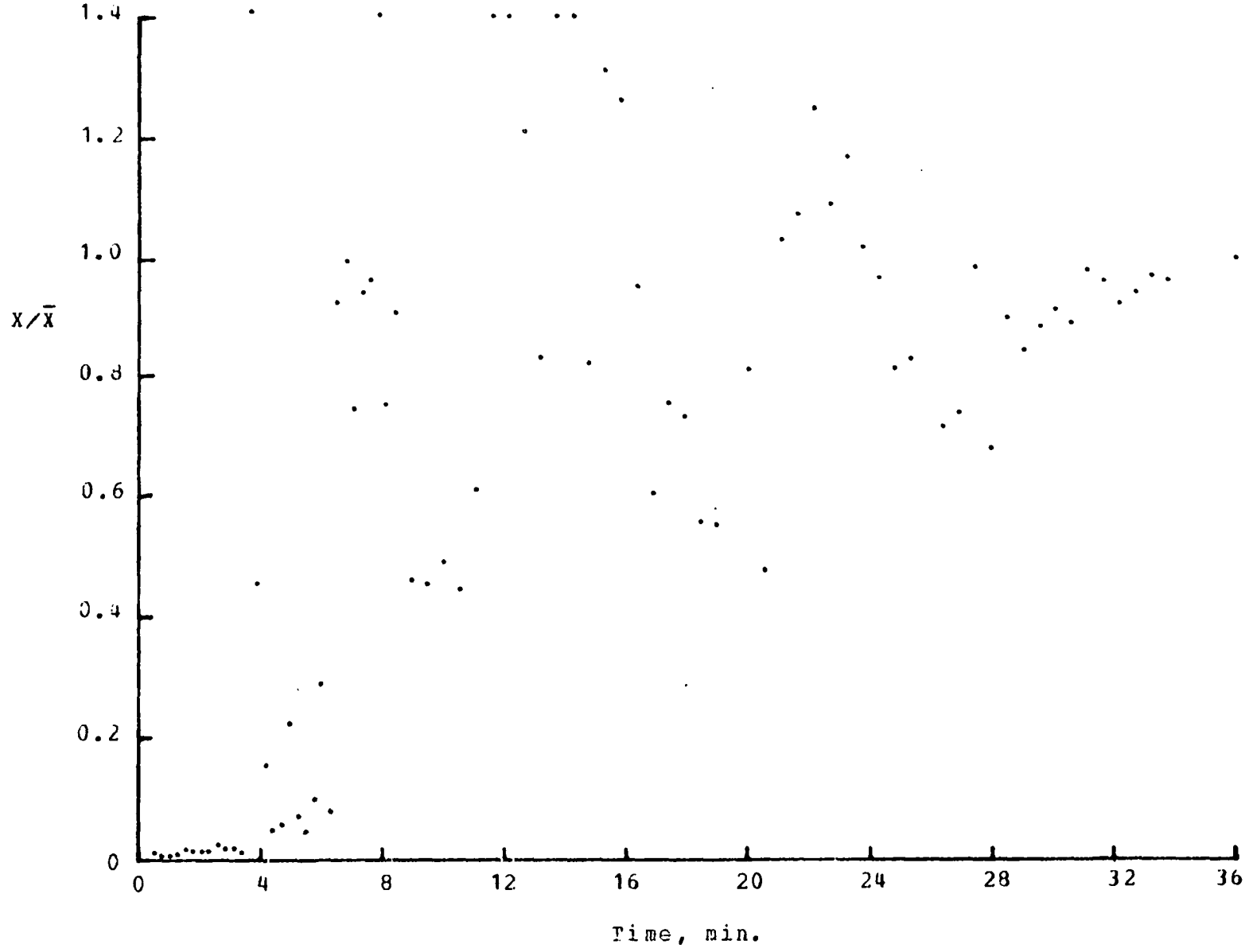
1.4
1.2
1.0
0.8
0.6
0.4
0.2
0
X/X̄
0
4
8
12
16
20
24
28
32
36
Time, min.

Figure 41. Mixing curve of Set 2, run 11

Parameters: u = 0.152 ft./sec.

N = 25 rpm

%M = 13.0%

H = 28.0 in.

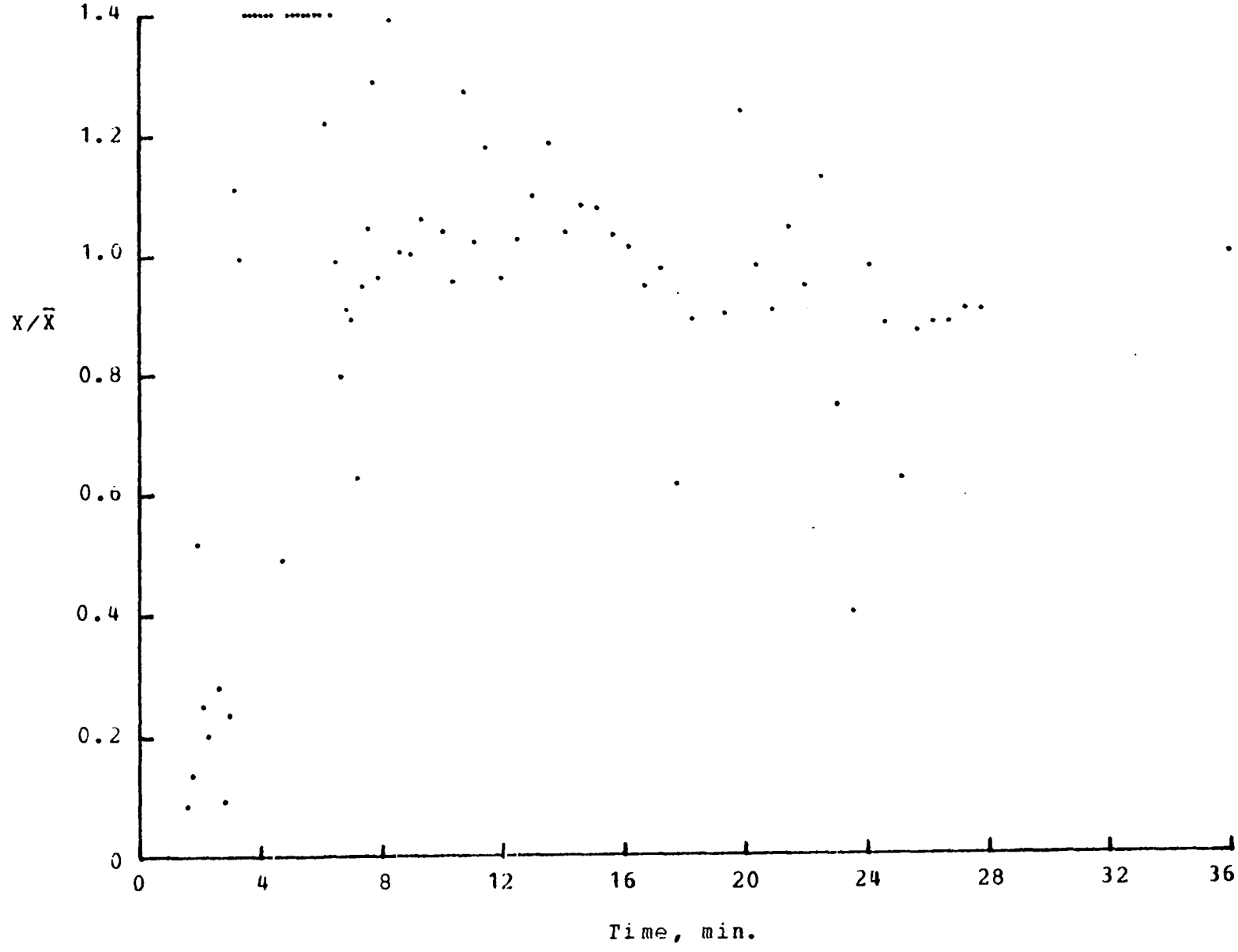
1.4
1.2
1.0
0.8
0.6
0.4
0.2
0
X/X̄
0
4
8
12
16
20
24
28
32
36
Time, min.

Figure 42. Mixing curve of Set 1, run 10

Parameters: u = 0.152 ft./sec.

N = 25 rpm

%M = 13.2%

H = 28.0 in.

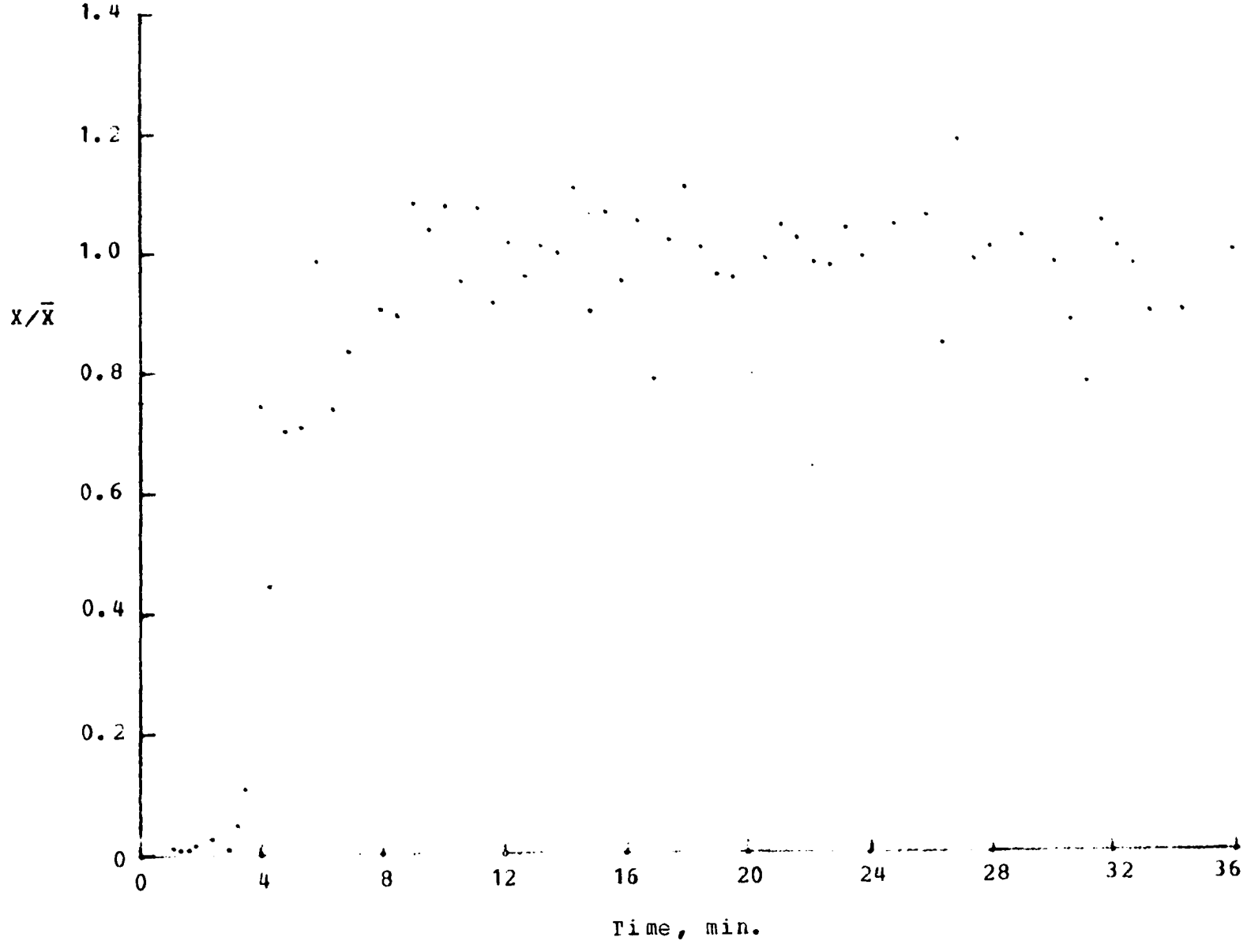
1.4
1.2
1.0
0.8
0.6
0.4
0.2
0
X/X̄
0
4
8
12
16
20
24
28
32
36
Time, min.

Figure 43. Mixing curve of Set 2, run 12

Parameters: u = 0.20 ft./sec.

N = 50 rpm

%M = 12.9%

H = 27.1 in.

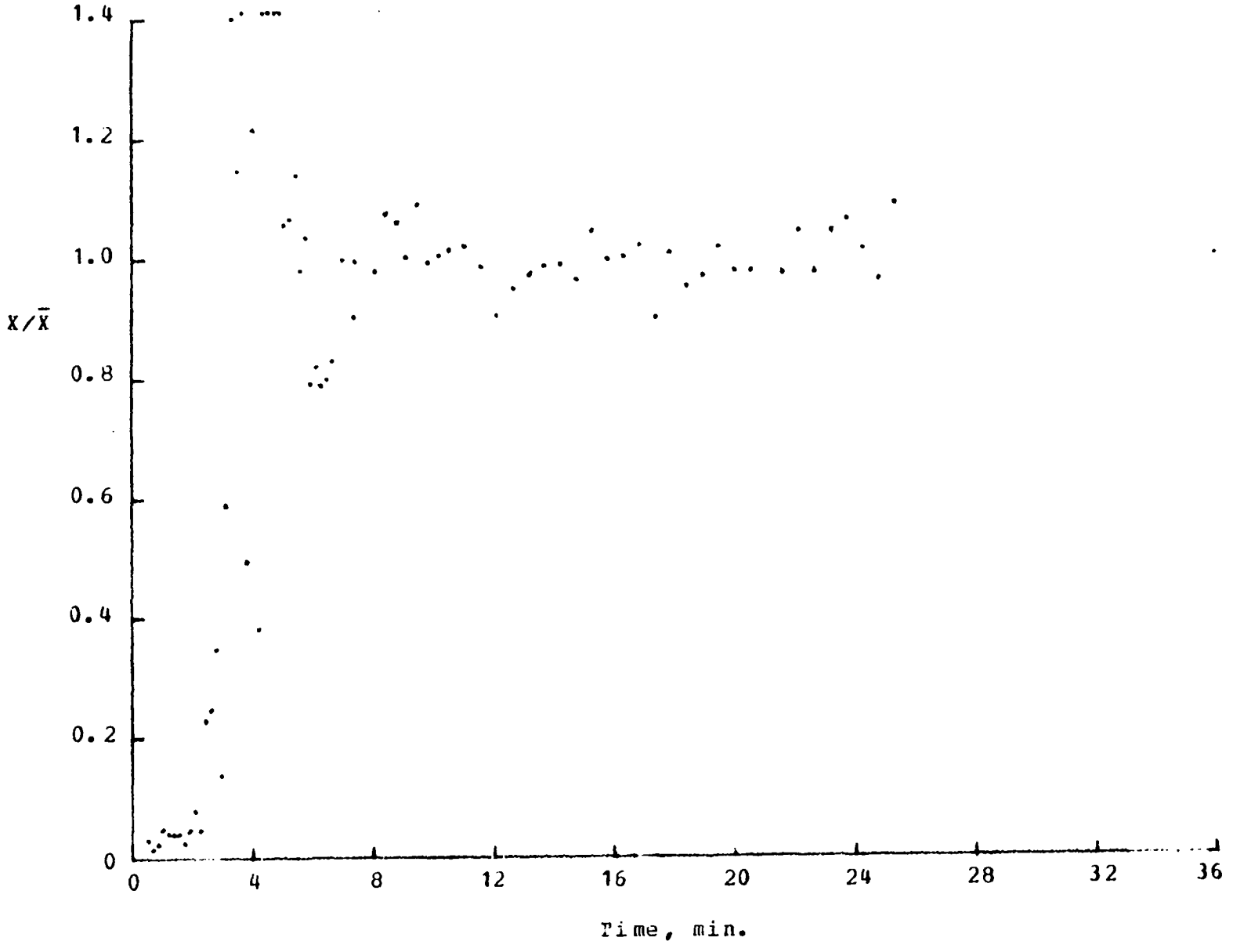
1.4
1.2
1.0
0.8
0.6
0.4
0.2
0
X/X̄
0
4
8
12
16
20
24
28
32
36
Time, min.

Figure 44. Mixing curve of Set 13, run 10

Parameters: u = 0.35 ft./sec.

N = 50 rpm

%M = 13.8%

H= 31.0 in.

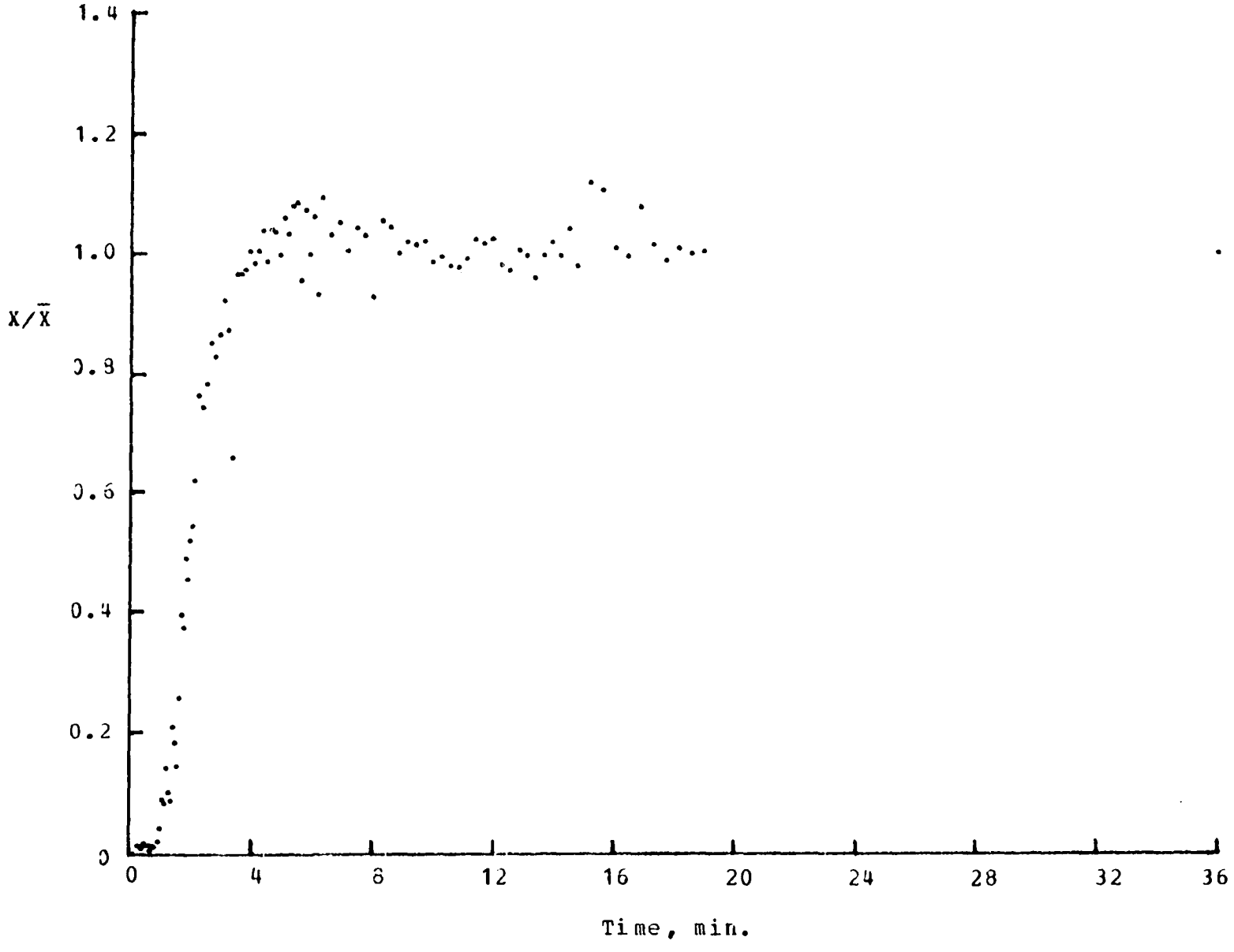
1.4
1.2
1.0
X/X̄
0.8
0.6
0.4
0.2
0
0
4
8
12
16
20
24
28
32
36
Time, min.

mixed to steady state concentration as fast as they were added. Third, none of the samples (above a minimum size which is a function of the relative numbers of particles of each component) would exhibit a concentration outside the range of the other samples. Finally, the mixing index would be that of a completely random distribution of mixture components (as discussed in the Literature Review).

In the real world, a very good mixer would provide a short minimum mixing time (lag time is usually unimportant compared to the minimum mixing time), would produce very few steady state samples having concentrations outside the range of the others, and would yield a mixing index close to that of a random mixture of the components. In practice, these stringent requirements are seldom encountered in most solids mixing application. What is important is economically meeting the specifications of the product mixture. Different applications have different tolerance levels for the four characteristics of the mixing curve.

The time required for adding tracer to the top of the fluidized bed was short, about 5 sec. or less (data are listed in Table 23, Appendix C). The mixing curves for the deep beds (all runs except those of Sets 7 and 14) show a significant lag time, 2 to 5 min., required for the tracer material to travel down the column. The lag time for the 12.5 in. deep settled beds (Sets 7 and 14) was shorter, 20

sec. to 1 min.

Following the lag time, two types of transient concentration profiles were observed. In one type, the overdamped response case, the tracer concentration increased more or less linearly (Figures 42 and 44), overshot the final concentration range (concentrations larger than 1.4 have been shown at the 1.41 level in the mixing curves), and then settled down to a steady state condition or fluctuations about the average concentration. Occasionally, a sample of either relatively large or small concentration was obtained in the steady state region.

In the second type of unsteady state behavior, the underdamped response case (Figures 40, 41, and 43), a very heterogeneous condition existed (at least in the lower bed section from which the samples were withdrawn). After the lag time, the sample concentration suddenly increased to a very large value which was followed in rapid succession by very much lower values and then more high values and the cycle was continued. With time, the amplitude of the fluctuations damped out to the same final steady state condition observed after the first type of unsteady state behavior. The duration of the individual high or low concentration periods was irregular. The amplitude and period of the underdamped type of response to the addition of tracer was fairly random and was not reproducible.

In fact, the underdamped and the overdamped responses were observed with the same fluidization conditions (Figures 41 and 42). Whether the type of response obtained was a function of the uniformity of the tracer distribution across the bed surface or dependent on the phase of the bed expansion cycle (discussed in the Fluidization Characteristics section) or on the random occurrence of bubbles was not evident. Both types of responses occurred over much of the range of operating conditions used. The length of the transient period, of course, was smaller when the bed was fluidized at the better mixing conditions where steady state was quickly achieved. In these cases, the overdamped response curve had a steep slope, but not as steep as that of the underdamped response curve. Sometimes sampling was not quick enough to determine much about the transient response at all (for example, flow conditioned flour, Figures 62 and 63).

Both types of transient concentration responses to the impulse addition of a tracer to the bed top were previously observed, under different conditions, for mixing curves determined from samples collected from the bottom half of fluidized beds (97).

The series of mixing curves (Figures 40 to 44) illustrates the effects of increasing fluidization gas velocity on the mixing process.

The mixing curve for a bed fluidized at 0.12 ft./sec. is shown in Figure 40. Very poor mixing of solids resulted. After a lag time of 4.0 min., the concentration increased to a very high value and just as suddenly dropped to low values for the next 3 min. or so. Very high values occurred periodically during the first 14 min. This suggested that a "front" of tracer was circulating through the bed, gradually being axially mixed with the flour. After 21 min., the largest amplitude fluctuations had damped out to smaller ones (±25% of steady state), but some cycling appeared to continue after that as all samples collected from 23 to 32 min. were below, but near, the average value calculated from the material balance. Since the other runs at this gas velocity also provided a poor, generally nonreproducible quality of mixing, a minimum mixing time of 21 min. was accepted for obtaining a coarse mixture.

On increasing the gas velocity to 0.15 ft./sec. (Figures 41 and 42), some improvement in mixer performance resulted. In Figure 41, it appeared that the tracer front was broader and was mixed quicker with the flour than where a gas velocity of 0.12 ft./sec. was used. In Figure 42, a region of high concentration values was not observed, but the underdamped response showed that enough mixing had occurred before the front reached the sampling tap so that the concentration built up gradually to the steady state level. As discussed

above, the reason for the occurrence of these two types of responses under the same operating conditions was not determined.

At a gas velocity of 0.20 ft./sec. (Figure 43), much better mixing was obtained. The tracer front moved more quickly down the column and was mixed faster with the flour to a more homogeneous mixture than at the lower gas velocities. Increasing the gas velocity still further, to 0.35 ft./sec. (Figure 44), resulted in the best mixing of tracer with pure flour observed in the deep beds (settled depth of 26 to 32 in.). The minimum mixing time was shorter and fewer samples of the apparent steady state mixture had concentrations much higher or lower than the rest.

In many runs with pure flour, the transient response, whether underdamped or overdamped, was linear during the period of initial rise. In quite a few runs, samples were collected at sufficiently short time intervals relative to the rate of concentration increase to clearly define the initial response. The very first concentration increase was sometimes linear (for example, Figures 59, 69, and 71 of Appendix C) but was more frequently nonlinear (for example, Figure 44 and Figures 53 and 63 of Appendix C). In these cases, the rate of increase in concentration accelerated until a maximum, constant rate of increase occurred. The

concentration either proceeded to overshoot the steady state level or the rate of change in concentration slowed to produce an overdamped response. Such an initially nonlinear, overdamped response had been previously observed in trace solids mixing in beds of cracking catalyst (97).

For all the mixing curves, especially those obtained with a gas flow above 0.12 ft./sec., most of the steady state sample concentrations fell within a small range of values about the mean level calcualted from the material balance. Usually 5 to 10% of the samples collected from the steady state bed had tracer levels above or below this range. In determining this range, as many samples were included as possible without resulting in a major change in the between sample variance caused by including one or two more points in the range. Points near the clearly transient region had to meet the additional criterion, discussed below, defining the start of the steady state region. For each material, the lower and upper limits of this concentration range are summarized for different gas velocities in Table 11 in terms of the percentage of the steady state average concentration. These limits observed for each run, in terms of the absolute tracer concentration as well as the percentage of the steady state average concentration, are listed in Table 24 of Appendix C. In flour beds (Figure 45), the steady state range defined by these limits narrowed as gas velocity was in-

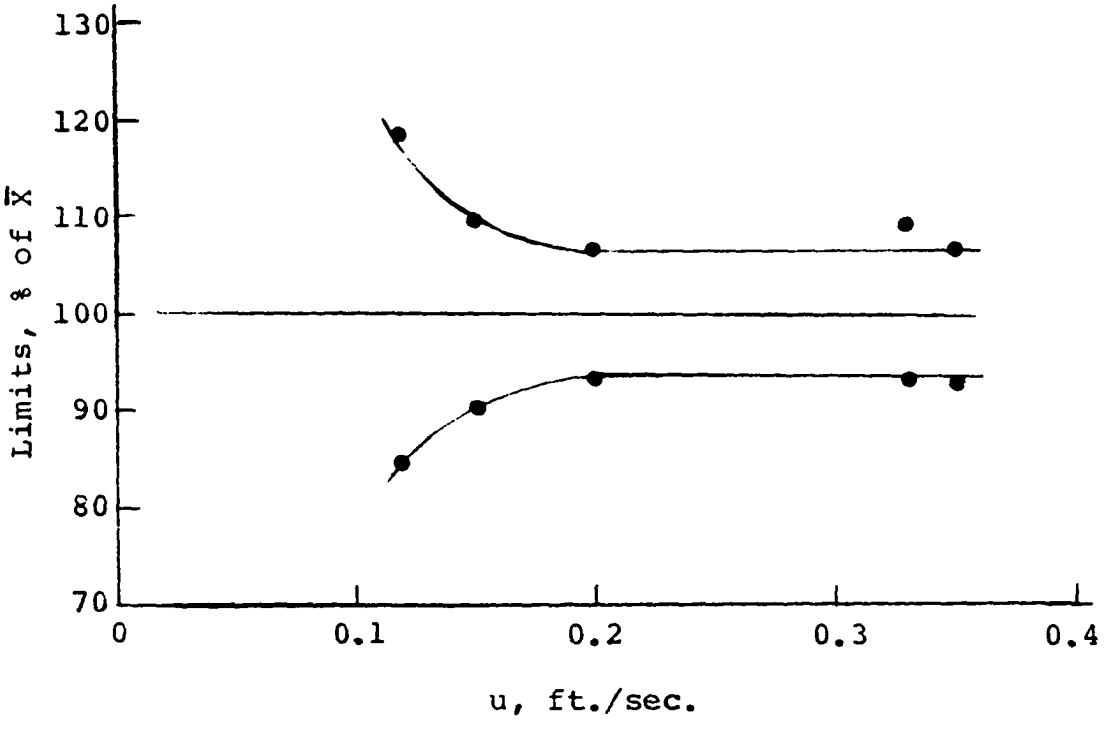

Figure 45. Mean steady state "natural" concentration limits versus gas velocity

creased. This indicated that most of the samples tended to lie closer to the average value as gas velocity increased. Thus mixture homogeneity was a function of gas velocity. Relatively little improvement resulted with gas velocities above 0.20 ft./sec, however. It seemed that a range of about ±7% of the average steady state concentration was the best range obtainable with pure flour. Flow conditioned flour had a slightly better range, ±5%, and showed a slight improvement with increasing gas velocity. Potato starch results were mixed; a range of ±6% was obtained for the first run but a wider range for the second run which was at a higher gas velocity. Both potato starch runs were flow conditioned by the added salt (discussed in Fluidization Characteristics).

The intersection of the steady state concentration limits with the unsteady state portion of the mixing curve was used as one criterion defining the start of the steady state mixing region. Another requirement was that the mixing curve must have reached the average concentration level expected from the material balance (or due to uncertainty in the material balance, that average value calculated from samples collected at times definitely long enough to be from the steady state mixture). Overshoot or a clearly oscillatory unsteady state response also must have damped down to within the concentration limits. The minimum time meeting the above requirements defined the attainment of steady state and is

Table 11. Summary of steady state flow sample concentration limits

Material	u, ft./sec.	Ave. concentration limits, % of $\bar{X}$ lower limit	upper limit
Flour III			
	0.12	84.4	118.6
	0.15	90.1	109.5
	0.20	93.1	106.6
	0.33	93.	109.
	0.35	92.5	106.5
Flour III with 1.0% Cab-O-Sil			
	0.06	95.	104.
	0.08	94.	103.
Potato Starch			
	0.15	94.	105.
	0.20	87.	107.

referred to as the minimum mixing time. Fluidization for at least this length of time from tracer addition would be required before samples of representative size collected from an effluent stream, would have the average steady state concentration level, the associated mixture homogeneity, and the percentage of samples having concentrations outside the concentration limits of the steady state mixture.

Having defined the steady state region as those samples collected after the minimum mixing time, a mixture homogeneity index (see Literature Review) such as the sample variance, can be calculated. In the present work, the sample variance

and the coefficient of variation (the standard deviation divided by the steady state average sample concentration) were the mixing indices used to describe the mixture. Including the samples with concentrations outside the range of the natural limits defined above (Table 11) would have an unduely large effect on the mixing index. These samples were excluded from the indices.

The minimum mixing time, concentration limits, and the mixture homogeneity are not independent. Enlarging the range of the concentration limits from the natural range used in this work, resulted in decreased mixture homogeneity and a smaller percentage of rejected samples. The minimum mixing time determined by the above method would generally decrease too. The lag time was not dependent directly upon the other three characteristics though the same basic particle motion mechanism determined all these characteristics.

For a few mixing curves, the natural limit of steady state concentration was ambiguous. One could determine two sets of characteristic values (having a common lag time) depending upon which characteristic was most important to minimize in a potential application. For a minimum sample variance criterion, the sample variation could be reduced some at the expense of increased mixing time without a significant change in the percentage of rejected samples. With the same data, a minimum mixing time criterion could be applied at the

expense of accepting a decreased mixture homogeneity, but perhaps not too great a decrease. Since a decision of the criterion to apply depends upon the requirements of the application, characteristics of the four ambiguous runs (Set 4, run 12; Set 12, run 11; Set 13, runs 10 and 11) were determined twice, once under each of the above criteria. Except where noted, no significantly different conclusions resulted from using one criterion or the other.

For each run, the four mixing characteristics, the steady state average concentration, and the coefficient of variation are summarized in Table 12.

In one run (Set 8, run 11), only about 60% of the zinc salt was injected initially. The 40% that remained in the injector was later added. Two step-responses resulted in that mixing curve (Figure 67, Appendix C). The two steady state variances were equal (Table 12). Since the lag time and, hence, the actual minimum mixing time for the second impulse was not accurately known, only the first response was included in the statistical analysis discussed later.

The average lag times and minimum mixing times of 31 in. deep beds of flour having a 13% moisture content are plotted as a function of gas velocity in Figure 46. Both times decreased nonlinearly with increasing gas velocity.

As one might expect, the deeper the bed, the longer it takes particles added at the top to travel to the bottom,

Table 12. Summary of steady state mixing samples (flow samples)

Set, Run No.	Lag time[3] min.	t_M min.	Samples in limits[1] mg. metal/g. n	ave.	S	C.V.[2] %	% Samples excluded[4] Low	High
1,10	3.0	8.0	41	1.195	0.073	6.09	2	7
1,11	4.0	7.1	40	0.383	0.044	11.4	6	10
1,12	3.5	6.2	49	1.249	0.038	2.96	0	4
2,10	4.0	21.0	24	1.162	0.167	14.4	0	0
2,11	3.4	8.5	32	0.419	0.036	8.51	5	10
2,12	2.5	7.0	38	1.261	0.059	4.62	0	0
3,10	2.9	8.1	21	1.090	0.040	3.64	0	0
3,11	5.0	14.4	37	0.410	0.039	9.44	11	7
3,12	5.5	9.6	46	1.271	0.081	6.33	2	0
4,10	7.5	17.0	36	1.127	0.034	2.98	0	0
4,11	7.0	17.0	38	0.347	0.020	5.60	3	0
4,12	3.4	7.0	46	1.353	0.060	4.38	0	2
	3.4	10.0	35	1.351	0.043	3.11	0	5
5,10	4.0	6.7	45	1.086	0.027	2.44	2	2
5,11	5.0	8.5	48	0.329	0.007	1.58	0	4
6,10	3.0	7.1	53	1.128	0.024	2.08	2	2
6,11	4.0	6.5	46	0.337	0.077	22.8	2	4
7,10	1.0	5.1	41	1.159	0.019	1.58	4	4
	1.0	6.1	37	1.159	0.019	1.58	0	3
7,11	1.0	3.0	54	0.273	0.008	2.37	5	5
8,10	3.4	9.1	37	1.039	0.023	2.16	3	5
8,11	4.7	8.9	18	0.192	0.011	5.18	5	5
	4.7	20.0	24	0.299	0.012	3.69	4	0

[1] See Table 24, Appendix C.

[2] Coefficient of variation, corrected for concentration measurement variance (87).

[3] Of tracer front.

[4] Concentrations not within limits listed in Table 24, Appendix C.

Table 12. (Continued)

Set, Run No.	Lag time min.	t_M min.	Samples in limits mg. metal/g. n	ave.	S	C.V. %	% Samples excluded Low	High
9,10	6.0	13.8	18	0.964	0.027	2.75	10	0
9,11	6.0	8.6	37	0.292	0.010	3.02	5	3
10,10	3.8	3.9	38	0.860	0.039	4.49	3	3
10,11	5.0	10.0	42	0.265	0.010	3.33	2	4
11,10	0.3	2.6	60	1.098	0.023	2.04	8	0
11,11	0.2	3.6	56	0.339	0.006	1.10	3	0
12,10	0.7	3.0	62	0.741	0.015	1.90	3	0
12,11	0.4	0.5	101	0.209	0.010	4.23	1	0
	0.4	1.5	85	0.208	0.010	4.25	1	0
13,10	1.5	4.3	51	1.203	0.040	3.30	4	4
	1.5	6.5	36	1.191	0.029	2.40	7	3
13,11	1.7	5.1	46	0.377	0.013	3.22	4	2
	1.7	6.5	37	0.380	0.012	2.91	5	3
14,10	0.4	2.0	29	1.419	0.057	4.00	9	6

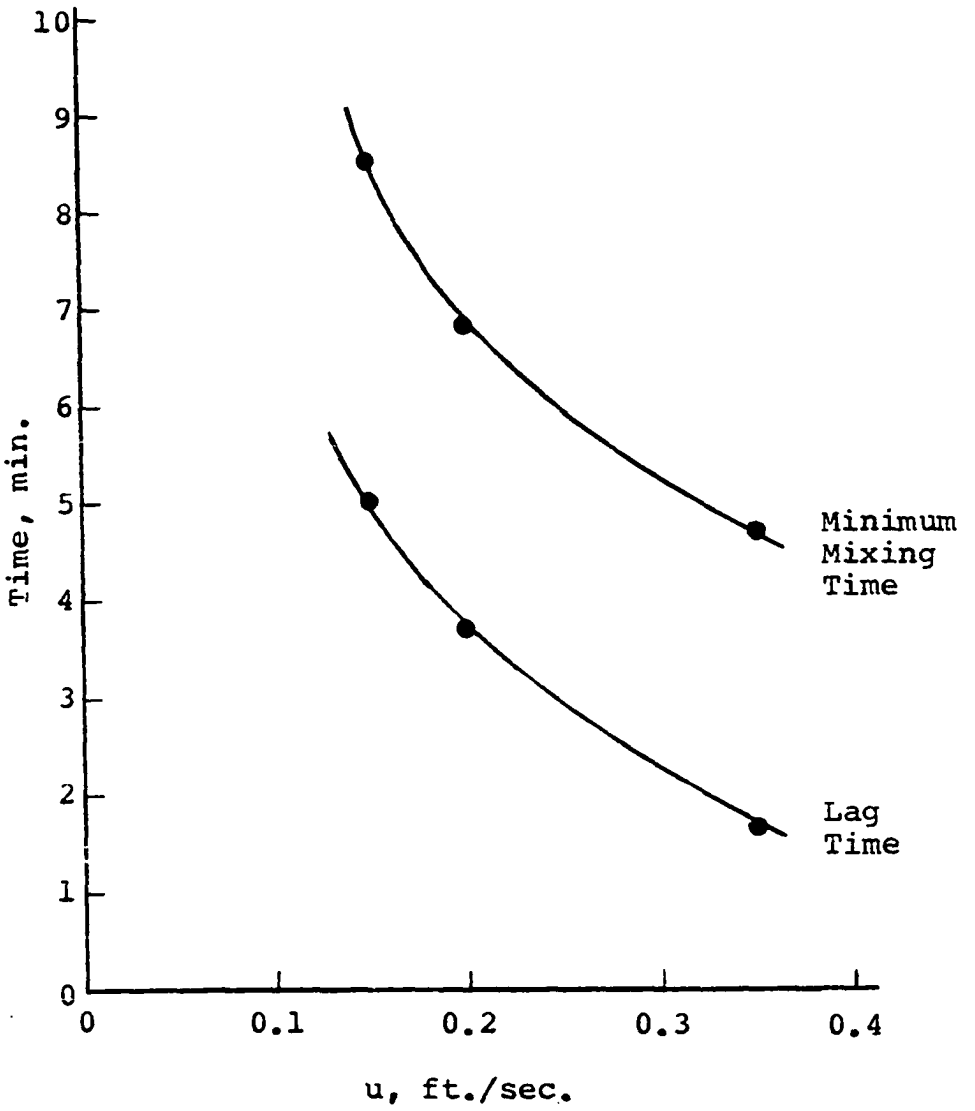

Figure 46. Average lag time and minimum mixing time versus gas velocity

Parameters: pure flour, %M = 13%

H = 31 in.

Figure 47. For the bed depth range used in these experiments, an increase in both lag time and minimum mixing time with increasing bed depth was observed. The 0.15 ft./sec. data showed that both characteristics had a common slope. The 0.20 ft./sec. data were more scattered than the 0.15 ft./sec. data and were not conclusive in indicating if the slopes could really be the same.

Extrapolation to much shallower beds leads to the erroneous conclusion of zero lag time, and probably also an erroneous minimum mixing time. Lateral mixing should be the rate controlling process for beds which are wider than they are tall whereas in deep beds with height several times greater than diameter, axial mixing should be the rate limiting process. Since lateral mixing may not have the same dependency on gas velocity as axial mixing, more time may be required for mixing a shallow bed than is indicated by extrapolation of the data in Figure 47. At very small bed depths, the gas would "punch" through the thin bed and, if particle motion ensued, poor mixing would be expected.

Figure 48 shows the effect of moisture content of the flour on the lag time and minimum mixing time. The lag time in the beds operated at a gas velocity of 0.20 ft./sec. showed a cubic relationship with moisture content. A maximum time occurred near the 8% moisture content level. Unfortunately, the 8% moisture level at 0.15 ft./sec. was not

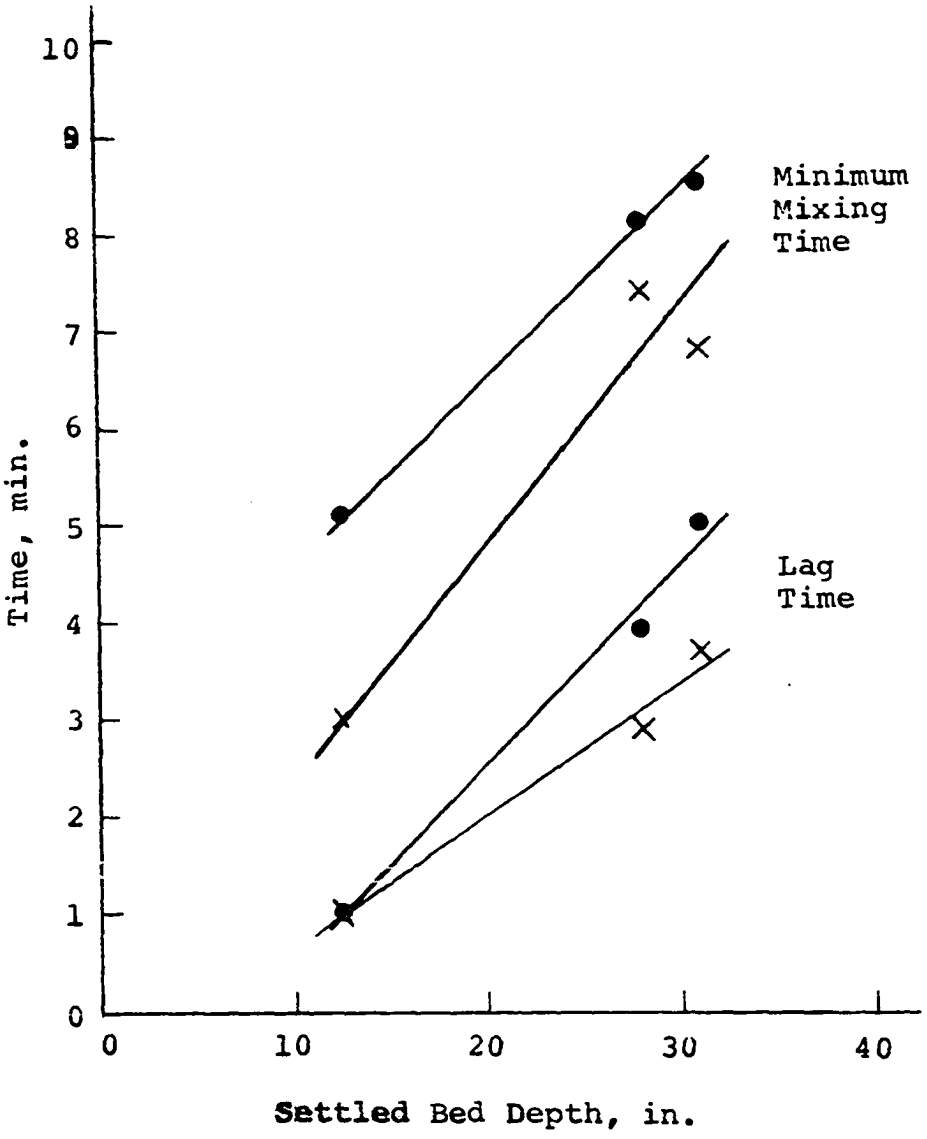

Figure 47. Average lag time and minimum mixing time versus bed height

Parameters: pure flour, %M = 13%

● u = 0.15 ft./sec.

X u = 0.20 ft./sec.

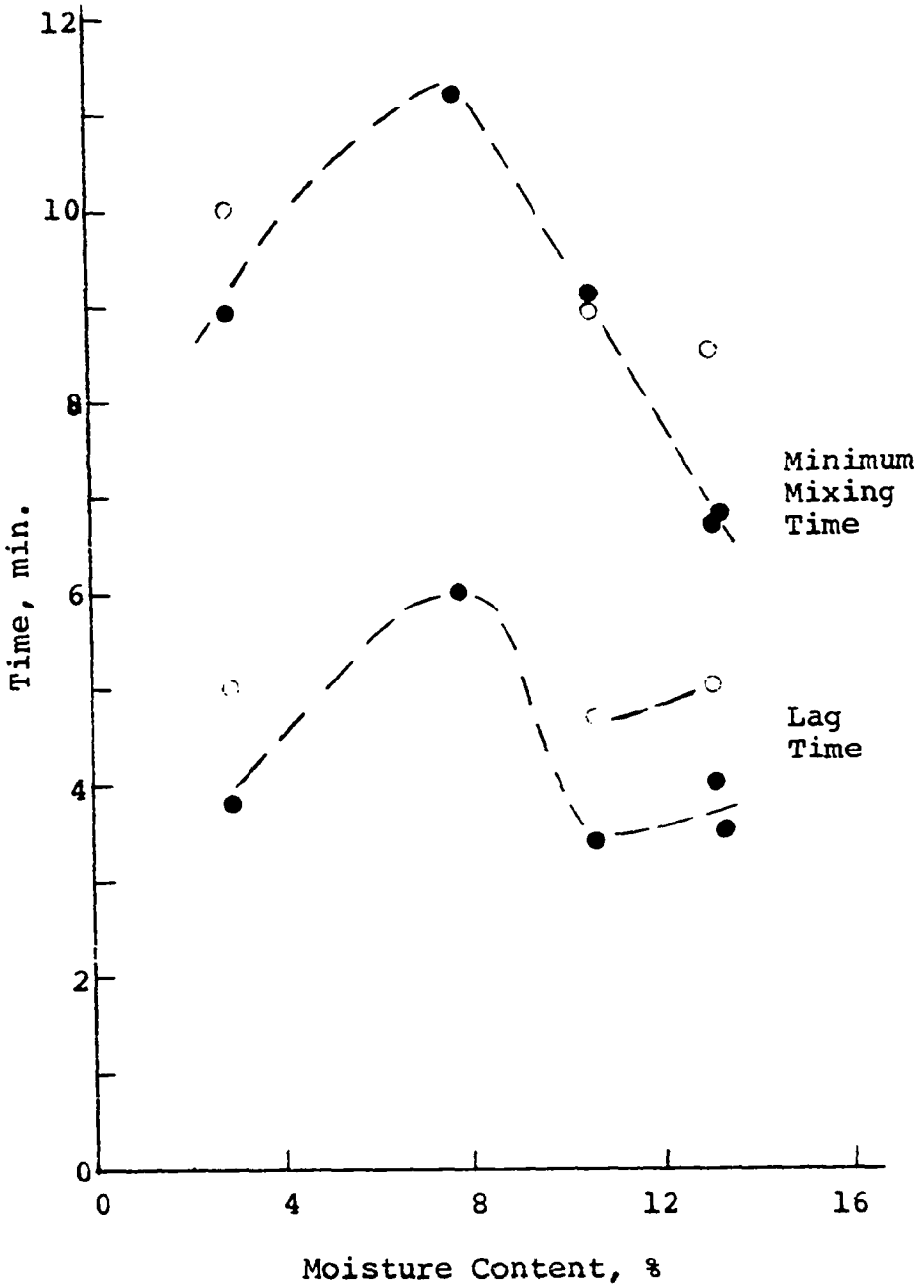

Figure 48. Average lag time and minimum mixing time versus flour moisture content

Parameters: H = 31 in.

○ u = 0.15 ft./sec.

● u = 0.20 ft./sec.

in the experimental design, so the order of dependence on moisture could not be determined at that fluidization velocity. In the residence time experiments, only a quadratic relationship was observed when beds were fluidized at 0.15 ft./sec. or slower gas velocities.

Contrary to the similarity in the response of the lag time and the minimum mixing time to changes in gas velocity or bed depth, the two times responded in entirely different ways to changes in moisture content. The minimum mixing time increased linearly as moisture was reduced from the 14% level to about the 8% level. However, at the 3% moisture level the minimum mixing time was significantly lower than at the 8% level. Again, the behavior for the 0.15 ft./sec. fluidization velocity could not be determined due to lack of data for the 8% moisture level. The existing data could be interpreted to either follow the quadratic form of the 0.20 ft./sec. data or linearly increase with decreasing moisture content.

Analysis of data

Statistical analyses were performed to test for significant effects on the mixing curve of each possible factor incorporated in the statistical design (Figures 22 and 24) of the mixing experiments. The effects of the fluidization parameters were tested on three of the four mixing curve char-

acteristics: the lag time, minimum mixing time, and the mixing index. The fourth characteristic, the percentage of samples outside the concentration range (Table 11) of most other steady state samples, was excluded from the analysis since all four characteristics were not independent. The concentration limits affected the minimum mixing time and the mixing index.

The mixing index chosen for the analysis was the steady state between sample variance of the nonnormalized concentrations since it is rather frequently used and is of industrial significance (71). The mixing index was evaluated for both the minimum between sample variance and the minimum mixing time criteria discussed above. The test statistics of these two cases were very frequently almost equal. Unless noted, the tests and results discussed below are for mixing index values based on the minimum between sample variance criterion, but the conclusions apply to both cases.

Analysis of variance and regression analysis require a constant variance of the dependent variable (13). Since this condition did not exist for the mixing curve characteristics, transformations similar to those used in the statistical analysis of the residence time experiments (see Statistical Analysis) were necessary. That the variances of the lag time and minimum mixing time were not constant with the factors being tested was indicated by the trends occurring in the

residual plots. There would be no trend if these variances were constant. As was the case with the residence times, the natural logarithm of the lag time or minimum mixing time was the transformation which removed the trends from the residual plots.

The transformation of the between sample steady state variances was also required since these variances were not uniformly distributed either. Taking the natural logarithm of the between sample variance indicated a trend in the variance of $\ln S^2$ which was inversely proportional to the degrees of freedom (the number of samples minus one) of the original, untransformed, sample variance. A constant variance was obtained by further multiplying $\ln S^2$ by the square root of the degrees of freedom of the original sample variance. Thus the models of the mixing index had $(n - 1)^{1/2} \ln S^2$ as the dependent variable.

The following factors were tested for significance in influencing the behavior of the three mixing curve characteristics.

gas velocity

bed depth

flour moisture content

material

stirrer speed

In addition, a test was made for the possible effect the

amount of tracer might have had on the mixing index.

Analysis of variance and regression analysis were performed on the lag time, minimum mixing time, and mixing index. As was the case with the residence time experiment (see Statistical Analysis), the factors of these tests were frequently nonorthogonal. The condition of nonorthogonality of the factors is contrary to an assumption of the usual analysis of variance test procedure and required that the analysis of variance tests be performed using less restrictive regression models as discussed in Appendix D. For the reasons discussed for the residence time experiment, the "all possibilities" method of model derivation was used in the mixing tests.

Tracer The weight of tracer added to a fluidized bed was determined by the requirements of the analytical procedure for measuring tracer concentration (87). Thus only 8.0 g. of zinc tracer were added to a 28 or 31 in. deep bed while 27.9 g. of copper tracer and 32.2 g. of nickel were added. Since the weights of the copper and nickel tracers were about the same level compared to the zinc, the copper and nickel data were pooled and treated as one level. A regression analysis (Table 54, Appendix D) showed there was no significant effect on the mixing index caused by these small levels of tracer added to the bed.

Gas velocity Fluidization gas velocity significantly affected the lag time (Tables 55 and 56 of Appendix D) and the minimum mixing time (Tables 57 and 58 of Appendix D), but not the mixing index (Tables 59 and 60, Appendix D) as indicated by regression analyses of the data of Sets 1 to 10 and 13. The lag time and minimum mixing time both decreased nonlinearly with increasing gas velocity (Figure 46). The minimum mixing time was found to also depend upon the square of the gas velocity (Tables 58 and 61, Appendix D). The lag time, however, was not dependent upon this term (Tables 56 and 62, Appendix D). The decrease from infinitely long lag time and minimum mixing time at or below the minimum fluidization velocity, 0.10 ft./sec., and the apparent asymptotic approach to some minimum lag time and mixing time agreed with the bubble mechanism of particle motion discussed in the Literature Review. At minimum fluidization conditions the bed is expanded some, but there is no bubbling and therefore no driving force large enough for much net particle movement.

As gas velocity is increased, the gas in excess of the minimum fluidization velocity flows through the bed as bubbles (101). The linear velocity of free flowing solids carried upward with the bubbles is proportional to the excess velocity (97). Also, as gas velocity increases, the rate of bubble generation increases. Since more solids are transported upward with increasing gas velocity, continuity re-

quires that more solids are also descending. It is currently not possible to quantitatively predict the behavior of solids in gas fluidized beds (101). Considering the bubble mechanism of particle motion, the solids velocity would be expected to increase with increasing gas velocity. Indeed the downward solids velocity was observed, in the residence time experiment discussed above, to increase linearly with increasing gas velocity. The nonlinearity of the lag time and especially the minimum mixing time may be a result of increased eddy diffusion occurring with increased gas velocity.

The local particle velocity is only one factor determining the net downward movement of solids as measured by the lag time or determining the net over-all movement measured by the minimum mixing time. Another important factor is the bubble size and frequency. The percentage of time the solids are moving upwards, or downwards but at a slow velocity, is dependent on the bubbles as discussed in the Literature Review. The higher the fluidization velocity, the greater the frequency of bubble passage becomes. With increased frequency of bubble passage, the more a particle might be expected to be moving upwards when compared with low fluidization velocities. The net downward travel in a given time period would be shorter than estimated from the local downward velocity. Since lateral solids movement occurs in the bubble wake, more frequent and larger bubbles would effect the mini-

mum mixing time more than the lag time. In the mixing of trace amounts of salt with flour, the minimum mixing time was found to be dependent on the square of the fluidization gas velocity while the lag time was dependent on only the linear power of the gas velocity.

Interactions of gas velocity with the moisture content of flour and with stirring speed were tested for effects on the lag time (Tables 62 and 63, Appendix D) and the minimum mixing time (Tables 61 and 64, Appendix D). Both of these two way interactions were insignificant for the lag time and also for the minimum mixing time. The interaction of gas velocity and the type of material (such as between flour and potato starch) was also found to be insignificant for lag time (Table 65, Appendix D). The test for this effect on the minimum mixing time was not performed.

That the mixing index was insignificantly affected by gas velocity (Tables 59 and 60, Appendix D) indicated that the between sample variances were equivalent at all gas velocities. The degree of homogeneity of the steady state mixtures, as defined above by excluding the small percentage of samples with very high or low concentrations compared to most samples, was independent of gas velocity. Gas velocity did affect the range of the steady state concentration limits within which most samples fell. The range was reduced by increasing the gas velocity up to 0.20 ft./sec. Above 0.20

ft./sec, no further decrease in sample range resulted. The interaction of gas velocity and moisture content of the flour was an insignificant factor for effecting the mixing index as was the square of the gas velocity (Tables 59 and 60 of Appendix D).

In summary, a longer time was required at the lowest fluidization gas velocity to achieve the same mixture homogeneity obtained at a higher gas velocity.

Brekken, et al. (11) reported improved mixing as gas velocity was increased in 12.5 and 23 in. deep, stirred, fluidized beds of flour. Kozulin and Kulyamin (59) reported that a gas velocity of three times the minimum fluidization velocity was an optimum gas velocity for similar stirred, fluidized beds of cohesive powders. As indicated in the Literature Review (Table 1), these powders were significantly denser than flour.

Bed depth Regression analysis of the data of Sets 1 to 10 and Set 13 showed that the settled bed depth had a significant effect on the lag time (Tables 55, 56, and 62 of Appendix D) and on the minimum mixing time (Tables 57, 58, and 61 of Appendix D), but not on the mixing index (Tables 59 and 60 of Appendix D). In other words, the mixture reached the same state of homogeneity in a shallow bed at steady state as was reached in a deep bed, but achieving this state required more time in the deep bed.

Both the lag time and the minimum mixing time increased proportionately (0.20 min./in.) with increasing bed depth (Figure 47) at 0.15 ft./sec. The minimum mixing time appeared to increase faster with increasing bed depth than the lag time when beds of flour were fluidized at the generally better mixing condition of 0.20 ft./sec. The limited amount of data obtained at a gas velocity of 0.20 ft./sec. was more scattered than that at the lower velocity and the slope of the lines in Figure 47 was not as well defined.

The finding that longer times were required in the deeper beds than in the shallow beds agreed with the general expectation that a proportionately longer time is required for particles to travel the longer distance down a deep bed under otherwise equal fluidization conditions.

The results of earlier experiments in which 12.5 in. deep beds were compared with 23 in. deep beds were inconclusive in determining whether the steady state sample variance was equal in beds of those two depths (11).

Moisture content The flour moisture content cubed was significant for lag time (Tables 55, 56, and 62 of Appendix D); the moisture content squared was significant for the minimum mixing time (Tables 57 and 58, Appendix D); but moisture content had no effect on the mixing index (Tables 59 and 60 of Appendix D). These conclusions were based on consideration of the data of Sets 1 to 10 and Set 13. The dependence

of lag time on moisture content cubed is illustrated by Figure 48. The maximum lag time for flour having a moisture content of 8% corresponds with the minimum solids velocity (Figure 37) found in the residence time experiments. The minimum mixing time also reached a maximum at 8% moisture content. As the flour moisture content decreased from 13% to 10% (Figure 48), the minimum mixing time unexpectedly decreased while the lag time increased. The data shown in Figure 48 indicate that the minimum mixing time and the lag time responded similarly as the flour moisture content decreased from 10% to 3%. The observed effect of moisture content on lag time and minimum mixing time might be accounted for by changes in powder cohesiveness.

No interaction of moisture content with gas velocity was found for any of the three mixing curve characteristics tested (Tables 59, 62, and 63 of Appendix D).

Stirrer speed From regression analysis of the data of Sets 1 to 10 and Set 13, it was concluded that stirrer speed had no effect on the lag time (Table 56, Appendix D), the minimum mixing time (Table 58, Appendix D), or the mixing index (Table 60, Appendix D). This supports the theory that the stirrer only serves to promote fluidization by preventing channels from developing in the bed. The improved fluidization resulting from the slow speed stirring used in these experiments itself was not dependent upon stirrer speed provid-

ed the level of stirring was sufficient to prevent channeling.

A previous study (11) was inconclusive regarding the effect of stirrer speed on the degree of mixing.

Material Analysis of variance tests of the data of Sets 5, 6, 11, and 12 indicated that the material fluidized had a very significant effect on the lag time (Table 66, Appendix D) and on the minimum mixing time (Table 67, Appendix D). An attempt was made to test the mixing index (Table 68, Appendix D), but the results were not conclusive. Generally, the better the quality of fluidization obtained with a given material (see Fluidization Characteristics), the better the mixing obtained.

The fluidization quality of the flour which had been flow conditioned with 1.0% Cab-O-Sil was very much better than that of pure flour or potato starch. The 1.0% Cab-O-Sil flour fluidized at a gas velocity of 0.06 ft./sec. (1.5 u_{mf}) showed mixing characteristics (Set 11, Table 12) which were generally very good compared to those of pure flour. A few samples were higher in concentration than the natural limit determined by the other steady state samples (Figure 72, Appendix C and Table 24, Appendix C). Increasing the fluidization velocity to 0.08 ft./sec. (2.0 u_{mf}) resulted in better mixing. After 5 min. from tracer addition, no samples were collected which were exceptionally high or low (Figure 73,

Appendix C) in tracer concentration. The mixing of a trace amount of salt with flour flow conditioned with 1.0% Cab-O-Sil and fluidized at 0.08 ft./sec. gave the best mixing observed in all the runs.

The mixing of a salt tracer with potato starch was much better than indicated by the rather poor qualtiy of fluidization observed with pure potato starch. This unexpected result occurred because the tracer salt significantly flow conditioned the potato starch (discussed in the Fluidization Characteristics section). The mixing was good. At 0.15 ft./sec. (Figure 74, Appendix C), only two steady state samples had a much higher concentration than the rest. The minimum mixing time was short (Table 12) but longer than for flour containing 1.0% Cab-O-Sil.

Surprisingly, increasing the gas velocity to 0.20 ft./sec. resulted in poorer mixing of potato starch than was obtained at 0.15 ft./sec. even though the bed contained additional tracer at the higher velocity which further flow conditioned the bed. At the higher velocity, the minimum mixing time was slightly longer due to a small overshoot (Figure 75, Appendix C). There was one steady state sample of very high concentration. The natural concentration limits of the steady state samples were much wider than at the lower gas velocity. The poorer mixing accompanying the generally better quality of fluidization might be a result of adding

less tracer in the second run than in the first run. This was the only clear case where an effect due the amount of tracer mixed was observed in the between sample variance.

Correlations

Correlations were developed which relate two of the mixing curve characteristics, lag time and minimum mixing time, to the significant fluidization parameters for mixing a trace amount of salt with pure flour. As discussed above, each of the factors tested had an insignificant effect on the steady state between sample variance. Since two levels of gas velocity are not sufficient for developing a meaningful correlation, no correlation was developed either for flour containing 1.0% Cab-O-Sil or for potato starch.

The lag time was dependent on gas velocity, bed depth, and the cube of the flour moisture content, while the stirrer speed was insignificant over the range tested, 25 to 100 rpm. The following correlation provided a good fit of the data as indicated by the coefficient of multiple determination, $R^2=0.88$ (Table 55, Appendix D). Following common practice, the linear and square moisture terms were included in the correlation too.

$$\ln \tau = -2.487 - 6.346u + 0.0810H + 0.1318\times10^{5}X_T - 0.1676\times10^{8}X_T^2 + 0.6220\times10^{10}X_T^3 \qquad [44]$$

This correlation was evaluated over the following range of the independent variables: gas velocity, 0.12 to 0.35 ft./sec.; bed depth, 12.5 to 31 in.; and moisture content, 2.9 to 14%, dry basis. Stirrer speed was insignificant over the range of 25 to 100 rpm.

The minimum mixing time was found to be dependent upon the gas velocity, the gas velocity squared, bed depth, and moisture content squared. Stirrer speed was insignificant over the range of 25 to 100 rpm. The data were fit by the following correlation

$$\ln t_M = 3.858 - 21.79u + 38.51u^2 + 0.03568H - 0.1156\times10^{4}X_T + 0.3353\times10^{7}X_T^2 \qquad [45]$$

The fit of the data by equation 45 was not as good as the fit of the data by equation 44. The coefficient of multiple determination was only 0.67 for the minimum mixing time correlation. The correlation was evaluated over the same range of independent variables as the lag time correlation.

Flow models

The mixing curves had two identifiable characteristics which were determined fairly accurately, the lag time and the minimum mixing time. The transient response between these times was best characterized as having a large random contri-

bution superimposed on the usual, smoothed response. Both types of response (underdamped or overdamped) occurred even when two beds were fluidized at the same conditions. Not enough samples were collected to adequately define the transient, underdamped response. The curves did show oscillations in concentration, but when compared with one another, the period and amplitude were not reproducible. This was understandable considering the random nature of the fluidized bed solids mixing process itself. Solids motion is dependent upon the apparently random passage of bubbles.

Having only two characteristics restricts the selection of possible models to those involving two parameters.

Two models for solids circulation in a batch, fluidized bed were found in the literature which had two parameters and which provided both underdamped and overdamped responses to a concentration step change depending upon the values of the model parameters. Both models did not model mixture homogeneity, but modeled the gross concentration.

The first model (9, 11) consisted of two equal sized, perfectly mixed tanks with solids circulation between the tanks, one stream containing a transport lag or dead time (Figure 49a). The parameters of this model are the dead time, τ, and the circulation rate, W. The model could be modified by including the relative tank size as a third parameter, but this parameter has been found to be rather unim-

Figure 49. Diagrams of mixing models

a. Two tank model (9,11)

b. Series of tanks model (69A)

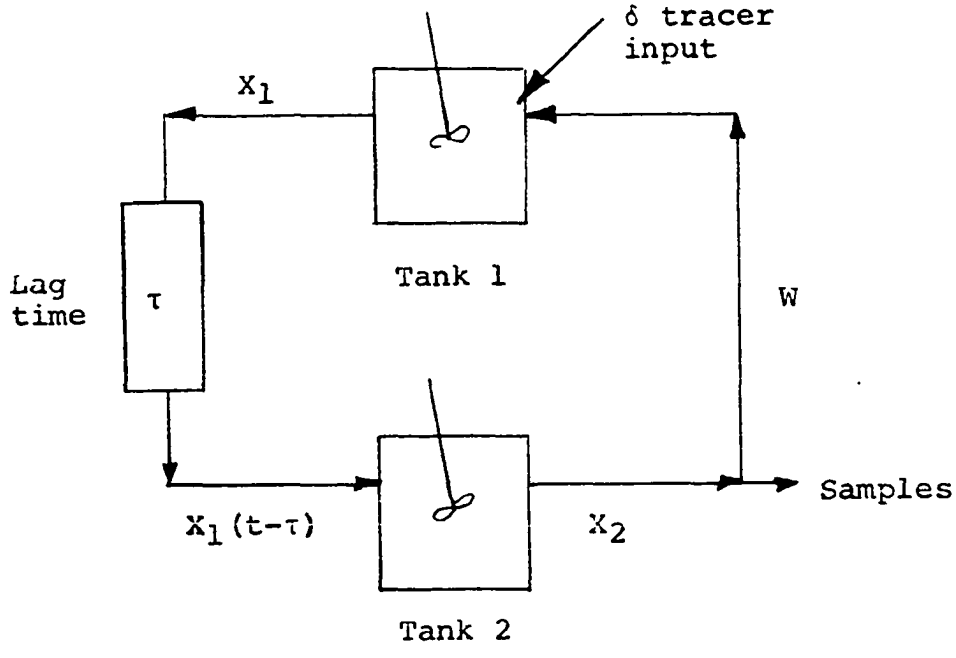
δ tracer
input
X_1
Lag
time
τ
Tank 1
W
Samples
$X_1(t-\tau)$
X_2
Tank 2

(a)

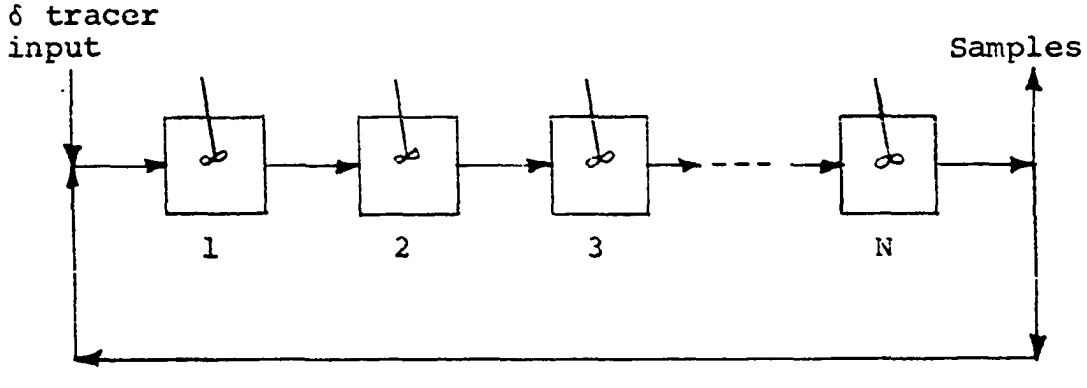
δ tracer
input
Samples
1
2
3
N

(b)

portant (9, 11). The stirred tanks physically correspond to the rather turbulent regions of the fluid bed above the gas distributor plate and at the bed surface. The local mixing by bubbles in the large middle bed region was allotted equally to the well mixed regions. The solids travel slowly down the column, requiring the lag time for the fastest complete cycle from the top to the bottom of the bed. Solids are quickly transported upwards by the bubbles.

The second model (69A) consisted of a series of stirred tanks with continuous recycle from the last tank to the first tank (Figure 49b). The parameters of this model are the time constant of the tanks (equal for each tank) and the number of tanks in the series, N. Physically, this model suggests that particles move through a series of well mixed zones, such as caused by the frequent passage of bubbles. On reaching the bottom, the model allows for solids to be rapidly transported back to the top. This model probably would not simulate the mixing of the deep beds of pure flour as well as it might simulate the other materials and shallow beds of flour at good mixing conditions. The lag of the concentration response to a step change in tracer fed to the system arises from the series of time constants. For the rather long lag times observed in the mixing of trace salts with flour, additional dead time may be required in order to fit the underdamped type of response.

In both models, if circulation is slow compared to the stirred tank holdup time, an overdamped response results.

Residence time and lag time

As discussed in the introduction to the Results and Discussion, two types of solids circulation rates were measured in this investigation of solids motion. The residence time of particle slip surface voids (cracks) moving down the column past a measuring grid was essentially a measure of the local downward velocity of particles at the wall. The rate of crack movement was previously found to be equivalent to that of a coal char tracer front and to the rate of movement of small, rubber particles (87). Since the cracks extended into the bed interior, one might suppose that this wall velocity would be representative of the interior as well.

The lag time indicated by the solids mixing curve is a measure of macroscopic circulation. The tracer particles that first arrived at the sampling tap could have arrived by either a route passing near the wall or an interior route. Particles may have arrived by both routes at essentially the same time. The region above the gas distributor plate is very turbulent and in this region an added lateral motion was imparted to the solids by the stirrer. Thus the additional distance particles arriving by an interior bed route would have to travel to reach the sample tap would be rapidly crossed. By whatever route the initial tracer particles

arrived at the tap, these particles traveled the whole length of the fluid bed.

The measured lag time and the measured local residence time may be compared in two ways. The local slip-stick downwards flow of solids observed in fluidized beds of flour might be averaged over time and approximated by plug flow. The lag time can then be estimated from the downward crack velocity observed as a function of elevation. Alternatively, an over-all particle velocity may be determined by dividing the measured fluid bed height by the measured lag time and may be compared to the local velocity averaged over the fluid bed height. Since the measured residence times were expressed as the harmonic average velocity while the velocity calculated from the measured lag time is a linear average velocity, the first alternative was chosen since the times could be compared on an equal basis.

The lag time calculated by averaging the upper and lower velocities was compared with the measured lag time as follows for the deep flour beds (26 to 31 in.):

Set No.	Calculated	Measured	Calculated	Measured
5	4.2	5.0	2.3	4.0
6	2.6	3.0	2.3	4.0
8	4.1	4.7	2.2	3.4
9	3.4	6.0	3.4	6.0
10	4.8	5.0	2.8	3.8

For the deep beds, the calculated lag time was always shorter than the measured time (4 to 43% difference). One would expect the calculated time to be shorter than the measured time since the residence time was a measure of downward moving cracks only whereas particles move upward during part of a typical journey to the bed bottom due to encounters with bubbles. Upward particle movement was not accounted for in the calculated lag times.

Settled Bed Tracer Distribution

When the stirrer and fluidizing gas were quickly turned off, fluidization suddenly stopped. The bed then rather slowly contracted to the settled bed state without much relative solids movement. Gas trapped as bubbles in the bed seeped through the settling bed, occasionally forming minute channels.

Samples of the settled bed were collected by the procedure described in the Fluidization Procedures section and were analyzed by the techniques described in the Analytical Techniques section.

The copper and zinc tracer concentrations of the samples removed from the settled bed following fluidization run 11 of Sets 5 through 13 (for operating conditions, see Figures 22 and 24 and also Table 6) are listed in Tables 25 to 33 of Ap-

pendix C. The settled bed samples were collected at the bed elevations and radial locations indicated in Figure 21 and Table 4. The copper tracer had been previously mixed during run 10. The sample concentrations are summarized as the overall average and standard deviation of each bed in Table 13. The average (and standard deviation) copper and zinc concentration at each elevation level of each bed are listed in Table 34, Appendix C.

No consistent pattern of average concentration or standard deviation was evident in either the overall bed values or the values for each elevation except that the topmost elevation (elevation A) had a zinc standard deviation which tended to be greater than that at lower elevations. The average concentration of some topmost layers were either larger or smaller than those at most lower elevations. This was probably due to material that had adhered to the wall above the bed during some of the run which fell to the surface about the time fluidization was stopped. For example, the copper, as well as the zinc, averages were low for the topmost levels of Sets 9 and 13, more so for samples near the wall. Even though the tracer injector was carefully removed after fluidization was stopped, a little tracer salt may have been knocked off the injector. For example, in Set 5 the zinc level was abnormally high, but the copper concentration was normal. Unmixed flour may have fallen from the wall and

Table 13. Summary of settled bed tracer concentrations

Set No.	Sample size[1] g.	Copper tracer n	Copper tracer $\bar{X}$ mg/g.	Copper tracer S mg/g.	Copper tracer C.V. %	Zinc tracer n	Zinc tracer $\bar{X}$ mg/g.	Zinc tracer S mg/g.	Zinc tracer C.V. %
5	0.736	66	1.01	0.033	3.23	65	0.337	0.035	10.3
6	0.721	66	0.978	0.035	3.54	66	0.336	0.029	8.52
7	0.791	34	0.975	0.039	3.96	34	0.288	0.015	4.95
8	0.871	67	0.990	0.048	4.85	66	0.320	0.020	6.08
9	0.843	72	0.954	0.077	8.05	72	0.287	0.027	9.26
10	0.856	72	0.905	0.079	8.71	72	0.296	0.612	207.
11	0.826	71	0.978	0.040	4.06	71	0.341	0.035	10.2
	0.151	36	0.971	0.047	4.81	36	0.332	0.059	17.7
12	1.015	72	0.619	0.011	1.57	71	0.193	0.023	11.7
	0.424	36	0.606	0.010	1.49	35	0.188	0.009	4.09
13	0.877	72	0.947	0.037	3.87	72	0.320	0.025	7.67
	0.440	36	0.966	0.034	3.48	36	0.322	0.026	7.98

[1] Average weight, dry basis.

tracer salt may have fallen from the injector in some cases (Sets 8, 10, and 11 had a large average concentration of zinc but the average copper concentration at the bed surface was low).

Good agreement was obtained between the overall bed average copper and zinc concentrations, the steady state average fluid bed samples, and the value calculated from the material balance (Table 14). The values calculated from the material balance had more uncertainty since usually four residence time runs and a fluidization characteristics run were performed before the mixing runs. Entrainment, sampling, make-up flour and moisture content changes had to be accounted for in the material balance. Set 14 involved only a fluidization characteristics run prior to the mixing run. Excellent agreement between the calculated and measured average concentration was obtained (87). In all runs, the tracer concentration of the entrained material collected in the filter was at the same level as the bed.

The experimental design enabled the following fluidization parameters to be tested for significant effects on the settled bed sample concentration variance: gas velocity, gas humidity, flour moisture content, bed height, and type of material fluidized. Following the "all possibilities" model building technique (discussed in the residence time experiment's Statistical Analysis section), a series of models of

Table 14. Average tracer concentration of fluid and settled bed samples

	Copper concentration, mg./g.							Zinc concentration, mg./g.				
	Run 10		Run 11			Run 12		Run 11			Run 12	
Set	M.B.[1]	F.B.[2]	M.B.	F.B.	S.B.[3]	M.B.	F.B.	M.B.	F.B.	S.B.	M.B.	F.B.
1	1.32	1.20	1.25	1.04	----	1.19	1.03	0.48	0.38	----	0.45	0.37
2	1.22	1.16	1.09	1.17	----	1.02	1.06	0.38	0.42	----	0.36	0.40
3	1.18	1.09	1.11	1.12	----	1.05	1.05	0.40	0.41	----	0.39	0.39
4	1.17	1.13	1.04	1.05	----	1.04	1.06	0.38	0.35	----	0.37	0.39
5	1.10	1.09	1.00	1.03	1.01			0.37	0.33	0.34		
6	1.19	1.13	1.05	1.07	0.98			0.38	0.34	0.34		
7	1.20	1.16	0.94	0.94	0.97			0.36	0.27	0.29		
8	1.12	1.04	1.08	0.98	0.99			0.38	0.30	0.32		
9	1.03	0.96	1.00	0.95	0.95			0.35	0.29	0.29		
10	1.03	0.86	0.97	0.86	0.90			0.34	0.27	0.30		
11	1.14	1.10	1.03	1.00	0.96			0.37	0.34	0.34		
12	0.75	0.74	0.63	0.60	0.62			0.22	0.21	0.19		
13	1.06	1.20	0.96	1.08	0.95			0.33	0.38	0.32		
14	1.42	1.42	----	----	----							

[1] Concentration calculated from material balance.

[2] Average concentration of steady state fluid bed samples.

[3] Average concentration of settled bed samples.

the fluidization parameters and the elevation in the settled bed were proposed and tested. Neither the elevation nor the gas velocity, gas humidity, material, flour moisture content, or the bed depth had a significant effect at the 5% significance level. This was confirmed by a large model which incorporated all these parameters (Table 69, Appendix D).

Another analysis of variance test was made to determine if settled bed concentration varied between elevations and radial locations. The two way interaction of elevation and radial location was also included in the model. Fluidization parameters were lumped as the conditions effect (see the residence time experiment's Statistical Analysis section). The radial locations were the three annuli of equal area shown in Figure 21. The inner area had radii of 0.25 and 1.75 in.; the middle area, 1.75 and 2.46 in.; and the outer wall area, 2.46 and 3.0 in. Since sample number 12 was not taken in the first few sets for all elevations, sample 12 was omitted. The set of factors was thus made orthogonal with respect to elevation. The results of this test (Table 70, Appendix D) indicated that all factors were significant. Since this was rather unexpected, further analysis was performed by determining the significance of a series of comparisons.

The following comparisons were made:

1. upper half of the bed versus the lower half
2. elevation A versus elevation C

3. elevation B versus the average of elevations A and C
4. elevation D versus elevation F
5. elevation E versus the average of elevations D and F
6. front (samples numbers 1, 2, 3, 4, 7, 8) versus rear (5, 6, 9, 10, 11) of the bed
7. samples along tube 1 versus those along tube 2 (see Figure 21)
8. outer versus middle radial locations (Figure 21)
9. outer versus inner radial location.

In calculating a comparison's F statistic, the better estimate of error determined in the analysis of variance test (Table 70, Appendix D) was used. All comparisons except numbers 1 and 2 were insignificant at the 5% significance level (Table 71, Appendix D). Comparisons 1 and 2 both involved the topmost elevation level which as discussed above was not representative due to contamination. It was therefore concluded that no segregation had occurred in the fluidized beds studied. This agreed with the well mixed state indicated by the lack of dependency of the between sample variance of the fluid bed samples.

A comparison of the standard deviation of the flow samples (Table 12) with the corresponding settled bed samples

(Table 13) showed the flow samples to generally have a significantly lower standard deviation than the settled bed samples. This comparison was clouded by the exclusion of the flow samples which were outside the limits of the rest as discussed above. Including those samples, however, would have resulted in less meaningful a comparison. Physically, the lower variance of the flow samples would mean the flow samples were mixed as they were collected.

Several reasons why the mixing of a small amount of one component into a large batch is frequently difficult compared to mixing a large amount of the component may be cited(40): more rigorous criteria of mixedness, the manner of charging, and difficulty in obtaining the small enough particle size needed for a good quality mixture without introducing segregation effects.

Scale of Scrutiny

The tracer concentration variance as a function of sample size of samples collected from steady state mixtures was investigated for each material (Sets 11, 12, and 13). The objective in this phase of the solids mixing experiments was to find the smallest scale of scrutiny the mixture could be subjected to and yield a between sample variance equivalent to that of the larger samples. The representativeness of the larger samples would be confirmed if the samples of smaller

size had a variance equal to (or smaller than) that of the larger samples.

The small samples were prepared, as described in the Procedures of Fluidization Experiments section, from samples collected close to the regular sized samples. The mixtures were from beds which had been well fluidized, especially those of run 11.

The regular sized flow samples ranged from 0.5 to 1.3 g. The regular sized settled bed samples averaged 0.88 g, for the pure flour on a dry basis, 0.83 g. for the 1.0% Cab-O-Sil flour, and 1.0 g. for potato starch. Since the settled bed samples were weighed out, the size range was narrow compared to the flow samples which were regularly used as collected.

The sample sizes and the between sample variance are summarized in Table 15 for each material. The regular samples corresponding to the 30 flow samples of each size and the 36 settled bed samples are also indicated.

The results verify that the regular size samples were representative. If sample size was not representative, one would expect the between sample variance to be significantly larger for the smaller samples than for the larger samples. The data show that the same (or even smaller) variance resulted for samples about half as large or less than the regular samples.

Table 15. Sample size and standard deviation of steady state sample concentration

Material	Type of Sample	Sample Size[1] g.	Copper S mg./g.	Zinc S mg./g.
Pure Flour (Set 13)	Flow	0.74[2]	0.035	---
		0.18	0.124	---
		0.088	0.567	---
		0.79[2]	0.024	0.026
		0.26	0.093	0.029
	Settled bed	0.88[2]	0.042	0.026
		0.44	0.034	0.026
Flour with 1.0% Cab-O-Sil (Set 11)	Flow	1.15[2]	0.059	---
		0.15	0.037	---
		1.07[2]	0.016	0.008
		0.35	0.037	0.010
	Settled bed	0.85[2]	0.049	0.045
		0.26	0.047	0.059
Potato Starch (Set 12)	Flow	1.19[2]	0.016	0.0009
		0.17	0.018	0.0011
		0.085	0.093	0.066
	Settled bed	1.02[2]	0.011	0.024
		0.42	0.010	0.009

[1] Average weight, dry basis.

[2] Size regularly used in mixing study.

The minimum scale of scrutiny for pure flour was 0.26 g. The 0.18 g. flour samples had a larger variance than the corresponding samples of the size (0.74 g.) regularly used for determining the mixing curve. The potato starch had a minimum scale of scrutiny of 0.17 g. for the mixture of run 11.

For flour with 1.0% Cab-O-Sil, samples as small as 0.15 g. had a variance equivalent to the larger samples. The smallest size tested was limited by the accuracy of the analytical technique. For the smaller samples, a blank correction was required and made. The minimum scale of scrutiny thus appeared to be about 0.15 g. or smaller for the flour containing 1.0% Cab-O-Sil. It is not possible to test smaller samples without modifying the procedure to enable handling the very small samples and measuring the very low tracer levels that would be involved.

PART 5. CONCLUSIONS AND RECOMMENDATIONS

CONCLUSIONS

Residence Time Experiments

The following conclusions are based on the results of the experimental study of the residence time of particle slip surface voids (cracks) observed in stirred, fluidized beds of flour.

1. The method of measuring the downward crack movement was satisfactory. The measured residence time was independent of the observer. Any bias in selecting cracks to time was uniform among the four observers. The downward crack velocity was found to be independent of the distance traveled over a range of 1 to 3 in. Any difference in residence time between flour beds prepared and operated under identical conditions was insignificant.

2. The following operating factors significantly affected the rate of crack movement down the bed: fluidization gas velocity, location, and bed depth. The velocity of the downward moving cracks was proportional to the fluidization gas velocity over the range studied (0.12 to 0.20 ft./sec.). The crack velocity increased linearly as the crack moved down the column. An interaction of gas velocity and location existed such that a maximum rate of movement resulted at an elevation of 12.5 in. above the gas distributor plate when the bed was fluidized at 0.20 ft./sec. At the

lower location, the shallow (12.5 in.) bed had cracks that moved slower than those at the same relative height above the distributor in the deep beds (26 to 32 in.). Otherwise the crack velocity in the shallow bed was generally the same as in the deep beds.

3. The type of material fluidized and the flour moisture content affected the downward crack velocity significantly. Reducing flour cohesiveness by adding 0.5% Cab-O-Sil resulted in increased crack velocity compared to the pure flour. The rate of crack movement in the flour with 0.5% Cab-O-Sil increased linearly with fluidization gas velocity and at a greater rate of increase than with pure flour. The moisture content had a higher order effect on crack velocity. A minimum crack velocity occurred with a bed of 8% moisture content, dry basis.

4. The following variables had no effect on the downward crack velocity. The stirrer speed had an insignificant effect on the downward crack velocity over the range studied (25 to 150 rpm). Using the nitrogen gas dry, as received, or using nitrogen gas of 28% relative humidity had no influence on the crack velocity. The presence of the salt tracer added in the mixing experiments had little, if any, effect on the residence time.

5. The harmonic average velocity of the downward crack movement was very adequately correlated by equation 32 for

beds of pure flour and by equation 33 for beds of flour containing 0.5% Cab-O-Sil. The correlations are applicable over the range of operating conditions listed in Table 10.

6. The residence time results agreed qualitatively with the mechanism of particle motion proposed by Rowe et al. (108) and further discussed by Rowe (101).

7. The wall-to-bed heat transfer coefficients (previously measured (84, 85)) were correlated with the harmonic average velocity of the downward moving cracks by equation 40. Since the range of data was small, the data were also correlated by a linear correlation, equation 39.

8. The relationship (equation 40) between the wall-to-bed heat transfer coefficients and the harmonic average velocity of the downward moving cracks did not disagree with the surface renewal packet model (35, 63, 79) of unsteady state heat transfer from the wall to the fluidized bed.

Trace Solids Mixing

The following conclusions were based on the results of the experimental investigation of the batch mixing of trace amounts of metal salt with flour or starch in a stirred, fluidized bed.

1. The methods of studying solids mixing were satisfactory. The material balance for the added salt closed. The scale of scrutiny of the samples was representative. The

procedure of collecting samples from a known location in the settled bed was workable.

2. The lag time before tracer added to the bed top appeared in samples withdrawn from the bed bottom was dependent upon gas velocity, bed depth, flour moisture content, and type of material fluidized. Lag time decreased with increasing gas velocity over the range studied (0.12 to 0.35 ft./sec.). Lag time increased linearly with increasing bed depth (12.5 to 31 in.). Moisture content had a higher order effect with a maximum lag time occurring at 8% moisture content, dry basis. Generally, the better the quality of fluidization, the shorter was the lag time. Potato starch was flow conditioned by the added tracer which resulted in a shorter lag time.

3. Lag time was independent of stirrer speed over the range tested (25 to 100 rpm). In addition, there was no interaction of gas velocity and moisture content or of gas velocity and stirrer speed or of gas velocity and material fluidized.

4. The time required to achieve the steady state mixture, the minimum mixing time, was dependent upon the fluidization gas velocity, bed depth, flour moisture content, and the material fluidized. The minimum mixing time decreased nonlinearly with increasing fluidization velocity over the range studied (0.12 to 0.35 ft./sec.). The minimum mixing

time increased linearly with increasing bed depth. Flour moisture content had a quadratic effect with the minimum mixing time reaching a maximum at 8% moisture content, dry basis. Mixing was faster for the bed of flour containing 1.0% Cab-O-Sil and for the potato starch bed which was flow conditioned by the added tracer salt.

5. The minimum mixing time was independent of stirrer speed (25 to 100 rpm). There was no interaction either between gas velocity and moisture content or between gas velocity and stirrer speed.

6. From 85 to 95% of all samples collected during the steady state portion of each mixing curve fell within a relatively narrow band of tracer concentration. The width of this band decreased with increasing gas velocity up to 0.20 ft./sec. and were then a constant ±7% of the average steady state concentration for gas velocities of 0.20 ft./sec. to 0.35 ft./sec., the highest velocity used.

7. The between sample variance of the steady state samples (after omitting 5 to 15% of the outlying samples) was independent of the fluidization gas velocity, bed height, stirrer speed, flour moisture content, and the amount of tracer salt mixed over the operating range indicated in Table 6. There was no interaction between gas velocity and moisture content. The same degree of mixture homogeneity was thus generally achieved in each run since mixing was allowed

to proceed long enough for an equally well mixed final mixture regardless of operating conditions.

8. The variance in concentration of the settled bed samples was independent of the following fluidization parameters: material, gas velocity, bed height, flour moisture content, and gas humidity. The samples were also independent of elevation or radial location in the bed. Thus no segregation occurred.

9. The mixing results do not disagree with the mechanism that solids motion and mixing are induced by bubbles (101, 108).

RECOMMENDATIONS

During the course of the investigation of residence time and of mixing of trace amounts of solids in fluidized beds of cohesive powders such as flour and potato starch, several areas were encountered which should receive further study. In addition, recommendations for further particle motion studies are made.

1. A technique for measuring the cohesiveness of powders is needed that would apply to the very cohesive powders of interest. Having a better measure of powder flowability than the angle of repose (which was found to be an inadequate technique (87)) would allow a better comparison of fluidization characteristics and particle motion to be made between different materials. It might then be possible to correlate the effects of moisture content and other variables such as particle size which also affect the powder cohesiveness and the the resulting particle motion as measured by such parameters as the lag time, miniminum mixing time, and the residence time.

The relationship between the occurrance, population density, and size of particle slip surface voids and the powder flowability could also be investigated.

2. It is recommended that the residence time and heat transfer studies be extended to other materials covering a wide range of particle size, density, and cohesiveness. A

particularily fruitful experiment would use beds of flour flow conditioned with Cab-O-Sil at concentrations between 0 and 0.5% by weight. Three levels of fluidization gas velocity would be benefical. Doing this experiment would extend the range of the harmonic average velocity of the cracks and enable a better test of the surface packet renewal model of heat transfer to be made. Furthermore, during the same experiment, the minimum fluidization velocity could be determined and correlated with a measure of cohesiveness, the amount of added Cab-O-Sil. Also, the entrainment rate could be measured and compared with the present results, possibly leading to a better understanding of that phenomenon.

3. Information on the characteristics of bubbles in beds of cohesive powders is very limited in the published literature. Quantitative data is especially scarse. Since bubbles exert a major influence on particle motion, a study of the bubbles is of basic importance to understanding particle residence time and mixing. Specifically, the frequency of bubbles passing close enough to the wall to exert an influence on particles at the wall is needed for a detailed analysis of the relationship of residence time and heat transfer. (Manual observation of the particle slip surfaces may give some indication fo the frequency of such bubbles.) The fraction of the heater covered by bubbles is of interest for fitting the residence time and heat transfer data. Since

larger bubbles might affect particle motion more than small ones, it would be desirable to measure size also. It is suggested that techniques for measuring bubble properties be developed for application in beds of cohesive powders. It is further recommended that means of generating bubbles of known size, location, and frequency be developed for such beds so that studies similar to those which have been very fruitful with free-flowing powders may be tried with cohesive powders, particularily the displacement of a colored tracer layer.

4. Several variations of the mixing experiment would yield a better understanding of the results of the present mixing curves. The tracer should be added as a slug to the bed surface while maintaining only 0.5 in. clearance between the extended injector plug and the bed. The tracer added in such a manner would not be dispersed over the surface. Comparing the mixing curves obtained with dispersed tracer and the curves obtained using a slug of tracer would indicate if the type of unsteady state response is related to the tracer addition. In another type of experiment, a series of samples of the settled bed obtained during the unsteady state period of mixing would show the movement of tracer down the column and how much cycling of tracer occurs.

5. Better seals are required for closing the sample ports. A thicker polyethylene film more securely retained such as by a rubber stopper shaped to the bed curvature would

be more suitable for operating deep beds at high gas velocities. Having such seals, the column could be attached to the recycle gas system used on another column. Mixing studies could then be performed at much higher gas velocities.

6. A quicker, cheaper, and accurate analytical technique for measuring tracer concentration would be very desirable. One approach would be to mix an acidic or basic salt with the flour and slurry a weighed sample with 5% methanol solution. The pH would then be measured. Any technique must be shown to be accurate!

7. The effect of additional stirrer blades mounted at intervals up the column with and without the use of vertical baffles could result in improved mixing through increased shear.

8. The mixing of other materials and using more levels of tracer concentration and tracers of different particle size would enable a better evaluation of mixing performance.

9. An especially interesting continuation of the present mixing study would be to mix salts of increasing particle density with the flour to see when segregation becomes significant.

LITERATURE CITED

1. Allen, Terrence. Particle size measurement. London, United Kingdom, Chapman and Hall Ltd. c1968.

2. American Society for Testing Materials. Committee E-1. A. S. T. M. special technical publication 447. Philadelphia, Pa., Author. c1969.

3. Ashton, M. D. and Valentin, F. H. H. The mixing of powders and particles in industrial mixers. Transactions of the Institution of Chemical Engineers 44: T166-T188. 1966.

4. Baerns, M. Properties of fluidized beds of finely divided solids. Unpublished paper presented at Symposium on Fundamental and Applied Fluidization, Part 1. Second Joint AIChE-IIQPR meeting, Tampa, Florida. May 1968.

5. Baerns, Manfred. Effect of interparticle adhesive forces on fluidization of fine particles. Industrial and Engineering Chemistry Fundamentals 5: 508-516. 1966.

6. Baskakov, A. P. and Filippovskii, N. F. Experimental study of heat transfer between a fluidized bed and vertical and inclined sheets. Inzh. Fiz. Zh. 20(1): 5-10. 1971. Original not available; abstracted in Chemical Abstracts 74: 101027x. 1971.

7. Beck, H. V. Displacement gas meters. Philadelphia, Pennsylvania, American Meter Division, The Singer Company, Incorporated. c1970.

8. Bourne, J. R. Blending calculations for two product specifications. British Chemical Engineering 13: 834-836. 1968.

9. Brekken, Roger Allen. Gas fluidization of wheat flour in a stirred bed. Unpublished Ph.D. thesis. Ames, Iowa, Library, Iowa State University of Science and Technology. 1968.

10. Brekken, R. A., Lancaster, E. B. and Wheelock, T. D. Fluidization of flour in a stirred aerated bed: Part I. General fluidization characteristics. Chemical Engineering Symposium Series 66, No. 101: 81-90. 1970.

11. Brekken, R. A., Lancaster, E. B. and Wheelock, T. D. Fluidization of flour in a stirred aerated bed: Part II. Solids mixing and circulation. Chemical Engineering Symposium Series 66, No. 105: 277-284. 1970.

12. Bridgewater, J. The mixing of cohesionless powders. Powder Technology 5: 257-260. 1971.

13. Brownlee, K. A. Statistical theory and methodology in science and engineering. 2d in science and engineering. 2nd. ed. New York, N. Y., John Wiley and Sons, Inc. c1965.

14. Cadle, R. D. Particle size determination. New York, N. Y., Interscience Publishers, Inc. 1955.

15. Christiansen, Leonard Rufus. Mixing studies on starch pastes and slurries. Unpublished Ph.D. thesis. Ames, Iowa, Library, Iowa State University of Science and Technology. 1973.

16. Chung, Benjamin T. F., Fan, L. T. and Hwang, C. L. A model of heat transfer in fluidized beds. Journal of Heat Transfer 94: 105-110. 1972.

17. Clift, Roland and Grace, John R. Bubble coalescence in fluidized beds: comparison of two theories. American Institute of Chemical Engineers Journal 17: 252-254. 1971.

18. Clift, Roland and Grace, J. R. Coalescence of bubbles in fluidized beds. AIChE Symposium Series 67, No. 116: 23-33. 1971.

19. Clump, Curtis W. Mixing of solids. In Uhl, Vincent W. and Gray, Joseph B., eds. Mixing. Volume 2. pp. 263-286. New York, N. Y., Academic Press, Inc. 1967.

20. Corella, J. and Otero, A. R. Fluidization of mixtures of solids of distinct characteristics. II. Segregation in totally fluidized beds. An. Quim. 67: 1221-33. 1971. Original not available; abstracted in Chemical Abstracts 76: 129419s. 1972.

21. Coulter Electronics, Incorporated. Instruction and service manual for the Coulter Counter Model TA. Hialeah, Florida, Author. 1973.

22. Davidson, J. F. and Harrison, D. Fluidised particles. Cambridge, United Kingdom, University Press. 1963.

23. Donsi, G., Massimilla, L., Crescitelli, S. and Volpicelli, G. Solid flow pattern at the wall of a fluidization column induced by single bubbles. Powder Technology 6: 217-224. 1972.

24. Dow, W. M. and Jakob, M. Heat transfer between a vertical tube and a fluidized air-solid mixture. Chemical Engineering Progress 47: 637-648. 1951.

25. Fan, L. T., Chen, S. J., and Watson, C. A. Solids mixing. Industrial and Engineering Chemistry 62, No. 7: 53-69. 1970.

26. Fan, L. T., Chen, S. J. and Watson, C. A. Solids mixing. Annual Reviews of Industrial and Engineering Chemistry, 1970: 22-56. 1972.

27. Florin, Gerd. Continuous drying in a fluidized bed and its uses in the food industry. Ind. Chim. Belge 35: 103-106. 1970. Original not available; abstracted in Chemical Abstracts 123418m. 1970.

28. Fomichev, A. G. and Gvozdev, V. D. An investigation of the mixing of granular materials in continuously operating fluidized bed equipment. International Chemical Engineering 4: 609-613. 1964.

29. Fried, E. M. Performance characteristics of a fluidized bed of wheat flour. Unpublished M.S. thesis. Ames, Iowa, Library, Iowa State University of Science and Technology. 1965.

30. Gabor, John D. Laterial solids mixing in fluidized - packed beds. American Institute of Chemical Engineers Journal 10: 345-350. 1964.

31. Galle, E. L. Flour pasteurization. U. S. Patent 3585049. 1971. Abstracted in Food Science and Technology Abstracts 3: 11M1300. 1971.

32. Garcia, Luis A. and Gulden, Ernesto E. Fluidized - bed particle coating. SAFYBI 8: 252-270. 1968. Original not available; abstracted in Chemical Abstracts 73: 28866t. 1970.

33. Geldart, D. The effect of particle size and size distribution on the behavior of gas-fluidized beds. Powder Technology 6: 201-215. 1972.

34. Geldart, D. Types of gas fluidization. Powder Technology 7: 285-292. 1973.

35. Gelperin, N. I. and Einstein, V. G. Heat transfer in fluidized beds. In Davidson, J. F. and Harrison, D. Fluidization. pp. 471-540. New York, N. Y. Academic Press, Inc. 1971.

36. Genetti, W. E., Schmall, R. A. and Grimmett, E. S. Effect of tube orientation on heat transfer with bare and finned tubes in a fluidized bed. AIChE Symp. Ser. 67(116): 90-6. 1971. Original not available; abstracted in Chemical Abstracts 77: 22179g. 1972.

37. Gillow, R. and Teders, R. Flour agglomeration. Canadian Patent 790010. 1968. Abstracted in Food Science and Technology Abstracts 1: 1M48. 1969.

38. Godard, K. and Richardson, John Francis. Minimum stable bubble volumes and bubble collapse rates in gas fluidized beds. The Canadian Journal of Chemical Engineering 47: 350-352. 1969.

39. Goossens, W., Dumont, G. and Spaepen, G. Fluidization of binary mixtures in the laminar flow region. Unpublished paper presented at American Institute of Chemical Engineers meeting, Chicago, Illinois, November 1970.

40. Gren, U. Solids mixing - a review of present theory. British Chemical Engineering 12: 1733-1737. 1967.

41. Guilbault, Lawrence J. Dry blending an agglomerated material with powdered material for preparing coating compositions for use in fluidized beds. U. S. Patent 3,541,043. November 17, 1970. Abstracted in Chemical Abstracts 74: 23953e. 1971.

42. Harnby, N. The statistical analysis of particulate mixtures. Part 1. The sampling of mixtures and the resultant precision of estimates based on the sample. Powder Technology 5: 81-86. 1971.

43. Harnby, N. The statistical analysis of particulate mixtures. Part 2. The application of social survey statistical techniques to solids mixing problems. Powder Technology 5: 155-165. 1971.

44. Haywood, Harold. The evaluation of powders. Journal of Pharmacy and Pharmacology 15: 56T-74T. 1963.

45. Hogg, R., Mempel, G. and Fuerstenau, D. W. The mixing of trace quantities into particulate solids. Powder Technology 2: 223-228. 1969.

46. Hutchinson, J. B. Steam treatment of wheat: a new type of flour. Chemistry and Industry: 1084. 1963.

47. Irani, R. R. Evaluation of particle size distributions obtained from electrolytic resistivity changes. Analytical Chemistry 32: 1162-1164. 1960.

48. Irani, Riyad, R. and Callis, Clayton F. Particle size: measurement, interpretation, and application. New York, N. Y., John Wiley and Sons, Inc. c1963.

49. Irani, R. R. and Fong, W. S. Measurements of the particle size distribution of flour. Cereal Chemistry 38: 67-75. 1961.

50. Jackel, S. S. and Belshaw, F. Encapsulated ferrous sulphate protects baking mixes, flour from rancid flavours. Food Processing 32, No. 5: 28-29. 1971. Original not available; abstracted in Food Science and Technology Abstracts 3: 12M1337. 1971.

51. Jackson, M. R., Iglarsh, H. and Salkowski, M. J. Sample-size induced errors in the transformation of particle size distributions. Powder Technology 3: 317-322. 1970.

52. Jacob, A. and Osberg, G. L. Effect of gas thermal conductivity on local heat transfer in a fluidized bed. The Canadian Journal of Chemical Engineering 35: 5-9. 1957.

53. Jones, Trevor M. Measuring cohesion in powders. Manufacturing Chemist and Aerosol News 39, No. 3: 38-40. 1968.

54. Kato, Kunio and Wen, Chin Yung. Bubble assemblage model for fluidized-bed catalytic reactors. Chemical Engineering Science 24: 1351-1369. 1969.

55. Kent, N. L. Technology of cereals (with special reference to wheat). New York, N. Y., Pergamon Press, Inc. c1966.

56. Khvastukin, Yu. I. Heat exchanger with a fluidized bed for preheating a sulfur concentrate. Khim. Prom. (Moscow) 47: 553. 1971. Original not available; abstracted in Chemical Abstracts 75: 78485e. 1971.

57. Koppel, Lowell B., Patel, R. D. and Holmes, John T. Statistical models for surface renewal in heat and mass transfer. Part 3. Residence times and age distributions at wall surface of a fluidized bed, application of spectral density. American Institute of Chemical Engineers Journal 16: 456-464. 1970.

58. Koppel, Lowell B., Patel, R. D. and Holmes, John T. Statistical models for surface renewal in heat and mass transfer. Part 4. Wall-to-fluidized bed heat transfer coefficients. American Institute of Chemical Engineers Journal 16: 464-471. 1970.

59. Kozulin, N. A. and Kulyamin, A. F. Mixing of powdered materials in a fluidized bed. International Chemical Engineering 5: 157-161. 1965.

60. Kranz, Allen Henry. Acid modification of wheat flour in a fluidized bed reactor. Unpublished M.S. thesis. Ames, Iowa, Library, Iowa State University of Science and Technology. 1966.

61. Kristensen, H. Gjelstrup. Statistical properties of random and non-random mixtures of dry solids. Part 1. A general expression for the variance of the composition of samples. Powder Technology 7: 249-257. 1973.

62. Kristensen, H. Gjelstrup. Statistical properties of random and non-random mixtures of dry solids. Part 2. Variance - sample size relationships derived by autocorrelation theories. Powder Technology 8: 149-157. 1973.

63. Kunii, D. and Levenspiel, Octave. Fluidization engineering. New York, N. Y., John Wiley and Sons, Inc. 1969.

64. Kunz, Robert G. Minimum fluidization velocity: fluid cracking catalysts and spherical glass beads. Powder Technology 4: 156-162. 1971.

65. Lacey, P. M. C. Developments in the theory of particle mixing. Journal of Applied Chemistry 4: 257-268. 1954.

66. Lese, H. K. and Kermode, R. I. Heat transfer from a horizontal tube to fluidized bed in the presence of unheated tubes. The Canadian Journal of Chemical Engineering 50: 44-48. 1972.

67. Leva, M. Fluidization. New York, N. Y., McGraw-Hill Book Company, Inc. 1959.

68. Leva, Max. The use of gas-fluidized systems for blending particulate solids. In Rottenburg, P. A. and Shepherd, N. T., eds. Proceedings of the Symposium on the Interaction between Fluids and Particles, London, 1962. pp. 143-150. London, The Institution of Chemical Engineers. ca. 1963.

69A. Levenspiel, Octave. Chemical reaction engineering. 2nd ed. New York, N.Y. Wiley and Sons, Inc. c1972.

69B. Lines, R. W. Some observations on sampling for particle size analysis with the Coulter Counter. Powder Technology 7: 129-136. 1973.

70. Littman, Howard. Solids mixing in straight and tapered fluidized beds. American Institute of Chemical Engineers Journal 10: 924-929. 1964.

71. Lloyd, P. J. and Yeung, P. C. M. Mixing of powders. Chemical and Process Engineering 48, No. 10: 57-61. 1967.

72. Makishima, Shin-ichi and Shirai, Takashi. Dead zone piled on the plate immersed in a fluidised bed. Journal of Chemical Engineering of Japan 2: 124-125. 1969.

73. Malecki, G. J., Shinde, P., Morgan, A. S., Jr. and Farkas, D. F. Atmospheric fluidized bed freeze drying. Food Technology 24: 601-617. 1970.

74. Marc De Chazal, L. E. and Hung, Yen-Chi. A study of the effect of sample size on the analysis of power (sic) mixtures. American Institute of Chemical Engineers Journal 14: 169-173. 1968.

75. Marsheck, R. M. and Gomezplata, A. Particle flow patterns in a fluidized bed. American Institute of Chemical Engineers Journal 11: 167-173. 1965.

76. Massimilla, L. and Westwater, J. W. Photographic study of solid - gas fluidization. American Institute of Chemical Engineers Journal 6: 134-138. 1960.

77. Merry, J. M. D. and Davidson, J. F. "Gulf Stream" circulation in shallow fluidized beds. Transactions of the Institution of Chemical Engineers 51: 361-368. 1973.

78. Michaels, Alan S. and Puzinauskas, Vytautus. Evaluating performance characteristics of mechanical mixing processes: the dextrose-kaolinite-water system. Chemical Engineering Progress 50: 604-614. 1954.

79. Mickley, H. S. and Fairbanks, D. F. Mechanism of heat transfer to fluidized beds. American Institute of Chemical Engineers Journal 1: 374-384. 1955.

80. Miller, Frederick Thomas. Residence time distribution in a fluidized bed reactor. Unpublished M.S. thesis. Ames, Iowa, Library, Iowa State University. 1974.

81. Miller, Kalman J. and Edwards, Richard Modlin. Gas-solids mixing and heat transfer studies in incipiently fluidized beds of nonuniform cross-sectional area. Industrial and Engineering Chemistry Process Design and Development 8: 232-240. 1969.

82. Molochnikov, N. V. and Lovchinovskii, E. V. Use of fluidized bed for drying and mixing iron ore charge materials. Stal' 30(5): 394-7. 1970. Original not available; abstracted in Chemical Abstracts 73: 68828p. 1970.

83. Morris, D. R., Gubbins, K. E. and Watkins, S. B. Residence time studies in fluidized and moving beds with continuous solids flow. Transactions of the Institution of Chemical Engineers 42: T323-T333. 1964.

84. Nazemi, Abolhassan. Heat transfer in fluidized beds of flour and starch. Unpublished Ph.D. thesis. Ames, Iowa, Library, Iowa State University of Science and Technology. 1969.

85. Nazemi, Abolhassan. Heat transfer in fluidized beds of glass beads, Microthene, and potato starch. Unpublished paper. Ames, Iowa, Iowa State University, Department of Chemical Engineering. 1970.

86. Nazemi, Abolhassan, Lancaster, E. B. and Wheelock, T. D. Heat transfer in fluidized beds of flour and starch. AIChE Symposium Series 67, No. 116: 106-113. 1971.

87. Nielsen, Richard Howard. Techniques for determinimg particle mixing and circulation in gas fluidized beds of flour. Unpublished M.S. thesis. Ames, Iowa, Library, Iowa State University. 1974.

88. Oldshue, James Y. Mixing. Industrial and Engineering Chemistry 57: No. 11: 115-123. 1965.

89. Orcutt, J. C. and Carpenter, B. H. Bubble coalescence and the simulation of mass transport and chemical reaction in gas fluidized beds. Chemical Engineering Science 26: 1049-1064. 1971.

90. Ormos, Zoltan, Mozes, Otto and Bolla, Laszlo. Granulation of pharmaceutical powders in fluidized layers. Hung. Halasyztott G616 (cl. B 01j). February 28, 1972. Abstracted in Chemical Abstracts 77: 39255b. 1972.

91. Orr, Clyde and Dallavalle, J. M. Fine particle measurement. New York, N. Y., Mac Millan Company. 1959.

92. Othmer, D. F. Fluidization. New York, N. Y., Reinhold Publishing Corporation. 1956.

93. Partridge, B. A., Lyall, E. and Crooks, H. E. Particle slip surfaces in bubbling gas-fluidized beds. Powder Technology 2: 301-305. 1969.

94. Perry, J. H., ed. Chemical engineers' handbook. 4th ed. New York, N. Y., McGraw-Hill Book Co., Inc. c1963.

95. Pilpel, N. The cohesiveness and tensile strength of powders. Manufacturing Chemist and Aerosol News 40, No. 2: 29-31. 1969.

96. Poole, K. R., Taylor, R. F. and Wall, G. P. Mixing powders to fine scale homogeneity: studies of batch mixing. Transactions of the Institution of Chemical Engineers 42: T305-T315. 1964.

97. Potter, O. E. Mixing. In Davidson, J. F. and Harrison, D., eds. Fluidization. pp. 293-381. New York, N. Y., Academic Press, Inc. 1971.

98. Randolph, Alan D. and Larson, Maurice A. Theory of particulate processes. New York, N. Y., Academic Press, Incorporated. 1971.

99. Roth, Douglas Duane. Thermal conductivity of starch particles. Unpublished M.S. thesis. Ames, Iowa, Library, Iowa State University of Science and Technology. 1969.

100. Roth, Douglas D., Tsao, George T. and Lancaster, Earl B. Thermal conductivity of starch granules. Die Starke 22: 40-44. 1970.

101. Rowe, P. N. Experimental properties of bubbles. In Davidson, J. F. and Harrison, D., eds. Fluidization. pp. 121-191. New York, N. Y., Academic Press, Inc. 1971.

102. Rowe, P. N. and Everett, D. J. Fluidised bed bubbles viewed by x-rays. Part 1. Experimental details and the action of bubbles with solid surfaces. Transactions of the Institution of Chemical Engineers 50: 42-48. 1972.

103. Rowe, P. N. and Henwood, G. A. Drag forces in a hydraulic model of a fluidized bed. Part 1. Transactions of the Institution of Chemical Engineers 39: 43-54. 1961.

104. Rowe, P. N., Nienow, A. W. and Agbim, A. J. Mechanisms by which particles segregate in gas - fluidized beds. Binary systems of near - spherical particles. Transactions of the Institution of Chemical Engineers 50: 310-323. 1972.

105. Rowe, P. N., Nienow, A. W. and Agbim, A. J. Preliminary quantitative study of particle segregation in gas - fluidized beds. Binary systems of near - spherical particles. Transactions of the Institution of Chemical Engineers 50: 324-333. 1972.

106. Rowe, P. N. and Partridge, B. A. Particle movement caused by bubbles in a fluidised bed. In Rottenburg, P. A. and Shepherd, N. T., eds. Proceedings of the Symposium on the Interaction between Fluids and Particles, London, 1962. pp. 135-141. London, The Institution of Chemical Engineers. ca. 1963.

107. Rowe, P. N. and Partridge, B. A. An x-ray study of bubbles in fluidised beds. Transactions of the Institution of Chemical Engineers 43: T157-T175. 1965.

108. Rowe, P. N., Partridge, B. A., Cheney, A. G., Henwood, G. A. and Lyall, E. The mechanisms of solids mixing in fluidized beds. Transactions of the Institution of Chemical Engineers 43: T271-T286. 1965.

109. Rowe, P. N. and Sutherland, K. S. Solids mixing studies in gas fluidized beds. Part 2. The behavior of deep beds of dense materials. Transactions of the Institution of Chemical Engineers 42: T55-T63. 1964.

110. Russo, J. V. and Doe, C. A. Heat treatment of flour as an alternative to chlorination. Journal of Food Technology 5: 363-374. 1970.

111. Schofield, C. and Zaidi, S. H. R. Trends in the mixing of solids and slurries. Chemical and Process Engineering 52, No. 7: 62-64. 1971.

112. Singh, B., Fryer, C. and Potter, O. E. Solids motion caused by a bubble in a fluidized bed. Powder Technology 6: 239-244. 1972.

113. Sutherland, K. S. Solids mixing studies in gas fluidized beds. Part 1. A preliminary comparison of tapered and non-tapered beds. Transactions of the Institution of Chemical Engineers 39: 188-194. 1961.

114. Svarovsky, L. A contribution to the use of the log- probability paper for particle size measurement. Powder Technology 7: 351-352. 1973.

115. Syromyotnikov, N. I. Conductive component for external heat transfer in a fluidized bed. Inzh. Fiz. Zh. 21: 979-84. 1971. Original not available; abstracted in Chemical Abstracts 76: 87765u. 1972.

116. Tailby, S. R. and Cocquerel, M. A. T. Some studies of solids mixing in fluidized beds. Transactions of the Institution of Chemical Engineers 39: 195-201, 237. 1961.

117. Talmor, Eliyahu and Benenati, Robert F. Solids mixing and circulation in gas fluidized beds. American Institute of Chemical Engineers Journal 9: 536-540. 1963.

118. Toomey, R. D. and Johnstone, H. F. Heat transfer between beds of fluidized solids and the walls of the container. Chemical Engineering Progress Symposium Series 49, No. 5: 51-63. 1953.

119. Tsen, C. C, Kulp, K. and Daly, C. T. Effects of chlorine on flour proteins, dough properties, and cake quality. Cereal Chemistry 48: 247-255. 1971.

120. Valentin, F. H. H. Mixing of powders and particulate solids. Chemical and Process Engineering 46, No. 4: 181-187. 1965.

121. Valentin, F. H. H. Mixing of powders, pastes and non-Newtonian fluids. Chemical and Process Engineering 48, No. 10: 69-71. 1967.

122. Valentin, F. H. H. The mixing of powders and pastes: some basic concepts. The Chemical Engineer No. 208: CE99-CE106. 1967.

123. Vance, Frank P. Statistical properties of dry blends. Industrial and Engineering Chemistry 58, No. 6: 36-44. 1966.

124. Varilek, Randall Eugene. Continuous fluidization of wheat flour. Unpublished M.S. thesis. Ames, Iowa, Library, Iowa State University. 1973.

125. Verloop, J., de Nie, L. H. and Heertjes, P. M. The residence time of solids in gas-fluidized beds. Powder Technology 2: 32-42. 1968.

126. Weast, Robert, C., ed. Handbook of chemistry and physics. 47th ed. Cleveland, Ohio, The Chemical Rubber Company. c1966.

127. Weidenbaum, S. S. Mixing of solids. Advances in Chemical Engineering 2: 209-324. 1958.

128. Wheelock, T. D. and Lancaster, E. B. Thermal properties of wheat flour. Die Starke 22: 44-48. 1970.

129. Wheelock, T. D. Literature review on fluidized bed systems relevant to wheat flour modification. Ames, Iowa, Iowa Engineering Experiment Station, Iowa State University of Science and Technology. January 1, 1966.

130. Williams, J. C. The mixing of dry powders. Powder Technology 2: 13-20. 1968.

131. Williams, J. C. The properties of non-random mixtures of solid particles. 3: 189-194. 1970.

132. Williams, P. C. Particle size analysis of flour with the Coulter Counter. Cereal Science Today 15: 102-106, 112. 1970.

133. Wilson, J. T. and Donelson, D. H. Comparison of flour particle size distributions measured by electrical resistivity and microscopy. Cereal Chemistry 47: 126-134. 1970.

134. Woollard, I. N. M. and Potter, O. E. Solids mixing in fluidized beds. American Institute of Chemical Engineers Journal 14: 388-391. 1968.

135. Zenz, F. A. and Othmer, D. F. Fluidization and fluid-particle systems. New York, N. Y., Reinhold Publishing Corporation. 1960.

ACKNOWLEDGMENTS

I heartily thank Dr. T. D. Wheelock for his general supervision (under-which one's decision was encouraged), valuable process suggestions, and constructive criticisms, all of which contributed to professional maturity.

Dr. Norman Harnby, University of Bradford, United Kingdom, deserves special thanks and appreciation for his invaluable expert guidance, constructive suggestions, and inspiration.

Acknowledgment and thanks for supporting help and services is extended to several individuals: Dr. Richard Mensing for his help in performing the statistical analysis, Dr. H. T. David for his guidance in constructing the statistical design, Dr. Richard Kniseley for his expert help and advice in the operation and repair of the small spectrophotometer, and Dr. John Lemish whose help in obtaining the use of the large spectrophotometer contributed to the success of the mixing experiments.

Many of the experiments and analyses reported could be performed only with more difficulty without the fine laboratory assistance of Paul Magee, Larry Nesbit, Mary Northwood, Gbekelolowa (Tunde) Oguntimein, and Mike Schmidt.

In addition to the assistance of the above individuals, the existence and success of this project was made possible by firm financial support. The fine sponsorship of this

project and the funding from grants provided by the United States Department of Agriculture were both greatly appreciated.

I also greatly thank the Iowa State University Graduate College and the National Science Foundation for the Traineeship and its renewal for 3 years.

I thank Dr. Burnet and the Engineering Research Institute of Iowa State University for their support and financial aid.

Special thanks are due my family for their kind support, patience, and encouragement.

APPENDIX A. ADDITIONAL PARTICLE SIZE DATA

Figure 50. Cumulative size distribution by weight of tracer salts

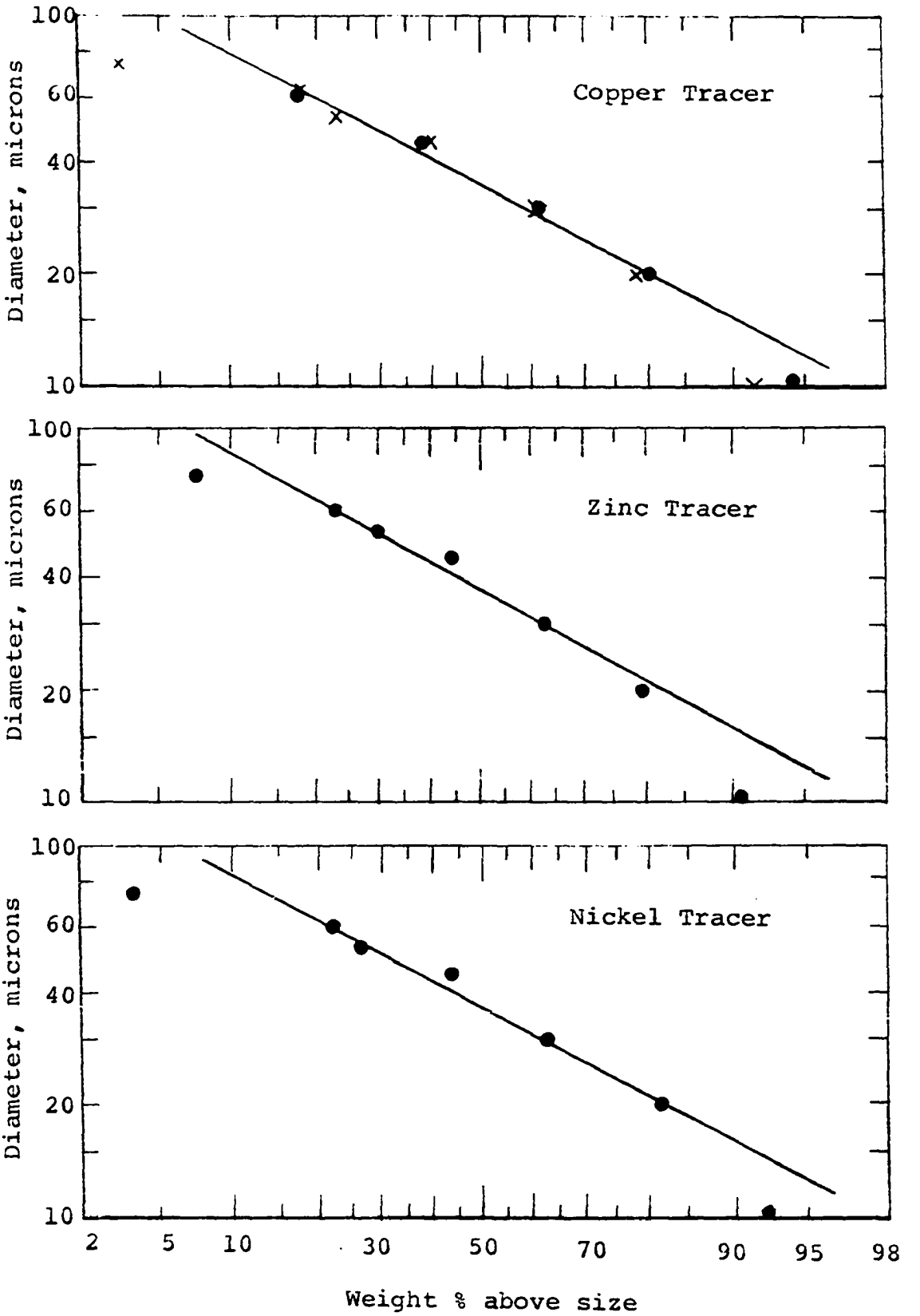
Copper Tracer
Zinc Tracer
Nickel Tracer
Diameter, microns
100
60
40
20
10
2
5
10
30
50
70
90
95
98
Weight % above size

Figure 51. Cumulative size distribution by weight of Microthene

○ = Microthene MN 710, trial 1

× = Microthene MN 710, trial 2

+ = Microthene MN 710, trial 3

● = Microthene MN 701

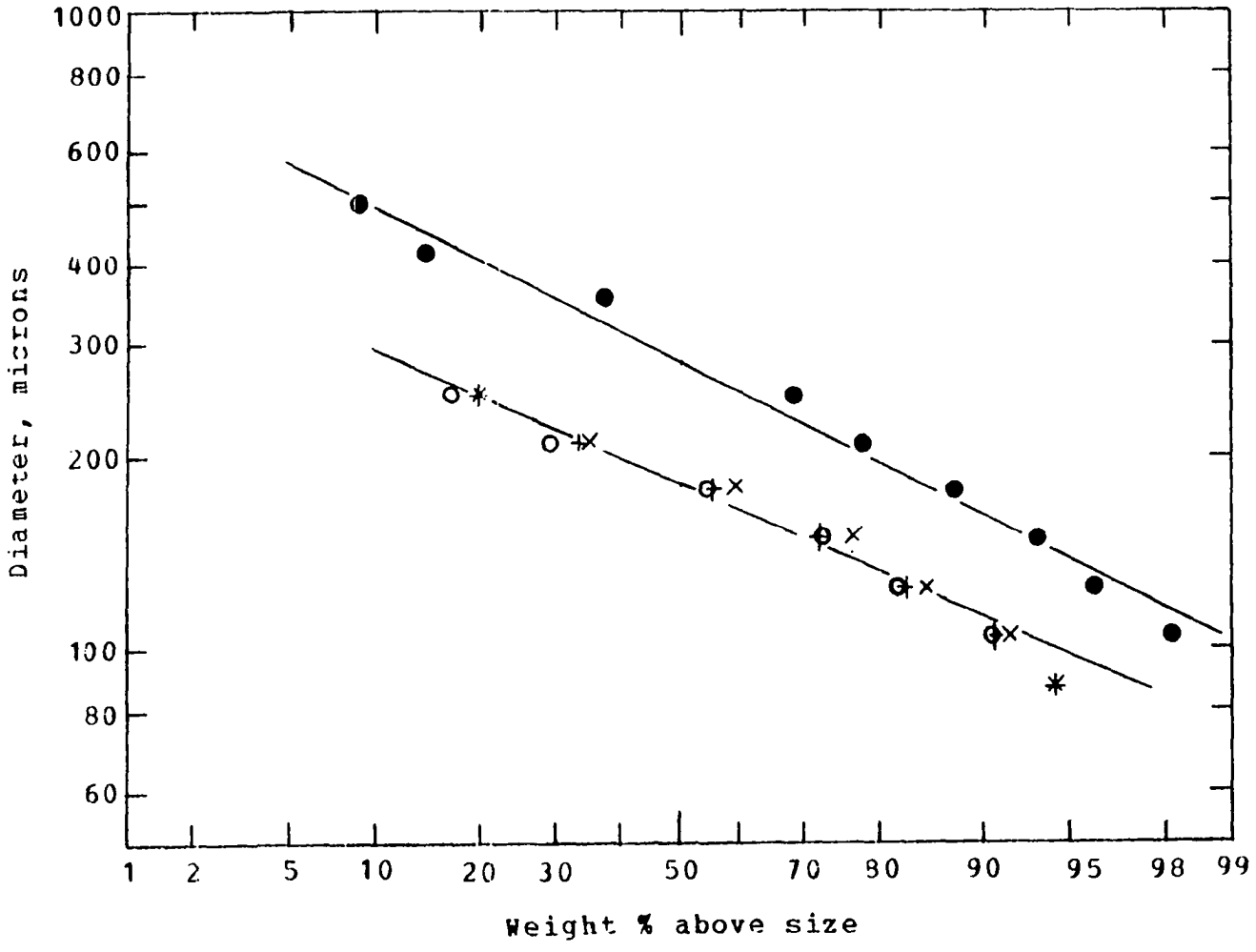
1000
800
600
400
300
200
100
80
60
Diameter, microns
1
2
5
10
20
30
50
70
80
90
95
98
99
Weight % above size

APPENDIX B. RESIDENCE TIME DATA

Table 16. Operating conditions, residence time experiments

Set, Run no.	Mass[2] g.	%M ave.	H in.	%RH	u ft./sec.	N rpm	Op.[1] Time min.
1,1	5635	14.2	27.8	28	0.152	50	65
1,2	5610	14.0	27.8	28	0.152	25	70
1,3	5525	13.7	27.8	28	0.200	50	65
1,4	5885	13.7	28.4	28	0.120	50	75
1,5	5820	13.5	28.0	28	0.152	100	55
1,6	5850	13.3	28.0	28	0.152	25	55
1,7	5805	13.1	27.5	28	0.152	25	75
1,8	5830	12.9	28.0	28	0.200	50	52
2,1	6880	14.7	28.6	28	0.120	50	70
2,2	6830	14.4	27.8	28	0.120	50	73
2,3	6835	14.1	28.1	28	0.120	50	70
2,4	6790	13.8	27.5	28	0.152	25	74
2,5	6810	13.9	27.8	28	0.200	50	76
2,6	6805	13.9	27.0	28	0.152	100	65
2,7	6765	13.8	26.6	28	0.152	50	77
2,8	6780	13.6	26.6	28	0.200	50	65
3,1	6540	14.5	27.8	28	0.152	50	77
3,2	6490	14.4	27.0	28	0.176	50	55
3,3	6505	14.1	26.5	28	0.152	100	70
3,4	6455	14.0	26.8	28	0.200	100	62
3,5	7245	13.9	29.3	28	0.152	25	85
3,6	7175	13.8	29.0	28	0.120	50	95
3,7	7210	13.6	29.0	28	0.200	25	65
3,8	7145	13.4	28.5	28	0.152	50	83
3,9	6040	13.0	25.3	28	0.152	50	61

[1]Operating time from start of fluidization to end of fluidization.

[2]Weight at start of run (from material balance), wet basis.

Table 16. (Continued)

Set, Run no.	Mass g.	%M ave.	H in.	%RH	u ft./sec.	N rpm	Op. Time min.
4,1	6575	14.6	27.3	28	0.152	150	85
4,2	6525	14.4	27.0	28	0.152	100	80
4,3	6545	14.2	27.0	28	0.200	50	71
4,4	7020	14.1	27.8	28	0.120	100	86
4,5	7050	14.1	28.3	28	0.152	25	48
4,6	7035	13.9	28.0	28	0.120	50	86
4,7	6995	13.7	27.6	28	0.120	25	80
4,8	6965	13.6	27.5	28	0.152	50	75
4,9	6320	13.5	26.3	28	0.152	50	65
5,1	7180	13.4	31.3	28	0.152	50	40
5,2	7150	13.2	31.1	28	0.200	50	37
5,3	7160	13.1	31.1	28	0.120	50	45
5,4	7130	13.1	31.0	28	0.152	50	42
6,1	6850	13.6	30.3	28	0.152	50	45
6,2	6785	13.5	30.3	28	0.120	50	55
6,3	6765	13.5	30.3	28	0.200	50	25
6,4	6720	13.2	30.0	28	0.152	50	45
7,1	2685	13.7	12.5	28	0.120	50	33
7,2	2675	13.4	12.5	28	0.200	50	33
7,3	2650	13.3	12.3	28	0.152	50	46
7,4	2625	13.2	12.0	28	0.152	50	--
8,1	7230	11.6	30.8	0	0.200	50	42
8,2	7235	11.3	30.8	0	0.152	50	45
8,3	7210	11.3	30.8	0	0.120	50	72
8,4	7165	10.9	30.4	0	0.152	50	47
9,1	7410	7.9	32.3	0	0.152	50	48
9,2	7365	7.8	32.1	0	0.120	50	55
9,3	7390	7.8	32.1	0	0.152	50	56
9,4	7375	7.8	32.1	0	0.200	50	35

Table 16. (Continued)

Set, Run no.	Mass g.	%M ave.	H in.	%RH	u ft./sec.	N rpm	Op. Time min.
10,1	7220	2.9	31.8	0	0.152	50	35
10,2	7205	2.9	32.0	0	0.120	50	52
10,3	7200	2.9	32.0	0	0.200	50	31
10,4	7180	2.9	32.0	0	0.152	50	47
11,1	7425	15.4	31.5	0	0.152	50	24
11,2	7375	14.9	31.5	0	0.120	50	44
11,3	7370	14.6	31.0	0	0.200	50	43
11,4	7330	14.5	31.0	0	0.152	50	38
11,5	6650	13.6	30.9	0	0.106	50	62
11,6	6630	13.4	30.5	0	0.084	50	51
11,7	6580	13.1	30.2	0	0.071	50	60
11,8	6590	12.8	29.6	0	0.084	50	30

Table 17. Cracks failing to travel full distance, Sets 1 to 6

Set, Run	Upper location: Good Total %	Upper location: Fail Pass d=1 in.	Upper location: Fail Pass d=3 in.	Lower location: Good Total %	Lower location: Fail Pass d=1 in.	Lower location: Fail Pass d=3 in.
1,1	71	0.11	0.40	89	0	0.13
2	87	0.03	0.12	93	0.03	0.07
3	34	0.51	1.91	97	0.01	0.03
4	81	0	0.05	89	0	0
5	88	0.03	0.14	93	0.01	0.04
6	96	0	0.03	89	0.01	0.10
7	83	0.03	0.18	94	0.01	0.06
8	47	0.22	1.11	94	0.03	0.07
2,1	80	0.08	0.13	89	0.02	0.07
2	73	0.08	0.29	92	0	0.04
3	73	0.03	0.16	93	0.02	0.04
4	83	0.04	0.16	95	0	0.03
5	54	0.22	0.86	96	0	0.04
6	80	0.05	0.20	96	0.03	0.03
7	81	0.11	0.24	97	0	0.03
8	52	0.31	0.92	90	0.06	0.12
3,1	83	0.06	0.20	99	0	0.01
2	78	0.10	0.27	97	0	0.03
3	99	0	0.12	99	0	0.01
4	64	0.20	0.56	97	0	0.03
5	86	0	0.13	99	0	0.01
6	77	0.02	0.12	94	0	0.03
7	77	0.10	0.30	94	0.03	0.07
8	80	0.08	0.17	99	0	0
9	80	0.08	0.23	100	0	0
4,1	77	0.12	0.27	95	0.01	0.05
2	79	0.02	0.23	100	0	0
3	51	0.39	0.96	89	0.06	0.13
4	67	0	0.23	91	0.02	0.04

Table 17. (Continued)

Set, Run	Upper location			Lower location		
	Good Total %	Fail Pass d=1 in.	Fail Pass d=3 in.	Good Total %	Fail Pass d=1 in.	Fail Pass d=3 in.
4,5	93	0.05	0.06	93	0.04	0.07
6	73	0.11	0.22	84	0	0.04
7	64	0.06	0.33	83	0	0.02
8	75	0.06	0.31	96	0	0.04
9	94	0.03	0.07	99	0.01	0.01
5,1	76	0.14	0.32	96	0.02	0.04
2	66	0.39	0.53	83	0.10	0.20
3	81	0.09	0.18	89	0	0.08
4	80	0.17	0.25	85	0.04	0.18
6,1	69	0.16	0.45	89	0.05	.012
2	84	0.14	0.20	88	0.06	0.13
3	46	0.84	1.15	90	0.05	0.10
4	51	0.56	0.97	98	0	0.02

Table 18. Cracks failing to travel full distance, Sets 7 to 11

Set, Run	Upper Good Total %	Upper Fail Pass	Mid Good Total %	Mid Fail Pass	Lower Good Total %	Lower Fail Pass	Lowest Good Total %	Lowest Fail Pass
7,1	100	0	100	0	98	0.02	100	0
2	100	0	100	0	92	0.09	100	0
3	98	0.02	100	0	97	0.03	98	0.02
4	98	0.02	98	0.02	98	0.02	100	0
8,1	77	0.29	92	0.09	97	0.03	100	0
2	83	0.20	91	0.10	83	0.11	100	0
3	89	0.08	89	0.06	96	0.04	100	0
4	81	0.18	90	0.07	100	0	95	0.05
9,1	85	0.14	81	0.24	93	0.08	98	0.02
2	82	0.22	91	0.10	100	0	87	0.16
3	86	0.16	89	0.10	100	0	100	0
4	80	0.24	90	0.11	91	0.10	100	0
10,1	88	0.14	97	0.04	96	0.04	100	0
2	85	0.04	93	0.04	89	0.10	96	0.02
3	95	0.05	92	0.11	100	0	100	0
4	93	0.07	96	0.04	93	0.08	100	0
11,1	85	0.18	--	----	96	0.04	--	----
2	93	0.06	--	----	98	0.02	--	----
3	85	0.18	--	----	100	0	--	----
4	90	0.11	--	----	93	0.07	--	----
5	91	0.10	91	0.10	92	0.09	85	0.17
6	84	0.19	86	0.17	84	0.19	69	0.44
7	88	0.14	95	0.05	93	0.07	85	0.17
8	89	0.11	89	0.12	93	0.07	84	0.20

Table 19. Summary of slip surface void times, upper and lower areas

Set, Run no.	Upper O[1] #	Upper d in.	Upper n	Upper $\bar{t}$ sec.	Upper s^2 sec^2	Lower O #	Lower d in.	Lower n	Lower $\bar{t}$ sec.	Lower s^2 sec^2
1,1	1	1	55	6.52	13.25	2	1	64	4.95	4.38
	1	2	55	16.30	73.83	2	2	64	10.09	15.46
	1	3	55	19.20	36.10	2	3	64	15.10	28.14
1,2	2	1	66	7.30	9.82	1	1	68	4.97	5.12
	2	2	68	15.41	44.72	1	2	70	10.80	37.11
	2	3	68	22.09	75.11	1	3	70	15.39	49.91
1,3	1	1	33	4.03	1.46	2	1	74	3.61	1.11
	1	2	33	7.35	4.75	2	2	74	6.91	2.64
	1	3	33	11.03	7.59	2	3	74	10.30	7.97
1,4	1	1	42	10.21	23.00	2	1	62	8.64	21.70
	1	2	41	21.17	106.35	2	2	64	17.48	91.73
	1	3	42	33.84	302.97	2	3	66	26.31	210.63
1,5	1	1	71	6.90	13.75	2	1	72	5.37	8.69
	1	2	68	12.79	24.64	2	2	72	9.91	20.97
	1	3	71	20.46	100.72	2	3	75	15.59	67.73
1,6	2	1	68	7.29	10.30	1	1	72	5.69	10.67
	2	2	65	13.48	25.26	1	2	72	10.49	22.54
	2	3	69	21.60	83.40	1	3	74	15.27	41.85
1,7	1	1	66	7.23	16.43	2	1	72	5.75	9.41
	1	2	67	14.83	74.39	2	2	72	11.09	30.29
	1	3	68	21.82	139.22	2	3	73	16.19	46.28
1,8	1	1	45	3.65	1.34	2	1	73	3.26	1.29
	1	2	45	6.89	1.91	2	2	73	6.37	3.40
	1	3	45	10.13	3.32	2	3	73	9.43	5.71
2,1	2	1	39	10.20	21.79	1	1	57	8.65	18.95
	2	2	40	21.41	62.81	1	2	58	17.09	77.50
	2	3	44	36.18	316.43	1	3	59	26.43	215.05
2,2	1	1	40	8.76	21.32	2	1	55	8.49	22.93
	1	2	39	16.23	42.82	2	2	55	16.97	99.25
	1	3	39	24.17	75.93	2	3	55	24.18	192.83

[1]Observer number.

Table 19. (Continued)

Set, Run no.	Upper O #	Upper d in.	Upper n	Upper $\bar{t}$ sec.	Upper s^2 sec^2	Lower O #	Lower d in.	Lower n	Lower $\bar{t}$ sec.	Lower s^2 sec^2
2,3	1	1	36	9.50	12.82	2	1	54	9.19	26.96
	1	2	37	19.48	101.18	2	2	54	17.69	84.33
	1	3	37	28.56	203.46	2	3	55	27.95	248.91
2,4	1	1	67	8.77	15.64	2	1	74	6.55	20.43
	1	2	70	18.09	83.34	2	2	76	12.91	57.23
	1	3	70	25.21	111.02	2	3	76	18.76	102.27
2,5	1	1	55	4.45	3.57	2	1	75	3.73	2.90
	1	2	55	8.75	7.80	2	2	75	7.52	7.06
	1	3	55	12.27	9.98	2	3	75	10.90	12.82
2,6	1	1	66	7.09	16.45	2	1	75	5.73	11.79
	1	2	66	14.77	61.61	2	2	76	11.81	40.35
	1	3	68	22.64	145.69	2	3	76	17.19	61.01
2,7	1	1	63	8.13	16.70	2	1	76	5.73	7.32
	1	2	62	14.73	33.90	2	2	76	11.19	22.96
	1	3	62	21.87	89.77	2	3	76	16.71	50.47
2,8	1	1	49	4.97	3.51	2	1	78	3.36	1.30
	1	2	49	9.40	5.85	2	2	78	6.52	4.86
	1	3	49	13.24	9.46	2	3	78	9.66	10.22
3,1	1	1	65	7.42	13.24	2	1	77	5.25	5.39
	1	2	65	14.16	31.51	2	2	77	10.83	29.57
	1	3	65	20.30	40.90	2	3	77	15.84	44.15
3,2	1	1	62	4.75	4.34	2	1	76	4.62	4.03
	1	2	62	10.17	7.97	2	2	76	9.12	8.66
	1	3	62	15.14	11.03	2	3	76	13.77	17.42
3,3	1	1	67	6.89	8.12	2	1	77	5.82	9.77
	1	2	68	15.50	66.79	2	2	77	11.51	37.89
	1	3	68	22.99	110.54	2	3	77	16.49	66.38
3,4	1	1	61	4.47	3.71	2	1	76	3.76	1.13
	1	2	61	8.51	5.62	2	2	76	7.56	2.32
	1	3	61	12.35	7.75	2	3	76	11.59	5.04

Table 19. (Continued)

Set, Run no.	Upper O #	d in.	n	$\bar{t}$ sec.	s^2 sec^2	Lower O #	d in.	n	$\bar{t}$ sec.	s^2 sec^2
3,5	1	1	68	7.62	20.39	2	1	77	5.72	10.78
	1	2	69	15.51	71.10	2	2	77	11.30	39.29
	1	3	67	22.33	115.13	2	3	77	16.46	75.16
3,6	1	1	39	10.83	23.87	2	1	59	9.61	27.17
	1	2	41	23.80	111.77	2	2	59	18.99	96.26
	1	3	43	38.06	293.39	2	3	59	27.99	200.49
3,7	1	1	69	4.30	2.72	2	1	73	3.13	0.91
	1	2	69	8.39	5.55	2	2	73	6.25	3.15
	1	3	69	12.37	7.35	2	3	73	9.38	6.55
3,8	1	1	64	8.39	22.03	2	1	77	6.24	14.07
	1	2	65	16.50	72.40	2	2	78	12.28	50.17
	1	3	66	25.05	165.33	2	3	78	17.44	69.09
3,9	1	1	65	6.24	7.74	2	1	78	4.44	6.00
	1	2	65	12.76	22.34	2	2	78	8.62	14.85
	1	3	66	19.33	72.79	2	3	78	12.74	25.03
4,1	1	1	59	7.29	12.83	2	1	78	5.18	5.23
	1	2	60	13.79	34.88	2	2	78	9.98	15.32
	2	3	62	22.19	113.77	2	3	78	15.14	47.20
4,2	1	1	54	8.11	22.83	2	1	77	4.63	6.85
	1	2	56	15.98	67.33	2	2	78	9.20	22.02
	1	3	56	22.30	93.74	2	3	78	13.54	33.42
4,3	1	1	54	4.01	2.58	2	1	72	3.11	1.02
	1	2	54	7.60	3.56	2	2	72	6.33	3.35
	1	3	54	11.31	4.35	2	3	72	9.63	6.54
4,4	1	1	37	11.62	30.29	2	1	47	8.30	22.13
	1	2	39	22.09	103.66	2	2	52	18.86	137.11
	1	3	40	32.72	309.82	2	3	52	29.82	503.27
4,5	1	1	60	7.09	16.73	2	1	69	5.59	11.48
	1	2	62	14.44	57.10	2	2	69	10.51	29.59
	1	3	62	21.96	87.23	2	3	69	14.88	36.55

Table 19. (Continued)

Set, Run no.	Upper					Lower				
	O #	d in.	n	t sec.	s^2 sec^2	O #	d in.	n	t sec.	s^2 sec^2
4,6	1	1	37	14.12	42.31	2	1	50	8.80	20.31
	1	2	36	24.14	134.99	2	2	53	18.33	99.20
	1	3	39	36.74	342.32	2	3	54	27.20	240.24
4,7	1	1	34	11.42	30.97	2	1	48	8.73	19.92
	1	2	36	22.34	105.45	2	2	53	19.29	114.57
	1	3	39	35.64	286.79	2	3	55	29.43	267.80
4,8	1	1	61	7.01	8.93	2	1	73	5.69	9.74
	1	2	62	15.26	80.15	2	2	75	11.47	47.22
	1	3	62	22.30	120.90	2	3	75	16.26	71.14
4,9	1	1	76	6.59	19.12	2	1	80	4.91	8.15
	1	2	76	11.81	35.04	2	2	80	9.49	18.53
	1	3	76	17.31	64.64	2	3	80	13.65	32.44
5,1	1	1	56	6.46	6.15	3	1	52	4.26	1.02
	1	3	56	16.80	17.81	3	3	52	12.62	2.25
5,2	1	1	57	3.57	2.72	3	1	59	2.79	0.21
	1	3	57	9.05	31.36	3	3	59	8.85	0.69
5,3	1	1	43	10.65	24.21	3	1	49	7.37	9.18
	1	3	45	33.05	302.76	3	3	51	22.95	101.61
5,4	1	1	53	7.64	9.24	3	1	55	4.63	1.74
	1	3	53	19.78	21.90	3	3	55	13.91	6.35
6,1	1	1	56	6.01	5.34	4	1	43	4.31	1.46
	1	3	56	16.59	13.47	4	3	43	12.49	7.51
6,2	1	1	51	9.54	23.62	4	1	53	5.95	5.43
	1	3	51	27.74	199.37	4	3	53	17.69	31.14
6,3	1	1	33	3.91	3.24	3	1	57	3.09	0.38
	1	3	33	11.27	5.81	3	3	57	9.62	1.21
6,4	1	1	39	6.64	3.50	3	1	55	4.54	1.12
	1	3	39	18.65	12.96	3	3	55	13.25	3.96

Table 19. (Continued)

Set, Run no.	Upper					Lower				
	O #	d in.	n	t sec.	S^2 sec^2	O #	d in.	n	t sec.	S^2 sec^2
7,1	1	1	54	8.05	1.64	3	1	52	7.56	0.92
7,2	1	1	54	3.78	0.30	3	1	47	5.58	1.25
7,3	1	1	53	6.27	1.77	4	1	62	6.34	1.02
7,4	1	1	53	6.22	1.00	4	1	61	6.29	1.23
8,1	1	1	48	3.09	1.56	3	1	58	2.76	0.21
8,2	1	1	55	6.21	4.52	3	1	55	4.48	1.70
8,3	1	1	50	12.20	36.86	3	1	52	7.40	13.51
8,4	3	1	50	7.62	11.88	1	1	62	5.42	4.19
9,1	1	1	58	8.33	15.30	4	1	52	6.33	4.79
9,2	1	1	49	13.93	21.92	4	1	52	8.53	13.45
9,3	4	1	51	9.22	27.95	1	1	56	6.00	7.13
9,4	1	1	49	5.10	5.63	4	1	51	4.07	0.94
10,1	1	1	51	7.42	3.79	4	1	54	5.29	0.73
10,2	1	1	46	10.88	28.74	4	1	32	12.92	553.80
10,3	1	1	56	4.04	1.85	4	1	56	3.96	0.41
10,4	1	1	57	7.95	6.91	4	1	52	5.09	1.72
11,1	1	1	51	5.55	4.85	1	1	55	4.18	2.24
11,2	1	1	55	11.23	25.98	1	1	57	6.50	7.37
11,3	1	1	61	3.38	1.71	1	1	61	3.16	0.28
11,4	1	1	53	6.93	5.16	1	1	55	4.51	2.28

Table 19. (Continued)

Set, Run no.	Upper					Lower				
	O #	d in.	n	t sec.	s^2 sec^2	O #	d in.	n	t sec.	s^2 sec^2
11,5	1	2	58	1.62	0.15	4	2	56	2.21	0.094
11,6	1	2	58	2.85	0.30	4	2	52	3.44	0.40
11,7	1	2	57	4.21	0.99	4	2	57	5.31	1.77
11,8	1	2	59	2.87	0.27	4	2	57	3.43	0.29

Table 20. Summary of slip surface void times, middle and lowest areas

Set, Run no.	Mid O[1] #	Mid d in.	Mid n	Mid t sec.	Mid S^2 sec^2	Lowest O #	Lowest d in.	Lowest n	Lowest t sec.	Lowest S^2 sec^2
7,1	1	1	54	7.55	1.15	3	1	53	7.46	1.85
7,2	1	1	54	4.56	0.59	3	1	49	7.91	6.15
7,3	1	1	54	5.97	0.66	4	1	61	6.57	2.02
7,4	1	1	53	6.09	1.42	4	1	62	6.33	1.25
8,1	1	1	57	3.11	0.83	3	1	46	4.02	4.75
8,2	1	1	60	6.24	5.70	3	1	60	4.13	6.93
8,3	1	1	50	10.40	20.39	3	1	54	7.04	7.02
8,4	3	1	56	5.83	10.37	1	1	58	4.76	1.43
9,1	1	1	50	6.38	14.81	4	1	55	5.64	6.59
9,2	1	1	49	9.55	20.69	4	1	45	9.44	22.05
9,3	4	1	50	7.01	10.28	1	1	56	5.98	4.98
9,4	1	1	55	4.55	2.22	4	1	56	4.75	0.76
10,1	1	1	56	5.61	2.41	4	1	56	5.54	1.02
10,2	1	1	48	10.35	23.17	4	1	55	7.39	20.06
10,3	1	1	55	4.09	1.02	4	1	56	4.52	0.75
10,4	1	1	55	7.23	11.35	4	1	56	5.30	1.81
11,1			--					--		
11,2			--					--		
11,3			--					--		
11,4			--					--		
11,5	1	2	58	1.79	0.19	4	2	52	2.46	0.17
11,6	1	2	59	2.96	0.32	4	2	43	3.76	0.58
11,7	1	2	62	4.56	1.10	4	2	52	5.30	2.51
11,8	1	2	59	3.20	0.28	4	2	51	3.85	0.42

[1] Observer number.

APPENDIX C. MIXING DATA

Table 21. Operating conditions, mixing experiments

Set, Run no.	Mass[2] g.	%M ave.	H in.	%RH	u ft./sec.	N rpm	Op.[1] Time min.
1,10	5805	13.2	28.0	28	0.152	25	34
1,11	5825	13.1	28.0	28	0.120	50	33
1,12	5865	13.1	27.6	28	0.152	100	33
2,10	6645	13.0	26.8	28	0.120	50	34
2,11	6755	13.0	28.0	28	0.152	25	28
2,12	6750	12.9	27.1	28	0.200	50	25
3,10	6900	13.2	28.5	28	0.200	100	22
3,11	6625	13.0	27.5	28	0.120	25	34
3,12	6435	12.9	26.8	28	0.152	25	33
4,10	9605	13.5	27.5	28	0.120	50	34
4,11	6980	13.6	28.3	28	0.120	100	33
4,12	6845	13.4	26.8	28	0.200	25	25
5,10	7150	13.1	31.0	28	0.200	50	25
5,11	7185	13.2	31.5	28	0.152	50	33
6,10	6715	13.4	29.9	28	0.200	50	33
6,11	7040	13.3	31.5	28	0.200	50	24
7,10	2675	13.0	12.5	28	0.152	50	20
7,11	2940	13.1	13.5	28	0.200	50	20
8,10	7105	10.6	32.3	0	0.200	50	25
8,11	6770	10.6	31.3	0	0.152	50	34
9,10	7335	7.8	32.4	0	0.200	50	22
9,11	7150	7.7	32.3	0	0.200	50	24
10,10	7135	2.8	32.0	0	0.200	50	24
10,11	7110	3.0	32.0	0	0.152	50	33

[1]Operating time from tracer addition.

[2]Weight at start of run (from material balance), wet basis.

Table 21. (Continued)

Set, Run no.	Mass g.	%M ave.	H in.	%RH	u ft./sec.	N rpm	Op. Time min.
11,10	7035	12.4	31.0	0	0.059	50	19
11,11	7160	12.6	31.5	0	0.080	50	19
12,10	10785	18.2	31.0	0	0.152	50	19
12,11	12060	18.0	33.0	0	0.200	50	19
13,10	7175	14.0	31.0	0	0.351	50	19
13,11	7340	13.8	32.1	0	0.351	50	19
14,10	2850	7.7	12.5	17	0.333	19	30

Table 22. Amount of material removed from bed during sampling

Set, run	No. of samples	% Bed mass removed[1]	% Change in bed depth[2]
1, 10	70	5.1	7.7
11	70	5.2	7.7
12	70	4.1	6.3
2, 10	80	3.8	4.4
11	77	4.0	7.7
12	74	5.7	5.9
3, 10	85	6.1	6.5
11	85	5.0	5.8
12	90	4.9	6.5
4, 10	81	5.6	5.3
11	90	5.5	7.6
12	91	4.6	0.5
5, 10	91	3.3	2.5
11	90	3.8	5.0
6, 10	90	3.6	2.1
11	91	4.3	4.1
7, 10	90	6.3	7.5
11	90	5.4	5.9
8, 10	91	3.7	3.2
11	91	3.7	4.2
9, 10	90	3.4	3.6
11	90	4.3	3.6
10, 10	90	3.4	3.6
11	90	4.3	4.9

[1]Samples plus purged material.

[2]Including loss by entrainment.

Table 22. (Continued)

Set, run	No. of samples	% Bed mass removed	% Change in bed depth
11, 10	100	4.4	5.1
11	100	3.8	6.3
12, 10	100	2.7	11.2
11	100	2.8	6.9
13, 10	100	3.0	3.8
11	100	3.3	4.0
14, 10	67	3.5	8.7

Figure 52. Mixing curve of Set 1, run 11

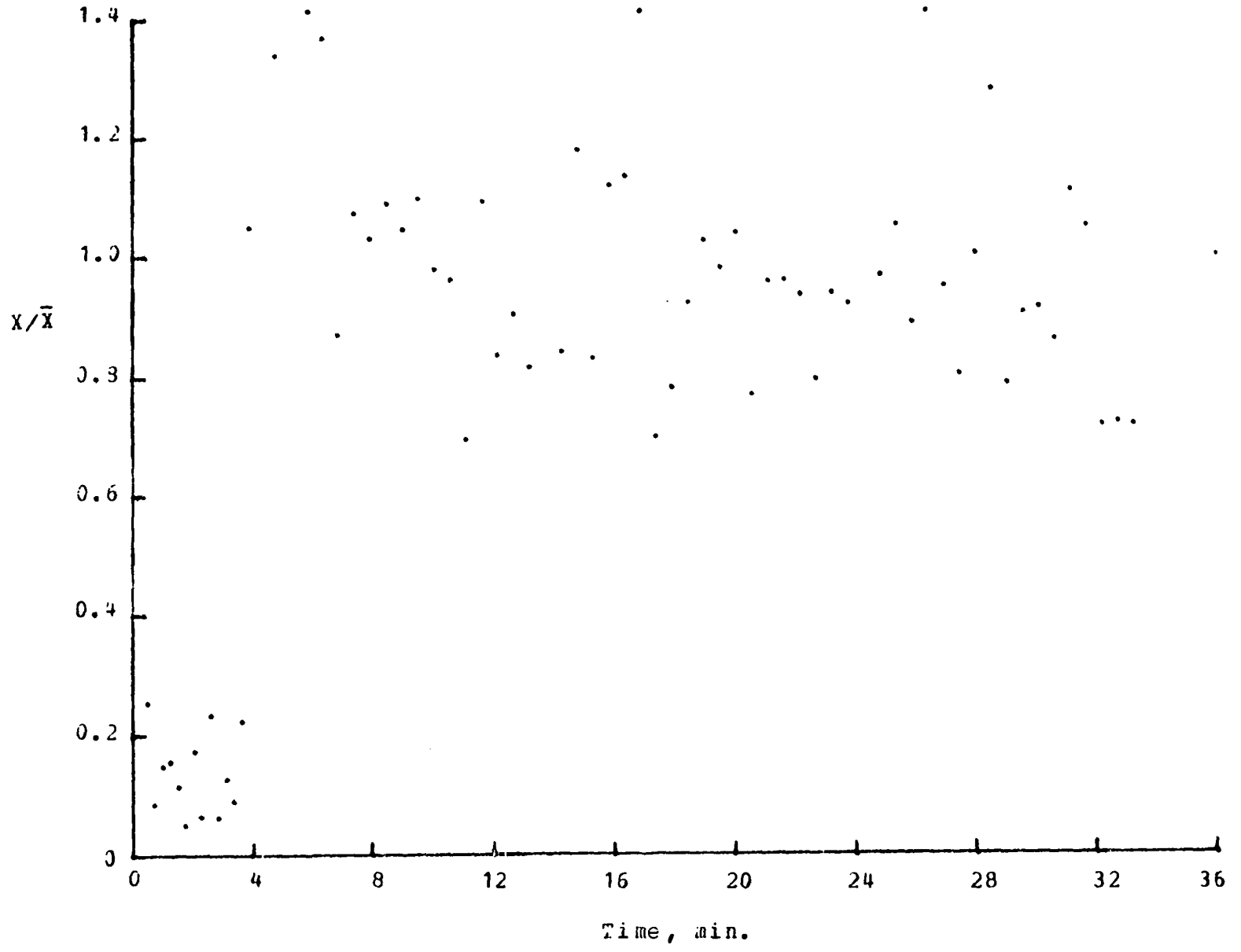
1.4
1.2
1.0
0.8
0.6
0.4
0.2
0
X/X̄
0
4
8
12
16
20
24
28
32
36
Time, min.

Figure 53. Mixing curve of Set 1, run 12

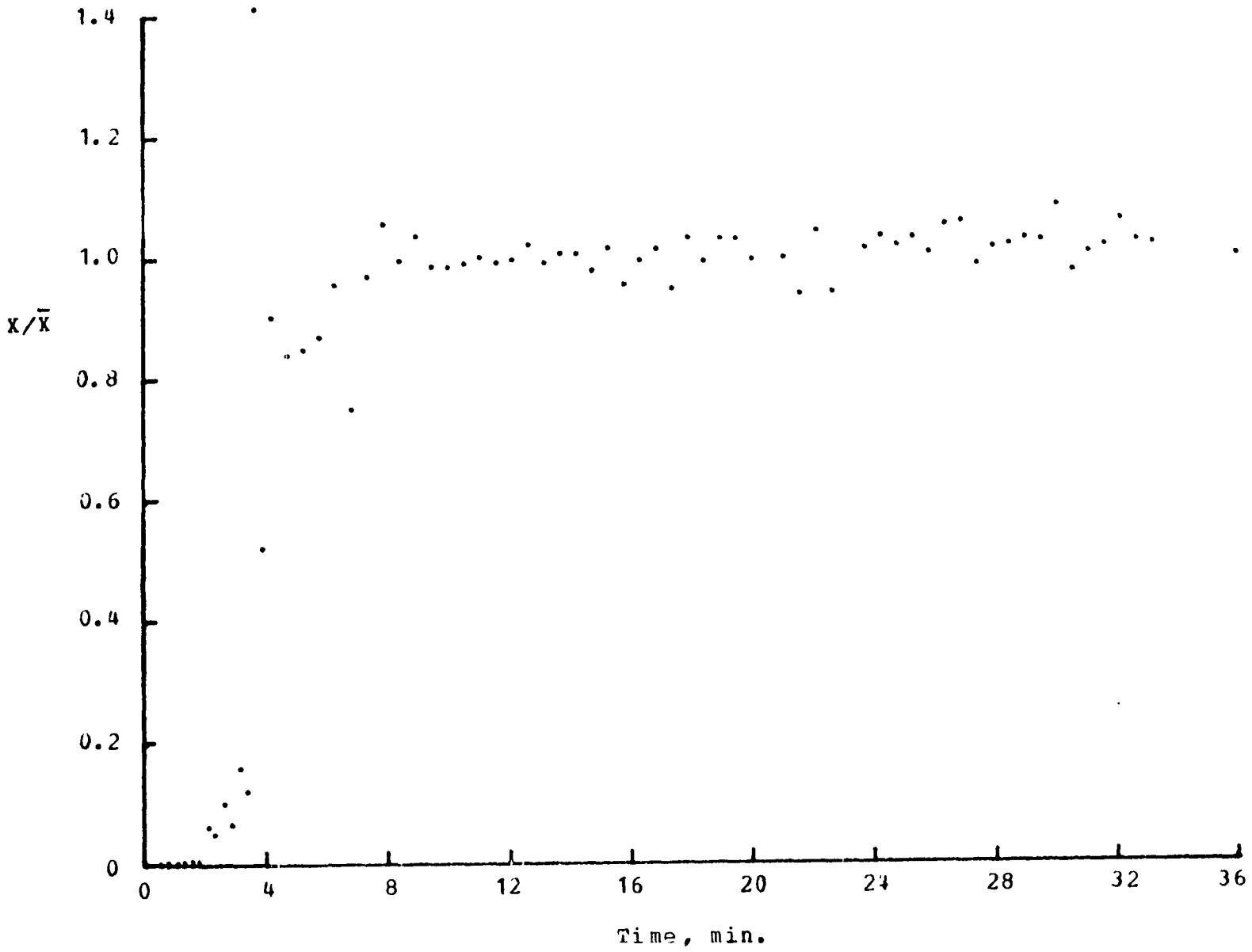
1.4
1.2
1.0
0.8
0.6
0.4
0.2
0
X/X̄
0
4
8
12
16
20
24
28
32
36
Time, min.

Figure 54. Mixing curve of Set 3, run 10

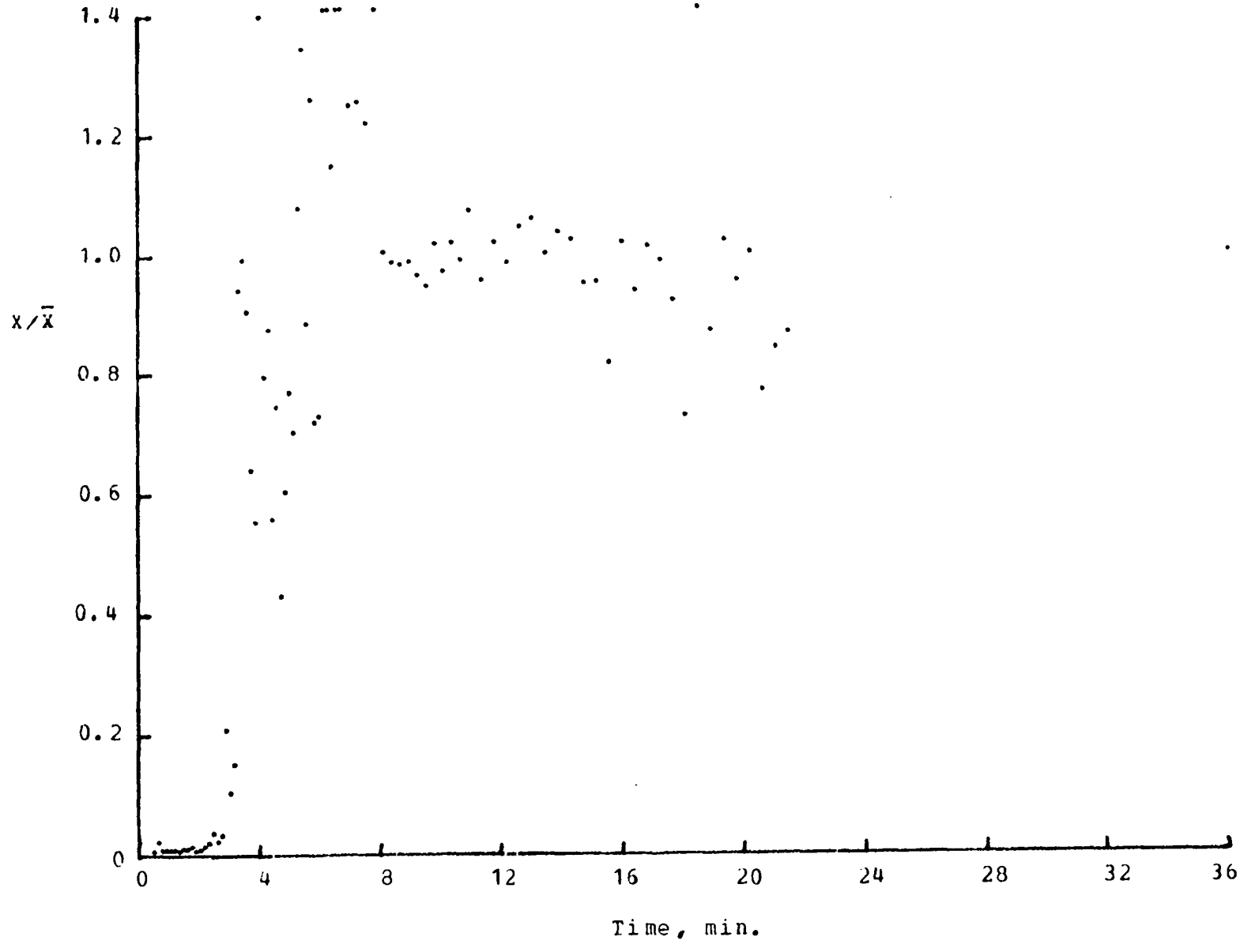
1.4
1.2
1.0
0.8
0.6
0.4
0.2
0
x/x̄
0
4
8
12
16
20
24
28
32
36
Time, min.

Figure 55. Mixing curve of Set 3, run 11

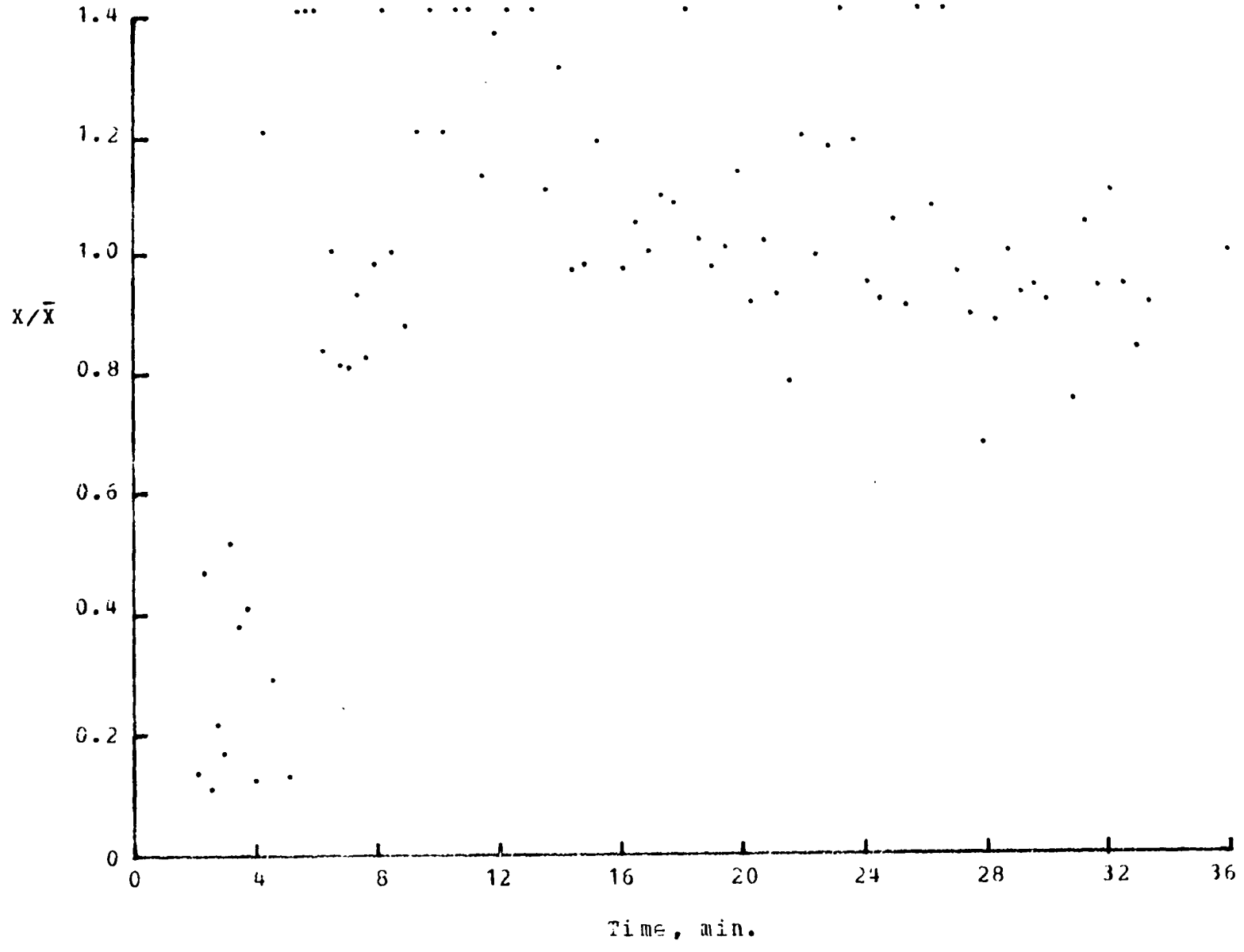
1.4
1.2
1.0
0.8
0.6
0.4
0.2
0
X/X̄
0
4
8
12
16
20
24
28
32
36
Time, min.

Figure 56. Mixing curve of Set 3, run 12

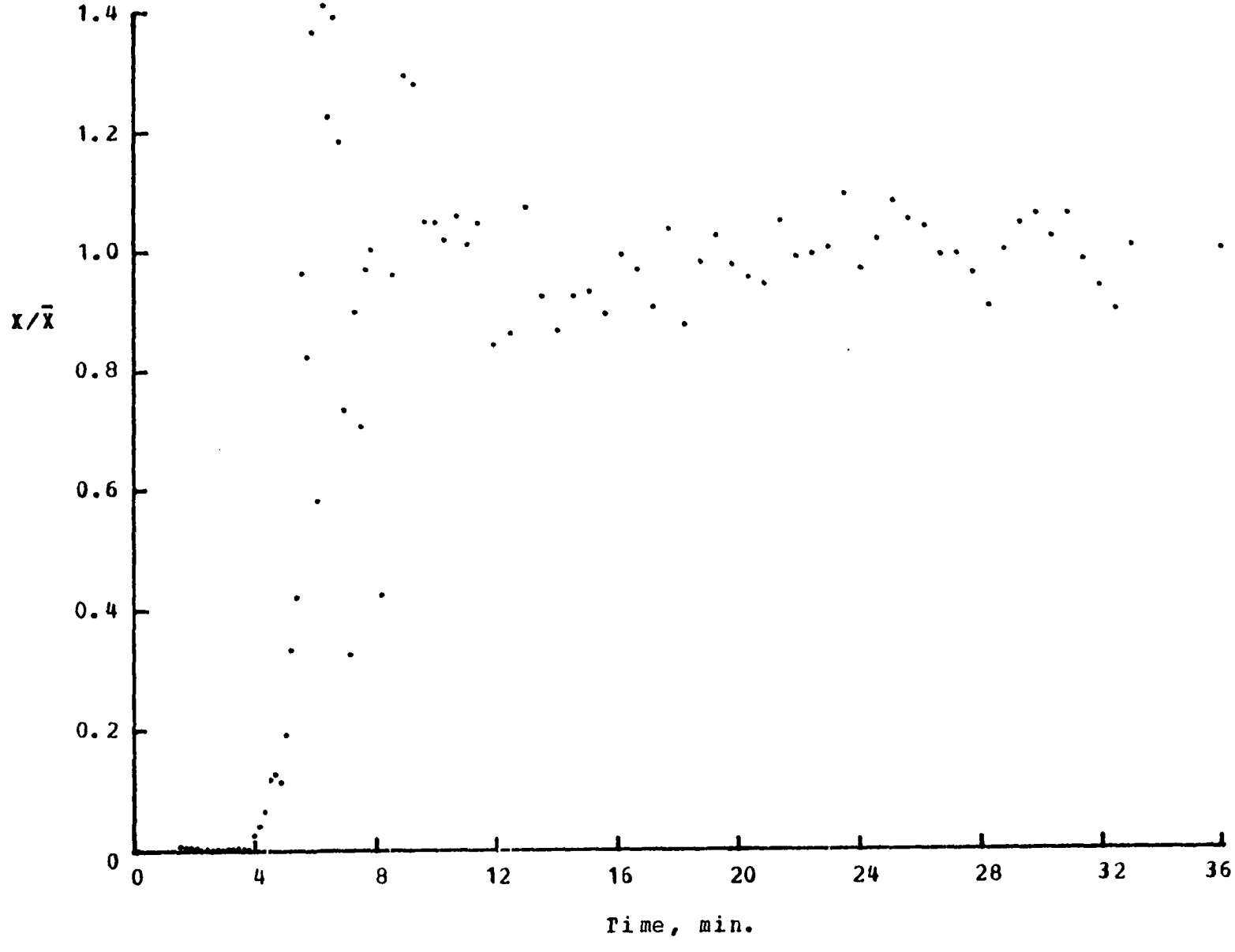
1.4
1.2
1.0
0.8
0.6
0.4
0.2
0
X/X̄
0
4
8
12
16
20
24
28
32
36
Time, min.

Figure 57. Mixing curve of Set 4, run 10

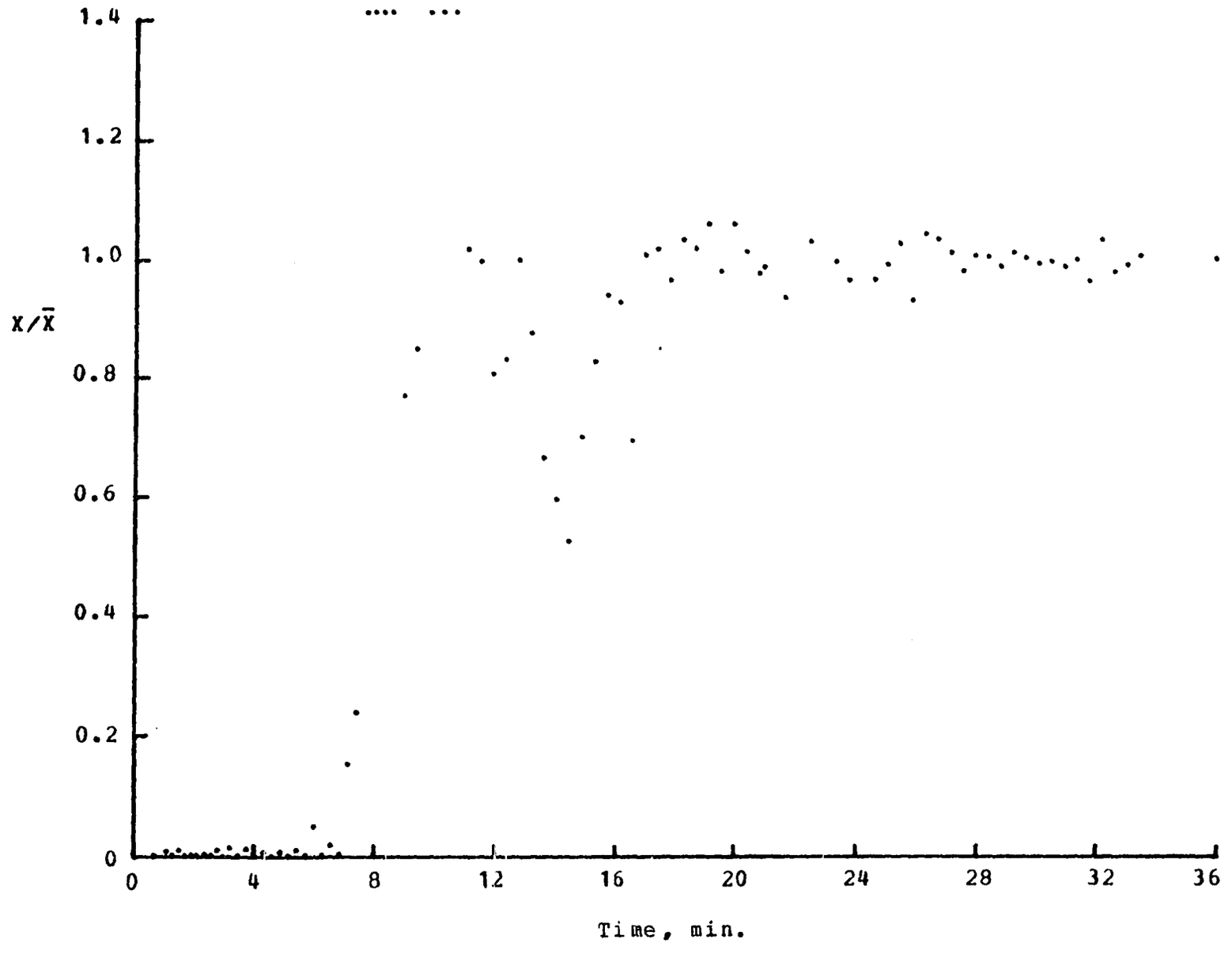
1.4
1.2
1.0
0.8
0.6
0.4
0.2
0
X/X̄
0
4
8
12
16
20
24
28
32
36
Time, min.

Figure 58. Mixing curve of Set 4, run 11

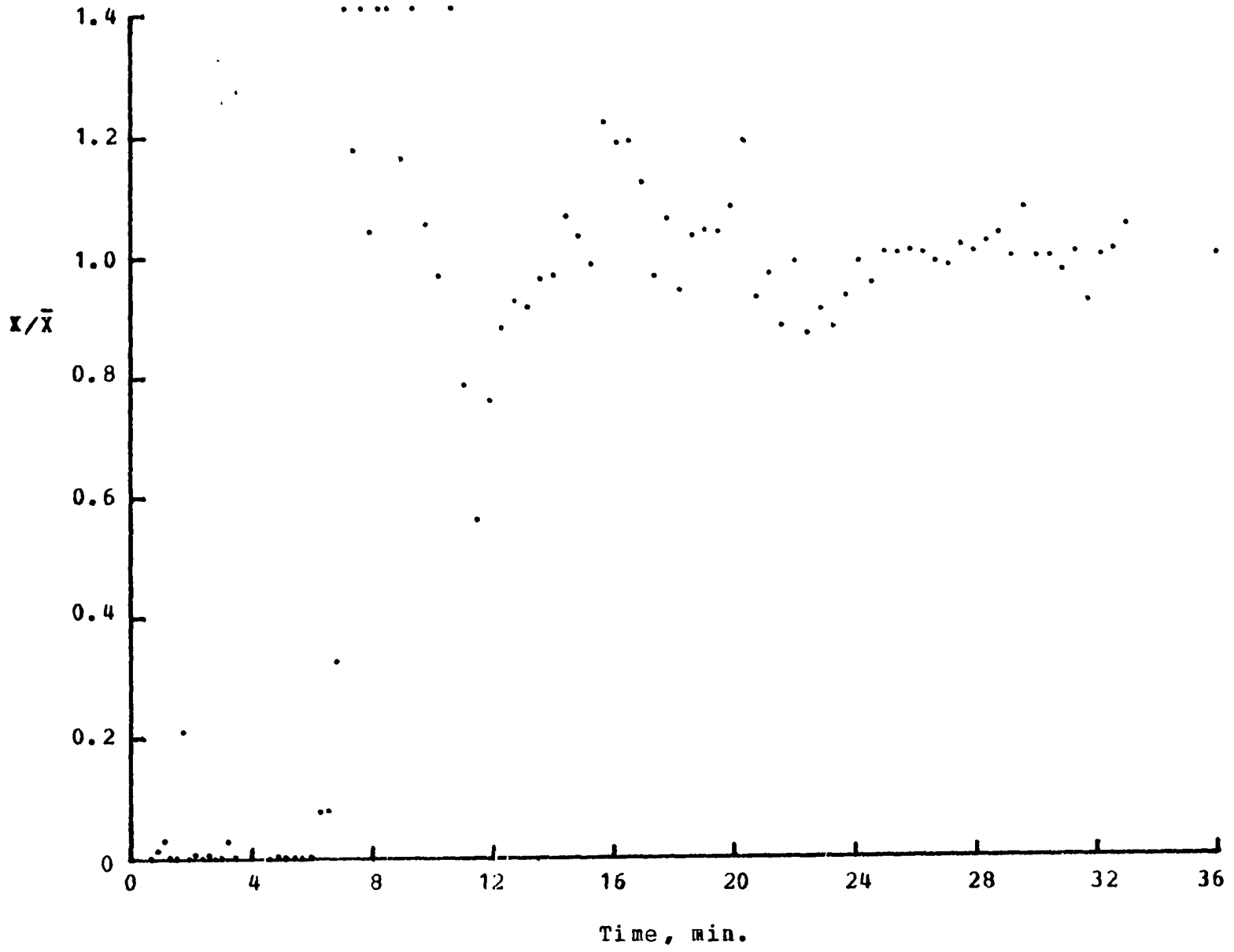
1.4
1.2
1.0
0.8
0.6
0.4
0.2
0
X/X̄
0
4
8
12
16
20
24
28
32
36
Time, min.

Figure 59. Mixing curve of Set 4, run 12

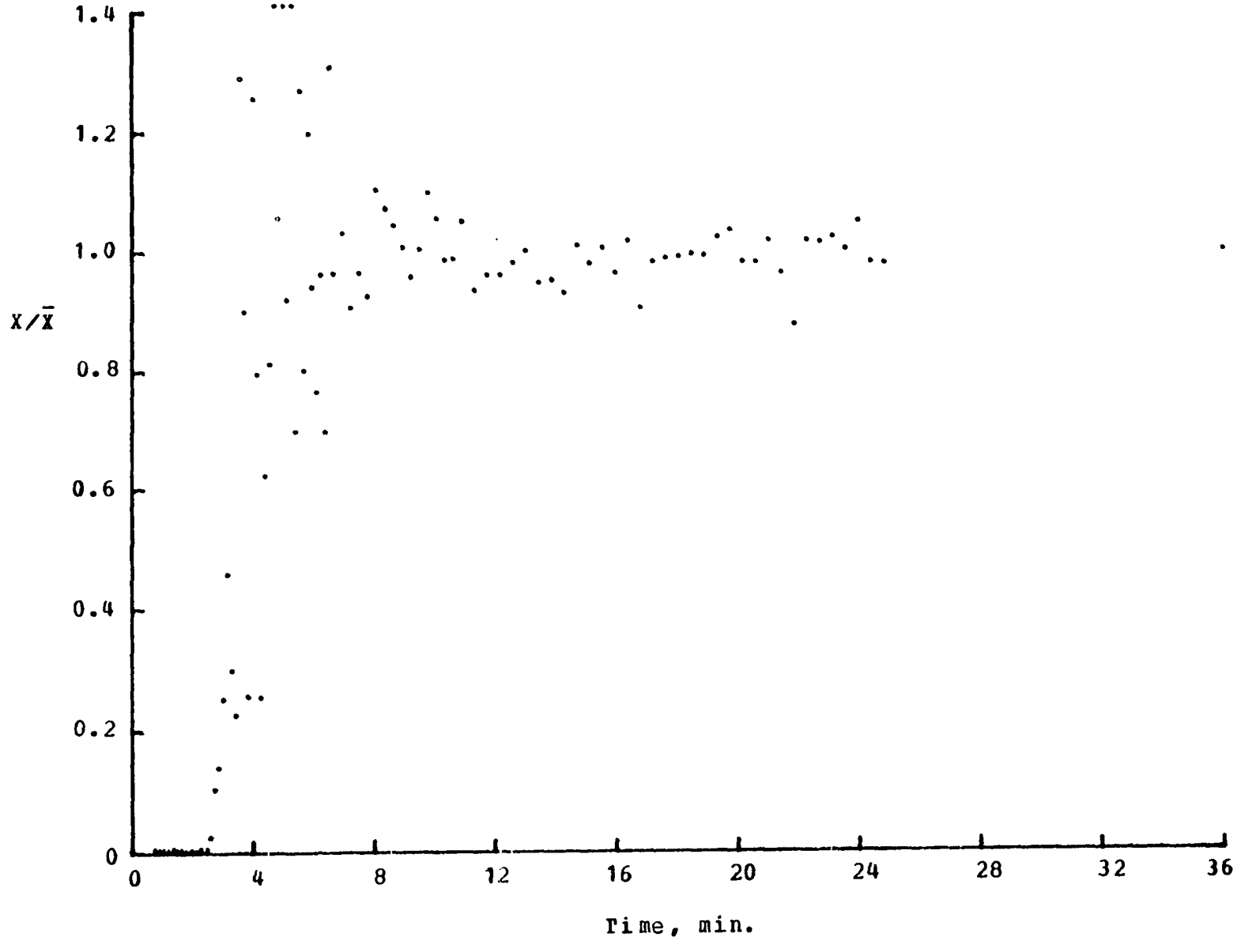
1.4
1.2
1.0
0.8
0.6
0.4
0.2
0
X/X̄
0
4
8
12
16
20
24
28
32
36
Time, min.

Figure 60. Mixing curve of Set 5, run 10

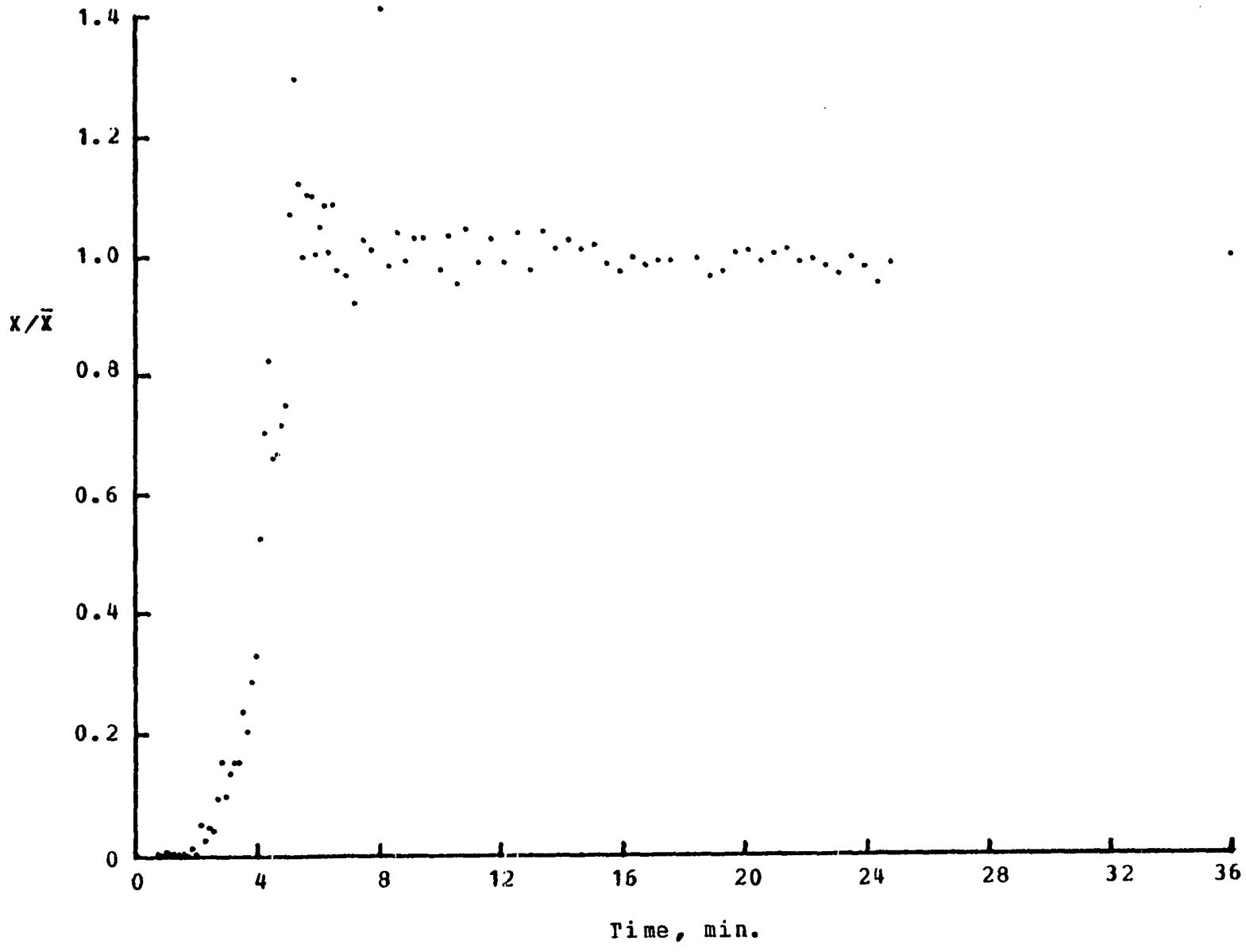
1.4
1.2
1.0
0.8
0.6
0.4
0.2
0
X/X̄
0
4
8
12
16
20
24
28
32
36
Time, min.

Figure 61. Mixing curve of Set 5, run 11

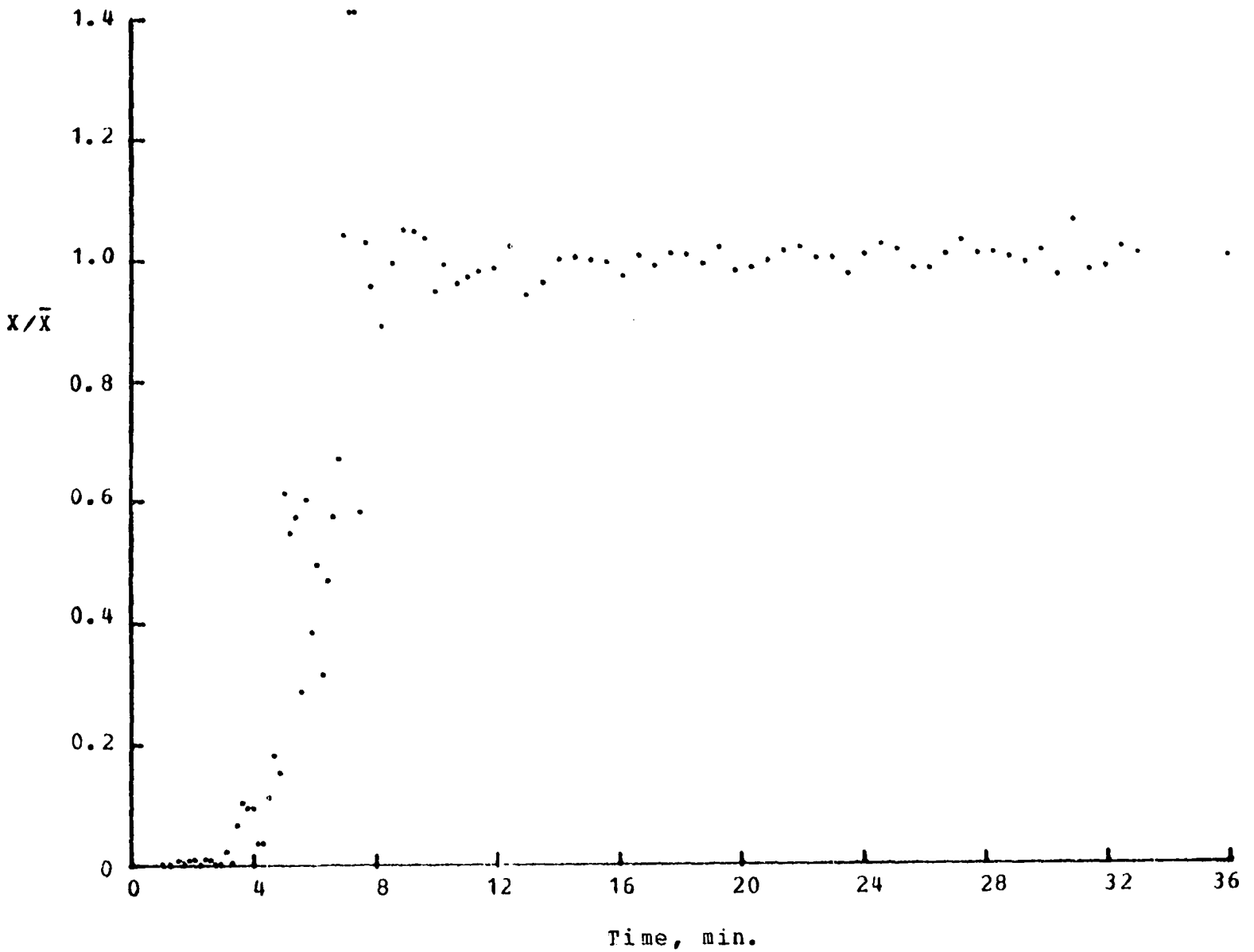
1.4
1.2
1.0
0.8
0.6
0.4
0.2
0
X/X̄
0
4
8
12
16
20
24
28
32
36
Time, min.

Figure 62. Mixing curve of Set 6, run 10

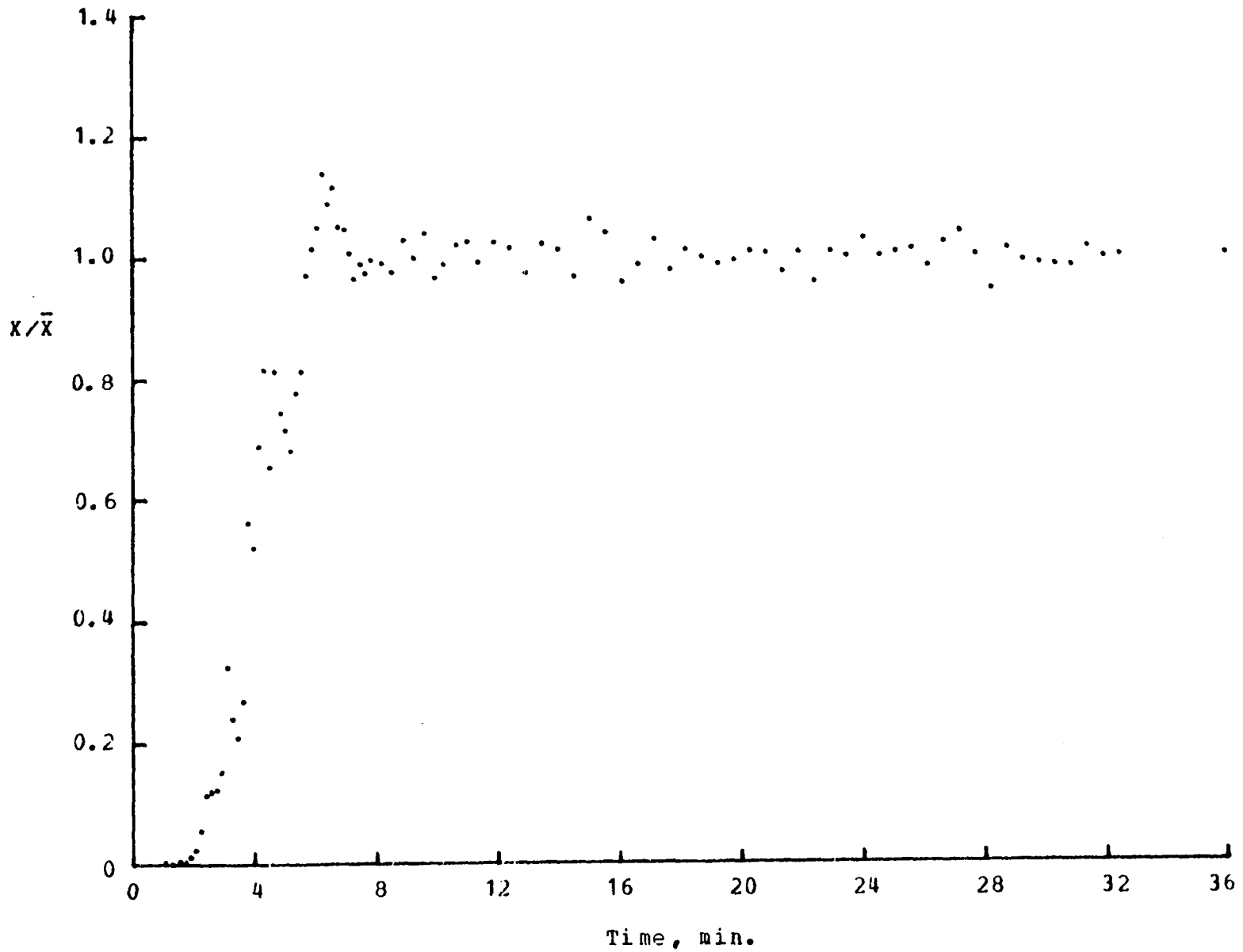
1.4
1.2
1.0
0.8
0.6
0.4
0.2
0
X/X̄
0
4
8
12
16
20
24
28
32
36
Time, min.

Figure 63. Mixing curve of Set 6, run 11

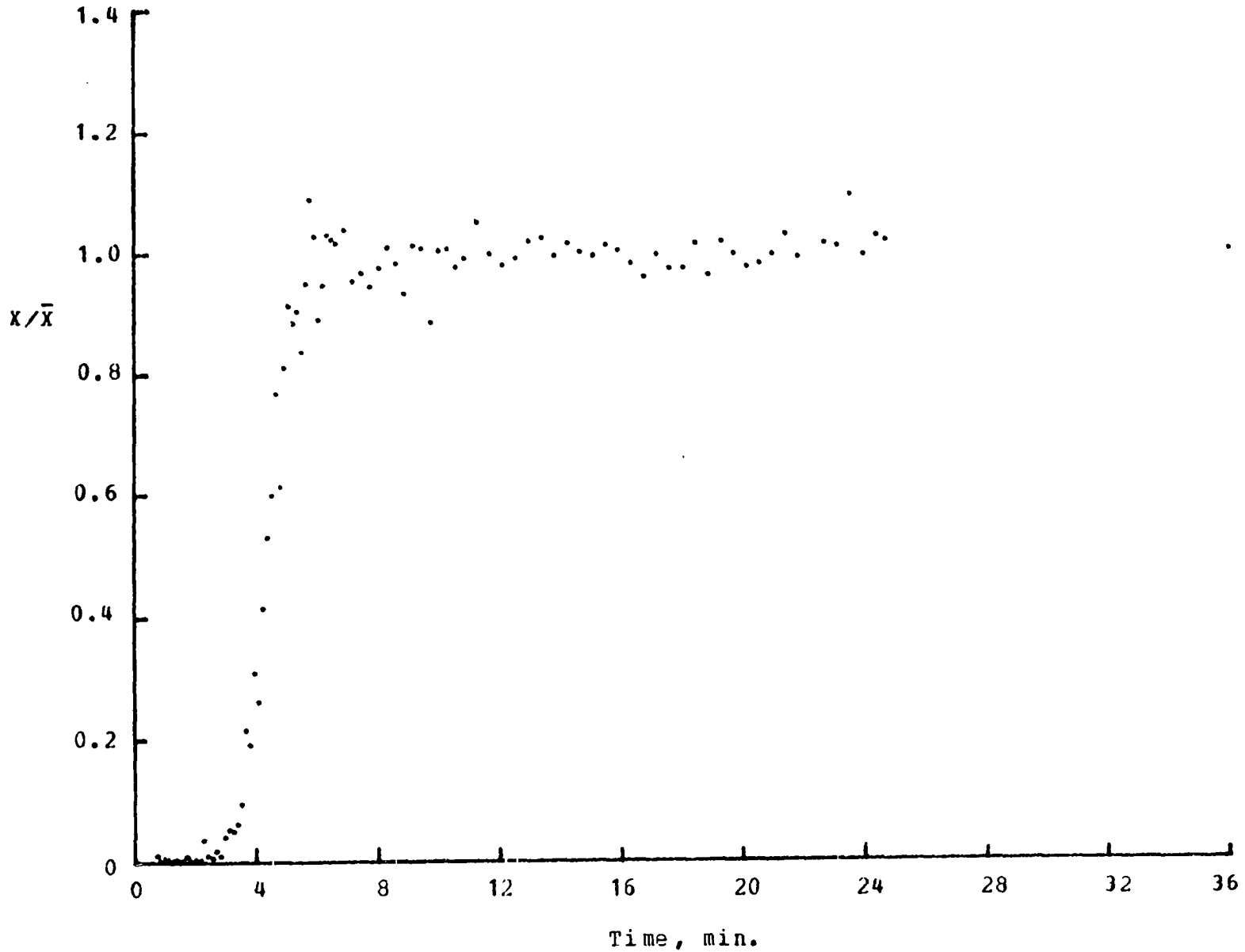
1.4
1.2
1.0
0.8
0.6
0.4
0.2
0
X/X̄
0
4
8
12
16
20
24
28
32
36
Time, min.

Figure 64. Mixing curve of Set 7, run 10

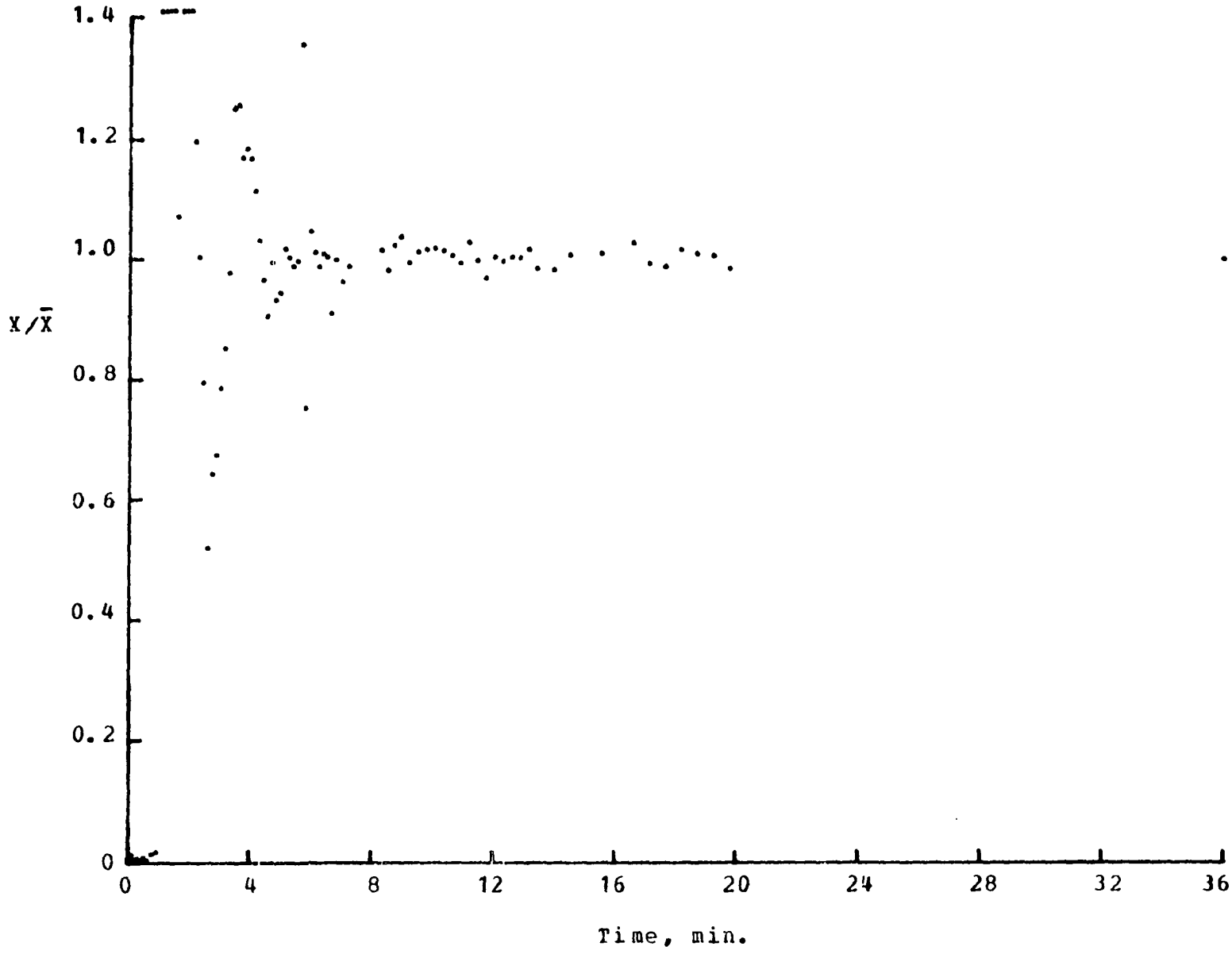
1.4
1.2
1.0
0.8
0.6
0.4
0.2
0
X/X̄
0
4
8
12
16
20
24
28
32
36
Time, min.

Figure 65. Mixing curve of Set 7, run 11

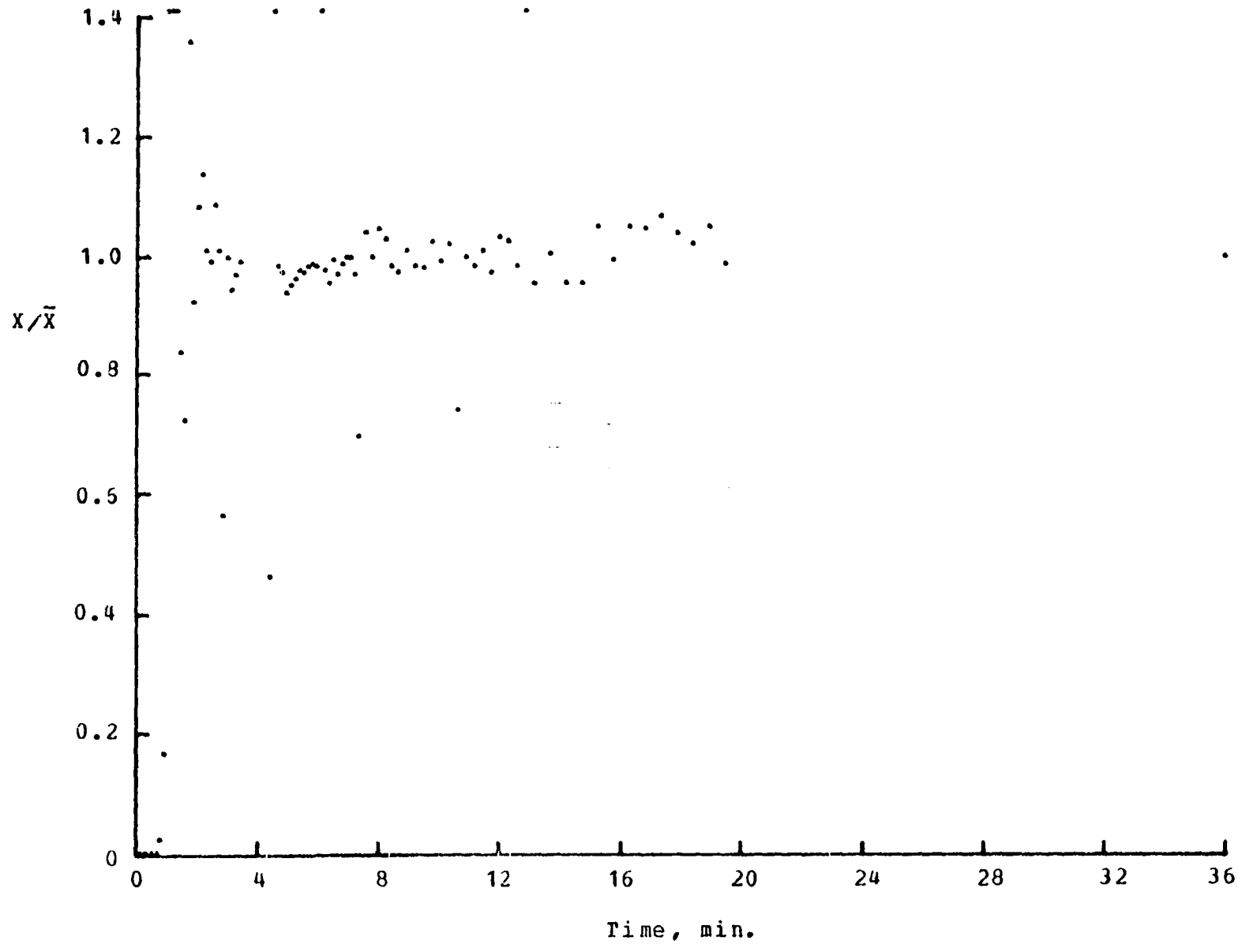
1.4
1.2
1.0
0.8
0.5
0.4
0.2
0
X/X̄
0
4
8
12
16
20
24
28
32
36
Time, min.

Figure 66. Mixing curve of Set 8, run 10

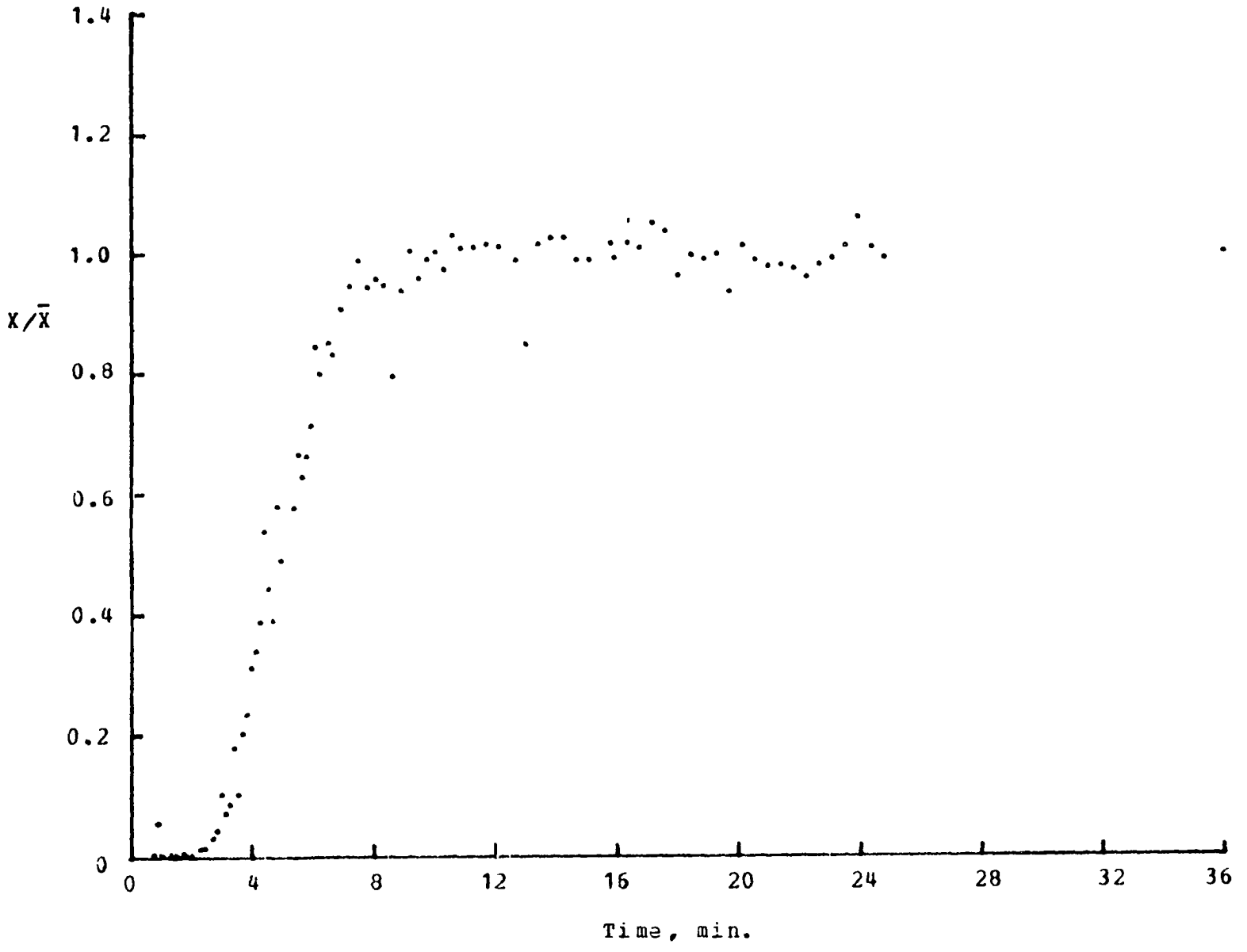
1.4
1.2
1.0
0.8
0.6
0.4
0.2
0
X/X̄
0
4
8
12
16
20
24
28
32
36
Time, min.

Figure 67. Mixing curve of Set 8, run 11

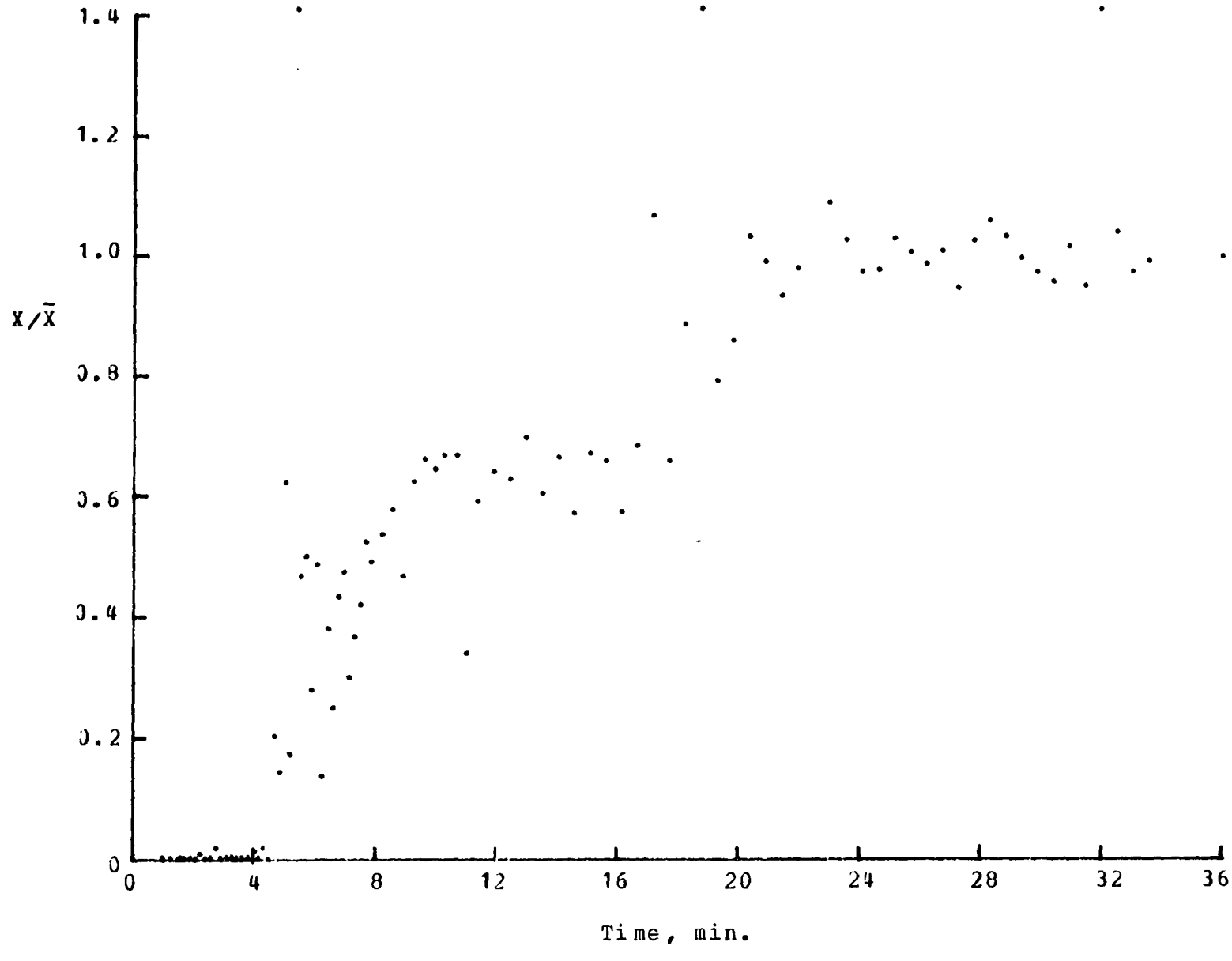
1.4
1.2
1.0
0.8
0.6
0.4
0.2
0
X/X̄
0
4
8
12
16
20
24
28
32
36
Time, min.

Figure 68. Mixing curve of Set 9, run 10

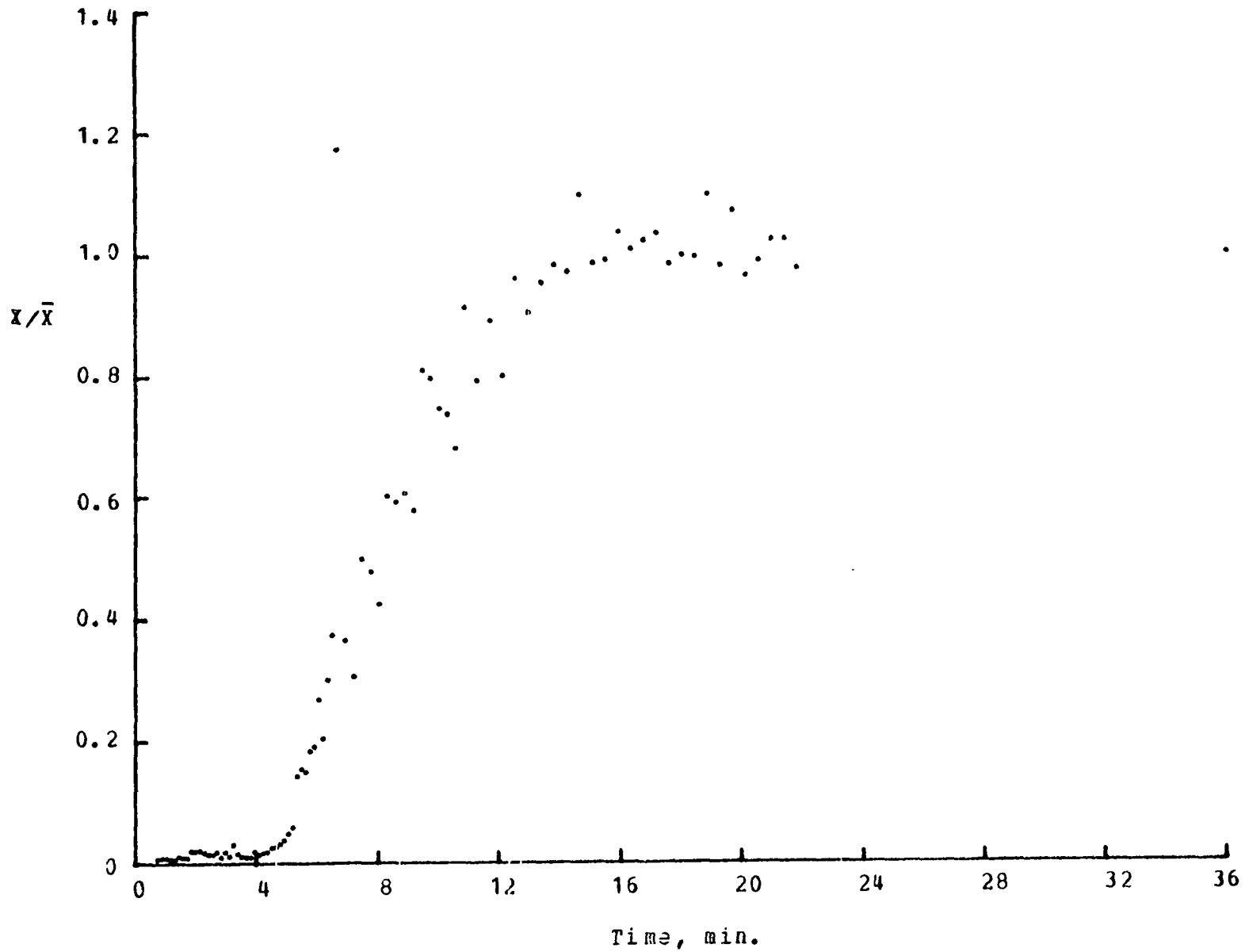
1.4
1.2
1.0
0.8
0.6
0.4
0.2
0
X/X̄
0
4
8
12
16
20
24
28
32
36
Time, min.

Figure 69. Mixing curve of Set 9, run 11

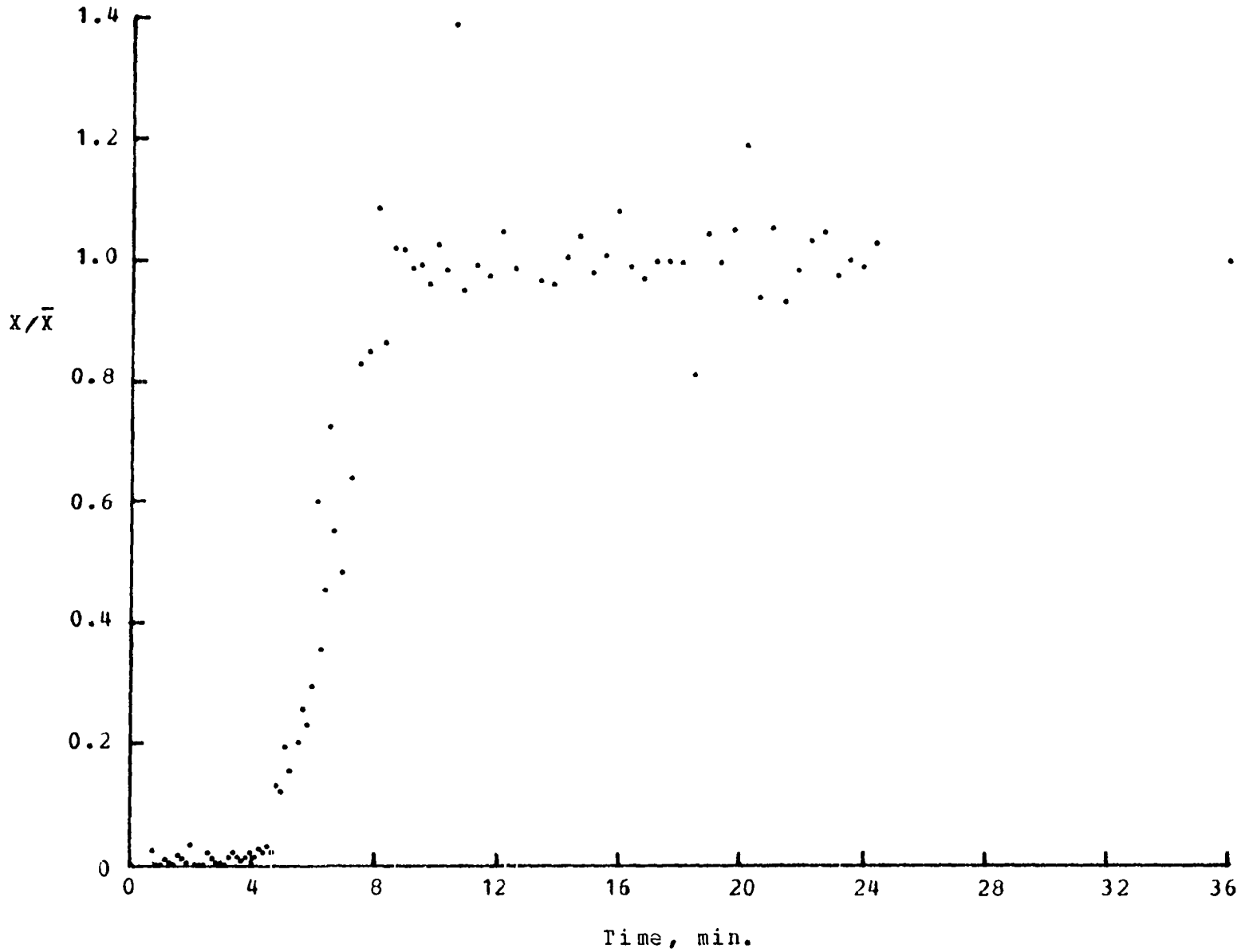
1.4
1.2
1.0
0.8
0.6
0.4
0.2
0
X/X̄
0
4
8
12
16
20
24
28
32
36
Time, min.

Figure 70. Mixing curve of Set 10, run 10

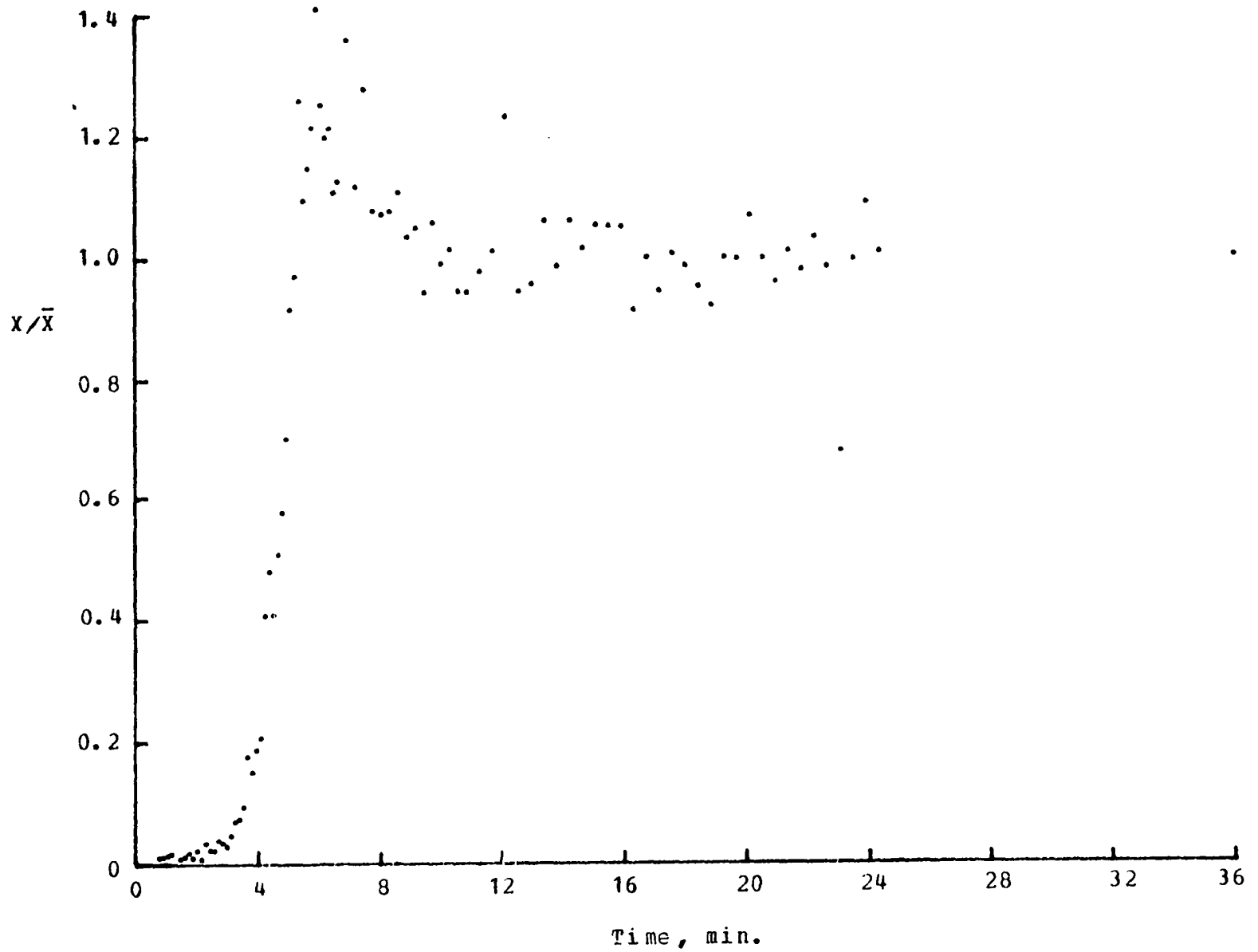
1.4
1.2
1.0
0.8
0.6
0.4
0.2
0
X/X̄
0
4
8
12
16
20
24
28
32
36
Time, min.

Figure 71. Mixing curve of Set 10, run 11

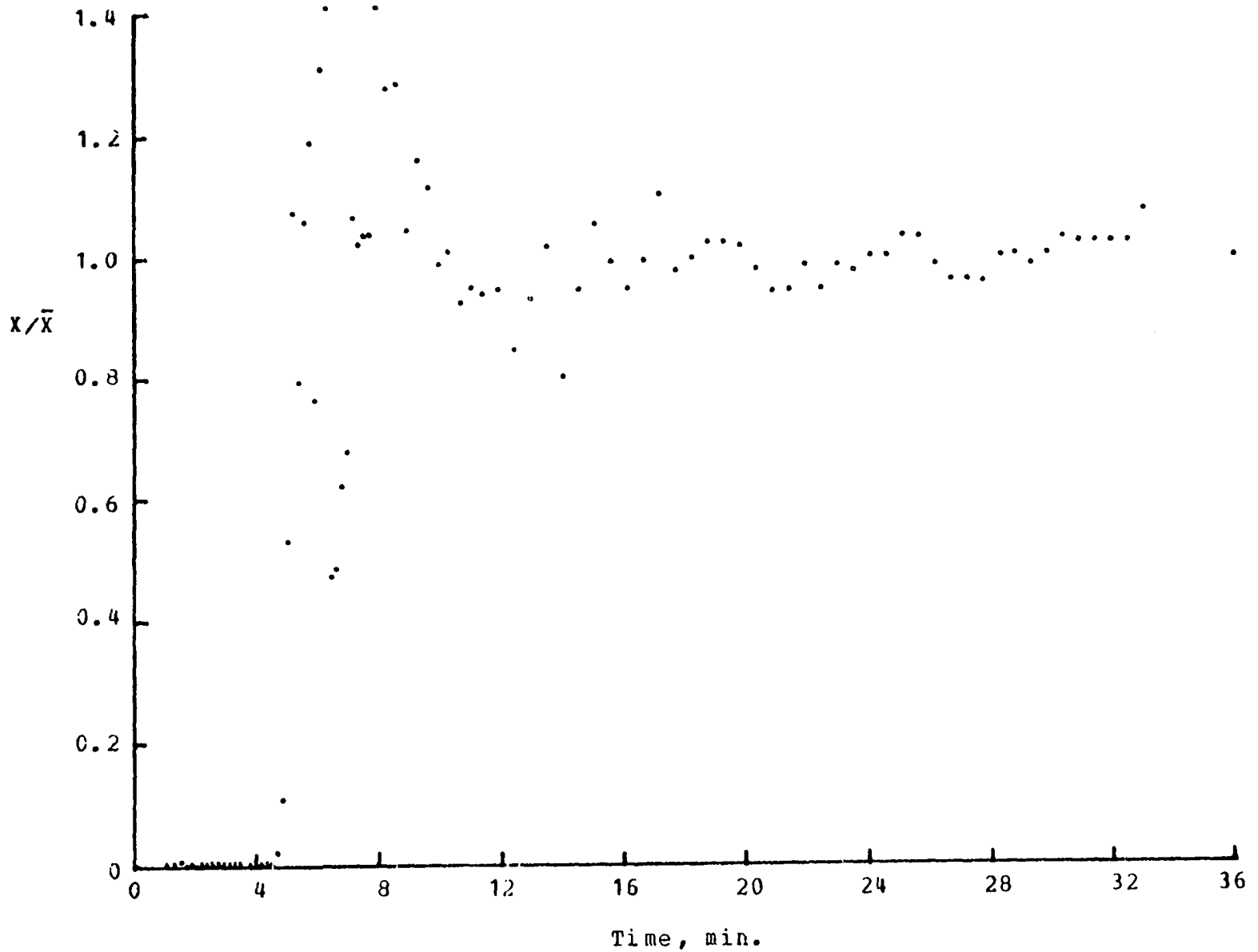
1.4
1.2
1.0
0.8
0.6
0.4
0.2
0
X/X̄
0
4
8
12
16
20
24
28
32
36
Time, min.

Figure 72. Mixing curve of Set 11, run 10

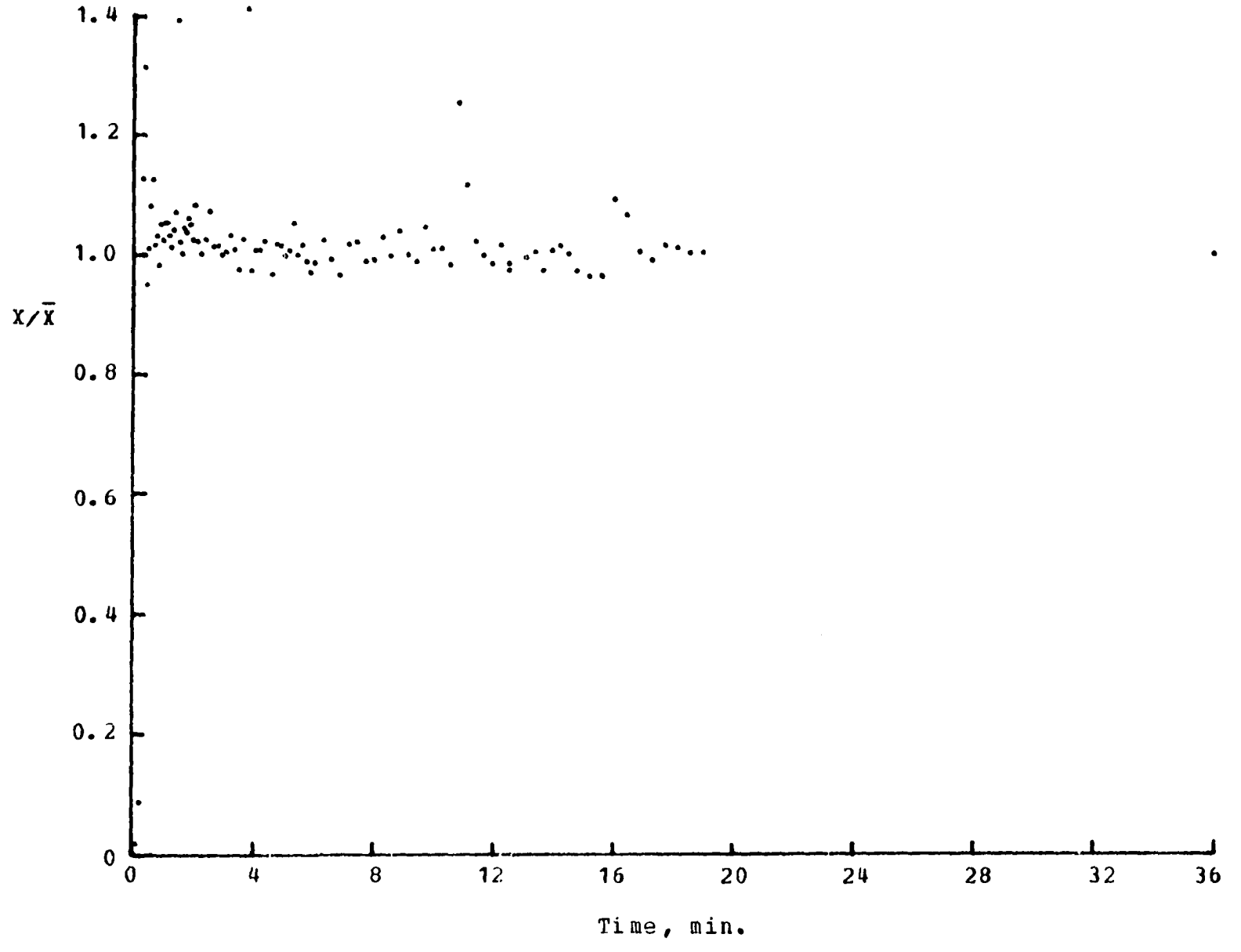
1.4
1.2
1.0
0.8
0.6
0.4
0.2
0
X/X̄
0
4
8
12
16
20
24
28
32
36
Time, min.

Figure 73. Mixing curve of Set 11, run 11

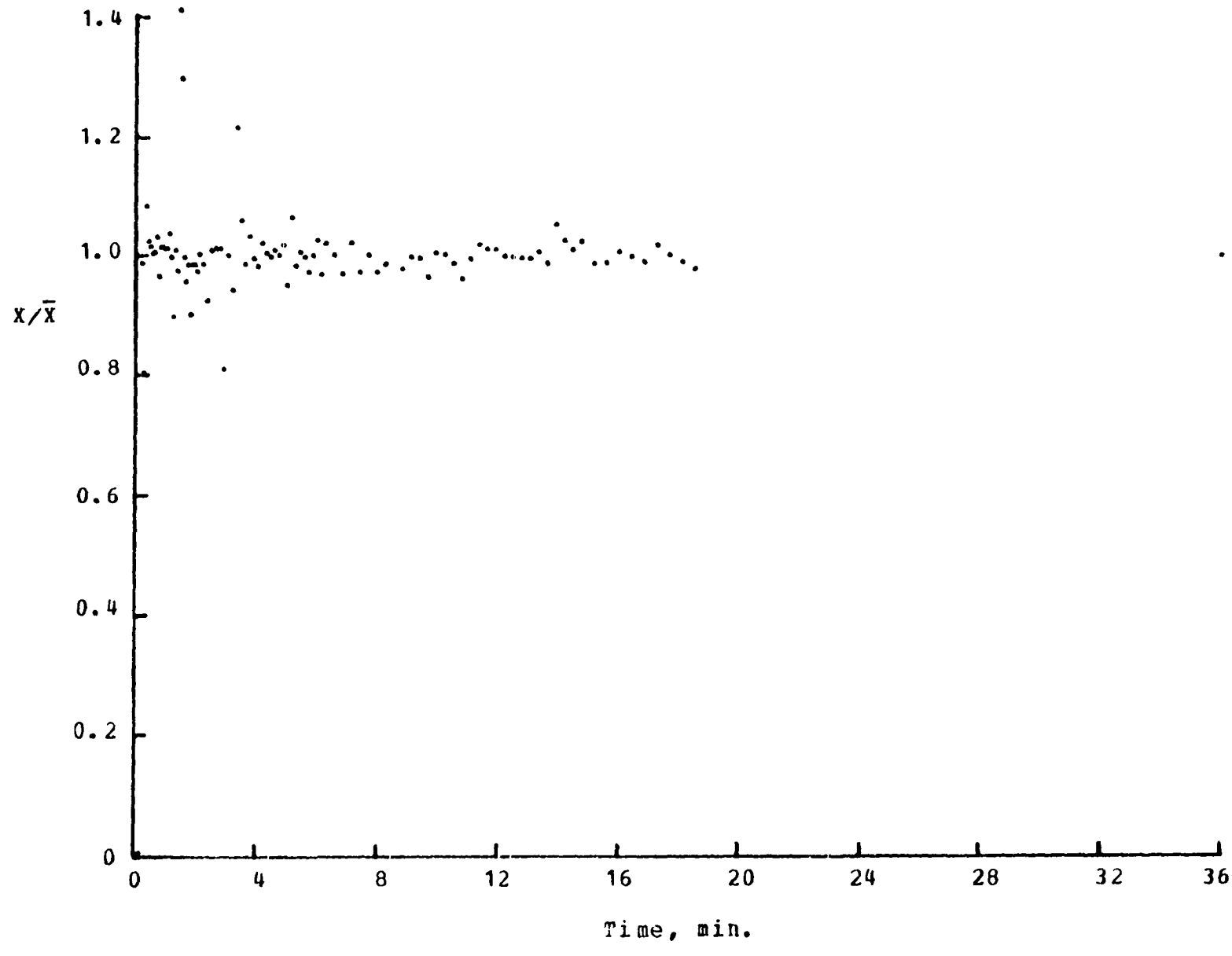
1.4
1.2
1.0
0.8
0.6
0.4
0.2
0
X/X̄
0
4
8
12
16
20
24
28
32
36
Time, min.

Figure 74. Mixing curve of Set 12, run 10

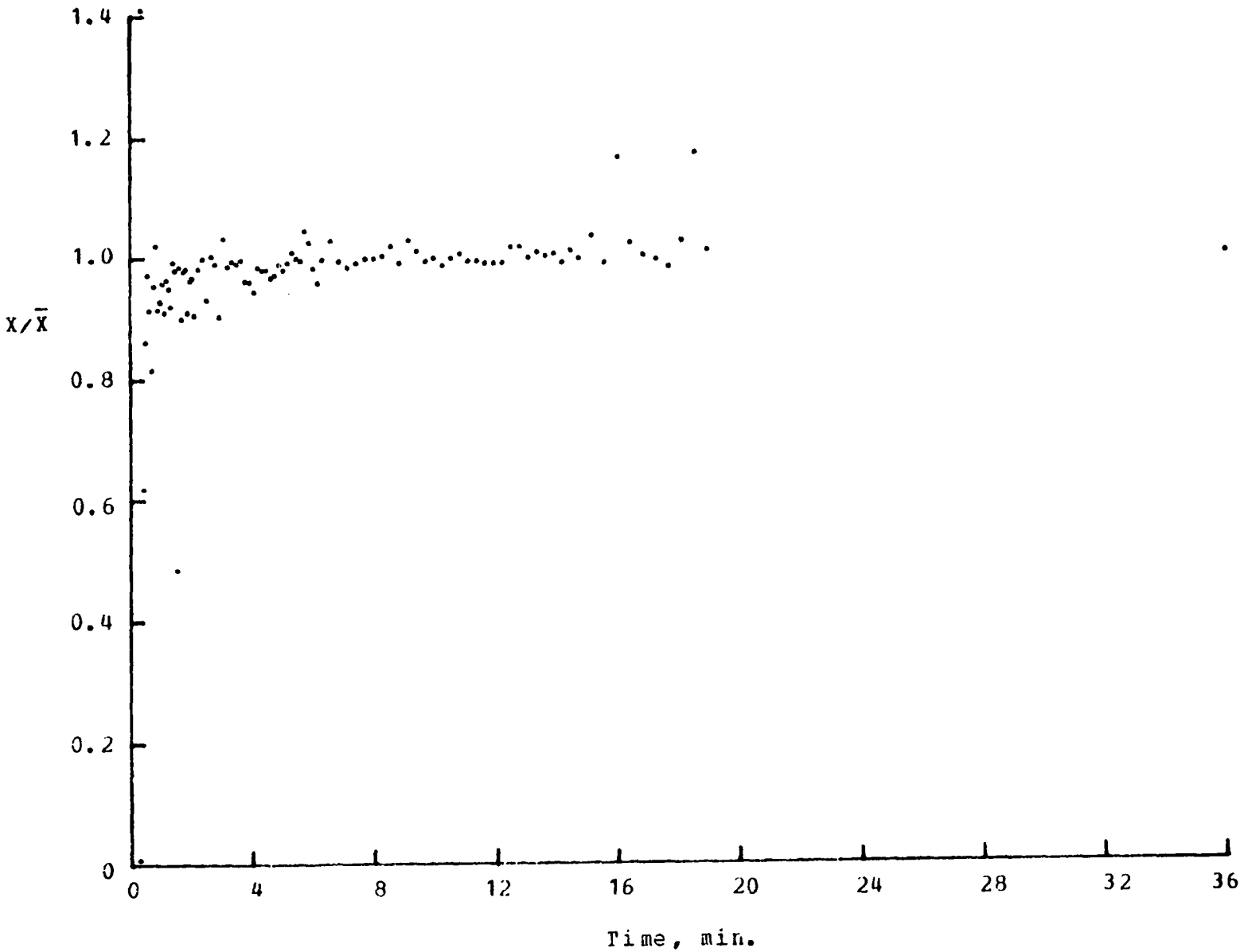
1.4
1.2
1.0
0.8
0.6
0.4
0.2
0
X/X̄
0
4
8
12
16
20
24
28
32
36
Time, min.

Figure 75. Mixing curve of Set 12, run 11

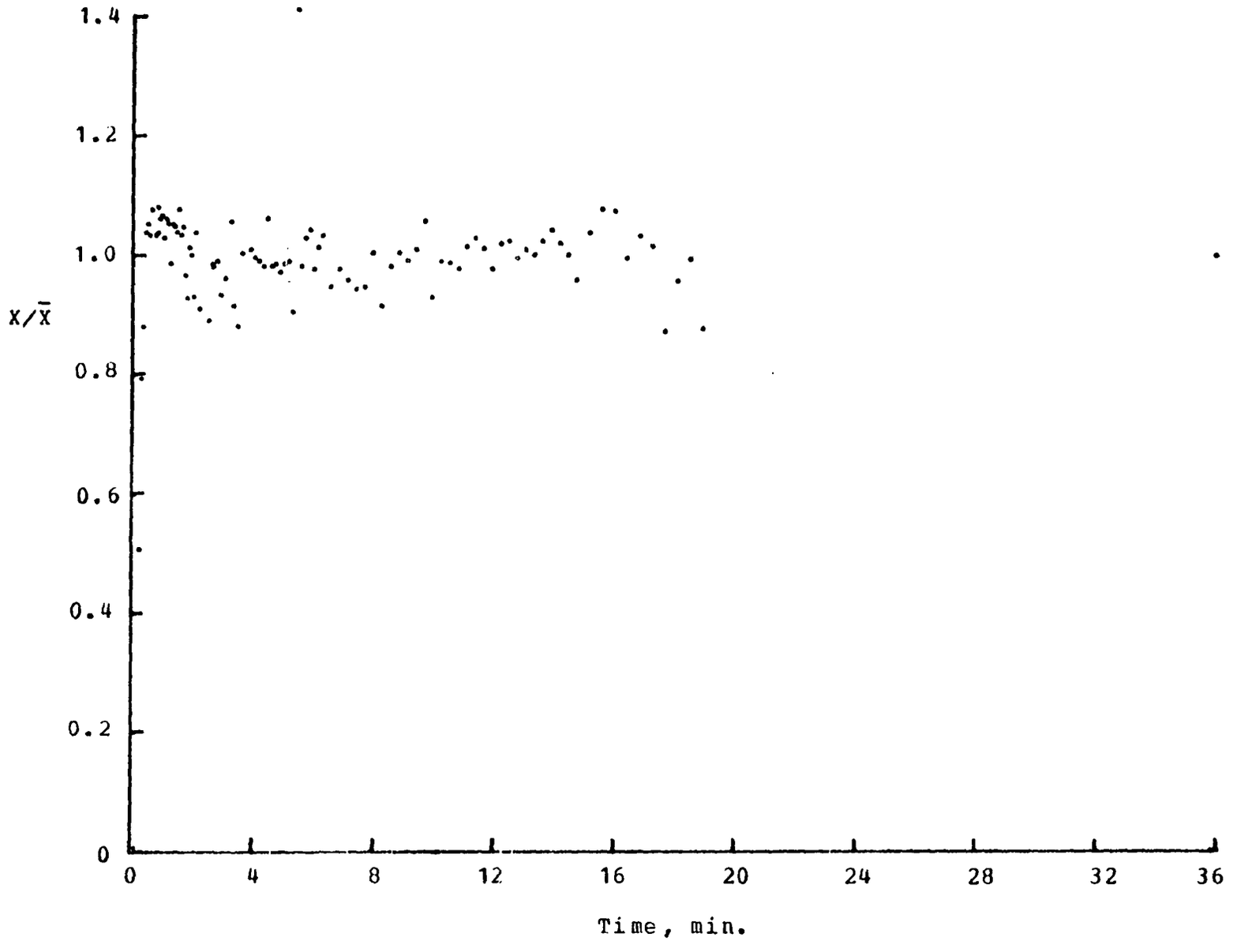
1.4
1.2
1.0
0.8
0.6
0.4
0.2
0
X/X̄
0
4
8
12
16
20
24
28
32
36
Time, min.

Figure 76. Mixing curve of Set 13, run 11

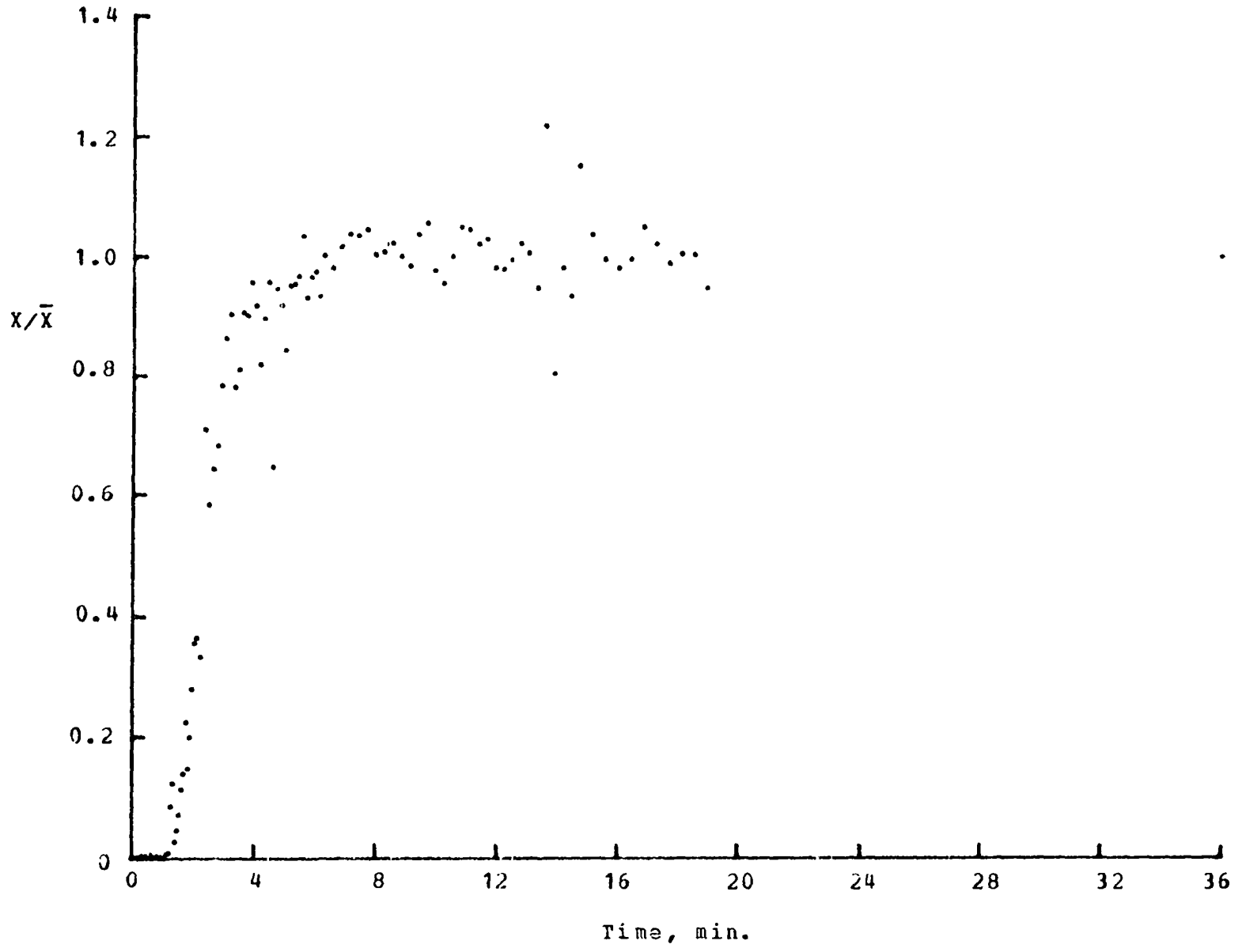
1.4
1.2
1.0
0.8
0.6
0.4
0.2
0
X/X̄
0
4
8
12
16
20
24
28
32
36
Time, min.

Figure 77. Mixing curve of Set 14, run 10

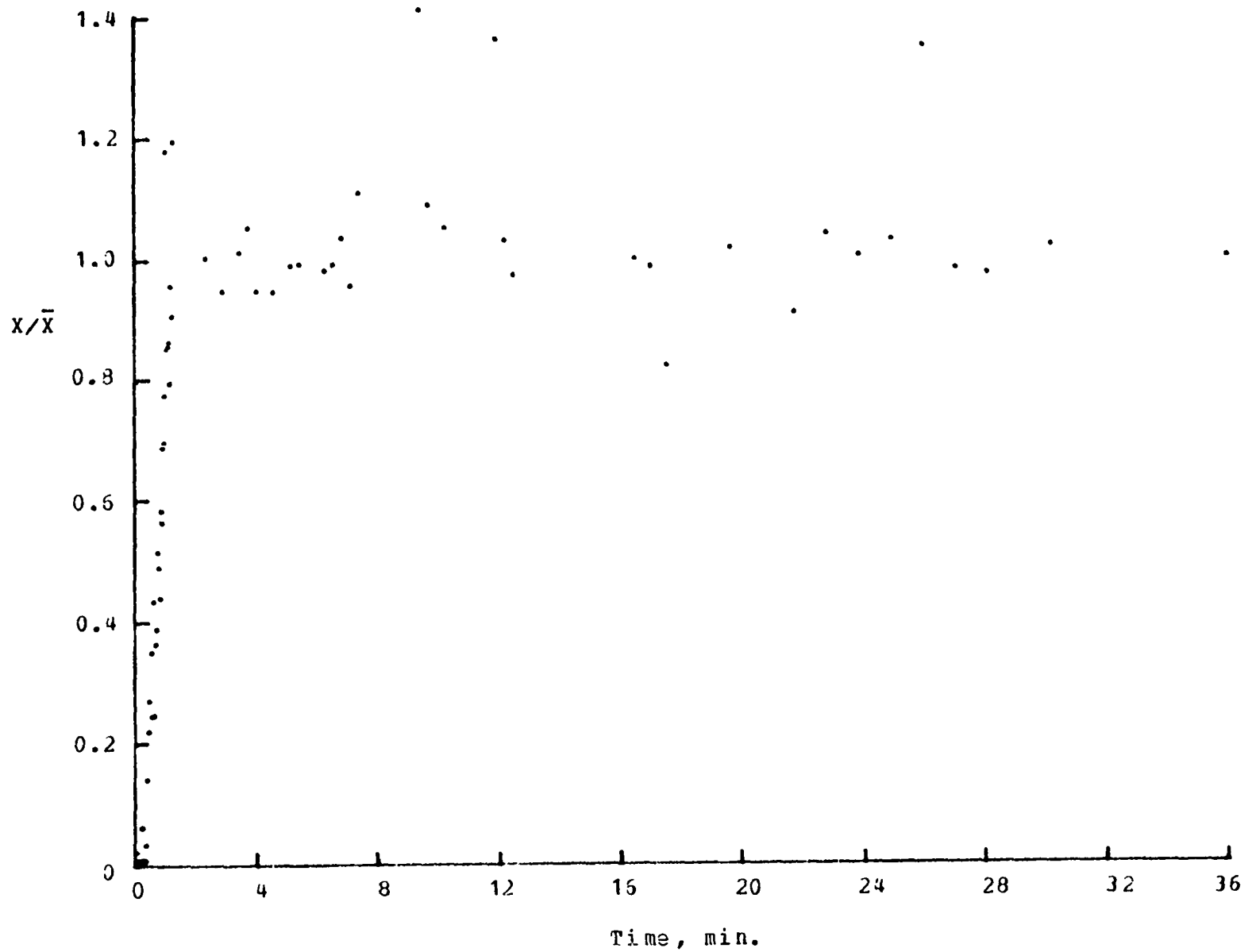
1.4
1.2
1.0
0.8
0.6
0.4
0.2
0
X/X̄
0
4
8
12
16
20
24
28
32
36
Time, min.

Table 23. Time required to inject tracer

Set, Run	Tracer	Time, sec.	Set, Run	Tracer	Time, sec.
3,13	Copper	<2.7	9,10	Copper	<5
11	Zinc	1.8	11	Zinc	-
12	Nickel	<3.9			
4,10	Copper	<3.5	10,10	Copper	2.8
11	Zinc	1.3	11	Zinc	1.8
12	Nickel	<3.9			
5,10	Copper	10	11,10	Copper	4.9
11	Zinc	<5	11	Zinc	<2
6,10	Copper	-	12,10	Copper	<2.7
11	Zinc	<3	11	Zinc	-
7,10	Copper	<5	13,10	Copper	5.1
11	Zinc	<5	11	Zinc	<3.1
8,10	Copper	3.3	14,10	Copper	
11	Zinc	<3.0			
			Average	Copper	<4.4
				Zinc	<2.9
				Nickel	<3.9

Table 24. Steady state flow sample concentration limits

Set, Run No.	t_M min.	Concentration limits mg. metal/g. Low	High	% of ave. Low	High
1,10	8.0	1.040	1.34	87	112
1,11	7.1	0.270	0.310	80	124
1,12	6.2	1.16	1.35	92	108
2,10	21.0	0.85	1.55	73	133
2,11	8.5	0.36	0.50	85	119
2,12	7.0	1.16	1.39	91	110
3,10	8.1	1.02	1.19	93	109
3,11	14.0	0.35	0.50	85	121
3,12	9.6	1.09	1.40	85	110
4,10	17.0	1.04	1.20	92	106
4,11	17.0	0.32	0.38	92	109
4,12	7.0	1.22	1.50	90	110
	10.0	1.25	1.44	92	106
5,10	6.7	1.03	1.14	94	104
5,11	8.5	0.315	0.35	95	106
6,10	7.1	1.08	1.18	95	104
6,11	6.5	0.32	0.355	94	105
7,10	5.1	1.11	1.20	95	103
	6.1	1.11	1.20	95	103
7,11	3.0	0.26	0.29	95	106
8,10	9.1	0.99	1.09	95	104
8,11	8.9	0.17	0.21	88	109
	20.0	0.28	0.325	93	108
9,10	13.8	0.925	1.03	95	106
9,11	8.6	0.27	0.31	92	106
10,10	8.9	0.79	0.94	91	109
10,11	10.0	0.25	0.29	94	109
11,10	2.6	0.105	0.115	95	104
11,11	3.6	0.32	0.35	94	103

Table 24. (Continued)

Set, Run No.	t_M min.	Concentration limits mg. metal/g. Low	High	% of ave. Low	High
12,10	3.0	0.70	0.78	94	105
12,11	1.5	0.182	0.225	87	108
	0.5	0.182	0.225	87	107
13,10	4.3	1.13	1.29	93	107
	6.5	1.13	1.25	94	104
13,11	5.1	0.35	0.40	92	106
	6.5	0.35	0.40	92	105
14,10	2.0	1.33	1.55	93	109

Table 25. Steady state settled bed concentrations, Set 5

Loc.	Dry weight g.	Copper mg/g.	Zinc mg/g.	Loc.	Dry weight g.	Copper mg/g.	Zinc mg/g.
A 1	1.0681	1.002	0.344	B 1	0.6287	1.001	0.329
A 2	1.0804	0.981	0.340	B 2	0.4348	0.989	0.476
A 3	1.0604	1.000	0.339	B 3	0.6024	1.046	0.345
A 4	0.7163	1.131	0.401	B 4	0.8386	1.031	0.344
A 5	0.8684	0.967	0.458	B 5	0.5241	0.973	0.321
A 6	1.2858	0.972	0.797	B 6	0.4230	0.969	0.324
A 7	0.9139	1.012	0.453	B 7	0.4360	0.998	0.328
A 8	1.0239	1.006	0.445	B 8	0.4737	0.982	0.325
A 9	0.8639	0.995	0.294	B 9	0.4398	1.000	0.325
A 10	0.8359	0.963	0.339	B 10	0.4396	0.978	0.330
A 11	0.8131	0.978	0.341	B 11	0.4723	1.016	0.320
C 1	0.7641	1.021	0.330	D 1	0.9853	0.984	0.328
C 2	0.6862	0.991	0.334	D 2	0.8971	1.031	0.342
C 3	0.7263	1.019	0.348	D 3	0.7473	-----	0.336
C 4	0.8741	1.018	0.349	D 4	0.9534	1.028	0.335
C 5	0.8459	0.999	0.335	D 5	0.6743	0.964	0.326
C 6	0.7067	0.990	0.321	D 6	0.4590	0.959	0.307
C 7	0.6944	1.015	0.341	D 7	0.6136	0.978	0.315
C 8	0.7054	1.007	0.335	D 8	0.7244	1.015	0.313
C 9	0.7735	1.021	0.348	D 9	0.8689	0.990	0.330
C 10	0.7803	1.025	0.329	D 10	0.6898	0.986	0.307
C 11	0.7683	0.989	0.314	D 11	0.7731	0.983	0.329
E 1	0.6232	1.155	0.327	F 1	0.6437	0.987	0.303
E 2	0.7243	1.008	0.324	F 2	0.7337	1.029	0.326
E 3	0.9358	1.015	0.338	F 3	0.7104	0.999	0.303
E 4	0.7477	1.016	0.325	F 4	0.6259	0.967	0.321
E 5	0.6745	1.038	0.319	F 5	0.6701	1.000	0.333
E 6	0.6588	0.987	0.317	F 6	0.6161	0.990	0.323
E 7	0.6578	1.019	0.318	F 7	0.6889	0.972	0.324
E 8	0.6777	1.011	0.329	F 8	0.7295	0.994	0.308
E 9	0.7442	1.001	0.329	F 9	0.7013	1.034	0.349
E 10	0.6865	1.034	0.328	F 10	0.8435	0.487	0.129
E 11	0.7589	0.975	0.310	F 11	0.7689	1.001	0.334
				F 12	0.7519	1.024	0.329

Table 26. Steady state settled bed concentrations, Set 6

Loc.	Dry weight g.	Copper mg/g.	Zinc mg/g.	Loc.	Dry weight g.	Copper mg/g.	Zinc mg/g.
A 1	0.7093	0.942	-----	B 1	0.6397	0.950	0.377
A 2	0.5181	0.971	0.324	B 2	0.8447	0.980	0.386
A 3	0.5147	0.971	0.356	B 3	0.7765	1.008	0.343
A 4	0.4332	0.958	0.298	B 4	0.7760	0.978	0.329
A 5	0.5472	1.044	0.323	B 5	0.7649	0.974	0.367
A 6	0.5293	1.052	0.332	B 6	0.8242	0.962	0.341
A 7	0.6809	0.977	0.354	B 7	0.7685	0.941	0.318
A 8	0.6090	0.921	0.396	B 8	0.7087	0.981	0.349
A 9	0.6114	0.973	0.348	B 9	0.8040	0.995	0.340
A 10	0.5312	0.962	0.339	B 10	0.7947	0.956	0.337
A 11	0.6203	0.967	0.385	B 11	0.8191	0.972	0.338
C 1	0.6248	0.960	0.318	D 1	0.6825	0.971	0.362
C 2	0.9265	0.995	0.343	D 2	0.9077	0.973	0.380
C 3	0.6258	0.967	0.324	D 3	0.8345	1.027	0.364
C 4	0.6070	0.972	0.376	D 4	0.6808	0.999	0.323
C 5	0.7763	0.966	0.326	D 5	0.7647	0.994	0.339
C 6	0.7496	0.941	0.338	D 6	0.7389	0.968	0.332
C 7	0.7794	1.453	0.323	D 7	0.7266	0.984	0.333
C 8	0.6690	0.954	0.335	D 8	0.6841	1.006	0.348
C 9	0.6455	1.015	0.349	D 9	0.6842	0.998	0.332
C 10	0.8648	0.853	0.346	D 10	0.6786	0.958	0.332
C 11	0.7541	0.963	0.369	D 11	0.9345	0.979	0.325
E 1	0.6879	0.938	0.317	F 1	0.7507	0.935	0.318
E 2	0.6848	0.971	0.329	F 2	0.8283	1.044	0.339
E 3	0.6780	1.003	0.326	F 3	0.9355	1.023	0.236
E 4	0.7065	0.994	0.341	F 4	0.7791	0.898	0.326
E 5	0.7046	1.019	0.345	F 5	0.6643	0.994	0.328
E 6	0.9261	0.991	0.257	F 6	0.6893	1.008	0.321
E 7	0.6594	0.990	0.328	F 7	0.7153	0.896	0.331
E 8	0.8122	0.967	0.335	F 8	0.6937	0.995	0.350
E 9	0.7244	1.040	0.351	F 9	0.7487	0.982	0.395
E 10	0.6671	0.986	0.331	F 10	0.7651	1.026	0.340
E 11	0.9914	0.978	0.218	F 11	0.6578	1.003	0.341
				F 12	0.6630	0.977	0.318

Table 27. Steady state settled bed concentrations, Set 7

Loc.	Dry weight g.	Copper mg/g.	Zinc mg/g.	Loc.	Dry weight g.	Copper mg/g.	Zinc mg/g.
D 1	0.6806	0.970	0.287	E 1	0.6947	0.979	0.285
D 2	0.6563	0.975	0.302	E 2	0.7701	0.965	0.287
D 3	0.7203	0.951	0.287	E 3	0.8012	0.965	0.285
D 4	0.6008	0.979	0.288	E 4	0.7092	1.005	0.295
D 5	0.7871	0.991	0.293	E 5	0.7711	0.986	0.290
D 6	0.5384	0.979	0.280	E 6	0.8078	0.978	0.291
D 7	0.7081	0.982	0.297	E 7	0.8012	0.826	0.287
D 8	1.1049	1.027	0.322	E 8	0.8172	0.985	0.289
D 9	0.6397	0.974	0.288	E 9	0.8120	1.006	0.296
D 10	0.5682	0.938	0.271	E 10	0.6867	0.973	0.287
D 11	0.8594	0.972	0.289	E 11	0.7749	0.972	0.280
F 1	1.1339	0.975	0.281				
F 2	0.7759	1.053	0.305				
F 3	0.8200	1.009	0.306				
F 4	0.7756	0.873	0.239				
F 5	0.9446	0.990	0.293				
F 6	1.0452	1.005	0.300				
F 7	0.7152	0.955	0.246				
F 8	0.7126	1.001	0.288				
F 9	0.9502	1.000	0.304				
F 10	0.8407	0.946	0.289				
F 11	0.7972	0.978	0.294				
F 12	0.8744	0.981	0.286				

Table 28. Steady state settled bed concentrations, Set 8

Loc.	Dry weight g.	Copper mg/g.	Zinc mg/g.	Loc.	Dry weight g.	Copper mg/g.	Zinc mg/g.
A 1	0.9198	0.973	0.320	B 1	0.7929	0.984	0.315
A 2	0.9525	1.018	0.329	B 2	0.9314	0.999	0.312
A 3	1.0656	0.993	0.337	B 3	0.8105	1.018	0.329
A 4	1.1280	0.924	0.369	B 4	0.6922	0.982	0.309
A 5	0.7715	0.959	0.324	B 5	0.7410	0.999	0.337
A 6	1.1137	0.961	0.364	B 6	0.7699	0.994	0.309
A 7	0.6600	0.985	0.538	B 7	0.7225	0.941	0.293
A 8	0.7176	0.955	0.371	B 8	0.9730	0.987	0.308
A 9	0.7873	0.981	0.310	B 9	0.8560	0.993	0.320
A 10	0.9474	0.929	0.287	B 10	0.7205	0.985	0.312
A 11	0.7525	0.917	0.266	B 11	0.8803	1.011	0.307
C 1	0.8703	0.977	0.310	D 1	0.8365	0.992	0.314
C 2	1.0970	0.994	0.320	D 2	0.7240	1.036	0.339
C 3	0.8025	1.003	0.315	D 3	0.9139	1.056	0.337
C 4	0.8161	1.017	0.316	D 4	0.7223	1.011	0.329
C 5	0.7612	0.972	0.303	D 5	0.8767	0.987	0.307
C 6	1.0036	0.976	0.311	D 6	0.9195	0.992	0.304
C 7	1.1168	0.989	0.317	D 7	0.9159	1.010	0.325
C 8	0.9925	0.982	0.309	D 8	1.0880	1.002	0.317
C 9	0.8322	1.027	0.317	D 9	0.7020	0.755	0.323
C 10	0.8082	0.959	0.306	D 10	0.7576	1.016	0.318
C 11	0.9377	0.949	0.293	D 11	1.0210	0.882	0.273
E 1	0.6893	0.986	0.310	F 1	0.9481	0.962	0.294
E 2	0.7973	1.010	0.330	F 2	0.9091	1.045	0.330
E 3	0.7837	1.021	0.333	F 3	0.9576	1.055	0.345
E 4	0.9003	0.994	0.320	F 4	0.8909	0.909	0.284
E 5	0.6909	0.999	0.310	F 5	0.8141	1.007	0.322
E 6	0.9824	1.008	0.361	F 6	0.8393	1.031	0.322
E 7	0.7636	1.022	0.316	F 7	0.8930	1.008	0.319
E 8	1.0328	1.051	0.332	F 8	0.9629	1.018	0.322
E 9	0.8505	1.058	0.329	F 9	0.8099	1.056	0.332
E 10	0.8551	1.000	0.315	F 10	0.8809	1.010	0.324
E 11	1.0320	0.916	0.377	F 11	0.8406	1.053	0.332
				F 12	0.9897	1.051	0.334

Table 29. Steady state settled bed concentrations, Set 9

Loc.	Dry weight g.	Copper mg/g.	Zinc mg/g.	Loc.	Dry weight g.	Copper mg/g.	Zinc mg/g.
A 1	0.9438	0.832	0.281	B 1	0.9687	0.934	0.284
A 2	0.7824	0.828	0.265	B 2	0.7988	1.017	0.299
A 3	0.8299	0.898	0.309	B 3	0.7262	1.030	0.307
A 4	1.0385	0.886	0.278	B 4	0.6412	1.053	0.299
A 5	0.9723	0.799	0.251	B 5	0.9193	0.968	0.293
A 6	1.0377	0.763	0.261	B 6	0.9138	0.873	0.266
A 7	0.7711	0.875	0.318	B 7	0.7717	0.985	0.283
A 8	0.7103	0.788	0.291	B 8	0.7552	1.000	0.295
A 9	0.9481	0.939	0.291	B 9	0.7903	1.025	0.299
A 10	0.7807	0.798	0.245	B 10	0.7794	1.007	0.294
A 11	0.9225	0.732	0.242	B 11	0.9629	0.909	0.268
A 12	0.8404	0.898	0.290	B 12	0.6527	1.026	0.446
C 1	0.7584	0.956	0.281	D 1	0.7606	1.012	0.304
C 2	0.7619	0.984	0.293	D 2	0.8938	0.996	0.292
C 3	0.9042	1.023	0.299	D 3	0.8542	1.040	0.317
C 4	0.7215	1.037	0.306	D 4	0.8246	0.997	0.291
C 5	0.8453	0.952	0.283	D 5	0.7546	0.994	0.293
C 6	0.9420	0.894	0.275	D 6	0.9401	0.928	0.269
C 7	0.8817	0.927	0.278	D 7	0.8871	0.937	0.281
C 8	1.0189	0.991	0.291	D 8	0.8770	0.994	0.285
C 9	0.8394	1.015	0.291	D 9	0.9523	1.021	0.301
C 10	0.8527	0.979	0.285	D 10	0.8201	0.936	0.280
C 11	0.8754	0.928	0.265	D 11	0.9096	0.920	0.268
C 12	0.6074	1.008	0.293	D 12	0.8526	1.015	0.292
E 1	0.8304	0.891	0.261	F 1	0.9181	0.884	0.260
E 2	0.8445	0.961	0.282	F 2	0.8378	1.083	0.315
E 3	0.8854	1.005	0.295	F 3	0.7998	1.019	0.304
E 4	0.8294	0.985	0.283	F 4	0.8691	0.874	0.262
E 5	0.7747	0.955	0.266	F 5	0.9171	1.036	0.306
E 6	0.9305	0.878	0.267	F 6	0.7820	1.049	0.306
E 7	0.8469	0.909	0.273	F 7	0.7478	0.923	0.266
E 8	0.8279	0.978	0.280	F 8	0.8923	1.009	0.290
E 9	0.9455	1.047	0.307	F 9	0.7177	1.017	0.291
E 10	0.8165	0.958	0.274	F 10	0.8476	0.956	0.271
E 11	0.8182	0.911	0.265	F 11	0.8028	1.009	0.299
E 12	0.8232	1.030	0.311	F 12	0.7891	1.077	0.321

Table 30. Steady state settled bed concentrations, Set 10

Loc.	Dry weight g.	Copper mg/g.	Zinc mg/g.	Loc.	Dry weight g.	Copper mg/g.	Zinc mg/g.
A 1	0.8652	0.795	0.286	B 1	0.7097	0.930	0.286
A 2	0.6926	0.881	0.271	B 2	0.6772	0.957	0.291
A 3	0.8470	0.694	0.243	B 3	0.8619	1.058	0.328
A 4	0.8218	0.797	0.293	B 4	0.7565	0.964	0.305
A 5	0.8498	0.788	0.547	B 5	0.7122	0.910	0.274
A 6	0.9510	0.778	0.647	B 6	0.9065	0.737	0.221
A 7	0.9247	0.831	0.397	B 7	0.9364	0.844	0.264
A 8	0.8460	0.874	0.288	B 8	1.0051	0.955	0.303
A 9	0.9836	0.819	0.418	B 9	0.7427	0.959	0.295
A 10	0.9186	0.814	0.386	B 10	0.6942	1.073	0.313
A 11	0.8226	0.805	0.283	B 11	1.0054	0.798	0.241
A 12	0.7568	0.901	0.311	B 12	0.8029	1.000	0.378
C 1	0.8258	0.930	0.286	D 1	0.7483	0.866	0.261
C 2	0.7595	0.948	0.284	D 2	0.8346	0.899	0.282
C 3	0.8630	0.994	0.300	D 3	0.7463	0.951	0.297
C 4	0.9235	0.966	0.303	D 4	0.8637	0.981	0.296
C 5	0.7740	0.969	0.287	D 5	0.7654	0.915	0.280
C 6	0.9653	0.860	0.257	D 6	0.9489	0.833	0.244
C 7	0.8253	0.906	0.278	D 7	0.9937	0.886	0.273
C 8	0.8252	0.935	0.285	D 8	0.9245	0.935	0.293
C 9	0.9531	0.950	0.292	D 9	0.7866	0.973	0.300
C 10	0.7808	0.899	0.269	D 10	0.8489	0.907	0.284
C 11	0.8706	0.824	0.257	D 11	0.9848	1.011	0.296
C 12	0.8285	0.978	0.293	D 12	0.7202	1.011	0.296
E 1	0.8266	0.926	0.284	F 1	0.8680	0.783	0.238
E 2	0.8452	0.988	0.288	F 2	0.9953	0.944	0.286
E 3	0.8459	1.005	0.305	F 3	0.8820	0.907	0.287
E 4	0.9726	0.967	0.296	F 4	0.8579	0.814	0.259
E 5	0.8502	0.915	0.285	F 5	0.8342	0.929	0.289
E 6	0.9470	0.850	0.325	F 6	0.7262	0.968	0.299
E 7	0.9638	0.884	0.275	F 7	0.9565	0.953	0.268
E 8	0.9747	0.971	0.299	F 8	0.9722	0.987	0.301
E 9	0.8810	0.944	0.293	F 9	0.7580	0.855	0.270
E 10	0.8812	0.933	0.280	F 10	0.7401	0.959	0.289
E 11	0.9748	0.726	0.231	F 11	0.8498	0.930	0.286
E 12	0.8237	0.987	0.300	F 12	0.9397	0.867	0.275

Table 31. Steady state settled bed concentrations, Set 11

Loc.	Dry weight g.	Copper mg/g.	Zinc mg/g.	Loc.	Dry weight g.	Copper mg/g.	Zinc mg/g.
A 1	0.8658	0.953	0.337	B 1	0.8980	1.013	0.354
A 2	0.7812	0.963	0.380	B 2	0.8577	0.997	0.343
A 3	0.8668	1.079	0.442	B 3	0.8440	0.978	0.332
A 4	0.9382	1.010	0.404	B 4	0.8794	0.984	0.346
A 5	0.7595	0.945	0.334	B 5	0.8094	0.988	0.340
A 6	0.8784	0.854	0.268	B 6	0.8986	0.958	0.286
A 7	0.9055	0.922	0.378	B 7	0.7578	1.025	0.350
A 8	0.7291	0.967	0.421	B 8	0.8507	1.002	0.357
A 9	0.8839	0.953	0.353	B 9	0.8093	0.991	0.345
A 10	0.7671	0.948	0.340	B 10	0.7309	1.013	0.342
A 11	0.8466	0.874	0.309	B 11	0.8743	0.984	0.342
A 12	0.8567	0.946	0.357	B 12	0.7741	1.008	0.348
C 1	0.8644	0.966	0.344	D 1	0.7101	0.986	0.332
C 2	0.8830	0.985	0.341	D 2	0.7840	0.995	0.342
C 3	0.8691	0.969	0.350	D 3	0.8309	0.993	0.350
C 4	0.7294	0.987	0.340	D 4	0.7522	0.984	0.347
C 5	0.8579	0.993	0.339	D 5	0.7918	1.017	0.350
C 6	0.7896	0.899	0.339	D 6	0.8834	0.985	0.345
C 7	0.8739	0.984	0.344	D 7	0.8815	1.001	0.345
C 8	0.8568	0.980	0.340	D 8	0.7896	0.978	0.346
C 9	0.8093	1.003	0.346	D 9	0.7720	1.000	0.341
C 10	0.8124	1.003	0.350	D 10	0.8503	0.914	0.305
C 11	0.8616	0.940	0.293	D 11	0.8871	0.510	0.254
C 12	0.7919	1.006	0.357	D 12	0.8554	0.970	0.327
E 1	0.8909	1.018	0.367	F 1	0.8892	0.939	0.318
E 2	0.8319	0.998	0.350	F 2	0.8523	0.974	0.339
E 3	0.8894	1.003	0.344	F 3	0.8656	0.984	0.354
E 4	0.7388	0.975	0.344	F 4	0.8755	0.865	0.289
E 5	0.7332	1.009	0.348	F 5	0.7277	1.003	0.347
E 6	0.8051	0.863	0.324	F 6	0.8204	0.993	0.345
E 7	0.7924	1.010	0.351	F 7	0.8722	0.963	0.334
E 8	0.8273	1.009	0.313	F 8	0.8282	0.990	0.338
E 9	0.8734	1.004	0.348	F 9	0.8415	0.998	0.346
E 10	0.8126	1.003	0.348	F 10	0.8821	1.006	0.345
E 11	0.8750	0.928	0.139	F 11	0.8122	1.003	0.342
E 12	0.7767	1.024	0.341	F 12	0.7963	0.986	0.345

Table 32. Steady state settled bed concentrations, Set 12

Loc.	Dry weight g.	Copper mg/g.	Zinc mg/g.	Loc.	Dry weight g.	Copper mg/g.	Zinc mg/g.
A 1	1.0182	0.608	0.208	B 1	1.0110	0.625	0.199
A 2	0.9871	0.617	0.203	B 2	1.0166	0.618	0.201
A 3	1.0061	0.615	0.206	B 3	1.0188	0.620	0.202
A 4	1.0177	0.614	0.200	B 4	1.0183	0.621	0.206
A 5	1.0147	0.610	0.198	B 5	1.0189	0.623	0.202
A 6	0.9658	0.619	0.192	B 6	1.0185	0.621	0.200
A 7	1.0179	0.629	0.200	B 7	1.0199	0.628	0.195
A 8	0.9949	0.631	0.204	B 8	1.0179	0.608	0.211
A 9	0.9890	0.616	0.200	B 9	1.0173	0.621	0.196
A 10	1.0096	0.613	0.186	B 10	1.0117	0.621	0.197
A 11	1.0122	0.612	0.201	B 11	1.0185	0.628	0.194
A 12	1.0220	0.606	0.205	B 12	1.0188	0.618	0.203
C 1	1.0170	0.621	0.195	D 1	1.0169	0.629	0.200
C 2	1.0129	0.612	0.191	D 2	1.0159	0.615	0.205
C 3	1.0146	0.603	0.201	D 3	1.0181	0.617	0.195
C 4	1.0173	0.617	0.203	D 4	1.0167	0.625	0.200
C 5	1.0174	0.611	0.200	D 5	1.0187	0.610	0.195
C 6	1.0171	0.621	0.184	D 6	1.0139	0.619	0.190
C 7	1.0183	0.629	0.200	D 7	1.0184	0.638	0.202
C 8	1.0196	0.628	0.201	D 8	1.0187	0.620	0.197
C 9	1.0141	0.619	0.203	D 9	1.0189	0.620	0.201
C 10	1.0197	0.623	0.202	D 10	1.0185	0.619	0.203
C 11	1.0162	0.622	0.110	D 11	1.0163	0.630	0.198
C 12	0.9794	0.616	0.199	D 12	1.0190	0.628	0.204
E 1	1.0180	0.608	0.196	F 1	1.0180	0.621	0.190
E 2	1.0177	0.614	0.103	F 2	1.0169	0.621	0.196
E 3	1.0170	0.617	0.195	F 3	1.0181	0.621	0.197
E 4	1.0177	0.629	0.200	F 4	1.0166	0.580	0.184
E 5	1.0182	0.611	0.192	F 5	1.0168	0.609	0.196
E 6	1.0134	0.618	0.104	F 6	1.0174	0.629	0.202
E 7	1.0175	0.610	0.192	F 7	1.0159	0.591	0.196
E 8	1.0182	0.614	0.197	F 8	1.0172	0.629	0.207
E 9	1.0180	0.640	0.208	F 9	1.0173	0.624	0.203
E 10	1.0183	0.599	0.191	F 10	1.0179	0.648	0.168
E 11	1.0179	0.656	0.024	F 11	1.0190	0.623	0.103
E 12	1.0181	0.624	0.199	F 12	1.0174	0.621	0.198

Table 33. Steady state settled bed concentrations, Set 13

Loc.	Dry weight g.	Copper mg/g.	Zinc mg/g.	Loc.	Dry weight g.	Copper mg/g.	Zinc mg/g.
A 1	0.8842	0.910	0.292	B 1	0.8683	0.946	0.308
A 2	0.8832	0.919	0.296	B 2	0.8696	0.932	0.321
A 3	0.8868	0.949	0.319	B 3	0.8573	0.941	0.321
A 4	0.8752	0.928	0.313	B 4	0.8689	0.972	0.328
A 5	0.8767	0.924	0.283	B 5	0.8719	0.952	0.326
A 6	0.8704	0.896	0.285	B 6	0.8850	0.944	0.324
A 7	0.8924	0.897	0.288	B 7	0.8774	0.963	0.324
A 8	0.8350	0.915	0.294	B 8	0.8314	0.956	0.316
A 9	0.9030	0.936	0.327	B 9	0.8686	0.973	0.332
A 10	0.8910	0.847	0.284	B 10	0.8701	0.948	0.326
A 11	0.9099	0.769	0.252	B 11	0.8766	0.947	0.316
A 12	0.8746	0.946	0.308	B 12	0.8298	0.968	0.335
C 1	0.8777	0.942	0.321	D 1	0.8779	0.951	0.322
C 2	0.8742	0.976	0.332	D 2	0.8792	0.967	0.328
C 3	0.8758	0.953	0.332	D 3	0.8793	0.978	0.336
C 4	0.8688	0.961	0.323	D 4	0.8766	0.989	0.357
C 5	0.8569	0.974	0.338	D 5	0.8789	0.967	0.323
C 6	0.8611	0.935	0.312	D 6	0.8767	0.935	0.323
C 7	0.8749	0.991	0.330	D 7	0.8786	0.945	0.322
C 8	0.8784	0.981	0.328	D 8	0.8789	0.961	0.336
C 9	0.8776	0.963	0.335	D 9	0.8775	0.969	0.334
C 10	0.8635	0.975	0.338	D 10	0.8778	0.940	0.328
C 11	0.8777	0.843	0.235	D 11	0.8791	0.958	0.261
C 12	0.8788	0.962	0.333	D 12	0.8770	0.964	0.331
E 1	0.8810	0.916	0.320	F 1	0.8794	0.915	0.301
E 2	0.8814	0.947	0.331	F 2	0.8791	0.986	0.352
E 3	0.8804	0.954	0.333	F 3	0.8787	0.956	0.332
E 4	0.8811	0.942	0.331	F 4	0.8790	0.958	0.328
E 5	0.8801	0.971	0.327	F 5	0.8792	0.978	0.350
E 6	0.8800	0.932	0.297	F 6	0.8800	0.977	0.351
E 7	0.8817	0.927	0.323	F 7	0.8780	1.031	0.351
E 8	0.8813	0.953	0.333	F 8	0.8786	0.981	0.343
E 9	0.8794	0.949	0.330	F 9	0.8786	0.987	0.340
E 10	0.8813	0.936	0.323	F 10	0.8797	0.989	0.347
E 11	0.8819	0.938	0.233	F 11	0.8789	0.973	0.342
E 12	0.8820	0.933	0.333	F 12	0.8795	0.938	0.332

Table 34. Summary of settled bed samples by elevation

Set	Elev.	Copper n	Copper Conc., mg./g. ave.	Copper S	Zinc n	Zinc Conc., mg./g. ave.	Zinc S
5	A	11	1.000	0.046	11	0.414	0.139
	B	11	0.998	0.024	11	0.342	0.045
	C	11	1.008	0.014	11	0.335	0.011
	D	10	0.992	0.025	11	0.324	0.012
	E	11	1.024	0.047	11	0.324	0.008
	F	12	0.957	0.149	12	0.307	0.058
6	A	11	0.976	0.039	10	0.346	0.029
	B	11	0.972	0.020	11	0.348	0.021
	C	11	1.004	0.154	11	0.341	0.019
	D	11	0.987	0.028	11	0.343	0.018
	E	11	0.989	0.027	11	0.316	0.041
	F	12	0.982	0.048	12	0.329	0.035
7	D	11	0.976	0.022	11	0.291	0.013
	E	11	0.967	0.049	11	0.288	0.005
	F	12	0.981	0.044	12	0.286	0.022
8	A	11	0.963	0.031	11	0.347	0.071
	B	11	0.990	0.020	11	0.314	0.012
	C	11	0.986	0.023	11	0.311	0.008
	D	11	0.978	0.058	11	0.317	0.018
	E	11	1.006	0.037	11	0.330	0.022
	F	12	1.017	0.044	12	0.322	0.017
9	A	12	0.836	0.063	12	0.277	0.024
	B	12	0.986	0.055	12	0.302	0.047
	C	12	0.975	0.044	12	0.287	0.011
	D	12	0.983	0.041	12	0.289	0.014
	E	12	0.959	0.054	12	0.280	0.016
	F	12	0.995	0.070	12	0.291	0.021
10	A	12	0.815	0.055	12	0.364	0.123
	B	12	0.932	0.099	12	0.292	0.041
	C	12	0.930	0.050	12	0.283	0.015
	D	12	0.931	0.057	12	0.284	0.017
	E	12	0.925	0.077	12	0.288	0.022
	F	12	0.908	0.064	12	0.279	0.018

Table 34. (Continued)

Set	Elev.	Copper n	Copper Conc., mg./g. ave.	Copper S	Zinc n	Zinc Conc., mg./g. ave.	Zinc S
11	A	12	0.951	0.058	12	0.360	0.048
	B	12	0.995	0.018	12	0.340	0.018
	C	12	0.976	0.031	12	0.340	0.016
	D	12	0.944	0.139	12	0.332	0.028
	E	12	0.987	0.046	12	0.326	0.061
	F	12	0.975	0.040	12	0.337	0.017
12	A	12	0.616	0.008	12	0.200	0.006
	B	12	0.621	0.005	12	0.201	0.005
	C	12	0.619	0.007	12	0.191	0.026
	D	12	0.623	0.008	12	0.199	0.004
	E	12	0.620	0.016	12	0.167	0.058
	F	12	0.618	0.018	12	0.187	0.028
13	A	12	0.903	0.050	12	0.295	0.020
	B	12	0.954	0.013	12	0.323	0.007
	C	12	0.955	0.039	12	0.321	0.028
	D	12	0.960	0.016	12	0.325	0.022
	E	12	0.942	0.015	12	0.317	0.029
	F	12	0.972	0.029	12	0.339	0.015

APPENDIX D. STATISTICAL TESTS

Statistical Techniques

The structure of the experimental design (see General Plan and the Results and Discussion of the residence time experiments) and the nature of the data collected required analyzing the data using several different techniques. The general type of analysis is illustrated by considering an experiment to measure the crack residence time, t, that involves just two factors, gas velocity and stirrer speed. Supose three levels of the gas velocity and two levels of stirrer speed were used.

To analyze the data of this experiment, a model for the residence time, t, must be proposed. Two alternative models can be considered, the "linear statistical" model or the "multiple regression" model.

Model 1. "Linear statistical" model

$$t_{ijk} = \bar{M} + A_i + B_j + (AB)_{ij} + E_{ijk}$$

$$i = 1, 2, 3 \qquad j = i, 2 \qquad k = 1, 2, \ldots n_{ij}$$

where

A_i = effect of the ith level of gas velocity

B_j = effect of the jth level of stirrer speed

$(AB)_{ij}$ = the interaction between the ith level of gas velocity and jth level of stirrer speed

An analysis using this model is usually summarized by the familiar analysis of variance table, Table 35.

Table 35. analysis of variance table for linear statistical model

Source	d.f.	Sum of Squares	Mean Squares	F
Gas velocity, u	2	SS(u)	MS(u)	MS(u)/E
Stirrer speed, N	1	SS(N)	MS(N)	MS(N)/E
Interaction, u*N	2	SS(u*N)	MS(u*N)	MS(u*N)/E
Error	$\sum n_{ij} - 6$	SS(E)	E	
Total (corrected)	$\sum n_{ij} - 1$			

Model 2. "Multiple regression" model

$$t_{ijk} = \bar{M} + \alpha_1 G_{1i} + \alpha_2 G_{2i} + \alpha_3 G_{3i} + \beta_1 S_{1j} + \beta_2 S_{2j} + (\alpha\beta)_{11} G_{1i} S_{1j} + (\alpha\beta)_{12} G_{1i} S_{2j} + (\alpha\beta)_{21} G_{2i} S_{1j} + (\alpha\beta)_{22} G_{2i} S_{2j} + (\alpha\beta)_{31} G_{3i} S_{1j} + (\alpha\beta)_{32} G_{3i} S_{2j} + \varepsilon_{ijk}$$

where $i = i, 2, 3$

$j = 1, 2$

$k = 1, 2, \ldots n_{ij}$

$G_{ml} = 1$ if $l = m$ and 0 if $l \neq m$

$S_{ml} = 1$ if $l = m$ and 0 if $l \neq m$

In terms of the multiple regression model, the analysis can be conducted in two possible directions, by the use of "sequential sum of squares" of by the use of "partial sum of squares". Both ways are based on the "additional sum of squares" principle.

The "sequential sum of squares" analysis is based on sequentially adding each term to the model and measuring the effect of each term, ignoring the effect of the other terms of the model. In the example experiment, the effect of gas velocity (u's of the model) is measured first while the stirrer speed and interaction are ignored. Then the effect of stirrer speed (N's of the model) is measured after adjustment for the gas velocity effect, but not the interaction, is made. In this manner, the analysis proceeds until all parameters have been added. The analysis can be summarized as in Table 36.

The sum of squares denoted by RSS( ) in Table 36 is the regression sum of squares based on a regression model with independent variable terms corresponding to the effect included in the argument, that is RSS($\bar{M}$,u) is the regression sum of squares for the model

$$t_{ijk} = \bar{M} + \alpha_1 G_{1i} + \alpha_2 G_{2i} + \alpha_3 G_{3i} + \varepsilon'_{ijk}$$

Thus the "additional sum of squares" due to adding gas veloc-

Table 36. Analysis of variance table for sequential sum of squares analysis of multiple regression model

Source	d.f.	Sum of Squares	Mean Squares	F
u ignoring N and (u*N)	2	$SS(u) = RSS(\bar{M},u) - RSS(\bar{M})$	MS(u)	MS(u)/E
N adjusted for u but not (u*N)	1	$SS(N\|u) = RSS(\bar{M},\underline{u},N) - RSS(\bar{M},u)$	MS(N)	MS(N)/E
u*N adjusted for u and N	2	$SS(u*N\|u,N) = RSS(\bar{M},\underline{u},N,u*N) - RSS(\bar{M},u,N)$	MS(u*N)	MS(u*N)/E
Error	$\sum n_{ij} - 6$	SS(E)	E	
Total (corrected)	$\sum n_{ij} - 1$	SST		

ity (the u's) to the model is

$$SS(u) = RSS(\bar{M},u) - RSS(\bar{M})$$

The "partial sum of squares" analysis is based on always measuring the effect of every term in the model after adjusting for all other terms. The analysis is thus like the sequential sum of squares analysis with every term "added last" to the model. The partial sum of squares analysis is summarized by Table 37.

For an experiment designed and conducted so that the factors and their interactions are all additative, then all three methods of analysis described above would be identical. The illustrative experiment has additative factors and interactions provided n_{ij} is the same for each i and j, that is the same number of measurements were made at all six combinations of gas velocity and stirrer speed. If these conditions were satisfied, the easiest model analysis would be that of the linear statistical model.

For many experiments, however, especially those involving many factors, it is uneconomical to include runs representing all possible combinations of the factors. It is more economical to not run some cells of the experimental design and to run fewer replications of other cells. Thus n_{ij} would not be constant. In this case, the factors are not additative and the three analyses are not identical. In

Table 37. Analysis of variance table for partial sum of squares analysis of multiple regression model

Source	d.f.	Sum of Squares
u adjusted for N and u*N	2	$SS(u \mid N,u*N) = RSS(\bar{M},u,S,u*N) - RSS(\bar{M},N,u*N)$
N adjusted for u and u*N	1	$SS(N \mid u,u*N) = RSS(\bar{M},u,N,u*N) - RSS(\bar{M},u,u*N)$
u*N adjusted for u and N	2	$SS(u*N \mid u,N) = RSS(\bar{M},u,N,u*N) - RSS(\bar{M},u,N)$
Error	$\sum n_{ij} - 6$	SS(E)
Total	$\sum n_{ij} - 1$	SST

fact, the linear statistical model and analysis could not be used since the model assumes the terms are additative. The alternative analyses, the sequential and partial sum of squares, do not involve that assumption.

In considering a given term of a model, the conclusion reached from a sequential F test may differ from the conclusion reached from a partial F test. In the illustrative experiment discussed above, the gas velocity may be significant as indicated by the sequential F test but be insignificant as indicated by the partial F test (at the reader's acceptable level of significance). This is not a contradiction, but means that if stirrer speed (or the interaction term) is included in the model, gas velocity has less effect. This in turn indicates that gas velocity and stirrer speed (or the interaction) are not orthogonal factors.

For convenience, the author's conclusions of significance, decided at the 5% significance level, have been indicated in the tables of this appendix. Usually for a factor to have been considered significant, F values determined by both the sequential F test and the partial F test must have been significant at the 5% level or greater. The exception occurred where a factor to the second or third power was significant by the above criteria but the factor itself tested as insignificant in one of the tests. In that case, it is accepted practice to include the lower order terms in the

model.

The overall fit of the model is indicated by the "coefficient of multiple determination", R^2, equation 30. This measures the model fit compared to that of a model consisting of just the constant mean value. R^2 approaches unity as the model accounts for more of the data's variance. Conversely, R^2 approaches zero for a total lack of fit.

Many of the data analyses summarized in this appendix were calculated using the multiple regression model with both the sequential and partial sum of squares analyses. This kind of analysis was required for these experiments because a large number of factors (see General Plan) were involved and not all combinations of factors were observed an equal number of times. The statistics presented in this appendix for these tests are the sequential F statistic (Seq. F), the partial F statistic (Part. F), and the level of significance of each F, "P > F". The degrees of freedom and error mean square are also reported.

Most of the statistical computations were performed using the Statistical Analysis System computer library package developed at North Carolina University, Raleigh, North Carolina as implemented at Iowa State University, Ames, Iowa. In this program, the significance of each F (or T) statistic was determined by calculating the highest significance level at which the hypothesis under consideration, H:

$w^2 = 0$ (or H: $b = 0$), may be rejected. This level of significance is commonly referred to as "P > F". The lower the P > F, the more significant a F (or T) statistic becomes. The level of significance means that if the experiment were repeated, P > F (or P > T) percent of the time, the experiment would indicate a different conclusion (that is, accepting H when in fact H is false). The level of significance reported for each F (or T) statistic is not predetermined as was the traditional procedure. With the significance reported in the current manner, the reader can decide for himself the level he considers significant for each F (or T) test.

Residence Time Tests

Table 38. Analysis of variance test for effect of observers 1 and 2 on residence time measurements

Data: (Set 1, run 2), (1,6), (1,7), (2,1), (2,2), (2,3)

Model: $\ln \bar{t} = \bar{M} + C + O + L + L*O$

d	Source	d.f.	Seq. F	P > F	Part. F	P > F	Sig.	R^2
1	C	1	70.84	0.0002	63.59	0.0003	yes	0.93
	O	1	0.013	0.907	0.013	0.907	no	
	L	1	17.18	0.005	17.18	0.005	yes	
	L*O	1	3.66	0.095	3.66	0.095	no	
	Error	7	M.S. = 0.00577					
2	C	1	45.30	0.0005	42.17	0.0006	yes	0.90
	O	1	0.197	0.672	0.197	0.672	no	
	L	1	12.97	0.009	12.97	0.009	yes	
	L*O	1	2.252	0.175	2.252	0.175	no	
	Error	7	M.S. = 0.00886					
3	C	1	43.73	0.0006	43.55	0.0006	yes	0.90
	O	1	1.194	0.311	1.194	0.311	no	
	L	1	13.43	0.008	13.43	0.008	yes	
	L*O	1	3.682	0.095	3.682	0.095	no	
	Error	7	M.S. = 0.0112					

Table 39. Analysis of variance test for effect of observers 1 and 3 or 4 on residence time measurements

Data: Sets 8 and 9

Model: $\ln \bar{t} = \bar{M} + C + L + O(S)$ (nested model)

Source	d.f.	Sum of Squares	Mean Square	F	F(0.95, d.f.,11)	Sig.
C	1	0.17597	0.17597	11.70	4.84	yes
L	1	0.32179	0.32179	21.40	4.84	yes
O	2	0.009337	0.004668	0.31	3.98	no
Error	11	0.16540	0.015037			
Total	15	0.672497				

Table 40. Analysis of variance tests for gas velocity, travel distance, and location effects on the harmonic average void rates

Data: Sets 8 to 10

Model: $\bar{v} = \bar{M} + S + U + D + L + U*L$

Source	d.f.	Seq. F	P > F	Part. F	P > F	Sig.	R^2
S	5	43.4	0.0001	14.4	0.0001	yes	0.95
U	2	695.	0.0001	695.	0.0001	yes	
D	1	2.70	0.100	2.70	0.100	no	
L	1	153.	0.0001	150.	0.0001	yes	
U*L	2	6.45	0.003	6.45	0.003	yes	
Error	84	M.S. = 0.000301					

Model: $\bar{v} = \bar{M} + S + U + L + U*L$

Source	d.f.	Seq. F	P > F	Part. F	P > F	Sig.	R^2
S	5	42.55	0.0001	14.08	0.0001	yes	0.95
U	2	682.	0.0001	682.	0.0001	yes	
L	1	151.	0.0001	147.	0.0001	yes	
U*L	2	6.323	0.003	6.323	0.003	yes	
Error	85	M.S. = 0.000307					

Table 41. Analysis of variance test for gas velocity, travel distance, and location effects on residence time

Data: Sets 5 and 6

Model: $\ln \bar{t} = \bar{M} + S + U + D + D*U + L + L*U + D*L + D*L*U$

Source	d.f.	Sum of Squares	Mean Square	F	F(0.95, d.f.,19)	Sig.
S	1	0.01180	0.01180	1.340	4.38	no
U	2	3.397	1.6984	192.	3.52	yes
D	1	9.011	9.011	1023.	4.38	yes
D*U	2	0.00706	0.00353	0.401	3.52	no
L	1	0.849	0.849	96.4	4.38	yes
L*U	2	0.0719	0.0360	4.09	3.52	yes
D*L	1	0.0150	0.0150	1.70	4.38	no
D*L*U	2	0.00479	0.00240	0.272	3.52	no
Error	19	0.1673	0.00880			
Total	31	13.53485				

Table 42. Analysis of variance tests of effects of stirrer speed, set, gas velocity, and location on residence time

Data: Sets 1 to 4, runs 1 to 8 except u = 0.175 ft./sec. and N = 150 rpm

Model: $\ln \bar{t} = \bar{M} + S + U + N + U*N + L + U*L + N*L + U*N*L$

d	Source	d.f.	Seq. F	P > F	Part. F	P > F	Sig.	R^2
1	S	3	17.8	0.0001	2.297	0.0926	no	0.96
	U	2	337.5	0.0001	156.8	0.0001	yes	
	N	2	0.495	0.619	0.046	0.955	no	
	U*N	4	0.835	0.513	0.835	0.513	no	
	L	1	102.7	0.0001	60.7	0.0001	yes	
	U*L	2	1.403	0.257	0.339	0.720	no	
	N*L	2	0.239	0.791	0.488	0.623	no	
	U*N*L	4	0.489	0.746	0.489	0.746	no	
	Error	39	M.S. = 0.00907					
2	S	3	19.6	0.0001	2.641	0.062	no	0.96
	U	2	398.9	0.0001	191.9	0.0001	yes	
	N	2	0.478	0.629	0.221	0.805	no	
	U*N	4	1.182	0.334	1.18	0.334	no	
	L	1	107.2	0.0001	48.6	0.0001	yes	
	U*L	2	5.20	0.010	3.50	0.039	yes	
	N*L	2	0.015	0.986	0.159	0.854	no	
	U*N*L	4	0.274	0.892	0.274	0.892	no	
	Error	39	M.S. = 0.00835					
3	S	3	20.8	0.0001	2.12	0.113	no	0.96
	U	2	421.2	0.0001	199.8	0.0001	yes	
	N	2	0.770	0.526	0.659	0.528	no	
	U*N	4	0.835	0.513	0.835	0.513	no	
	L	1	107.0	0.0001	44.28	0.0001	yes	
	U*L	2	4.88	0.013	3.85	0.029	yes	
	N*L	2	0.213	0.811	0.596	0.561	no	
	U*N*L	4	0.530	0.717	0.530	0.717	no	
	Error	39	M.S. = 0.00857					

Table 42. (Continued)

Model: $\ln \bar{t} = \bar{M} + U + N + L + S$

d	Source	d.f.	Seq. F	P > F	Part. F	P > F	Sig.	R^2
1	U	1	780.	0.0001	723.	0.0001	yes	0.94
	N	1	0.844	0.635	1.500	0.224	no	
	L	1	112.0	0.0001	112.0	0.0001	yes	
	S	3	2.33	0.083	2.33	0.083	no	
	Error	57	M.S. = 0.00858					
2	U	1	828.	0.0001	775.	0.0001	yes	0.94
	N	1	1.427	0.235	2.238	0.136	no	
	L	1	108.1	0.0001	108.1	0.0001	yes	
	S	3	2.64	0.057	2.64	0.057	no	
	Error	57	M.S. = 0.00870					
3	U	1	797.	0.0001	745.	0.0001	yes	0.94
	N	1	0.157	0.695	0.554	0.533	no	
	L	1	99.9	0.0001	99.9	0.0001	yes	
	S	3	2.23	0.093	2.23	0.093	no	
	Error	57	M.S = 0.00975					

Table 43. Analysis of variance tests for effects of moisture, gas velocity, and location on residence time

Data: Sets 8 to 10

Model: $\ln \bar{t} = \bar{M} + Mo + U + L + U*L + Mo*L$

Source	d.f.	Seq. F	P > F	Part. F	P > F	Sig.	R^2
Mo	2	15.4	0.0001	15.4	0.0001	yes	0.94
U	2	183.	0.0001	183.	0.0001	yes	
L	3	15.9	0.0001	11.1	0.0001	yes	
U*L	6	4.06	0.0049	4.06	0.0049	yes	
Mo*L	6	0.888	0.518	0.888	0.518	no	
Error	28	M.S. = 0.0135					

Model: $\ln \bar{t} = \bar{M} + Mo + U + L + U*L$

Source	d.f.	Seq. F	P > F	Part. F	P > F	Sig.	R^2
Mo	2	15.72	0.0001	15.72	0.0001	yes	0.94
U	2	187.	0.0001	187.	0.0001	yes	
L	3	16.18	0.0001	11.32	0.0001	yes	
U*L	6	4.146	0.005	4.146	0.005	yes	
Error	34	M.S. = 0.0133					

Table 44. Regression analysis of gas velocity and location effects on residence time in a deep bed

Data: Set 8

Model: $\ln \bar{t} = a + bU + cL + dU^2 + e(U*L)$

Source	d.f.	Seq. F	P > F	Part. F	P > F	Sig.	R^2
U	1	177.	0.0001	3.30	0.094	no	0.95
L	1	21.66	0.001	22.57	0.001	yes	
U^2	1	2.34	0.152	2.34	0.152	no	
U*L	1	15.82	0.003	15.82	0.003	yes	
Error	11	M.S. = 0.0118					

Regression coefficients:

Source	B values	T for H:B=0	P > |T|	Sig.
a	3.371	3.42	0.006	yes
b	-21.48	-1.82	0.094	no
c	0.091	4.75	0.001	yes
d	54.68	1.53	0.152	no
e	-0.479	-3.98	0.003	yes

Table 45. Regression analysis of gas velocity and location effects on residence time in a shallow bed

Data: Set 7

Model: $\ln \bar{\tau} = a + bU + cL + d(U*L)$

Source	d.f.	Seq. F	P > F	Part. F	P > F	Sig.	R^2
U	1	63.4	0.0001	9.31	0.010	yes	0.91
L	1	17.5	0.0016	33.6	0.0002	yes	
U*L	1	44.4	0.0001	44.4	0.001	yes	
Error	12	M.S. = 0.00432					

Regression coefficients:

Source	B values	T for H:B=0	P > |T|	Sig.
a	1.298	5.518	0.0003	yes
b	4.524	3.051	0.0098	yes
c	0.180	5.800	0.0002	yes
d	-1.306	-6.662	0.0001	yes

Table 46. Regression fits of flour harmonic average slip surface void velocities

Data: Sets 1 to 11, excluding u = 0.175 ft./sec., N = 150 rpm, run 9, and runs 5 to 8 of Set 11

Model: $\ln \bar{v} = a + bU + cL + dMo + e(U*L) + fH + gR$

Source	d.f.	Seq. F	P > F	Part. F	P > F	Sig.	R^2
U	1	1279.	0.0001	81.2	0.0001	yes	0.88
L	1	87.9	0.0001	61.0	0.0001	yes	
Mo	1	9.78	0.0024	19.2	0.0001	yes	
U*L	1	28.89	0.0001	28.3	0.0001	yes	
H	1	77.40	0.0001	68.9	0.0001	yes	
R	1	0.036	0.845	0.036	0.845	no	
Error	193	M.S. = 0.0190					

Model: $\ln \bar{v} = a + bU + cL + dMo + e(U*L) + fH$

Source	d.f.	Seq. F	P > F	Part. F	P > F	Sig.	R^2
U	1	1285.	0.0001	81.6	0.0001	yes	0.88
L	1	88.4	0.0001	61.5	0.0001	yes	
Mo	1	9.8	0.0024	39.0	0.0001	yes	
U*L	1	29.0	0.0001	28.4	0.0001	yes	
H	1	77.8	0.0001	77.8	0.0001	yes	
Error	194	M.S. = 0.0189					

Table 46. (Continued)

Regression coefficients:

Source	B values	T for H:B=0	P > |T|	Sig.
a	-3.446	-22.9	0.0001	yes
b	7.313	9.0	0.0001	yes
c	-0.0467	-7.8	0.0001	yes
d	0.0201	6.2	0.0001	yes
e	0.200	5.3	0.0001	yes
f	0.0207	8.8	0.0001	yes

Table 47. Additional regression fit of flour harmonic average slip surface void velocities

Data: Sets 1 to 11, excluding u = 0.175 ft./sec., N = 150 rpm, run 9, and runs 5 to 8 of Set 11

Model: $\ln \bar{v} = a + bU + cL + dMo + e(U*L) + fH + gMo^2 + hMo^3$

Source	d.f.	Seq. F	P > F	Part. F	P > F	Sig.	R^2
U	1	1389.	0.0001	88.2	0.0001	yes	0.89
L	1	95.5	0.0001	66.9	0.0001	yes	
Mo	1	10.6	0.0017	12.0	0.0010	yes	
U*L	1	31.4	0.0001	30.7	0.0001	yes	
H	1	84.1	0.0001	83.7	0.0001	yes	
Mo^2	1	7.2	0.0077	11.7	0.0011	yes	
Mo^3	1	10.5	0.0018	10.4	0.0018	yes	
Error	192	M.S. = 0.0175					

Regression coefficients:

Source	B values	T for H:B=0	P > |T|	Sig.
a	-2.605	-9.75	0.0001	yes
b	7.315	9.39	0.0001	yes
c	-0.0469	-8.18	0.0001	yes
d	-0.386	-3.37	0.0010	yes
e	0.200	5.54	0.0001	yes
f	0.0212	9.15	0.0001	yes
g	0.0504	3.42	0.0011	yes
h	-0.00184	-3.23	0.0018	yes

Table 48. Analysis of variance tests for effect of salt mixing experiments on solids residence time

Data: runs 8 and 9 of Sets 3 and 4

Model: $\ln \bar{z} = \bar{M} + S + Q$

where $\bar{z} = \ln \bar{t}$ averaged over upper and lower locations

d	Source	d.f.	Seq. F	P > F	Part. F	P > F	Sig.	R^2
1	S	1	0.158	0.924	0.001	0.980	no	0.71
	Q	1	4.811	0.160	4.811	0.160	no	
	Error	2	M.S. = 0.00824					
2	S	1	0.326	0.625	0.001	0.977	no	0.87
	Q	1	12.69	0.069	12.69	0.069	no	
	Error	2	M.S. = 0.00487					
3	S	1	0.587	0.524	0.067	0.812	no	0.83
	Q	1	8.91	0.096	8.91	0.096	no	
	Error	2	M.S. = 0.00587					

Table 48. (Continued)

Model: $\ln \bar{t} = \bar{M} + C + Q + L + L*Q$

d	Source	d.f.	Seq. F	P > F	Part. F	P > F	Sig.	R^2
1	S	1	0.340	0.589	0.002	0.970	no	0.89
	Q	1	10.35	0.024	10.35	0.024	yes	
	L	1	28.76	0.004	28.24	0.004	yes	
	L*Q	1	0.089	0.772	0.089	0.772	no	
	Error	5	M.S. = 0.00767					
2	S	1	0.583	0.516	0.002	0.968	no	0.93
	Q	1	22.73	0.006	22.73	0.006	yes	
	L	1	39.16	0.002	38.17	0.002	yes	
	L*Q	1	0.056	0.816	0.056	0.816	no	
	Error	5	M.S. = 0.00544					
3	S	1	0.991	0.633	0.113	0.747	no	0.91
	Q	1	15.0	0.012	15.0	0.012	yes	
	L	1	35.9	0.003	34.8	0.003	yes	
	L*Q	1	0.030	0.864	0.030	0.864	no	
	Error	5	M.S. = 0.00696					

Table 49. Test for material effect on harmonic average slip surface void velocity

Data: Set 11

Model 1: $\bar{v}_H = a + bU$

Source	d.f.	Sum of Squares	Mean Square	F	P > F	R^2
Regression	4	1.3325	0.3331	20.6	0.0001	0.88
Error	11	0.1778	0.0162			
Corrected Total	15	1.5102				

Model 2: $\bar{v}_H = a + bU' + cU''$

where U' = gas velocity effect for pure flour

U'' = gas velocity effect for flour iwth 0.5% Cab-O-Sil

Source	d.f.	Sum of Squares	Mean Square	F	P > F	R^2
Regression	5	1.4243	0.2849	33.16	0.0001	0.94
Error	10	0.0859	0.00859			
Corrected Total	15	1.5102				

Table 49. (Continued)

Model 3: $\bar{v}_H$ = a(Material i) + b(Material i *Location j) U

where i = pure flour or flour with 0.5% Cab-O-Sil
j = upper or lower locations

Source	d.f.	Sum of Squares	Mean Square	F	P > F	R^2
Regression	7	1.4354	0.2051	21.9	0.0004	0.95
Error	8	0.0748	0.00935			
Corrected Total	15	1.5102				

Partial F tests:

Test for common slope of lines for both materials:

$$F(1,10) = \frac{RSS(model\ 2) - RSS(model\ 1)}{MSE(model\ 2)}$$

$$F(1,10) = \frac{1.4243 - 1.3325}{0.00859} = 10.69$$

which is greater than F(0.99, 1, 10) = 10.04 so decision is that the slope of the lines depended on the material.

Test if slope was only a function of material and not location:

$$F(1,8) = \frac{RSS(model\ 3) - RSS(model\ 2)}{MSE(model\ 3)}$$

$$F(1,8) = \frac{1.4354 - 1.4243}{0.00935} = 1.187$$

Table 49. (Continued)

---

which is less than F(0.95, 1,8) = 5.32 so conclude location was not important.

Table 50. Regression fit of harmonic average slip surface void velocity for flour with 0.5% Cab-O-Sil

Data: Set 11, runs 5 to 8

Model: $\bar{v}_H = a + bu + cL$

Source	d.f.	Seq. F	P > F	Part. F	P > F	Sig.	R^2
u	1	233.9	0.0001	233.9	0.0001	yes	0.95
L	1	35.46	0.0001	35.46	0.0001	yes	
Error	13	M.S. = 0.00325					

Regression coefficients:

Source	B values	T for H:B=0	P > |T|	Sig.
a	-1.031	-9.871	0.0001	yes
b	17.34	15.29	0.0001	yes
c	0.0108	5.955	0.0001	yes

Heat Transfer Tests

Table 51. Regression analysis of heat transfer coefficients as function of gas velocity

Data: All flour-nitrogen system runs of Nazemi (84), pooled stirrer speed

Model: $h = a + bu$

Lower heat transfer surface:

Source	d.f.	Sum of Squares	Mean Square	F	P > F	R^2
Regression	1	756.52	756.52	463.5	0.0001	0.96
Error	19	31.011	1.632			
Total (corrected)	20	787.53				

Regression coefficients:

Source	B values	T for H:B=0	P > |T|	Sig.
a	-6.202	-5.35	0.0001	yes
b	172.36	21.81	0.0001	yes

Table 51. (Continued)

Upper heat transfer surface:

Source	d.f.	Sum of Squares	Mean Square	F	P > F	R^2
Regression	1	548.11	548.11	520.1	0.0001	0.96
Error	19	20.022	1.054			
Total (corrected)	20	568.13				

Regression coefficients:

Source	B values	T for H:B=0	P > |T|	Sig.
a	-7.435	-7.98	0.0001	yes
b	146.71	22.81	0.0001	yes

Table 52. Regression fit of heat transfer coefficients and harmonic average crack velocity, linear model

Data: Heat transfer coefficients from correlation of Table 50, mean harmonic average velocity of Sets 1 to 11, except run 9 and Set 11, runs 5 to 8.

Model: $h = a + b\bar{v}_H$

Upper heat transfer surface:

Source	d.f.	Sum of Squares	Mean Square	F	P > F	R^2
Regression	1	143.0	143.0	122111	0.0001	1.00
Error	2	0.00234	0.00117			
Total (corrected)	3	143.0				

Regression coefficients:

Source	B values	T for H:B=0	P > |T|	Sig.
a	3.898	123.4	0.0002	yes
b	70.628	349.4	0.0001	yes

Table 52. (Continued)

Lower heat transfer surface:

Source	d.f.	Sum of Squares	Mean Square	F	P > F	R^2
Regression	1	197.4	197.4	999999	0.0001	1.00
Error	2	0.000294	0.000147			
Total (corrected)	3	197.4				

Regression coefficients:

Source	B values	T for H:B=0	P > |T|	Sig.
a	5.290	422.4	0.0001	yes
b	74.628	1160.	0.0001	yes

Table 53. Regression fit of heat transfer coefficients and harmonic average crack velocity, square root model

Data: Heat transfer coefficients from correlation of Table 50, mean harmonic average velocity of Sets 1 to 11, except run 9 and Set 11, runs 5 to 8.

Model: $h = a(\bar{v}_H)^{1/2}$

Upper heat transfer surface:

Source	d.f.	Sum of Squares	Mean Square	F	P > F	R^2
Regression	1	830.2	830.2	337.2	0.0004	0.99
Error	3	7.386	2.462			
Total (uncorrected)	4	837.6				

Regression coefficients:

Source	B values	T for H:B=0	P > |T|	Sig.
a	39.80	18.36	0.0004	yes

Table 53. (Continued)

Lower heat transfer surface:

Source	d.f.	Sum of Squares	Mean Square	F	P > F	R^2
Regression	1	1483.	1483.	369.5	0.0003	0.99
Error	3	12.04	4.015			
Total (uncorrected)	4	1495.				

Regression coefficients:

Source	B values	T for H:B=0	P > |T|	Sig.
a	46.64	19.22	0.0003	yes

Mixing Tests

Table 54. Regression analysis of between sample variance of flow samples

Data: Sets 1 to 6, 13 (minimum S^2 criteria)

Model: $(n-1)^{1/2} \ln S^2 = a + bu + cN + dH + eTr$

where Tr = tracer effect

Source	d.f.	Seq. F	P > F	Part. F	P > F	Sig.	R^2
U	1	1.336	0.270	0.986	0.658	no	0.54
N	1	0.412	0.539	0.838	0.619	no	
H	1	9.553	0.009	8.600	0.012	yes	
Tr	2	1.475	0.267	1.475	0.267	no	
Error	12	M.S. = 80.41					

Table 55. Regression fit of lag time data for flour

Data: Sets 1 to 10 and 13

Model: $\ln \tau = a + bu + cH + dMo + eMo^2 + fMo^3$

Source	d.f.	Seq. F	P > F	Part. F	P > F	Sig.	R^2
u	1	46.2	0.0001	80.6	0.0001	yes	0.88
H	1	95.4	0.0001	78.7	0.0001	yes	
Mo	1	0.49	0.500	7.47	0.012	yes	
Mo^2	1	2.52	0.125	6.90	0.015	yes	
Mo^3	1	6.33	0.020	6.33	0.020	yes	
Error	20	M.S. = 0.0408					

Regression coefficients:

Source	B values	T for H:B=0	P > |T|	Sig.
a	-2.487	-2.433	0.0232	yes
b	-6.346	-8.979	0.0001	yes
c	0.081	8.869	0.0001	yes
d	132.	2.734	0.012	yes
e	-1675.	-2.627	0.015	yes
f	6219.	2.516	0.020	yes

Table 56. Additional regression analysis of lag time for flour

Data: Sets 1 to 10 and 13

Model: $\ln \tau = a + bu + cMo + dH + eN + fu^2 + gMo^2 + hMo^3$

Source	d.f.	Seq. F	P > F	Part. F	P > F	Sig.	R^2
u	1	43.99	0.0001	5.79	0.026	yes	0.89
Mo	1	13.43	0.0021	7.32	0.014	yes	
H	1	77.90	0.0001	70.40	0.0001	yes	
N	1	0.216	0.652	0.215	0.652	no	
u^2	1	0.211	0.655	0.839	0.625	no	
Mo^2	1	3.000	0.097	6.70	0.018	yes	
Mo^3	1	6.064	0.023	6.06	0.023	yes	
Error	18	M.S. = 0.0428					

Regression coefficients:

Source	B values	T for H:B=0	P > |T|	Sig.
a	-2.127	-1.865	0.076	yes
b	-10.14	-2.407	0.026	yes
c	133.8	2.706	0.014	yes
d	0.0795	8.390	0.0001	yes
e	0.000933	0.464	0.652	no
f	8.293	0.916	0.625	no
g	-1692.	-2.588	0.018	yes
h	6235.	2.462	0.023	yes

Table 57. Regression fit of minimum mixing time data for flour

Data: Sets 1 to 10 and 13

Model: $\ln t_M = a + bu + cH + du^2 + eMo + fMo^2 + gMo^3$

Source	d.f.	Seq. F	P > F	Part. F	P > F	Sig.	R^2
u	1	11.54	0.0033	13.87	0.0017	yes	0.67
H	1	14.71	0.0014	7.34	0.013	yes	
u^2	1	6.02	0.023	9.33	0.0064	yes	
Mo	1	0.73	0.593	0.028	0.862	no	
Mo^2	1	4.72	0.040	0.14	0.716	yes	
Mo^3	1	0.29	0.603	0.29	0.603	no	
Error	19	M.S. = 0.0825					

Regression coefficients:

Source	B values	T for H:B=0	P > |T|	Sig.
a	3.858	2.446	0.023	yes
b	-21.79	-3.724	0.0017	yes
c	0.0357	2.710	0.013	yes
d	38.51	3.063	0.0064	yes
e	-11.56	-0.168	0.862	no
f	335.	0.369	0.716	no
g	-1888.	-0.537	0.603	no

Table 58. Additional regression analysis of minimum mixing time for flour

Data: Sets 1 to 10 and 13

Model: $\ln t_M = a + bu + cMo + dH + eN + fu^2 + gMo^2 + hMo^3$

Source	d.f.	Seq. F	P > F	Part. F	P > F	Sig.	R^2
u	1	10.94	0.0041	13.15	0.0022	yes	0.67
Mo	1	1.510	0.233	0.0266	0.866	no	
H	1	12.44	0.0027	6.967	0.016	yes	
N	1	0.0194	0.886	0.0156	0.897	no	
u^2	1	6.401	0.020	8.900	0.0079	yes	
Mo^2	1	4.473	0.046	0.129	0.724	no	
Mo^3	1	0.273	0.613	0.273	0.613	no	
Error	18	M.S. = 0.0870					

Regression coefficients:

Source	B values	T for H:B=0	P > |T|	Sig.
a	3.875	2.383	0.027	yes
b	-21.80	-3.626	0.0022	yes
c	-11.51	-0.163	0.866	no
d	0.0357	2.640	0.016	yes
e	-0.000358	-0.125	0.897	no
f	38.52	2.983	0.0079	yes
g	334.6	0.359	0.724	no
h	-1885.	-0.522	0.613	no

Table 59. Regression analysis of between sample variance of steady state mixture flow samples

Data: Sets 1 to 10 and 13

Model: $(n-1)^{1/2} \ln S^2 = a + bu + cMo + dH + eu^2 + fMo^2 + gMo^3 + h(u*Mo)$

Source	d.f.	Seq. F	P > F	Part. F	P > F	Sig.	R^2
u	1	0.612	0.550	0.795	0.612	no	0.20
Mo	1	0.395	0.544	0.0784	0.779	no	
H	1	1.753	0.200	1.660	0.212	no	
u^2	1	0.0090	0.923	0.136	0.717	no	
Mo^2	1	0.0186	0.888	0.0007	0.977	no	
Mo^3	1	0.178	0.681	0.0019	0.965	no	
(u*Mo)	1	1.549	0.228	1.549	0.228	no	
Error	18	M.S. = 158.9					

Regression coefficients:

Source	B values	T for H:B=0	P > |T|	Sig.
a	-157.7	-1.772	0.090	no
b	434.9	0.891	0.612	no
c	852.8	0.280	0.779	no
d	0.74	1.288	0.212	no
e	207.2	0.368	0.717	no
f	-1118.	-0.027	0.977	no
g	7059.	0.044	0.965	no
h	-4248.	-1.245	0.228	no

Table 60. Additional regression analysis of between sample variance of steady state flow samples

Data: Sets 1 to 10 and 13

Model: $(n-1)^{1/2} \ln S^2 = a + bu + cMo + dH + eN + fu^2 + gMo^2 + hMo^3$

Source	d.f.	Seq. F	P > F	Part. F	P > F	Sig.	R^2
u	1	0.569	0.533	0.0945	0.760	no	0.14
Mo	1	0.367	0.558	0.204	0.661	no	
H	1	1.630	0.216	1.544	0.228	no	
N	1	0.171	0.687	0.173	0.685	no	
u^2	1	0.0087	0.924	0.0162	0.896	no	
Mo^2	1	0.0161	0.896	0.175	0.683	no	
Mo^3	1	0.168	0.689	0.168	0.690	no	
Error	18	M.S. = 171.0					

Regression coefficients:

Source	B values	T for H:B=0	P > |T|	Sig.
a	-85.55	-1.187	0.249	no
b	-81.87	-0.307	0.760	no
c	1411.	0.452	0.661	no
d	0.746	1.243	0.228	no
e	-0.0528	-0.415	0.685	no
f	72.87	0.127	0.896	no
g	-17288.	-0.418	0.683	no
h	65588.	0.410	0.689	no

Table 61. Regression analysis of minimum mixing time for flour

Data: Sets 1 to 10 and 13 (minimum S^2 criteria)

Model: $\ln t_M = a + bu + cMo + dH + eu^2 + f\,Mo^2 + gMo^3 + h(u*Mo)$

Source	d.f.	Seq. F	P > F	Part. F	P > F	Sig.	R^2
u	1	11.05	0.0040	2.367	0.138	no	0.67
Mo	1	1.525	0.231	0.052	0.817	no	
H	1	12.57	0.0026	7.039	0.016	yes	
u^2	1	6.462	0.019	9.17	0.0072	yes	
Mo^2	1	4.526	0.045	0.232	0.641	no	
Mo^3	1	0.276	0.611	0.400	0.541	no	
(u*Mo)	1	0.200	0.664	0.200	0.664	no	
Error	18	M.S. = 0.0861					

Regression coefficients:

Source	B values	T for H:B=0	P > |T|	Sig.
a	3.276	1.581	0.128	no
b	-17.48	-1.539	0.138	no
c	-16.17	-0.228	0.817	no
d	0.0356	2.653	0.016	yes
e	39.64	3.029	0.0072	yes
f	469.6	0.482	0.641	no
g	-2374.	-0.633	0.541	no
h	-35.52	-0.447	0.664	no

Table 62. Regression analysis of lag time for flour

Data: Sets 1 to 10 and 13 (minimum S^2 criteria)

Model: $\ln \tau = a + bu + cMo + dH + eu^2 + fMo^2 + gMo^3 + h(u*Mo)$

Source	d.f.	Seq. F	P > F	Part. F	P > F	Sig.	R^2
u	1	43.64	0.0001	1.074	0.315	no	0.89
Mo	1	13.33	0.0021	6.920	0.016	yes	
H	1	77.28	0.0001	69.89	0.0001	yes	
u^2	1	0.212	0.655	0.898	0.642	no	
Mo^2	1	2.957	0.099	5.630	0.028	yes	
Mo^3	1	6.033	0.023	5.171	0.034	yes	
(u*Mo)	1	0.071	0.788	0.071	0.788	no	
Error	18	M.S. = 0.0432					

Regression coefficients:

Source	B values	T for H:B=0	P > |T|	Sig.
a	-2.328	-1.588	0.127	no
b	-8.331	-1.036	0.315	no
c	132.0	2.631	0.016	yes
d	0.0795	8.36	0.0001	yes
e	8.779	0.947	0.642	no
f	-1637.	-2.373	0.028	yes
g	6039.	2.274	0.034	yes
h	-14.99	-0.267	0.788	no

Table 63. Analysis of variance tests for gas velocity, and stirrer speed effects on lag time

Data: Sets 1 to 6

Model: $\tau = \bar{M} + U + N + (U*N)$

Source	d.f.	Seq. F	P > F	Part. F	P > F	Sig.	R^2
U	2	3.48	0.089	3.24	0.100	no	0.57
N	2	0.059	0.943	0.099	0.906	no	
U*N	4	0.523	0.725	0.523	0.725	no	
Error	7	M.S. = 1.923					

Model: $\tau = \bar{M} + U + N$

Source	d.f.	Seq. F	P > F	Part. F	P > F	Sig.	R^2
U	2	4.21	0.043	4.18	0.044	yes	0.44
N	2	0.072	0.931	0.072	0.931	no	
Error	11	M.S. = 1.589					

Table 64. Analysis of variance tests for gas velocity and stirrer speed effects on minimum mixing time

Data: Sets 1 to 6 (lower S^2 criteria)

Model: $t_M = \bar{M} + U + N + (U*N)$

Source	d.f.	Seq. F	P > F	Part. F	P > F	Sig.	R^2
U	2	6.48	0.026	4.81	0.048	yes	0.66
N	2	0.147	0.865	0.065	0.938	no	
U*N	4	0.215	0.920	0.215	0.920	no	
Error	7	M.S. = 14.853					

Model: $t_M = \bar{M} + U + N$

Source	d.f.	Seq. F	P > F	Part. F	P > F	Sig.	R^2
U	2	9.07	0.005	9.26	0.005	yes	0.63
N	2	0.206	0.818	0.206	0.818	no	
Error	11	M.S. = 10.614					

Table 65. Analysis of variance test of gas velocity and material effects on lag time

Data: Sets 5, 6, 11, and 12

Model: $\tau = \bar{M} + Ma + U + (Ma*U)$

Source	d.f.	Seq. F	P > F	Part. F	P > F	Sig.	R^2
Ma	2	39.0	0.023	39.9	0.022	yes	0.98
U[1]	1	2.468	0.258	1.690	0.324	no	
Ma*U	2	0.841	0.543	0.841	0.543	no	
Error	2	M.S. = 0.333					

[1]Relative fluidization gas velocity, u/u_{mf}, used.

Table 66. Additional analysis of variance test of gas velocity and material effects on lag time

Data: Sets 5, 6, 11, and 12

Model: $\tau = \bar{M} + Ma + U$

Source	d.f.	Seq. F	P > F	Part. F	P > F	Sig.	R^2
Ma	2	42.4	0.004	43.4	0.004	yes	0.96
U[1]	1	2.682	0.176	2.682	0.176	no	
Error	4	M.S. = 0.307					

[1]Relative fluidization gas velocity, u/u_{mf}, used.

Table 67. Analysis of variance tests of gas velocity and material effects on minimum mixing time

Data: Sets 5, 6, 11, and 12 (minimum S^2 criteria)

Model: $\ln t_M = \bar{M} + Ma + U + (Ma*U)$

Source	d.f.	Seq. F	P > F	Part. F	P > F	Sig.	R^2
Ma	2	223.	0.004	230.	0.004	yes	0.99
U[1]	1	14.7	0.060	10.0	0.086	no	
Ma*U	2	13.4	0.069	13.4	0.069	no	
Error	2	M.S. = 0.0933					

Model: $\ln t_M = \bar{M} + Ma + U$

Source	d.f.	Seq. F	P > F	Part. F	P > F	Sig.	R^2
Ma	2	30.9	0.005	31.8	0.005	yes	0.94
U[1]	1	2.040	0.226	2.040	0.226	no	
Error	4	M.S. = 0.673					

[1]Relative fluidization gas velocity, u/u_{mf}, used.

Table 68. Analysis of variance test for gas velocity and material effects on between sample variance of steady state flow samples

Data: Sets 5, 6, 11, and 12 (minimum S^2 criteria)

Model: $(n-1)^{1/2} \ln S^2 = \bar{M} + Ma + U$

Source	d.f.	Seq. F	P > F	Part. F	P > F	Sig.	R^2
Ma	2	1.869	0.267	1.786	0.270	no	0.48
U	1	0.0047	0.947	0.0047	0.947	no	
Error	4	M.S. = 229.9					

Table 69. Analysis of variance test of settled bed samples

Data: Sets 5, 6, 8 to 13

Model: $S^2 = \bar{M} + C + El + Ra + (El*Ra) + E$

where El = elevation effect
Ra = radial location effect

Source	d.f.	Seq. F	P > F	Part. F	P > F	Sig.	R^2
C	7	107.9	0.0001	108.	0.0001	yes	0.67
El	5	7.458	0.0001	7.294	0.0001	yes	
Ra	10	3.964	0.0001	3.989	0.0001	yes	
El*Ra	50	1.509	0.017	1.509	0.017	yes	
Error	453	M.S. = 0.00155					

Table 70. Comparisons of settled bed samples

Data: Sets 5, 6, 8 to 13

Model: $y_{ijk} = \bar{M} + aC_{1ijk} + bC_{2ijk} + \ldots + E$

where C_m = comparison m
i = set up
j = elevation
k = sample

Source	d.f.	Seq. Sum of Squares	F	P > F	Sig.
C_1[1]	1	0.02220	5.649	0.017	yes
C_2	1	0.02731	6.951	0.0085	yes
C_3	1	0.003712	0.945	0.667	no
C_4	1	0.000396	0.101	0.750	no
C_5	1	0.002791	0.710	0.596	no
C_6	1	0.006439	1.639	0.198	no
C_7	1	0.002633	0.670	0.581	no
C_8	1	0.008430	2.145	0.140	no
C_9	1	0.003631	0.924	0.662	no
Error	516	M.S. = 0.00393			

[1]For key, see Settled Bed Tracer Distribution.